Modification of PTFE using low-pressure and atmospheric-pressure plasma methods

HANNAH IRENE BLACKNELL

MODIFICATION OF PTFE SURFACES USING LOW-PRESSURE AND ATMOSPHERIC-PRESSURE PLASMA METHODS

Hannah Irene Blacknell

PhD Thesis

Department of Chemistry

Durham University

2018

Declaration

The work undertaken and described in this thesis was undertaken at Durham University Chemistry Department between September 2014 and February 2018. It is the original work of the author except where otherwise stated or acknowledged and has not been submitted for a degree in this, or in any other university.

Statement of Copyright

Acknowledgments

This thesis would not have come to fruition were it not for my incredible support network of family, friends, and teammates. I would like to lay special thanks to my parents and sisters for their long-distance love and support. My incredibly close-distance support coming from my neighbours: Steve, Elaine, and family, who looked out for me every day. To Lottie, Phil, and Rudy for their unwavering love and continually offering me shoulders to cry on, food to comfort eat, and picking me up after every knock back. To Beth, Bekah, Erica, Kate, Sam and Simon for ensuring I always ate the good things in life.

The pain of my PhD drove me to sports in a big way. Throughout my PhD, Tigers Netball Club and Hartlepool Triathletes have been a welcome distraction from my studies, but also a hub of friendship and support. Particular mention to Andrea, Anna, Cheryl, Chloe, Darrel, Jenny, Jonny, Julie, Kirsty, Lesley, Naomi, Niall, Sam, Shelley, Susan, and Vanessa.

Day-to-day stresses were alleviated by fellow members of Lab 98, the Bain group, and my trips to see Annette, Karen, and Emma for coffee, hugs, and tears, usually all at once. I would like to expressly thank Dr AnnMarie O'Donoghue and Professor Colin Bain for all their help in pushing my thesis towards its closure. For developing my character, my lab skills, and my writing abilities, I would like to thank Professor Jas Pal Badyal FRS, and for financial funding P2i Ltd.

For Mum and Dad,
I never did give up

“Nolite te Bastardes Carborundorum”
-Margaret Atwood-

ABSTRACT

As an inherently chemically inert and physically stable polymer, PTFE has the potential to be used in medical applications as replacement ligaments or vascular stents. In the work presented in this thesis, atmospheric and low-pressure plasma processes were used to modify PTFE surfaces without altering the bulk properties of the substrate.

The coupling of two low-pressure gas plasma treatments together into a two-step process was investigated as a method of producing a stable hydrophilic PTFE surface. A roughening oxygen plasma treatment was used to create a high water contact angle (WCA) Cassie-Baxter surface, before an ammonia plasma treatment transformed it into a hydrophilic Wenzel state. Although these surfaces initially exhibited a WCA of <10°, solvent washing caused significant hydrophobic recovery which was attributed to the washing off of low molecular weight oxidised species (LMWOS).

Economically, an atmospheric-pressure plasma process is industrially favourable to low-pressure methods. The simple equipment required for a dielectric barrier discharge (DBD) process means that PTFE modification could be carried out in situ to prevent contamination or hydrophobic recovery being an issue in surgeries. The work presented here produced surfaces with a stable surface potential, the polarity of which was determined by the feed gas. Doping in water and/or ammonia molecules into inert feed gases was found to change the polarity of the surface potential.

The use of the theory of electrowetting to decrease the WCA of DBD plasma-treated surfaces was successful, although only a small decrease in WCA was observed on the charged surfaces. However, the surface potential of the substrates was used to initialise the grafting and subsequent polymerization of a number of monomers, as well as deposition of a sulfobetaine zwitterionic layer. The lowest WCA was produced by the dipping of DBD-charged PTFE substrates into an aqueous sulfobetaine solution which produced a WCA of <10° recovering to 39° after solvent washing.

The methods described in this thesis present a number of ways in which stable hydrophilic PTFE surfaces can be produced: an effective low-pressure treatment altered the wetting state of the surface using roughening effect, and DBD plasma-treated surfaces used the surface potential imparted by the plasma to initialise further grafting processes to achieve stable hydrophilicity.

LIST OF SYMBOLS USED

$\bar{r}$	Roughness ratio
A	Specific surface area per gram of solid
d	Thickness of dielectric
dA	Change in Helmholtz free energy
$d\omega$	Change in surface area
e	Charge of an electron
$E_{1,0}$	Zero point energy
F	Change in weight
f_1	Fraction of solid-liquid interface
f_2	Fraction of liquid-air interface
ħ	Planck's constant
l	Length of liquid intrusion into porous substrate
m	Mass of an electron
p	Perimeter of contact line
r	Pore radius
r	Radius of the wavefunction of an electron
R_1	Principle radius of curvature
R_2	Principle radius of curvature
t	Time for penetration into porous substrate
V	Volume of displaced liquid
V_p	Measured surface potential
W_A	Work of adhesion
γ	Surface tension
Γ	Surface excess, according to Gibb's isotherm
Δp	Pressure difference across the air/fluid interface
$\Delta \rho$	Difference between densities of liquid and air
ϵ	Dielectric constant of the insulator
ε_0	Vacuum permittivity
ε_r	Relative permittivity of substrate
η	Liquid viscosity
θ	Contact angle
θ_A	Advancing CA
θ_i	Intrinsic WCA of a charged surface
θ_{obs}	Observed CA

θ_R	Receding CA
θ_v	Observed WCA of a charged surface
θ_W	Wenzel equation calculated CA
θ_Y	Young's equation calculated CA
ρ	Density of solid
σ	Standard deviation
Σ	Surface potential density
φ	Work function of spectrophotometer
ϕ	Volume fraction of solid
Φ_D	Work function of the dielectric
Φ_M	Work function of the metal contacting the polymer

LIST OF ABBREVIATIONS

1-AI	1-Allylimidazole
1-VI	1-Vinylimidazole
4VP	4-vinyl pyridine
AA	Acrylic acid
AAm	Acrylamide
AFM	Atomic force microscopy
ALD	Atomic layer deposition
AM	Allyl mercaptan
AMPS	2-Acrylamido-2-methylpropylsulfoacid
APPJ	Atmospheric-pressure plasma jet
APTD	Atmospheric-pressure Townsend discharge
ATR-FTIR	Attenuated total reflectance Fourier-transform infrared spectroscopy
ATRP	Atom transfer radical polymerization
BE	Binding energy
CA	Contact angle
CuAC	Copper acetate monohydrate
DBD	Dielectric barrier discharge
DCSBD	Diffuse coplanar surface barrier discharge (a type of DBD)
DSA	Droplet Shape Analysis
ECA	Ethanol contact angle
FDBD	Filamentary dielectric barrier discharge

FWHM	Full width half maximum
GMA	Glycidylmethacrylate
HCA	Hexadecane contact angle
HEMA	2-Hydroxyethylmethacrylate
KE	Kinetic energy
LMWOS	Low molecular weight oxidised species
MPEG	Methoxy-poly(ethylene glycol)
OES	Optical emission spectroscopy
PE	Poly(ethylene)
PEG	Poly(ethylene glycol)
PTFE	Poly(tetrafluoroethylene)
RMS	Roughness mean squared
SEM	Scanning electron microscopy
SLAN	Slot antenna microwave plasma source
SSS	Sodium 4-styrenesulfonate
TAPP	Transferred atmospheric-pressure plasma
TMS	Tetramethylsilane
WCA	Water contact angle
XPS	X-ray photoelectron spectroscopy

CONTENTS

Chapter 1: Introduction

1 INTRODUCTION

1.1 POLYTETRAFLUOROETHYLENE

Like most great inventions, the discovery of polytetrafluoroethylene (PTFE) was serendipitous. Roy J. Plunkett, of Chemours Jackson Laboratory, noted that a frozen compressed sample of the monomer tetrafluoroethylene had polymerized spontaneously, forming PTFE. This white and waxy polymer sparked interest as it was virtually inert to all chemicals. [1,2]

By 1945, Chemours (later to become DuPont) had trademarked Teflon™, and was using the slippery and inert properties of PTFE for coating cookware and as a stain repellent on textiles. Teflon™ has transformed the polymer industry, such that DuPont were awarded the National Medal of Technology in 1990 for their development and commercialization of synthetic polymers.[1] It is no surprise therefore, that over 200,000 tonnes of PTFE are produced globally each year, making it one of the key polymers of the modern world.[3]

PTFE is a fluoroplastic, which is the traditional name for a carbon and fluorine containing polymer. If a fluoropolymer is fully fluorinated, it is called a perfluoropolymer to distinguish it from a fluoroelastomer, which are fluorocarbon based rubbers that contain alkyl groups in the polymer chain such as vinylidene fluoride, and perfluoromethylvinylether.[4] PTFE is classified as a homopolymer on account of it being made by polymerizing a single monomer into long chains. PTFE has a carbon backbone, and all the pendant groups are single fluorine atoms, with the polymer chains running to thousands of monomer units. The only two bonds present in the polymer are the very strong C–C and C–F covalent linkages. It is the strength of these bonds which give rise to basic low friction and inert properties of PTFE. As PTFE is fully fluorinated, all the carbon atoms are “shielded” from chemical attack by the pendant groups, thus resulting in a chemically stable and resistant polymer. This fluorine sheath also keeps the friction coefficient (0.05–0.08 static) and the surface energy (18 mN m^{-1}) low.[7]

The size of the fluorine atom in the pendant groups of PTFE restricts the rotation of the carbon-carbon bonds. Some of this can be explained by sterics, as fluorine atoms are electron dense atoms and so there is some lone-pair repulsion that is also involved.[5] The combinations of these effects results in the pendant groups being arranged in a helical fashion, to minimise the interaction between pendant groups, Figure 1. The amount of turns and angles between groups in a PTFE helical chain is affected by the temperature. Below 19 °C, the chain takes the H-136 form, where there are 6 turns for every 13 pendant groups. Between 19 and

30 °C, the H-157 structure is adopted, which is characterized by 15 groups for every 7 turns. [6]

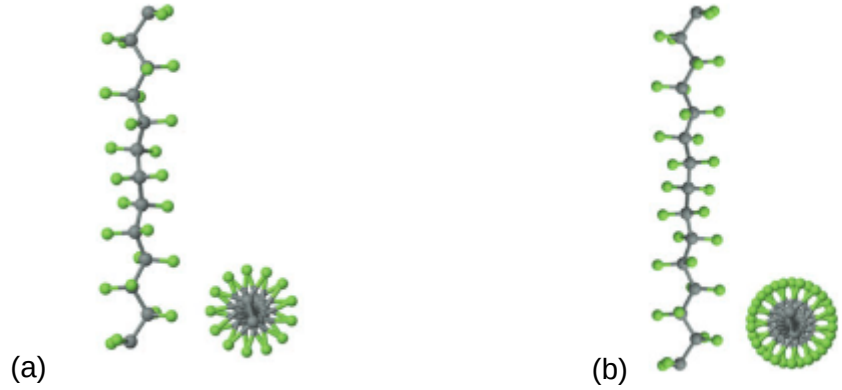

Figure 1: Molecular structure of PTFE. Pendant groups are arranged in a helical structure in order to minimise interactions. (a) Below 19 °C, the H-136 form is adopted by PTFE chains. (b) At room temperature, PTFE is arranged in the H-157 structure. Images adapted from article by C. Wang *et al.*[6]

Recent developments in the production of PTFE films and sheets have given rise to the doping of other species into the PTFE during the polymerization process in order to produce different grades of PTFE. For example, DuPont has a range of doped PTFE called Teflon™ NXT Resins, Dyenon™, and TFM™ which incorporate less than 1% of the copolymer PPVE (perfluoropropyl vinyl ether) into the PTFE. This allows for the retention of beneficial chemical, thermal and low friction properties, as well as creating extra desirable properties such as 'weldability', and improved permeation resistance.[7] Due to their high viscosity PTFE films cannot be melt-processed, and so are made by sintering PTFE powder together to form a film.[8] In the case of Goodfellow PTFE films, which are used in this thesis, the PTFE powder is pressed into a press mould before heating in an oven to fuse the granules together into a block. This block is then cut into films using a "skiving" process whereby a large blade peels the film off the bulk rod. This process causes uniaxial striations on the surface of the film, which can be viewed using various microscopy techniques.[9,10] These striations result in a "rolling hills" type roughness of the surface, which affects the wettability of the PTFE.

1.1.1 Properties of PTFE

As with any material, there are both advantageous and undesirable properties to using a material for a particular application. With PTFE being facile and cheap to obtain, it is often commercially beneficial to absorb the costs of any undesirable

properties of the polymer, as switching to another suitable material would incur greater costs overall.

PTFE is chemically inert to the majority of substances, which makes it safe for use in the food industry and as a container for many industrial chemical processes. As previously mentioned in Section 1.1, the spatial arrangement of the atoms of a PTFE strand results in a fluorine 'sheath' around a carbon backbone which is responsible for the low surface energy and low friction coefficient of the polymer.[7] PTFE is often deemed as a benchmark for low surface energy materials.[11] The surface energy is governed by the intermolecular forces between the solid and the liquid.[11] For polymer surfaces, the surface energy is chiefly determined by the surface composition, in the case of PTFE, the fluorine pendant groups. The very low friction coefficient is what gives PTFE its slippery properties which make is useful for the transportation of substances along tubes and pipes in an industrial plant. These are also the properties capitalized on by DuPont with their famous non-stick Teflon^{TM} pan range.

Polymers are generally relatively insulating anyway, however the fluorine sheath arrangement of PTFE results in it being almost uniformly electrically inert. As a result the surface and volume electrical resistivity of a PTFE substrate are both high.[7]

The melting point of a PTFE resin or sheet is an indication of the degree of crystallinity of the polymer, the higher the melting point, the larger the degree of crystallinity of the sample.[7] Amorphous (disordered) areas exist where the polymer chains are not aligned with each other. The opposite of amorphous is crystalline, where the polymer chains exhibit long-range translational order, and are parallel, and closely packed together, increasing the strength and number of intermolecular bonding interactions. Disrupting this crystalline structure by melting requires a significantly larger amount of thermal energy than when melting the amorphous regions, hence the increased observed melting point of highly crystalline PTFE.[7]

The degree of crystallinity in granular PTFE is significantly higher than that of any sheet or film. This is owing to the fact that the manufacturing process for sheets, films, and rods requires the PTFE powder to be sintered to form a single solid. This heating process results in a decrease in the melting point of the polymer as more amorphous regions are introduced.[12] This change is shown in the observable decrease in the melting point when moving from newly polymerized PTFE (340–345 ^{o}C) to PTFE products such as sheets and films (327 ^{o}C).[12]

There are many different types of PTFE; films, sheets, and porous membranes, all of which have different wettabilities and surface architecture which

makes it difficult to compare the changes in the hydrophobicity induced by different surface treatments. In this thesis all the work is carried out on a non-expanded PTFE sheet substrate (from Goodfellow Ltd.) which is non-porous but does have significant roughness to it with the exception of the linear striations which are a result of the manufacturing method. Where comparisons are made with literature results, the nature of the substrate is commented upon if it is significantly different to that which is used in this work.

1.2 THEORY OF WETTABLE SURFACES

People have been trying to understand why some surfaces are wettable and some are not for centuries; Aristotle, Archimedes, and Galileo were the early minds occupied with the theory of surface wettability.[13] Initially this desire for information was for the sake of fundamental understanding, but in the modern world, the driver is economics. The wettability of surfaces within industrial processes can have a significant role in the efficacy, for example in the printing, lubrication, oil recovery, textile, and spray coating industries. Additional to wettable surfaces, there are many applications that desire a liquid repellent surface, for example for self-cleaning, filtration and electrical protection purposes.

1.2.1.1 Static Contact Angles

The wetting of a surface is a thermodynamic process governed by the energy of three different interfaces; the solid-liquid, the solid-air, and the liquid-air (Figure 3).[14,15] The zone where the solid, liquid and air phases meet is termed the 'three-phase contact line' and this point is key in determining the wettability of the surface. The contact angle (CA) is defined as the angle between the solid-liquid interface and the liquid-air phase, i.e. the angle at which the droplet sits upon the surface.[16] The shape of a droplet that is residing on a surface is determined by the surface tension of the liquid, and the gravity acting on the droplet.[17] In the bulk of the liquid, every molecule is pulling and being pulled by neighbouring molecules, resulting in a net force of zero. However, those molecules presenting at the surface of the droplet (the interface of the liquid with either the surface or the air), are being pulled inwards towards the bulk, and there is no balancing force pulling from the air or the surface. This imbalance of forces causes an internal pressure, and so the liquid contracts to minimize the surface free energy (Figure 2).[17]

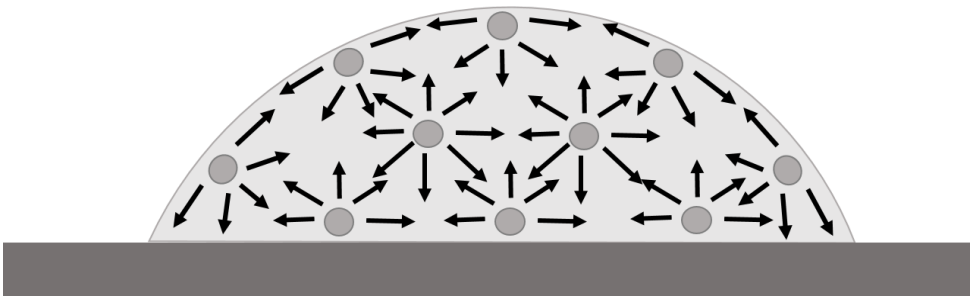

Figure 2: Surface tension of a droplet of liquid on a surface. The interfacial molecules have an imbalance of forces compared the bulk and so the droplet contracts to minimize the surface free energy. Based on schematic by Y. Yuan and T.R. Lee. [17]

The Young's equation (Equation 1.1) describes how the CA (θ) is related to the various interfacial tensions between the solid, liquid, and air phases. First defined in 1805, this equation was intended to determine the CA of a liquid on an ideal surface based on the mechanical equilibrium between the aforementioned interfacial tensions.[18]

$$cos\Theta = \frac{\gamma_{sa} - \gamma_{sl}}{\gamma_{la}}$$ Equation 1.1[18]

where γ is the surface tension at the solid-air, solid-liquid and liquid-air interfaces. Young's equation was the first significant attempt to quantify and predict the wettability of a surface, however it only describes an ideal surface. Dupré furthered this work, deriving a new equation that took into account the reversible work of the adhesion (W_A) at the solid-liquid interface (Equation 1.2).[18] Thermodynamically, the energy required to keep the two phases apart must be equal to the free energy change of the system.

$$W_A = \gamma_{sa} + \gamma_{la} - \gamma_{sl}$$ Equation 1.2[18]

The amount to which a droplet spreads on a surface is influenced by the viscosity and surface tension of the liquid, but also the character of the substrate: the chemistry and the topography. Liquids can either interact favourably with the surface (affinity), or they can exhibit unfavourable interactions.

A small CA (less than 90°) indicates an affinity for this liquid by the surface, so if the liquid were water, the surface would be described as hydrophilic. If the CA is large (greater than 90°), the surface has a low affinity for the liquid, and would be described as hydrophobic if the liquid were water. The way in which a droplet rolls along the surface, termed the hysteresis, is also an important parameter to consider. For a surface that is very resistant to wetting, the CA will be greater than 150°, and have low hysteresis (<5°), and the surface is described as superhydrophobic.

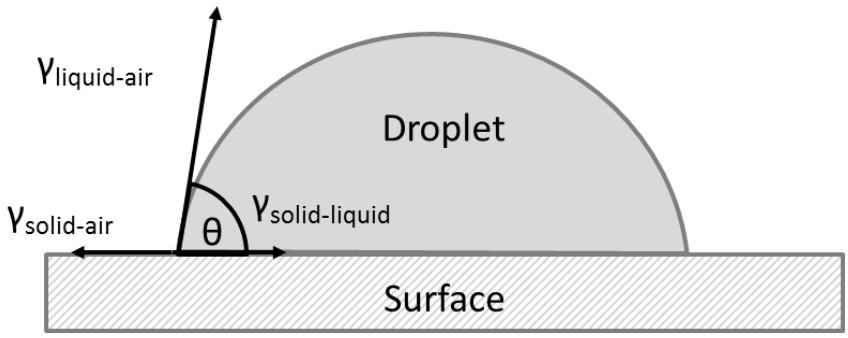

Figure 3: Diagram of the surface tension forces acting upon a droplet on a surface. The balance between these tension energies determines the observed contact angle of the droplet on the surface. The CA is measured at the three-phase contact line between the solid-liquid and liquid-air interfaces, labelled θ.

1.2.1.2 Contact Angle Hysteresis

For ease, often a static angle is quoted as a measure of the wettability of a surface. This is measured when the droplet has equilibrated with the surface, and the shape of the droplet is no longer changing, i.e. the most stable state. There are however many metastable states in which a droplet on a surface can exist. These will not usually have CA equal to the static CA.

In addition, the definition of a truly superhydrophilic or superhydrophobic surface is concerned not only with the measured water contact angle (WCA) but also with the CA hysteresis (θ_H). This is a measure of how 'sticky or slippy' the surface is. The hysteresis is defined as the difference between the advancing and receding CAs. The advancing CA (θ_A) is the angle measured when the droplet incident on the surface and is 'advancing' or spreading across an 'unwetted' fresh surface. The receding CA (θ_R) is measured when a droplet is coming away from an already wetted surface. The advancing angle can be measured by increasing the droplet size on the surface by adding liquid to a static droplet. Similarly, the receding angle is measured by withdrawing liquid from the surface. Equation 1.3 gives the CA hysteresis as the difference between these two angles:

$$\theta_H = \theta_A - \theta_R \qquad \text{Equation 1.3}$$

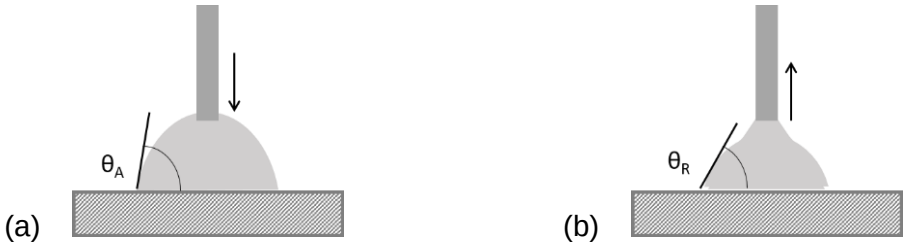

Figure 4: Schematic of (a) advancing CA, and (b) receding CA on a surface.

Chiefly, θ_H is affected by the surface roughness and any heterogeneity upon the surface. A rough surface can result in the θ_A being higher than expected if it is pinned between two topographical features on the surface. Additionally, the θ_R would be lower than expected if the droplet is unable to easily withdraw from the surface. This results in an overall high hysteresis.

1.2.1.3 Influence of Surface Roughness

The previously mentioned Young's equation (Equation 1.1) was based on an ideal surface, i.e. a perfectly smooth and uniform surface. This is not an accurate representation of real world substrates, which will not be completely uniform, but also will have some kind of surface structure, be that on the nano-, micro- or the macro-scale. The influence of this surface roughness is not something that was accounted for in the Young's equation, and so further additions had to be made in order to quantify the effect that roughness had on the observed CA. These came in the form of the Wenzel and Cassie-Baxter wetting states.

In 1936, Wenzel proposed an additional equation which would take into account the effect of the roughness and non-symmetrical nature of a rough surface on the apparent contact angle, Equation 1.4.[15]

$$\cos\theta_W = \bar{r}\cos\theta_Y$$

Equation 1.4[15]

where θ_Y is the predicted CA based on the Young's equation, θ_w is the observed contact angle, and $\bar{r}$ is the average roughness ratio, defined as the actual surface area divided by the geometric surface area. This measures the increased surface roughness with respect to the size, and hence calculated surface area, of the substrate.

For surfaces with a CA of less than 90°, an increase in the roughness of the surface will cause a decrease in the observed CA. Mathematically speaking, this is

due to the nature of the cosine graph, Figure 5. However, if one is to think about the nature of wetting a rough surface, this can be explained by a difference in the specific energy content of the wetted surface interface and the dry solid interface. If the wetted area has a lower specific energy than that of the dry area, then the droplet will spread spontaneously to minimize the solid surface energy. During spreading, energy will be released as the wetted area under the droplet increases, and energy will be consumed as the free liquid upper interface over the solid surface is increased. For the same geometric surface area of solid substrate and volume of liquid droplet, a rough surface will have a greater real surface area in contact with the droplet. This in turn means that a greater decrease in the solid surface energy can be achieved on a rough surface by the droplet spreading, leading to a decrease in the observed contact angle relative to a non-rough substrate. If the surface is rough, then the real surface area of the solid that is wetted will be larger than the geometric surface area of free liquid at the upper surface of the droplet. Therefore more energy will be released than consumed, and the droplet will spread further, thus the observed CA will be lower. In the case of a hydrophobic surface with a WCA greater than 90°, the dry solid interface has the lower specific energy, and so the droplet will spontaneously bead up. In essence, a roughened substrate will exacerbate the intrinsic wetting or repellent nature of the surface in comparison to its smooth counterpart.

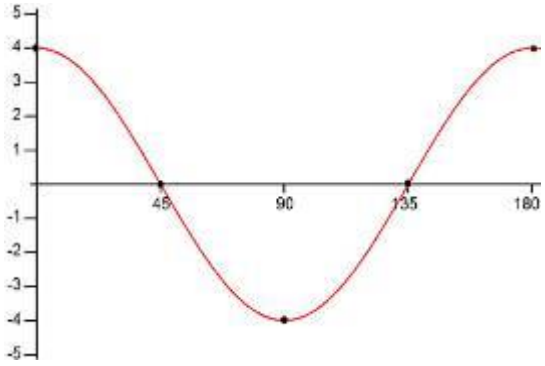

Figure 5: Form of cosine graph. Drawn is a graph of y=4cosθ, spanning 0–180° on the x-axis.

The alternative to this Wenzel wetting is a composite surface, termed the Cassie-Baxter state. In a Wenzel state, the droplet permeates into the roughness of the surface, whereas in the Cassie-Baxter state, there is air trapped between the droplet and the surface, hence the term composite surface, Figure 6.[19] If the surface does not obey the Wenzel equation, whereby an untreated CA of <90° will

decrease after roughening and a CA of >90° will increase after roughening, then it can be deduced that the surface is in the Cassie-Baxter state. The observed CA can be determined using the Cassie-Baxter equation,[19] Equation 1.5, which takes into account the fraction of the solid-liquid interface (f_1) and the fraction of the liquid-air component (f_2).

$$\cos\theta_{obs} = f_1 \cos\theta_{int} - f_2$$

Equation 1.5[19]

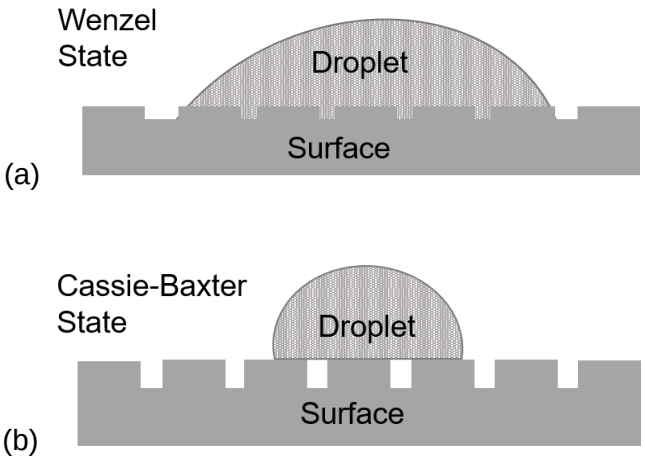

Figure 6: Wetting states of a surface. Schematic (a) depicts the Wenzel wetting state whereby the droplet permeates into the roughness of a surface, causing a decrease in observed contact angle. Schematic (b) shows the Cassie-Baxter state where air pockets are trapped in the surface roughness between the surface and the droplet. The result of which is an increase in the observed contact angle of the droplet with the surface.

1.2.2 Measuring the Contact Angle of a Surface

In industrial process plants, the CA of a surface is often measured to determine how clean a surface is. For example glass and silicon substrates should exhibit total wetting with water, forming a duplex film across the whole surface rather than a droplet with a measureable WCA.[20] If a water droplet does not completely wet the surface, then it is clear that there is some contamination on the surface, and so it must be cleaned. In this case, it may not be necessary to even obtain a WCA, but simply to determine it is not equal to zero. In this thesis, the CA of a surface is the major method for determining the efficacy of a plasma treatment process, and thus the techniques by which CAs are measured are explained thoroughly here.

1.2.2.1 Drop Shape Analysis

There are a few different experimental methods by which the CA of a surface with a liquid can be measured. The most common method by which the CA is determined is drop shape analysis (DSA).[21] This uses an image of a static droplet on a surface and calculates the CA by measuring the points of intersection between the droplet and the baseline (Figure 3). In this method, a microliter droplet is placed on the surface using a syringe, and this is captured using a camera. The contour analysis is calculated using grey-scale analysis of the image to determine where the baseline (or substrate) is and where the droplet is. Once this is determined for the image, the CA is calculated using a geometric model which fits the contour of the droplet, Figure 7.[22]

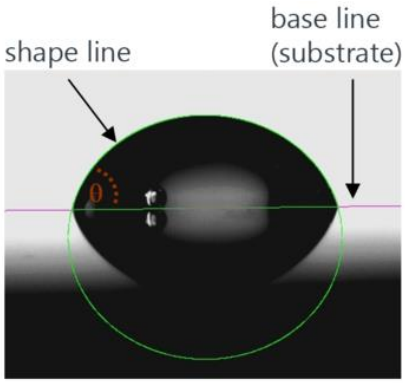

Figure 7: Image of droplet on a substrate surface. The baseline is shown in pink, and the calculated geometric model is shown in green. The CA is indicated by the orange angle labelled θ. Image reported by Kruss-Scientific.[22]

DSA is a direct method of measuring the CAs of a surface. It is facile and requires minimal equipment and training compared to other CA measurement techniques. The measured CA are reliable and repeatable given that the conditions are unaltered. The accuracy and reliability of the measurements can be improved by mechanical additions, such as an automated syringe drive, and the incorporation of a vibration quenching stage.

1.2.2.2 Captive Bubble Analysis

Rather than a droplet of liquid being placed on a surface like in DSA, captive bubble analysis works by creating a droplet of air within the desired liquid and measuring the CA of the air bubble on the surface. The captive bubble method was coined by Taggart *et al.* in 1930 to analyse frothing agents.[17,23,24] The CA of the liquid of the surface can then be determined by subtracting the captive bubble angle away from 180°.

An advantage of using this method rather than the standard DSA is that the surface is kept under a saturated equilibrium atmosphere whilst the CA is determined. Furthermore, captive bubble technology may also give an indication of the gas/surface interaction. This can be useful when looking at gas adsorbing materials, especially as different gas behaviours can easily be investigated.[25,26]

Although theoretically the captive bubble and sessile drop methods may both be used in order to measure the WCA of a surface, the two methods do not always give concordant results. Reasons postulated in the literature for this include the entrapment of air upon a rough surface increasing the apparent contact angle, the homogeneity of the surface, the porosity of the surface, and the size of the droplet (or bubble) used.[13,27,28]

1.2.2.3 Wilhelmy Plate Method

An alternative to this method is the Wilhelmy Plate method (WPM), which is rather more complex in terms of set up, Figure 8. However, it allows for measurement of the surface tension of the liquid and the interfacial tension between two liquids as well as an indirect determination of the CA between a liquid and solid.[29] A smooth platinum or glass plate mounted with the sample is brought down vertically until it is in contact with the liquid, and the change in weight is measured using a balance.[30,31] This measured change in weight (F) is the buoyancy and the force of wetting. The force of gravity is also included in the weight change, but this remains constant. This measured value can be used to calculate the CA of the substrate (θ) using the liquid surface tension (γ_{la}), and the perimeter of the contact line (p) which is the size of the plate. Additional terms required for the calculation of the CA using Equation 1.6 are the acceleration of gravity (g), the volume of the displaced liquid (V), and the difference between the densities of air and the liquid ($\Delta\rho$).[30]

$$F = \gamma_{la}\, p \cos\theta - V\, \Delta\rho g$$

Equation 1.6[30]

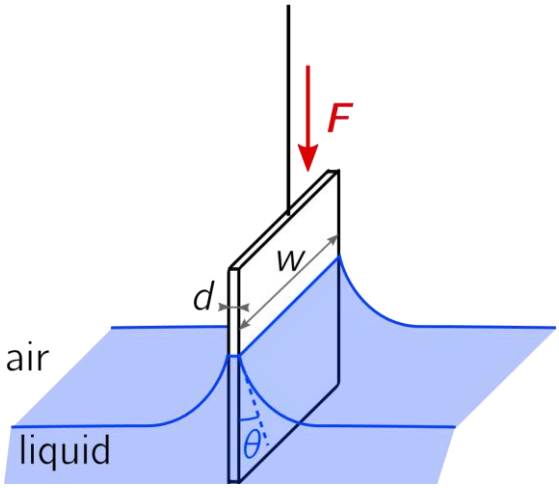

Figure 8: Schematic of Wilhelmy plate method. Shown is the vertical plate being pushed into the liquid, and labelled is the CA (θ). Source: WikiCommons. [32]

As an indirect force method, the WPM uses no optical methods, and depends on only the measurement of weight and length. These can both be measured with a high degree of accuracy, and are free from user decision making, and therefore subjectivity. As the depth of immersion is an average already, the calculated CA is already an average of the whole surface, this can be observed as an advantage, but it does fail to account for any heterogeneity that may be present at the surface.[30] Disadvantages of the method include that the sample must be a regular shape, in order to allow precise measurement of the perimeter and the wetted length.

1.2.2.4 Capillary Method for Porous Materials

When a droplet is placed on a porous surface, often the droplet will penetrate into the material, making optical measures of the contact angle impossible. The porous architecture of the surface also means that the CA will be higher than for the equivalent smooth surface, which has been shown thermodynamically.[17,33] The capillary method developed by Washburn in 1921, whereby the depth to which the liquid penetrated the porous substrate was measured as a function of time. This can be subsequently used to then calculate the CA indirectly, Equation 1.7.[17,34]

$$l^2 = \frac{r\, t\, \gamma_{lv} cos\theta}{2\eta}$$

Equation 1.7[17]

where *l* is the depth of liquid intrusion into the surface, *r* is the pore radius, *t* is the time taken for the liquid to penetrate the substrate, θ is the CA, η is the bulk liquid viscosity, and γ_{lv} is the liquid surface tension. Initially this method was determined in order to determine the CA of a powder cake, which is inherently porous. Further additions were made by Bartell who incorporated the idea that the pressure of the wetting liquid column must be balanced by the capillary pressure in order to reach equilibrium, and thus obtain a static CA measurement, Equation 1.8.[17]

$$\Delta P = \frac{2\gamma_{lv}\cos\theta}{r}$$

Equation 1.8[17]

where ΔP is the change in pressure, and the other terms are as defined for Equation 1.7.

$$\Delta P = \frac{\gamma_{lv}\cos\theta\,\phi\,A\,\rho}{1-\phi}$$

Equation 1.9[17]

Both Washburn and Bartell's equations fall foul of the fact that the pore radius is not consistent in a powder cake. Thus the Laplace-White equation was developed, Equation 1.9, which is a strict thermodynamic expression of the change in pressure (ΔP). In the equation, ϕ is the volume fraction of the solid, *A* is the specific surface area per gram of solid, and ρ is the density of the solid.

1.3 PLASMA MODIFICATION

Plasma describes a macroscopically neutral substance containing many free electrons and ions that are interacting with each other, but also exhibiting collective behaviour due to Coulombic forces.[35] When a significant amount of heat or a high voltage is applied across a gas, electrons in the gas molecules are excited to higher energy states. If the energy increase is sufficient, the gas is converted to a plasma. A plasma contains ionised gas molecules, high energy electrons, and neutral species, and behaves as a single entity.

Naturally occurring plasmas make up the majority of the Universe, as the main component of stars. Lightning is also an example of plasma, where a sudden high voltage discharge occurs between either two charged clouds, or a charged cloud and the Earth. As well as naturally occurring plasmas, plasma can be made artificially at either low-pressures like on the outer surface of stars, or at atmospheric-pressures like in the case of lightning. The nature of the plasma is affected by the pressure, the voltage being passed across the gas, the nature of the gas, and the properties of the substrate being treated.

As the species within a plasma are so high in energy, they can react with substrates that would ordinarily be unreactive. This is important for the work in this thesis owing to the inert nature of PTFE under standard conditions. Industrially, the use of plasma is appealing because it is a “clean” method which uses no solvents in order to modify surfaces. In the age of striving to be “greener” and more environmentally friendly, this is important in the reduction of waste from a process, but the lack of solvents also has a significant cost benefit.

Plasma modification is the altering of a surface topography or composition using a plasma, and is a very surface specific method, unlike some wet chemical methods. The surface will be modified whilst the bulk properties of the material remain unaltered. This is of particular benefit for example when trying to alter the wettability of a surface to a particular liquid in filtration applications. Generally a material is suitable for an application owing to its bulk properties over its surface properties, and the surface is easily modified using a plasma technique.

1.3.1 Modifying PTFE

PTFE is deemed a hydrophobic, not superhydrophobic, surface with a high water contact angle (WCA) and a low hysteresis. This can be attributed to the low surface energy, caused by the highly fluorinated nature of PTFE.[36] Although most polymers do not have ideal properties for a specific application, they can usually be modified

in order to bring about the desired surface properties.[37,38] Although there are a number of wet chemical methods by which this can be done, these can also alter the bulk properties of the material. In contrast, plasma can be used in order to modify the surface without changing the bulk properties.[39]

1.3.1.1 Application Areas

Although PTFE has numerous advantageous properties, there are situations where modification can further augment its performance. The inert nature of PTFE is beneficial in that if something is made of PTFE it will not rust or age like some other materials. However this also results in PTFE having almost no adhesive properties. It is therefore very difficult to apply coatings to PTFE or to adhere PTFE to another surface. In the past, the applications of PTFE as for example non-stick coatings for cookware and textiles have exploited the inert and slippery nature of PTFE. However in the drive to apply PTFE to more complex applications, such as heart stents and wound dressings, the ability to modify PTFE surfaces has become necessary.

One of the applications where PTFE has the potential to be a real player is in that of medical implants. Replacement hips for example that are made out of PTFE were thought be longer lasting than some of the more traditional metal versions, which are combinations of polyethylene (PE) and stainless steel, titanium, chromium, or cobalt. This has already been tried, some 50 years ago Teflon^{TM} total hip arthroplasty (THA) operations were widely carried out, and then subsequently further operations were carried out on patients after the PTFE hip replacements were shown to fail catastrophically.[40,41,42] The replaced joint wore out far quicker than the metal or ceramic counterparts. With surface modifications to the PTFE substrates, it is possible that the issue of wear can be counteracted, in a similar way to the use of a membrane between older joints can increase the lifetime of the joint.[42]

When considering PTFE as an alternative to other materials for medical implants, the significant disparity in cost between these two materials is a major consideration, but also the advent of 3D printing makes it easy to print tailor designed body parts for an individual. The same is also true of replacement ligaments or tendons, and heart stents, Figure 9. In all of these situations, one of the key properties of the material is that it needs to haemocompatible. As blood is chiefly composed of water, the hydrophilicity of the material is imperative to the body not rejecting the implant as a foreign body. As a cheap and readily

available material that is chemically and thermally stable, PTFE is a suitable material for these implants. However, it could be made more suitable by increasing the hydrophilicity of the surface layer. Plasma modification can be used to modify the very top layer of the PTFE implant, making this part hydrophilic by removing some of the fluorine atoms from the surface and replacing them with polar groups containing oxygen or nitrogen.

From an economic perspective, plasma-modified PTFE is useful for these medical implants as it is an inexpensive material for making the implants, and the method of plasma modification is also inexpensive, and furthermore has green credentials as it produces limited waste. However when looking at the idea from a humanitarian point of view, these PTFE substrates have the potential to be used in developing countries to provide life-changing health improvements, for example by providing a less expensive alternative to metal hip replacements. PTFE is repellent to the majority of dust and bacteria particles as it has such low adhesive properties and is chemically inert. This means that in locations where there are large amounts of airborne particles e.g. places where pollution is a serious issue, then these PTFE replacements will remain comparatively clean. Additionally, a plasma treatment process can be done in situ (i.e. in a hospital theatre) using relatively simple equipment meaning that the implant is clean before entering the body in surgery, seriously reducing the chance of infection.

(a)  (b) 

(c) 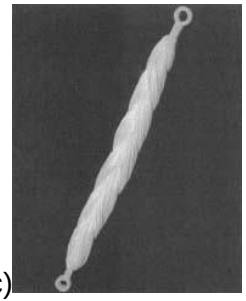

Figure 9: Uses of PTFE within the medical industry. (a) Replacement hip joint; (b) wound dressings; (c) artificial replacement tendon for use in ankle/foot. Source: WikiCommons.

An alternative use of PTFE in the medical industry is in wound dressings. When dressing an open wound, the chief priority is keeping the wound clean and preventing infection. As PTFE is not biocompatible, this means that it is “clean” as no bacteria will easily cultivate upon the surface. The main limitation with using PTFE as a wound dressing is that in order to allow adhesion of the PTFE dressing to the wound, an adhesive layer must be successful attached to the PTFE. Through modifying the PTFE surface, this can be possible. This works by disrupting the fully

fluorinated structure of the PTFE and replacing it with more reactive groups such as sulfur, nitrogen, or oxygen containing groups. This can be done using a wet chemical or a plasma modification method. One of the advantages of the plasma method is that a mask can be placed over the area that the wound will come into contact with, meaning that this area will remain unmodified, retaining its bacteria-repellent properties.

As well as the medical field, there is potential for the use of plasma-treated surfaces as filtration devices. This is of particular importance for atmospheric plasma-treated surfaces as this treatment involves the incorporation of charge into the polymer surface, discussed more in Chapter 4, and Section 1.3.4.4. This charged surface can be used in conjunction with the increased hydrophilicity to produce air filtration devices, for which there is already an established market. These devices filter particulates out more effectively than traditional porous size exclusion filters, as the electrostatic attraction means smaller particles can be 'caught' by the filter. PTFE makes a good potential candidate for an electrostatic filtration device owing to its high charge storage capacity, and low charge mobility. The use of atmospheric plasma to impart charge of the surface is quick and effective. Polypropylene surfaces were modified by P.C. Raynor *et al.* for use in hospital air conditioning units, and were proved to be more effective than their uncharged counterparts.[43] However similar modification of PTFE has not been investigated in the literature.

1.3.2 Hydrophobic Recovery

There is however a major stumbling block with the use of plasma techniques to modify PTFE surfaces, and that is the stability of this hydrophilicity on the surface. When using gas plasmas, there is no film deposition, merely the removal/addition of surface groups. This is problematic as the WCA tends to increase with time after removal from the plasma chamber; this phenomenon is well documented and referred to as hydrophobic recovery.[10,44]

Although the process is well documented, there is some disagreement in the literature as to exactly what causes hydrophobic recovery.[10,30,44,45] After a hydrophilizing plasma treatment, the PTFE surface has polar groups present on the surface, which result in unfavourable increased surface energy. In order to reduce the surface energy, these modified polymer chains move from the solid-air interface into the bulk, and are replaced by unmodified polymer chains from the bulk polymer. The net result of this that the modified polymer surface is no longer

exhibits the modified properties, but simply those of the starting polymer, Figure 10. There is a debate in the literature as to whether it is the surface groups moving into the bulk or the bulk groups moving to the surface.[46,47,48,49] Although this is possibly purely philosophical as the net result is the same since both occur, the only question is which causes the other to happen.

Figure 10: Schematic depicting the effect of surface reconstruction after plasma hydrophilizing plasma surface treatment of a hydrophobic polymer.

It is widely reported that the environment in which samples are stored has a marked effect on the observed WCA of the surface after gas plasma treatments. For example, D.J. Wilson *et al.* reported two mechanisms of hydrophobic recovery depending on the storage medium; reaction of the surface with the storage medium, and surface relaxation.[50] Samples that were not placed in ambient air – but instead wrapped in aluminium foil immediately after plasma treatment still underwent hydrophobic recovery, even though there would be minimal hydrocarbon contamination.[50] Samples that were stored in PBS (phosphate-buffered saline) for any period of time showed less increase in PBS contact angle over time, indicating that the storage in the wetting liquid reconditions the surface.[50] The retardation/reversal of hydrophobic recovery by storage in a polar medium means that for the medical applications, where the surrounding environment is an aqueous solution, the ageing of the surfaces in air is irrelevant to the end use.

Under atmospheric conditions, it is well known that there will be deposition of carbonaceous compounds onto a surface. The degree of aerial contamination is dependent not only on the rate of surface bombardment which can be estimated using the kinetic theory of gases, but also the volatile organic compound (VOC) content of the surrounding atmosphere.[51]

One further reason for hydrophobic recovery was reported by Greenwood *et al.* and Guckenberger *et al.* to be due to the removal of low molecular weight oxidised species (LMWOS) from the surface.[52,53] These can be reliably removed from a plasma-treated polymer surface using adhesive tapes, or a solvent wash process (1:1 v/v solution of propan-2-ol and cyclohexane).

1.3.3 Why hasn't this problem been solved already?

The issue of hydrophobic recovery has retarded the achievement of a stable hydrophilic PTFE surface. The main reason for this is the disparity between how the stability of the plasma-treated surfaces has been determined. Very few plasma-treated surfaces are washed at all, some are only analysed immediately after plasma treatment, and some are analysed after an arbitrary amount of time in air.

The lack of a defined method to determine how to analyse the stability of a plasma-treated surface has mostly come from the desire within the research community to only publish the best data. Unless there is a reason that the surface recovering back to a higher WCA is a good thing for the particular application being assessed or if the unstable PTFE surfaces is a bench mark for some better treatment, then it likely that the recovery of the plasma-treated surface to a higher CA is simply outside the scope of the publication.

Aside from the stability of the plasma-treated surfaces, the nature of plasma treatments, including the equipment and exact conditions, plays a major role in the modification of the surface that is observed. The feed gas, the pressure, the power, and duration of the plasma all play a major role, but also the flow rate, the exact geometry of the plasma chamber, and the position and orientation of the substrate. All of these variables in the plasma process, and the same variables in the CA measurement method and washing process mean that there is significant variation between the works reported between different groups.

1.3.4 Prior Art

1.3.4.1 Low-pressure Single-Step

The most commonly used plasma method of modifying PTFE substrate to increase hydrophilicity is low-pressure, single-step, gas plasma treatments. Low-pressure plasma is typically deemed as being below 1 mbar, and the plasma feed gas is introduced into a chamber, after evacuation of the air, at a set flow rate in order to maintain the low-pressure. Low-pressure plasma is the most commonly used as it produces a glow discharge which is uniform in its appearance and thus its character. This allows for even and consistent plasma modification of a sample. The size of the substrate is hindered only by how big the chamber is as the plasma can be made to fill the available space, meaning it is very suitable for industrial scale-up.

Almost all gas plasma treatments resulted in a decrease in the WCA, indicating an increase in hydrophilicity of the PTFE surfaces. The only exception to this was oxygen plasma treatments which resulted in either a significant increase in the WCA, ranging from 105° to 'too hydrophobic to measure',[54,55,56,57] or in a significant decrease in WCA (to 23–41°).[58] The disparity between these two can be attributed to the variation in the PTFE substrate. The substrates that exhibited hydrophilization after oxygen plasma treatment were porous ePTFE materials, for use in vascular grafts.[58]

In terms of hydrophilic surface modifications of non-expanded PTFE, the lowest reported WCA for a single-step gas plasma was 4°, which was reported by W. Hai *et al.* after treatment of PTFE with argon and ammonia water plasma (100 W, 15 min, flow rate Ar, NH_3, and H_2O were 24.4, 0.28, and 0.13 mmol min^{-1} respectively).[59] However, as the limit of reliable measurement of the WCA using a sessile drop method is widely deemed to be approximately 10°, the reported value of 4° which also has no error value associated with it should not be considered accurate. Additionally no wash process was carried out, and from the FE-SEM images, there appears to be significant roughening of the surfaces potentially leaving a large amount of LMWOS which would cause a much lower initial WCA until they have been removed by a wash process.

The lowest WCA reported for a single-step gas plasma treatment that can be considered reliable, i.e. not at the limit of the analysis technique, was obtained using a thermal ammonia plasma, where an advancing WCA of 16° was reported. In this case as well as heating the samples during the plasma treatment, no solvent wash process was employed either.[60]

When solvent washing is taken into account, the lowest WCA achieved was an advancing WCA of 53°, and a receding WCA of 15° after washing in methanol (1 h Soxhlet extraction). After 10 h these surfaces exhibited hydrophobic recovery to approximately adv. 70°.[61]

1.3.4.2 Low-pressure Multi-Step

In comparison with single-step gas plasma treatments, the use of sequential plasma treatments is under-researched. For the most part, any treatments which follow a gas plasma treatment are wet chemistry deposition or grafting steps. Two hydrophilizing gas plasma treatments (hydrogen then ammonia) were arranged in tandem by P. Favia *et al.* to produce what they described as a stable surface that did not exhibit hydrophobic recovery (24° to 40° after 8 days storage in air).[62]

In terms of combining a hydrophobizing plasma treatment combined with a hydrophilizing treatment, there is nothing reported in the literature. However the use of an oxygen plasma treatment combined with a hydrogen plasma treatment has been reported by Shin *et al.*.[63] They reported that the oxygen plasma treatment step results in hydrophilization of the surface (reduction of the WCA from 115° to 80°), but also significant roughening (RMS increase from 12 nm to 70 nm). When the combination of oxygen and hydrogen plasma treatments were used, the WCA was not an improvement in comparison to the single-step hydrogen plasma treatment they reported (two-step 60°, hydrogen treatment 52°).[63] The paper is in Korean, and not published elsewhere, making it difficult to determine the experimental protocol, but to the best translation available, it appears that there was not any solvent washing process, or investigation of the stability of the surfaces created using this method.

There are no solvent washed surfaces that have undergone multi-step plasma processes reported in the literature, so the effect of LMWOS removal has not been previously investigated for two-step processes.

1.3.4.3 Low-pressure Plasma + Wet Chemistry step

One of the areas that has been perhaps more explored is the use of a plasma treatment step as a PTFE ‘activation’ method. As PTFE is inert, grafting of other monomers onto the surface is generally quite ineffective unless the surface structure is significantly disrupted. For the most part a simple gas plasma such as argon or hydrogen is used as a method to ‘activate’ the surface prior to a wet

chemistry step. Generally this wet step has the aim of depositing a stable film onto the PTFE.

In some cases, more than one plasma step is employed in order to promote successful grafting in the wet chemistry step. For example, C-Y. Tu *et al.* reported the use of sequential hydrogen plasma and ozone plasma treatment as a method to activate the PTFE surface prior to monomer grafting in solution.[64] They reported that the hydrogen plasma treatment facilitated an otherwise ineffective ozone treatment in order to produce surface peroxides for grafting. The wettability of the surface prior to grafting processes was not reported.[64]

1.3.4.4 Atmospheric-Pressure Single-Step

As well as low-pressures, it is possible to create plasmas at atmospheric-pressure, just like naturally occurring lightning. The appeal of atmospheric-pressure plasma is mostly economic; there is no need for vacuum equipment, liquid nitrogen, or pumping systems, and also no risk of production delays due to loss of vacuum. The drawback to atmospheric plasma is that for the most part, the discharge is not a glow plasma, but resembles little lightning bolts striking the surface, termed micro-discharges. This also means that the modification of the surface is not completely homogenous, and the location of the micro-discharges can be significantly affected by surface defects.

In the literature, the majority of atmospheric plasma treatments that are reported are for air, which is of course the easiest medium within which to create a plasma. The hydrophilicity induced by air atmospheric plasma varies from 46–95°.[65,66,67,68,69,70,71,72,73,74,75] This can mostly be attributed to the different plasma generation techniques, which will be discussed further in Chapters 2 and 4. Atmospheric plasma can be created by having a dielectric such as air between two parallel plates, one earthed and one provided with a high voltage. The plasma is created as a way of breaching that interelectrode gap and completing the circuit. This is called dielectric barrier discharge (DBD) and is the method used in the work presented in this thesis. Alternative methods involve creating a plasma plume or jet within a tube which is fired at the surface.

Further increases in the hydrophilicity of PTFE surfaces were made after using a mixture of nitrogen and hydrogen as the feed gas, resulting in a WCA of approximately 25°.[76,77] This significant decrease was attributed to a large degree of defluorination of the surface induced by the plasma. As seen before with the low-pressure plasma treatments, most of the plasma-treated samples are not exposed

to any kind of wash process, meaning that the stability of these surfaces must be called into question. This is especially important given that an alternative use of DBD plasma is to create charged polymer surfaces for use as electrets. Electrets are permanently charged materials that are created by being subjected to a strong electric field;[78] these are further discussed in Chapter 4. The presence of a charge on the PTFE substrate will cause the water droplets to jump towards the surface, and the phenomenon of 'electrowetting' will be observed. This means that the observed WCA will be significantly reduced on account of the charge rather than the composition or topography of the surface, which is further discussed in Chapter 4.

1.3.4.5 Atmospheric-Pressure Plasma as an Activation Step

There are no reported multi-step atmospheric-pressure plasma processes, however, there are some occasions where the 'activated' PTFE is used in a subsequent wet chemistry step in order to graft a film, much like that mentioned in Section 1.3.4.3. In this way, more significant surface modification can be made. For example, Z-Y. Xi *et al.* reported the grafting of a 4:1 ratio film of acrylic acid and sodium 4-styrenesulfonate onto the surface of air DBD plasma-treated PTFE.[79] After grafting, the surfaces were washed in DI water (10 h Soxhlet extraction) before being dried overnight in a vacuum oven at 40 °C. This resulted in a stable WCA of 36°, which was the lowest reported through any grafting process.

1.3.4.6 Alternative Methods

Plasma modification methods are not the only, or indeed the most common, method by which PTFE can be modified to be hydrophilic. There are a number of wet chemical methods by which PTFE has shown to be hydrophilized effectively, for example using sodium naphthalenide solution.[80] M. Gabriel *et al.* and G. Tae *et al.* both used a dip coating process to graft polyethylene glycol (PEG) molecules onto PTFE substrates to improve the wettability and adhesive properties of PTFE.[80,81]

An alternative approach is the use of non-ionic surfactants to coat the PTFE surface. K. Szymczyk *et al.* reported the effective use of an aqueous solution of two such surfactants to improve the hydrophilicity of PTFE substrates. The lowest WCA achieved was approximately 65°.[82]

A longer process was investigated by C. Zilio *et al.* where dip processes were performed sequentially to produce a thicker coating on plasma-treated PTFE surfaces to improve the hydrophilicity of the surface.[83] In their method, an oxygen

plasma was used to activate the polymer surface with hydroxyl groups prior to submersion in a mixture of *N*-acryloyloxysuccinimide poly(diemethylacrylamide) and glycidyl methacrylate poly(dimethylacrylamide).

A similar approach is the layer-by-layer atomic layer deposition (ALD) method, whereby self-limiting reactions deposit monolayers onto the surface.[84,85] Often these methods also use a plasma pre-treatment step to prepare the surface for grafting of the first layer. Work by A.K. Roy *et al.* produced PTFE surfaces grafted with an Al_2O_3 ALD coating, which has an air stable WCA of 40°.[86]

The plasma processes employed in this thesis are advantageous over the alternative methods produced here as the plasma processes are solventless. As previously mentioned, the need for environmentally benign industrial processes means that the lack of waste associated with solvent-free processes gives plasma processes a significant advantage for the future over wet chemical methods.

1.4 THESIS SCOPE

In this thesis, the aim is to create a stable hydrophilic surface that does not exhibit hydrophobic recovery over time. The wider aim was producing films which can be used in the medical industry for cheaper, safer, and cleaner implants that will last for a long time in the body with no rejection issues, and will perform their function as stents, ligaments, or joint replacements.

Initially low-pressure plasma methods were used to achieve stable hydrophilic surfaces. The use of single-step plasma treatments has been widely investigated, and although some very hydrophilic surfaces have been produced, the stability of these surfaces has been mostly overlooked. The extensive literature base of single-step plasma treatments was used to determine which gas plasma treatments could be coupled together in order to achieve an improved hydrophilic surface. The concept of sequential gas plasma treatments is something that has not been widely investigated in the literature. This work took a two-pronged approach to using sequential plasma treatments, initially looking at using multiple hydrophilizing plasma treatments in order to increase the hydrophilicity of the PTFE substrate. The second method was to couple a hydrophobizing and roughening oxygen plasma treatment with a hydrophilizing gas plasma treatment in order to create a Wenzel wetting state.

Additionally, with the idea of developing countries in mind, a similar aim of developing a stable hydrophilic PTFE surface was to be achieved using simple atmospheric plasma methods. Atmospheric plasma methods require very limited equipment, and so if a suitable method can be determined that can be performed in situ, then plasma modified medical implants can be made cheaply in areas where access to expensive equipment and implants is not possible.

Finally the imparting of surface charge onto PTFE substrates that occurs during DBD plasma treatment can be utilised as a method by which to promote grafting of monomers onto the surface to improve the hydrophilicity of the surface even further.

This thesis comprises of an overall experimental methods chapter which describes the theory of the techniques employed in this thesis. Subsequent chapters include the precise experimental details as well as thorough literature reviews, reported results and discussion for these plasma processing methods. All conclusions are summarised in the final chapter along with discussion of future work.

Chapter 2: Experimental Methods

2 EXPERIMENTAL METHODS

2.1 INTRODUCTION

A number of surface modification and analysis techniques were utilised in order to produce and characterise the PTFE substrates presented in this thesis. These analysis techniques were used to track changes in the wettability, morphology, topography, and chemical structure of the surfaces. This chapter is a brief summary of the techniques used in this thesis.

2.2 PLASMA SURFACE MODIFICATION

Plasma is defined as a volume of quasi-neutral ionised gas molecules that behave as a collective entity due to the dominance of the local concentration of charge on the movement of particles.[87] Resulting from this collective behaviour, a gas plasma will "flow" in a manner similar to that of a liquid. This property is why in the late 1920s, Langmuir referred to plasma as 'fourth state of matter'.[88] Plasmas can be in equilibrium, whereby all the neutrals, ions, and electrons within the plasma are in thermal equilibrium. This is termed 'natural' plasma, and is produced under extreme heat, such as in stars.[89] Alternatively a plasma can be non-equilibrium, or 'cold', such as that described in this thesis. Non-equilibrium plasmas have a lower degree of ionisation, and the ions and neutral species remain close to ambient temperature, whilst the electrons have a much higher temperature.[89]

As a process, plasma surface modification is popular as it is a 'clean' method for altering the physical and chemical properties of a surface with no waste or solvent use.[90] This work focuses on gaseous plasma surface modification, where a plasma is created by placing a potential through a gas and thus igniting it.[91] Through the use of a gas plasma modification method, it is possible to avoid many of the pitfalls of wet chemical methods, for example residual solvent, and swelling of the material.[92] There are a number of different types of cold plasma ignition; dark discharge (prior to spark ignition), normal glow discharge, abnormal glow discharge and arc discharge.

Plasma can be used to modify the surface properties of an inert material without altering the bulk properties.[90] Upon reaching a polymer surface, plasma can initiate either a degradation reaction or a modification reaction. More often than not, these two processes occur both competitively and simultaneously.[91] If the dominant reaction is the degradation process, then atoms will be removed from the surface, and the polymer will be 'etched'. This can lead to changes in the wettability of the

surface owing to the removal of polar or non-polar groups. This loss from the polymer also results in a net weight loss, however it must be noted that this only affects the top layers of the polymer surface as plasma cannot penetrate into the bulk. If the modification process prevails, the properties of the surface will also be changed, however not due to etching. When modifying a porous substrate, plasma fills all the available space, and so any exposed surface will be modified, which includes pores in a substrate. Plasma can also be used to pattern a surface using a mask process: any area that is covered will remain unmodified, whereas all exposed areas will be plasma-treated.

2.2.1 Low-Pressure Non-Equilibrium Plasma Treatment

There are two overarching categories of plasma modification apparatus: those that operate at atmospheric-pressure, and those that use vacuum pump technology to operate in the region of less than 1 mbar.

The low-pressure apparatus used in this work focuses on glow discharge plasma which is inductively coupled. Inductive coupling refers to the use of external electrodes to provide a potential and thus ignite plasma of the gas within a glass reactor.[91] The electrical power is transferred to the gas from the RF supply through the electric field created by RF current flowing through the copper coil wound around the cylindrical reactor.[93] Inductively coupled plasma generally has a higher plasma density and lower amount of ion scattering than its counterpart produced from capacitive sources.[94]

Electrons are accelerated within the plasma through the presence of an alternating RF electromagnetic field, and this causes reaction at the surface.[95] Bond cleavage and ionization of the species in the plasma can initiate either degradation or modification processes at the surface, which will result in surface changes. The degree of modification that occurs at the surface is chiefly influence by the plasma power and treatment duration, but also influenced by the species present in the plasma, and hence the feed gas.

2.2.2 Atmospheric-Pressure Plasma Treatment

Plasmas which can be ignited under atmospheric conditions are generally more easily scaled up for industrial applications. Removing the low-pressure aspect of the system results in the possibility for continuous rather than batch processing.

Non-equilibrium discharge is created in this work using dielectric barrier discharge (DBD). The possible operating pressures for this technique are 75–760

Torr, although in this case, the technique was used at atmospheric-pressure (approximately 760 Torr). DBD plasma apparatus involves two electrodes positioned a few millimetres apart. There is a dielectric between these electrodes which prevents dangerous arcing, and induces a more controlled plasma discharge. In this case the PTFE sample is insulating and can act as a dielectric.

Unlike the aforementioned low-pressure glow discharge plasma, DBD plasma is non-uniform and so the plasma treatment of the surface is often uneven. DBD plasma ignition involves the passing of a high voltage to the 'live' electrode, and this induces the potential to be passed across the interelectrode gap to the 'earthed' electrode via micro-discharges. These micro-discharges look similar to little lightning bolts bridging the gaps. The distribution of these micro-discharges is influenced by the surface of the dielectric, any defects or contaminants on the surface would cause the discharge to strike more frequently in that position, much like lightning will strike metal poles more than empty ground.

2.3 CONTACT ANGLE ANALYSIS

As previously discussed in Chapter 1, the shape of a liquid drop is dependent on a number of factors: the free energy of the surface, the composition of the surface, and the morphology of the surface. The sessile drop method involves the deposition of a droplet of liquid (in this case chiefly water, but also ethanol and hexadecane), on a flat surface, using an automated syringe dispensing unit. The measurement of the contact angle of the droplet with the surface is calculated from an image captured using a mounted camera.

It must be noted that regardless of the method by which the CA is measured, the observed CA may be a function of the size of the droplet (or bubble in the case of the captive bubble method).[96,97] To this end, it is important to ensure that the droplet or bubble size is the same or at least similar in order to draw meaningful comparisons between observed contact angles. In this report, all static CAs are measured for a 1 µL droplet of liquid, and although comparisons may be drawn between those measured here, and those reported in the literature, some care must be taken over these as they may not all use the same size droplet.

In this thesis, advancing and receding CAs are measured using the dynamic CA method, where liquid is removed or added respectively to a static droplet present on the surface.

2.4 X-RAY PHOTOELECTRON SPECTROSCOPY

X-Ray photoelectron spectroscopy (XPS) is used to analyse quantitatively the composition of the surface of a sample. Generally XPS uses a monochromatic beam of X-rays that hit the surface and cause photoemission of electrons from both the core and valence shells of the atoms within the surface into the vacuum. This emission of electrons is known as the photoelectric effect, and was discovered by Hertz in 1887.[98] Further development by Rutherford and Moseley developed both the understanding of the theory of X-ray photoemission and also the technique of XPS.[98,99,100] The kinetic energy (KE) of the emitted electrons as they impact the detector is determined by the binding energy (BE) of the level they originate from. Elemental identification is possible as each element has a characteristic set of binding energies. Additionally, the environment surrounding the atom will influence slightly the kinetic energy of the ejected electrons resulting in a method by which to determine the number of environments in which that element is found. The nature of these environments is determined as the induced charge on the nucleus is dependent on the functional group in which is the element is situated.

In XPS spectra, there are multiple different types of emission lines present. For first row elements, which are all that is pertinent to this thesis, these include the main photoelectron line, which is the most intense and well defined peak in a spectrum. The photoemission lines are caused by the ejection of electrons from core levels into the vacuum. To be ejected, the photoelectron must have KE sufficient enough to overcome the BE of the core level of an element, Equation 2.1.

$$KE = h\nu - BE - \varphi \qquad \text{Equation 2.1}^{101}$$

where *KE* is the kinetic energy of ejected photoelectron, *hv* is the incident X-Ray energy, *BE* is the binding energy of electron, and φ = the work function of the spectrophotometer.[106] The value of *hv* must be a lot greater than φ, which means that the photon energy is higher than the energy required to promote a core electron into the vacuum level.[102,103]

Auger lines are caused by secondary electron emissions. If a second electron relaxes from a higher energy level down into the core, the energy released may be sufficiently high enough to permit the ejection of an Auger electron from the valence band of the atom into the vacuum.[104,105]

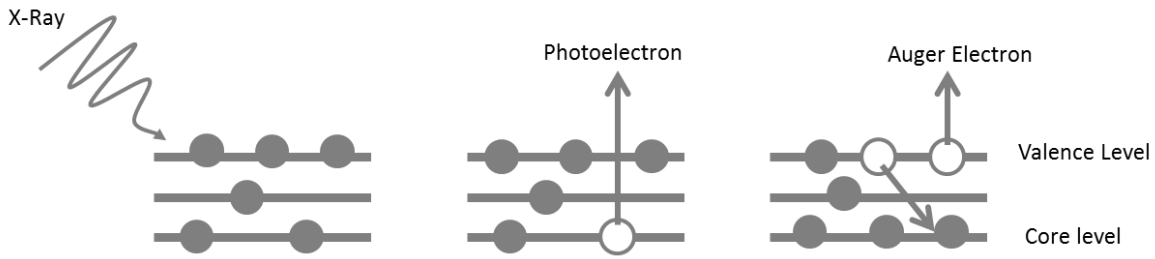

Figure 11: Schematic representation of photoemission process of XPS.[106] The wavy line represents the X-ray incident on the sample. The grey circles represent electrons in core and valence levels. The white circles indicate holes where electrons used to be.

Historically the j-j coupling method is used to describe the Auger electrons in an XPS spectrum, for example KLL. The *K* represents the core level hole, the *L*s denotes that the two vacancies are in the L shell.[98,102] This scheme of coupling is key for heavy atoms, where the spin-orbit coupling is large.

The second descriptor of coupling is the Russell-Saunders scheme (also known as L-S coupling). This is more important for first row elements which are the focus of this thesis, where j-j coupling can chiefly be ignored.[107] In a many electron system, *L* is the total orbital angular momentum quantum number, and *S* is the total spin quantum number, which together give *J*, the spin-orbit total angular momentum quantum number.[108] Russell-Saunders coupling is based on the assumption that when spin-orbit coupling is weak, effectively all orbital momenta are operating cooperatively. The permitted values of J are given by the Clebsch-Gordan series, Equation 2.2.[108]

$$J = L+S, L+S-1, \ldots, |L-S| \qquad \text{Equation 2.2}^{108}$$

When X-rays are incident upon the surface, a small number of the electrons are scattered elastically from the surface, meaning no energy is lost from these electrons. However most of the incident electrons will interact strongly with the surface and therefore will lose energy.[109] This gives rise to inelastic back scattering from the surface. The result of inelastic scattering can be seen as a stepped background on the XPS spectra. At higher BE, i.e. lower KE, the background is higher as there is multiple scattering events.

Although for the most part, a monochromator is located in series with the X-ray source, it is possible to run XPS analysis without this piece of equipment. The non-monochromated X-rays will create satellite peaks on the XPS spectrum.[103,110] For each main peak that is observed, smaller peaks will be observed at a specific

displacement and at a specific percentage of the area of the main peak. The size and displacement of these satellite peaks is determined by the machine and X-ray anode being used.

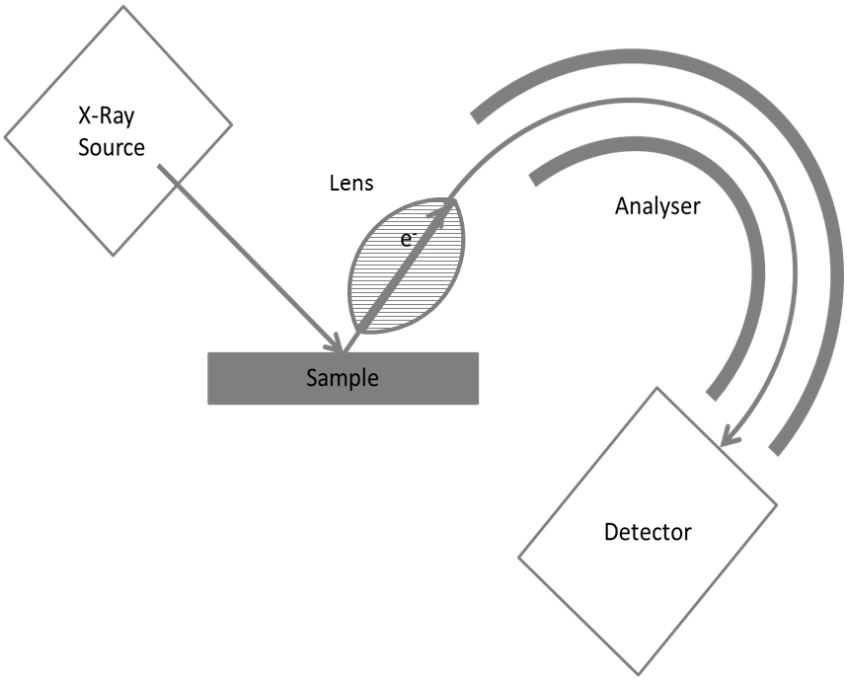

Figure 12: Schematic representation of XPS equipment for analysis of surface composition. The X-ray source is incident on the sample, from which either photoelectrons or Auger electrons are ejected. These are accelerated towards the concentric hemispherical analyser through a lens where the electrons are separated according to their kinetic energies. The electrons are collected at the detector which is an electron multiplier and from analysis of this data, surface composition is determined.

The hemispherical analyser works by only allowing electrons with a certain KE to pass all the way round to the detector, Figure 12. Those with too high, or too low, energy will hit either the inner positive hemisphere or the outer negative hemisphere and be neutralized. In order to produce a full spectrum, a retard plate is used. Using a negative voltage on the retard plate, the electrons can be slowed down until they have the correct 'pass energy'. Through altering the negative voltage across the retard plate, electrons with differing KEs can make it through the analyser to the detector.[102,104,105,106]

The peaks within a XPS spectrum all have a peak width, this is caused by several contributions. These include the lifetime broadening (homogenous broadening), different chemical environments (inhomogeneous broadening), different relaxation pathways and final states, and can also be due to instrumental factors. The breadth of a peak is defined as the full width half maximum (FWHM), and is governed by this broadening.[101]

In order to ascertain quantitative data about the XPS spectra, it is important to fit a curve to the data. The area under this curve is representative of the amount of that particular element present on the surface of the sample.[111] A number of function types can be used to fit the data; commonly Gaussian or Lorentzian functions.[109] Due to the asymmetric nature of the data, it is usually necessary to fit a number of Gaussian-Lorentzian peaks, and use the sum of these peaks to fit the data. In this thesis, a Shirley background is subtracted prior to the fitting of a number of Gaussian-Lorentzian functions.[111]

2.5 OPTICAL EMISSION SPECTROSCOPY (OES)

The radiation of ions and neutrals within a plasma often lies in the visible spectrum region. The result of this is that the colour of the plasma is indicative of the heavy particles present, and hence the feed gas of the plasma.[112] A quick visual inspection of the colour of the plasma will allow characterization of at least the main gas present in the plasma. For example, helium plasma is pink, nitrogen plasma is orange/pink, and hydrogen plasma is purple.[112]

Where a more in depth analysis of the plasma composition is required, for example to check for air contamination in the chamber, optical emission spectroscopy (OES) can be used. OES is the most used in-situ method for monitoring real time changes in a plasma during an experiment, and is non-invasive and independent of large RF frequencies or strong magnetic fields.[112,113,114] The technique is based on the analysis of the spontaneous emission of photons by ions that have been excited using RF discharge.[115]

OES is used to detect the spectrally dispersed photons emitted after excitation and relaxation of electrons into and from excited states. [116,116,117] This emission is detected in this work using an optical fibre, and gives a picture of the excited species within the plasma, but not the ground state species.[117]

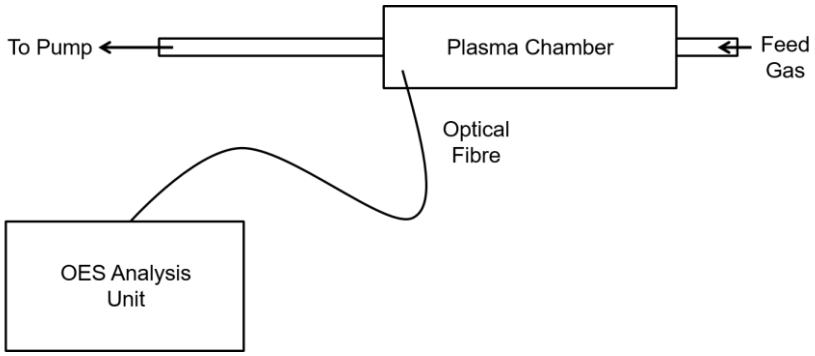

Figure 13: Schematic of OES apparatus.

The positioning of the optical fibre influences both the intensity of the emission measured, and the degree of background interference. There are two configurations for the optical fibre: axial and radial. Axial is where the plasma is observed end-on, and radial is where the plasma chamber is perpendicular to the optical fibre. The radial positioning reduces the effect of spectral and background interferences by limiting the observation volume significantly in comparison to axial viewing.[115] In this report, OES is used as a diagnostic tool in the radial position to determine if any contamination is present in the plasma.

2.6 ATOMIC FORCE MICROSCOPY (AFM)

Atomic Force Microscopy (AFM) is a surface characterisation technique that allows the topography of a surface to be studied at very high resolution. The lateral resolution of the AFM technique is governed mostly by the sharpness of the tip. With modern equipment it is possible to image single atoms. Unlike traditional optical microscopy, AFM measures the change in forces between a probe and the surface to map topography. This allows the height of each undulation on the surface to be measured accurately, which can then be plotted into a coloured height contour map which gives a visual representation of the micro- and nano-scale surface features.

The concept of AFM is that a sharp probe which measures force is used to determine how the surface topography changes. The probe is mounted on a cantilever that allows it to move up and down, and over the undulations of the surface. The X and Y directions give a 2D scan, but in order to get a 3D scan, the Z direction must also be recorded. The Z direction is determined by the recorded force which is measured by changes in the angle of the cantilever. These small changes in angle are detected by beam deflection method, where a laser is incident on the cantilever, and as the cantilever moves, the laser is deflected slightly (Figure 14).

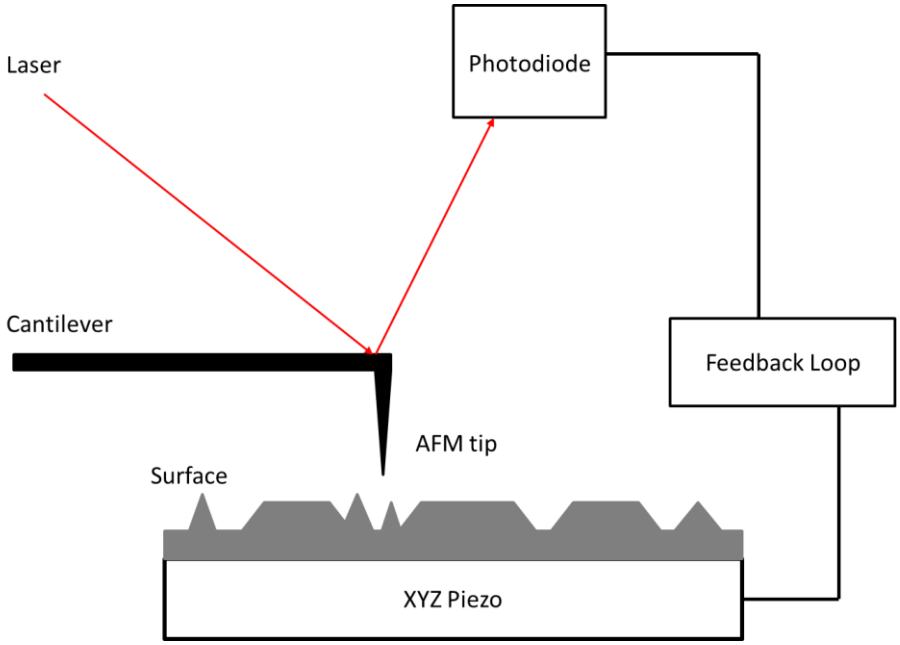

Figure 14: Schematic of AFM apparatus. As the sharp tip moves across the features of the surface, the cantilever angle moves slightly. The deflection angle is measured by the degree of deflection of the laser as it hits the photodiode. This is fed into the feedback loop which controls the XYZ piezo and the height of the surface in comparison to the AFM tip.

There are a number of different modes in which AFM can be used, the most common of these are traditional contact mode and the newer tapping mode. In this study, tapping mode and Bruker's own ScanAsyst mode are used. In the first, the tip vibrates at a resonant frequency resulting in oscillation with an amplitude typically greater than 20 nm over the surface as it scans.[118] ScanAsyst mode is similar except that the feedback is automatically controlled to reduce the likelihood of loss of contact with the surface, thus giving rise to sharper images. The main advantage of a tapping mode over traditional contact mode AFM is that the surface is not subject to sideways forces that can cause damage to the surface by the removal of loosely bonded groups.[119] This is important in this work, as plasma modification of PTFE produces LMWOS on the surface, which are easily dislodged.

2.7 SCANNING ELECTRON MISCROSCOPY (SEM)

Scanning electron microscopy (SEM) allows for the study of the topography of a sample surface using a beam of high energy electrons (0.5–40 keV).[89] The concept of SEM was first described by M. Knoll in 1935, but was produced and marketed by Sir Charles Oatley in the early 1950s.[120,121,122] Modern SEM machines can produce high resolution images with in some cases detail down to 25 Å, with a good depth of field.[123]

Electrons are generated from a field emission gun or tungsten filament, and accelerated through a series of apertures and electromagnetic lenses to produce a thin high energy beam.[120,123] This beam initiates the emission of secondary electrons from the surface core orbitals. This emission occurs as the incident electrons impart enough energy to overcome the ionisation potential of the surface atoms. The emitted secondary electrons have a significantly lower energy (usually <50 eV) than those focused on the surface.[89] By holding a positively biased grid close to the surface, these secondary electrons can be accelerated towards the detector for collection.

The high resolution of the images obtained using SEM are a product of the small spot size (0.4–2 nm) of the electron beam, and the limited escape depth of the secondary electrons. As the secondary electrons have low KE, and thus a short mean free path, the technique is very surface specific.[89,120]

2.8 FOURIER TRANSFORM INFRARED SPECTROSCOPY (FTIR)

Infrared spectroscopy is cheap and swift method by which to identify changes in functional groups in a solid or a liquid. For the majority of functional groups, the molecular vibration at transition lie in the infrared region. If the transitions between vibrational energy levels of molecules, i.e. the bending and stretching motions of a covalent bond that correspond to a change in dipole moment, match the energy of infrared photos, then distinctive absorption features will be observed in the spectrum.[89120]

The Fourier transform addition to the tradition IR method, is typified by the splitting of the incident light into two beams that each cover of the whole frequency range (5000–400 cm^{-1}).

2.8.1 ATR-FTIR

In this thesis, ATR-FTIR is used, this is a standard FTIR spectrometer fitted with an ATR (attenuated total reflection) accessory. ATR-FTIR is suited to analysing PTFE as it does not require a reflective surface, working instead through evanescent waves. These waves extend into the sample, and as they cannot propagate through the solid, the amplitude of the waves decrease with distance, making it more surface specific. ATR works by measuring the changes in an internally reflected beam once it has come into contact with the sample. The IR beam is focused on a crystal with a high refractive index at a set angle using a mirror. An evanescent wave is created by the internal reflectance, and this extends

beyond the surface of the crystal into the sample which is in contact with the crystal. The way in which this evanescent wave behaves is what is measured. If the sample absorbs a particular wavenumber of IR radiation, the evanescent wave will be attenuated before returning to the crystal and being directed by another mirror to the detector.[124] The standing wave that is created at the interface between the crystal and the substrate is able to penetrate into the sample, this is known as the standing wave penetration depth, and is 1.73 μm in the mid IR region for KSR-5 crystal,[125] (Figure 15). In order to generate the IR spectrum of the sample, the background absorbance of the crystal in air is subtracted from the beam that is detected (I_A).[89]

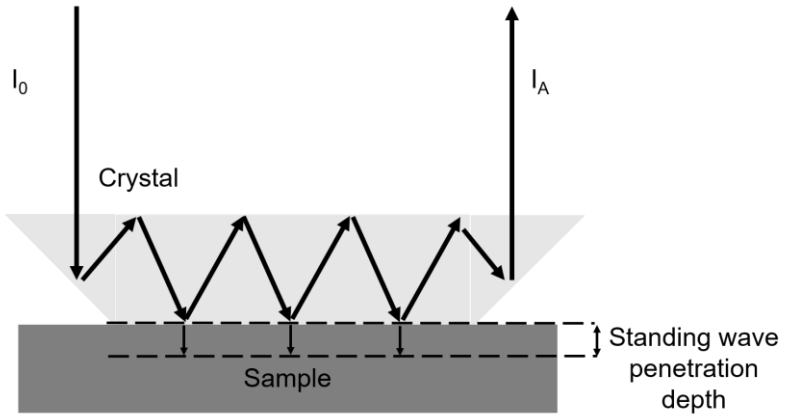

Figure 15: Total internal reflection of I_0 within the Diamond cut KSR-5 (thallium bromoiodide) crystal, and the resultant standing wave that penetrates the sample. Adapted from schematic by S. Morsch.[89]

2.9 SURFACE TENSION MEASUREMENTS

When gravity and other fields can be neglected, a liquid droplet will always adopt a shape that minimizes its surface area. This is generally a spherical shape as this has the lowest surface to volume ratio.[126] Although a sphere has the lowest surface to volume ratio, gravity and interactions with a surface can influence the shape of the droplet, which is the basis of CA analysis, Section 2.3. Surface tension can be defined as the force per unit length (N m^{-1}), or the free energy per unit area (J m^{-2}).[127]

Surface effects are a combination of the Gibbs and the Helmholtz energies. The Helmholtz free energy is the maximum work done by a system at a constant volume and temperature, whereas the Gibbs free energy is the same but at constant pressure and temperature.[128,129]. The work done to form the surface of a liquid at a constant temperature and volume (i.e. the droplet is not advancing or receding) can be expressed in terms of the surface tension (γ), change in surface

area ($d\omega$), and the change in the Helmholtz free energy (dA), Equation 2.3.[126] The surface tension is therefore a proportionality between the surface area and the Helmholtz free energy. As the surface area decreased, the Helmholtz energy will also decrease, and so the liquid surface will contract. In the work presented is this thesis, the system is open, but the pressure remains constant. At ambient pressures, the Gibbs and Helmholtz energies are indistinguishable.

$$dA = \gamma \, d\omega$$

Equation 2.3[126]

The surface tension of a liquid droplet is often thought of as an “elastic skin” which holds the droplet in the shape that has the lowest free energy. This skin-like quality is a tangible model for the imbalance of forces between the surface, the surrounding vapour, and the bulk that actually holds the shape.[130]

In this thesis, surface tension measurements are taken of the wash liquors after plasma-treated PTFE surfaces have been solvent washed. Solvent washing of these surfaces resulted in hydrophobic recovery being observed, which could be due to the reported removal of LMWOS. If solvent washing removes these oxidised species, these will remain in the wash liquor, and analysis of the surface tension of this could provide insight into the amount of LMWOS present. Fluorocarbons reduce the surface tension, and so a decrease in surface tensions should be observed if there are fluorine-containing fragments washed off. Hydrocarbon chains have lower surface tensions than their oxygen-containing functional group counterparts,[130] and so an increase in oxygen containing species should cause a small increase in the surface tension. However, when considering dilute species, there can only be a decrease in surface tension observed, according to Gibb’s Isotherm, Equation 2.4. Additionally, the length of the carbon chain in these ‘washings’ should be considered, as when carbon chain length is increased, the observed surface tension generally decreases, Figure 16.[130]

$$\Gamma = -\frac{1}{nRT}\frac{d\gamma}{d\,lnC}$$

Equation 2.4[131]

where Γ is the surface excess, in this case of the LMWOS washed from the surface, γ is the observed surface tension, and C is the concentration of the LMWOS.

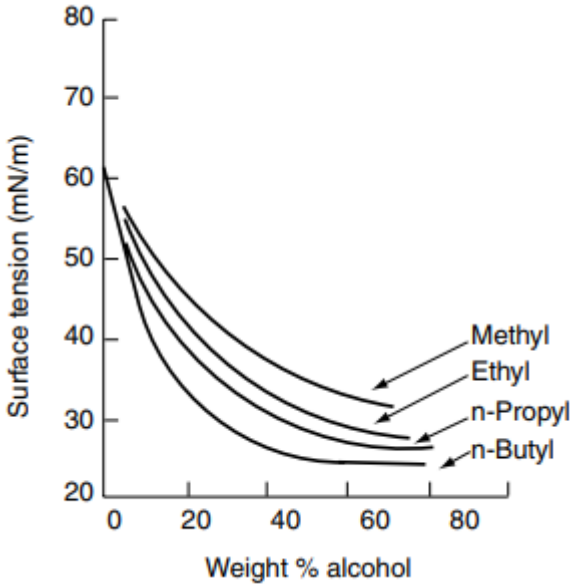

Figure 16: Effect of carbon chain length on the surface tension of water. Here illustrated using methanol, ethanol, propanol, and butanol. Taken from work by D. Myers.[130]

It should however be added, that the incorporation of these LMWOS into the surfaces means the solutions are not behaving as “ideal” liquids, and thus the orientation and mixing of these LMWOS in the solution should also be thought of. For example, polar molecules will orient themselves to present their aliphatic chains away from a non-polar solvent, much like in a lipid bilayer. This will mean that the oxygen containing groups are “buried” in the bulk of the wash liquor, and so the characteristic increase in surface tensions is not perhaps observed. Providing that the molecule size is relatively small, rather than macromolecular, the effect of this should be minimal.

2.10 SURFACE CHARGE MEASUREMENTS

As PTFE is an insulating material, it can accumulate and store charge easily. This charging can be exacerbated by plasma treatments. Electrostatic voltmeters can be used to accurately measure the charge without physically touching the surface, and therefore not altering the surface. This is achieved using an electrostatic chopper for low drift, and negative feedback for accuracy and probe-to-surface spacing insensitivity.

In this thesis, the Isoprobe 244 is used, it contains a probe (model 1017E) that has a small aperture (1.75 mm) that allows the electrode to “look” at the surface. A tuning fork chopper is used to “chop” the A.C. signal, this has a set starting oscillation executed by the tuning fork drive. The oscillation of this tuning

fork is influenced by the charge on the surface that is seen through the aperture, (Figure 17).[132]

A sensitive electrode allows for changes in the oscillations of the tuning fork to be detected, and fed into the feedback circuit. The feedback circuit promotes incremental changes in the oscillation of the tuning fork. These are made until the oscillation provided to the tuning fork by the circuit (input) and that induced by the surface (output) match. At this point the readout on the LCD display will be a true representation of the surface voltage.[132]

The null feedback system consists of a phase sensitive detector which is used to match the oscillation of the tuning fork with that induced by the surface, which is displayed on the LCD screen. A feedback circuit is where the outputs of a circuit are fed back into the circuit as inputs. In this case, this occurs until the output voltage is the same as the surface voltage (null feedback loop).[132]

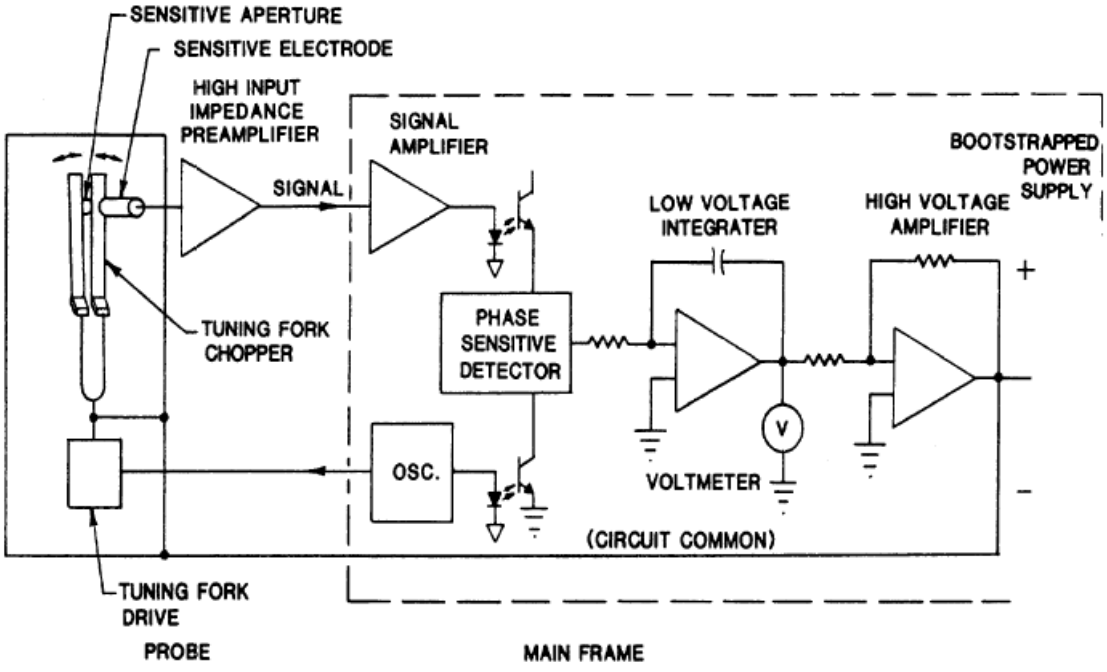

Figure 17: Simplified block circuit diagram of electrostatic voltmeter, Monroe Electronics Isoprobe 244.[132]

2.11 GAS CHROMATOGRAPHY MASS SPECTROMETRY (GC-MS)

GC-MS is two separate techniques arranged in series with one another; first a gas chromatography (GC) apparatus, and then a mass spectrometer. The GC is used to separate volatile gas mixtures into their component molecules. This allows the mass spectrometer to analyse each species as it is eluted from the GC column. The

tandem set-up of apparatus means that the MS method which is not adept at analysing mixtures can be effectively used.[133]

GC is a well-established technique whereby the sample mixture is injected into a column, and is carried through this by an inert carrier gas; in the work presented, this is helium. The long capillary column is coated with in this case a liquid, and the degree to which the mixture substances interacts with the column determines how long it takes to travel through. In this way the mixture is separated out, and each component part is eluted from the column at a different time, termed the retention time.

In the case of GC-MS, these components are ionized (often by electron ionization using an electron beam) and then the charged gas phase species are separated according to the mass and charge values.[133,134]

In a similar manner to the surface tension analysis of the wash liquors, GC-MS was used as a tool to probe the composition of the wash liquors with the aim of determining the type of groups washed from the surface that promote hydrophobic recovery.

Chapter 3: Two-Step Low-Pressure Gas Plasma Treatment of PTFE Surfaces

3 TWO-STEP LOW-PRESSURE GAS PLASMA TREATMENT OF PTFE SURFACES

3.1 MOTIVATION

Through the use of gas plasma treatments it is possible to modify the surface of polytetrafluorethylene (PTFE) without altering the bulk properties of the polymer. Gas plasma modification is preferable to liquid plasma modification or plasma deposition processes in that it is more easily scaled up for industrial applications. Plasma treatments produce far less waste than traditional wet chemical methods owing to the solvent-less nature of the processes.

In this chapter, the coupling of low-pressure (0.2 mbar) gas plasma treatments together is investigated as a method by which a stable low WCA surface could be produced. The modified PTFE surfaces are analysed in terms of their hydrophilicity, and the most hydrophilic surfaces are investigated using surface analysis techniques to determine the mechanism by which the hydrophilization has occurred.

3.2 WETTABILITY OF PLASMA-TREATED SURFACES

3.2.1 Single-Step Gas Plasma Treatment

Gas plasma treatment of PTFE surfaces is an area with a lot of scope for vast reduction of the water contact angle (WCA) of PTFE surfaces whilst retaining the properties of the bulk polymer.

Many different feed gases have been used for low-pressure plasma treatments of PTFE surfaces, including argon, air, nitrogen, hydrogen, and ammonia. Table 1 is a summary of the lowest reported WCA in the literature for gas plasma treatment of PTFE. Included is the WCA after plasma treatment, and any reported changes in the surface upon storage in air, or after solvent washing. Further literature data is available in the Supplementary Information, Section 7.1.

Table 1: Summary of prior art for the static WCA after single-step gas plasma treatment of PTFE.

Gas	Power / W	Time / s	WCA Before / °	WCA Aged in Air / °	WCA After Washing / °	Ageing Comment	Ref.
Argon	8.3	500	30	Not given	No solvent washing process	Not reported but in other work by same group, recovery to approx. 110°	135
	30	3600	30	70	No solvent washing process	Chemical etching process prior to the argon plasma treatment. Recovery to 70° within 1 hour	136
	8.3	600	<10	75	No solvent washing process	96 hours in air, samples repeatedly measured and water droplets not washed from the surface	137
	Not given	120	Adv. 88, rec. 18	Not given	Adv. 88, rec. 18 Samples washed in deionised water and air dried over silica gel	Samples stored in deionised water	138
	Not given	1200	Adv. 25, no rec. given	Not given	No solvent wash process	Not given, and note that samples were heated during plasma treatment	139
Nitrogen	20	1800	34	Not given	No solvent washing process	Not given	140
Ammonia	350 W Microw	120	Adv. 53, rec. 15	70	Adv. 53, rec. 15	Recovery to approx. 70° after 10 h	141

	ave plasma				Samples washed for 1 h with a Soxhlet extraction in methanol immediately after treatment		
	Not given	120	Adv, 75, rec. 20	Not given	Adv, 75, rec. 20 Samples washed in deionised water and air dried over silica gel	Not given, and note that samples were stored in DI water	138
	Not given	180	Adv. 16, no rec. given	Not given	No solvent wash process	Not given, and note that samples were heated during plasma treatment	139
Oxygen	20	600	111	Not given	No solvent washing process	Not given	140
Hydrogen	100	10	62		84 Rinsed with acetone, no rinse duration given	Recovery to 84° after acetone washing	142
Air	10	180	38	>70	>50° after storage in water for 20 days.	Aged to >100° after storage in air at 100°C, >70° after 20 days in ambient conditions, >50° after storage in water at 22°C.	143
Water + Argon	400	120	24	60	No washing process	Aged to 60° after 100 h	144
CO_2 + Argon	2.31	20	89	Not given	No solvent washing process	Not given	145
CH_4 + Nitrogen	50	60	52	88	No solvent washing process	Recovery to 88 after 25 days storage in air	146
Argon + Ammonia-water	100	900	4	Not given	No solvent washing process	Not given	147

A major issue with the comparison of literature is that many papers have only reported the WCA of the surface immediately after plasma treatment, and have not taken the stability, or indeed instability of the surface into account. The aforementioned plasma-treated surfaces (Table 1) are a combination of surfaces

that have been tested for stability and those that have not. One of the key problems with gas plasma-treated PTFE is that of hydrophobic recovery, whereby over time some of the hydrophobic nature of the PTFE is regained, quantified by measuring the WCA.

The lowest reported WCA of 4° was reported by W. Hai *et al.* after treatment of PTFE with argon and ammonia water plasma (100 W, 15 min, flow rate Ar, NH_3, and H_2O were 24.4, 0.28, and 0.13 mmol min^{-1} respectively), Table 1.[147] The limit of reliable measurement of the WCA using a sessile drop method is widely deemed to be approximately 10°, so the reported value of 4° which has no error value associated with it should not be considered accurate. Additionally no wash process was carried out, and from the FE-SEM images (Figure 18), there appears to be significant roughening of the surfaces potentially leaving a large amount of LMWOS which would cause a much lower initial WCA until these have been removed.

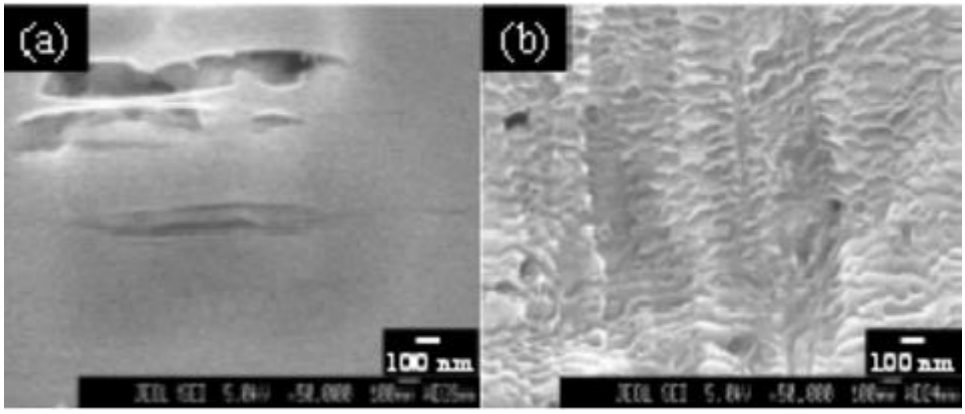

Figure 18: FE-SEM images at 50 000 magnification and 5.0 kV electron acceleration voltage of PTFE (a) as received, WCA 118°, and (b) treated with Ar/NH_3-H_2O plasma (100 W, 15 min, 0.8 mbar), WCA 4°.[147]

For a single feed gas, the lowest WCA achieved was 30° and this was using argon as the feed gas, Table 1. Again, there was no wash step prior to WCA measurement.[135,136] When aerial ageing is taken into consideration, the best reported aged sample was after treatment with water and argon mixture, where the WCA was 60° after 100 h (4 days 4 h).[144] Due to the lack of wash process on this sample, it is not possible to accurately determine the reason for the observed hydrophobic recovery, or asses the stability of the surface, or compare this with the work achieved in this study. The best solvent washed samples were plasma-treated using ammonia (350 W microwave plasma, 120 s), and subsequently washed in methanol (Soxhlet extraction, 1 h) and achieved an adv. angle of 53°, and a rec. angle of 15°.

Hydrophobic recovery is generally reported in the literature to be caused by surface reconstruction, whereby groups from the polymer bulk will migrate and present on the surface to lower the surface energy. After a hydrophilizing plasma treatment, the surface has polar groups present on the surface, which result in unfavourable surface energy. In order to reduce the surface energy, these modified polymer chains are moved from the solid-air interface into the bulk, and replaced by unmodified polymer chains from the bulk polymer. The net result of this that the modified polymer surface is no longer exhibiting the modified properties, but simply those of the starting polymer. There is a debate in the literature as to whether it is the surface groups moving into the bulk or the bulk groups moving to the surface.[148,149,150,151] Although as previously mentioned, this is possibly purely philosophical as the net result is the same: both occur, the only question is which causes the other to happen. There is additional evidence to suggest that there is condensation of the surface hydroxyl groups that are introduced during plasma treatment, discussed in reference to PDMS by N. Zachariaha *et al.*[49]

Another reason given for hydrophobic recovery is the gradual removal of low molecular weight oxidised species (LMWOS) from the surface.[152] O.D. Greenwood (1997) reported the LMWOS present on the surface caused hydrophobic recovery of plasma-treated non-fluorine-containing unsaturated phenyl polymers (polystyrene, PET, poly ether ether ketone (PEEK), poly(bisphenol carbonate), poly(ether sulfone), and poly(bisphenol sulfone)).[152] In this work, the LMWOS were effectively removed using a solvent wash process (propan-2-ol/cyclohexane, 1:1 solution by volume, 2 min). Similarly, work by Guckenberger *et al.* indicated that LMWOS could be reliably removed from a plasma-treated polymer surface using adhesive tapes, and thus induce hydrophobic recovery of the surface.[153]

Furthermore it is well known that, under atmospheric conditions, there will be deposition of carbonaceous compounds onto a surface. The degree of aerial contamination is dependent not only on the rate of surface bombardment which can be estimated using the kinetic theory of gases, but also the VOC content of the surrounding atmosphere.[154]

Work by M. Mortazavi *et al.* into the development for a model for diffusion-driven hydrophobic recovery in plasma-treated PTFE showed a synergistic relationship between diffusion and molecular reorientation in the surface. Both of which are thermodynamically driven non-equilibrium processes.[48]

Z. Kolska *et al.* reported changes in argon plasma-treated PTFE (8.3 W, 400 s, 0.1 mbar, no wash process) over a duration of 96 hours of storage in air.[137] Through the use of AFM, XPS, WCA and zeta-potential measurements, they concluded that

immediate drastic surface changes occur in order to reduce the surface energy of the sample. In contrast to that observed in polyolefins (previous work),[155] no reorientation of oxidised species towards the bulk is seen, instead it is indicated by the AFM that the roughness decreases sharply in the first 24 h and then increases. This is hypothesised to be due to spontaneous reorientation of the LMWOS on the surface.[137]

Work by J. Hyun on the mobility of oxygen plasma-treated PET (poly(ethylene tetraphthalate), 180 W, 60 s, 0.13 mbar, no wash process) surfaces reported that the hydrophobic recovery of a polymer surface can be reduced using an annealing step (130 °C, 1–24 h).[156] As the chain mobility in the amorphous region of the polymer is reduced by annealing, the fraction of immobile polar groups on the surface is increased, and thus the WCA remains lower.[156]

The storage medium for samples prior to analysis is important because the properties of the storage medium can affect how the hydrophobic and hydrophilic moieties on the substrate surface restructure.[48,157,158] For example, if stored in water, a plasma-treated PTFE surface will retain more of its hydrophilic character. For this reason, those studies where the samples were stored in water prior to WCA analysis are not included in Table 1. After ammonia plasma treatment, X. Xie *et al.* reported a WCA of approximately 10° for PTFE, however prior to analysis these samples were stored in deionised water. Additionally, these samples exhibited full hydrophobic recovery back to the original WCA of untreated PTFE (approximately 110°) after only being stored in air for a few days.[159]

D.J. Wilson *et al.* reported two mechanisms of hydrophobic recovery depending on the storage medium; reaction of the surface with the storage medium, and surface relaxation.[158] Samples that were not placed in ambient air – but instead wrapped in aluminium foil immediately after plasma treatment still underwent hydrophobic recovery. Even though there would be minimal hydrocarbon contamination from the surrounding environment.[158] Samples that were stored in PBS (phosphate-buffered saline) for any period of time showed less increase in PBS contact angle over time, indicating that the storage in the wetting liquid reconditions the surface – through chemical reaction.[158]

Table 2: Summary of causes of hydrophobic recovery, and how to determine which of these is the major cause of it in this work.

Cause of Hydrophobic Recovery	**How to test for it**	**Prior Art**	**Ref.**
Removal of LMWOS from surface	Wash surfaces in PROPAN-2-OL/Cyclohexane solution in order to remove these – use WCA/AFM/XPS of washed vs unwashed to prove this.	Guckenberger *et al.* used adhesive labelling tape to remove LMWOS from plasma-treated hydrophilic polystyrene surfaces. This induced hydrophobic recovery to 51° (from 15°) and according to XPS imparted very little Si onto the surface.[153] Greenwood *et al.* reported that the globular features present on the polymer surface after oxygen plasma treatment were diminished after solvent washing to give an overall smooth texture. The remaining globular features were attributed to incomplete chain scission and/or crosslinking to the surface.[152]	152,153, 160
Aerial Contamination	XPS Place samples in areas with different atmospheres. Back fill the chamber with nitrogen or compressed air and compare XPS when back filled with lab air.	Molecules from the gas phase are continually colliding with the surface. If they strike a vacant site on the surface then the gas molecule with be adsorbed. After impact with an occupied site, the adsorbate is reflected back into the gas phase.[51] At sufficiently low-pressures, the aerial contamination is vastly reduced, so as soon as the samples are removed from the plasma chamber, adsorption of aerial contaminants is significantly increased.	51, 161
Storage Medium	WCA will show if	Murakami *et al.* reported that	158, 160,

Polar liquids have been shown to retard hydrophobic recovery of plasma modified polymers incl. PTFE.	there is a difference XPS and AFM analysis will determine the effect this is having on the surface.	methanol-washed oxygen plasma-treated polystyrene (PS), polydimethylsiloxane (PDMS), and phenol-formaldehyde resin (PFR) exhibited different hydrophobic recovery when kept for 500 h in distilled water and under nitrogen. When the polymers were stored in water, the surface free energy of the surfaces approached that of water (72.8 mJ m^{-2}). Additionally it was observed that samples aged in nitrogen exhibited hydrophobic recovery which was reversed when the samples were stored in water.[160] Similarly, D.J. Wilson reported that storing plasma-treated PTFE in PBS prevented ageing.[158]	162, 163,164, 165
Crystallinity of polymer – those with high crystallinity (glass transition temperature) show a reduced hydrophobic recovery as the polymer chains are less mobile.	Glass temperature can be analysed using DSC (Differential Scanning Calorimetry) Note: In high power long treatment time plasmas, the temperature has the potential to reach T_g for some polymers.		162, 164, 166, 167, 168
Storage Temperature	Store samples at different temperatures and use WCA and/or XPS to determine if this makes a difference.	Nakamatsu *et al.* showed that storage at 100°C promoted a larger degree of hydrophobic recovery than when stored at 50°C.	143, 162, 169
Surface groups	XPS and FTIR	Work by R.K. Wells reported	153, 170

moving into the bulk to decrease surface energy		changes in the oxidised surfaces of polyethylene and polystyrene. The degree of crosslinking in the polystyrene surface reduced the amount of hydrophobic recovery observed.[170] Guckenberger stated that thermoplastics (of which PTFE is one) do not undergo surface diffusion.[153]	

3.2.2 Two-Step Gas Plasma Treatment

The use of a two-step gas plasma treatment rather than single-step is something that is comparatively under researched. In 2003, P. Favia *et al.* investigated the use of a hydrogen plasma pre-treatment (40 W, 60 s, 0.27 mbar) in tandem with an ammonia plasma treatment (20 W or 100 W, 60 s, 0.27 mbar). The aim of the hydrogen plasma step was to limit the hydrophobic recovery, and they reported a WCA of 40° (40 W H_2 followed by 20 W NH_3). They claimed this was stable, once recovery from 24° to 40° had occurred after 8 days storage in air, however no details of any solvent rinse process were given, and the water droplets appear to have been allowed to dry on the surface.[171]

Shin *et al.* reported oxygen (120 W, 90 s) and hydrogen (250 W, 90 s) sequential plasma treatments of PTFE resulting in improved roughness and hydrophilicity (untreated 12 nm, 115°, treated 122 nm, 60°) versus single-step oxygen plasma treatment (120 W, 90 s, 70 nm, 80°).[172] They reported a further decrease in the WCA when using O_2-H_2 two-step plasma treatment (60° after two-step 120 W, 90s O_2 and then 250 W, 90 s H_2 treatment) instead of single-step H_2 treatment (80° after 120 W, 90 s single-step H_2 treatment). Note that this sequential treatment is twice as long as any of the single-step treatments to which it is compared. Additionally this WCA (60°) was not as good as that achieved by a higher power (250 W, 90 s) single-step H_2 treatment (52°).[172] Although this paper is in Korean and not published in English, it appears that none of these samples were washed in any solvents prior to analysis.

Work by C-Y. Tu *et al.* reported the use of sequential hydrogen plasma and ozone treatment as a method to activate the PTFE surface prior to monomer grafting in solution.[173] They reported that the hydrogen plasma treatment facilitated

an otherwise ineffective ozone treatment in order to produce surface peroxides for grafting. The wettability of the surface prior to grafting processes was not reported.[64]

3.2.3 Single-Step Oxygen Plasma Treatment

In previously published work, oxygen plasma treatment of PTFE has been used to create superhydrophobic surfaces. The use of oxygen as a feed gas for plasma results in the roughening of the PTFE surface, and an associated increase in hydrophobicity. However it is postulated that the use of an oxygen pre-treatment step prior to a second hydrophilizing gas plasma treatment step could result in increased hydrophilicity of the final surface.

Note that stability of oxygen plasma-treated PTFE surfaces is reported by some groups in the literature to not be subject to hydrophobic recovery,[171] however, as many groups report that the surfaces are not stable.[176] Zanini *et al.* reported that samples with substantially increased surface roughness (plasma power ≥ 100 W) are less susceptible to post-plasma surface oxidation, and the OH functionalization penetrates into the bulk rather than just occurring at the surface (shown by XPS).[176]

Table 3: Summary of best prior art for the static WCA after single-step low-pressure oxygen plasma treatment of PTFE.

Power / W	**Time / s**	**WCA After Treatment / °**	**WCA Aged / °**	**WCA After Washing / °**	**Ageing Comment**	**Roughness**	**Ref.**
1000	Pulsed treatment for 1 h	160	148	No wash process	After 30 days	-	174
70	120	Too hydrophobic to measure	-	No wash process	-	Strong increase in RMS observed	140
100	900	Adv. 170, rec. 160	-	No wash process	-	SEM shows significant etching of the surface	175
20	600	Adv. 105, rec. 20	Adv. 115, Rec. 20	No wash process	Samples measured after 30 days storage in air	Decreased from 70 nm for untreated to 50 nm	176
300	600	Adv. 145, rec. 155	Adv.145, rec. 140	No wash process		Increased from 70 nm for untreated to 550 nm	176
300	20	-	41	No wash process	WCA measured	-	177

300	600	-	23	No wash process	20-24 h after treatment, samples not washed	-	177

The highest WCA (too hydrophobic to measure) was achieved after oxygen treatment (120 s, 70 W) by Vandencasteele *et al.*[140] The highest aged sample was after pulsed oxygen plasma treatment (1000 W, 1 h) which after 30 days recovered from 160° to 148°.[174] There were no reports of samples that were washed after plasma treatment.

3.2.4 Two-Step Oxygen then Non-Depositing Gas Plasma

As previously mentioned, Shin *et al.* combined hydrogen and oxygen treatments together with limited success. P. Favia *et al.* also used oxygen plasma (100 W, 60 s, 0.27 mbar) as a pre-treatment to NH_3 plasma treatment (20 W, 60 s, 0.27 mbar). This was shown to be ineffective in modifying the PTFE surface; the single-step oxygen plasma treatment did not increase the WCA, and the two-step treatment resulted in a stable surface of approx. 95°, although this surface was not washed.[171]

3.2.5 Summary

The lowest reported WCA after a solvent wash process was by J.P. Badey *et al.* after an ammonia plasma treatment (Adv. 53°, rec. 15°, samples washed for 1 h with a Soxhlet extraction in methanol immediately after treatment).[141]

3.3 CHARACTERIZATION OF PLASMA-TREATED SURFACES

3.3.1 AFM

The observed CA of a surface is affected by the composition of the surface, but also by the surface structure. The type of PTFE and the method by which it is manufactured has a significant effect on the appearance of the untreated polymer under AFM analysis. For the most part, there are no obvious features reported on the untreated PTFE, Table 4. Goodfellow PTFE, which is used in this work, is reported universally to have an uneven texture from the granular process, as well as tribological deformation resulting from the aforementioned manufacturing slicing process, Chapter 1.

Table 4: Summary of roughness values and reported features for untreated PTFE from the literature. Listed in ascending RMS value.

PTFE type	Wash Process	Scan Area	RMS / nm	Features Seen	Ref.
Goodfellow	Washed in ethanol	10 x 10 μm	Only images given	Untreated sample was smooth and featureless	178
Goodfellow	Isooctane	Not given	Only images given	Smooth and featureless	179
Goodfellow	Propan-2-ol/ Cyclohexane 50/50 mix	2 x 2 μm	Only images given	The constituent particles and surface voids are clearly discernible in the AFM micrograph of untreated PTFE. Also evidence of the tribological deformation from manufacturing process.	180
No brand name given	Not given	5 x 5 μm	Only images given	No clear features	181
DuPont	Washed ultrasonically in	5 x 5 μm	6.6	No information given	182

	ethyl alcohol				
Gaflon	Soxhlet extraction in methanol	1.5 x 1.5 μm	7.5	No information given	187
Goodfellow	None given	1 x 1 μm	9.2	No information given	183
Gaflon	Soxhlet extraction in methanol	5 x 5 μm	9.8	No information given	187
Gaflon	Soxhlet extraction in methanol	30 x 30 μm	14.4	No information given	187
Plumber's tape	15 mins ultrasonic bath in 1:8 solution of acetone:distilled water	1 x 1 μm	14 ± 2.3	No obvious features. A lot smoother than the sheet form. Alveolar features caused by oxygen/helium treatment	184
Goodfellow	Pure methanol then pure isooctane	5 x 5 μm	17	Undulations seen in the image, however no comment made	185
Goodfellow	Not given	Not given	18.8	No information given.	186
Gaflon	Soxhlet extraction in methanol	100 x 100 μm	22.2	Untreated surface has a smooth surface. Extended plasma treatment (argon) caused nano-hillocks to be formed.	187
Goodfellow	Methanol then pure isooctane	5 x 5 μm	25	Relatively smooth when untreated, rougher upon treatment.	188
Nitto Denko	Washed in acetone in ultrasonic washer	Not given	29.9	No description given.	189
Nünchritz	In ethanol in	10 x 10	40 ± 5	No details given.	190

GmbH	ultrasonic bath for 15 mins	µm			
Brand not given	Not given	10 x 10 µm	47.30	Described as having high surface roughness causing “inhomogenous” subsequent plasma treatment.	191
Goodfellow	Soxhlet extraction with acetone for 45 mins	10 x 10 µm	52	No description given.	192
Goodfellow	15 mins ultrasonic bath in 1:8 solution of acetone:distilled water	1 x 1 µm	50 ± 5.3	Constituent particles before pressing are discernible on the surface, the average size of which being 1 µm. Uniaxial alignment of surface texture is indicative of the tribological deformation during manufacture.	184
Goodfellow	30 min extraction with acetone, and rinsed with doubly distilled water.	10 x 10 µm	60	Surface described as rough.	193
Brand not given	Acetone then PROPAN-2-OL in succession	100 x 100 µm	70 nm	No description given, no obvious features, but surface is rougher than after O_2 plasma (10 mins treatment time, Power 20 W)	194
Goodfellow	Pure ethanol and then isooctane	225 x 225 µm	100	The surface is relatively smooth	195

				and featureless	
Brand name not given	Propan-2-ol	5 x 5 μm	239	No description given.	196
Nitto Denko	Not given	Not given	539	No description given.	197
Goodfellow	Sonicated in ethanol for 5 minutes	196.7 x 196.7 μm	1300 ± 300	Only comment made was it was not assumed to be smooth.	198

In terms of the reported roughness or RMS of the surface, there is a large range of values reported in the literature, for the most part the values are low (below 50 nm). However for larger scan sizes, an RMS as high as 1300 nm was reported for Goodfellow PTFE.[198] The variation in RMS value can be partly explained by the varying scan sizes, and this trend is observed in the results presented in this study, whereby larger scan sizes result in an average higher RMS.

M.E. Ryan *et al.* reported that there was evidence in the AFM of the manufacture process. Namely that there were “constituent particles and surface voids” visible on the surface, as well as evidence of tribological deformation as the surface texture is “uniaxially” aligned. [180]

3.4 EXPERIMENTAL

3.4.1 Plasmachemical Modification

PTFE substrates (10 x 15 mm samples, Goodfellow Cambridge Ltd., thickness 0.25 mm, FR301350/20, Batch no. 300291002) were washed in 1:1 v/v solution of propan-2-ol (99.5%, CAS no. 67-63-0, Fisher Scientific UK Ltd.) and cyclohexane (99% purity, CAS no. 110-82-7, Fisher Scientific UK Ltd.) for at least 5 min, and air dried (60 min) in a petri dish to minimize aerial contamination prior to plasma treatment.

The plasma treatments were carried out in a cylindrical glass reactor (5 cm diameter, 475 cm^3 volume) housed in a Faraday cage, (Figure 19). This was connected to a two stage rotary pump (model E2M2, serial no. 68120 FF, pumping speed 27 L min^{-1}, Edwards Vacuum Ltd.,) via a liquid nitrogen cold trap, with a base pressure of 5 $x10^{-4}$ mbar. A copper coil (6 mm diameter, 12 turns, spanning 101 mm) was externally wound around the glass reactor, and connected to a 13.56 MHz radio frequency (RF) generator (initially Tegal Corporation, subsequently using model ACG-3LP3, serial no. 5101, ENI Power Systems (now a part of MKS Instruments Inc.). An L-C matching unit was used to minimize the standing wave ratio (SWR) of power transmitted from the RF generator. The leak rate of the plasma apparatus was less than 9.2 $x10^{-9}$ mol s^{-1} throughout the experimental procedure. For each experiment, samples were placed in the glow region of the plasma, and in the remote region.

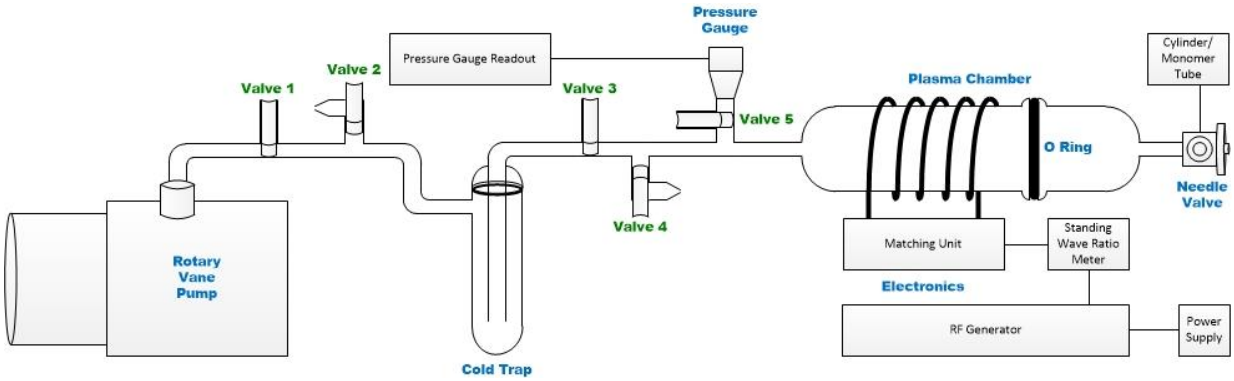

Figure 19: Schematic representation of low-pressure plasma reactor. Created by James Wigzell and reproduced with thanks.

The ammonia gas was introduced into the chamber from a lecture cylinder (ammonia anhydrous, purity 99.99+%, CAS no. 7664-41-7, Catalogue no. 29,499-3, Lot no. 01919E2, Aldrich Chemical Co.). The flow rate of ammonia gas into the

chamber through the Swagelok metering valve (part code SS-SS4, Swagelok Teeside Fluid Systems Technologies Ltd.) was 1.22 $x10^{-7}$ mol s^{-1}.

For the oxygen plasma treatment (2–50 W, 3–600 s, 0.2 mbar), oxygen was introduced to the chamber from an outdoor cylinder (99.5% purity, size W, Barcode 21001178436564, BOC Ltd.) through a wall mounted regulator and metering valve (part code SS-SS4, Swagelok Teeside Fluid Systems Technologies Ltd.). Instead of using the standard rotary pump oil, a Fomblin oil (ID JT291, Series YLVAC 06/C, Code H11301019, Ausimont UK Ltd.) pump (E2M2 FOM pump, serial number 68120 FF, Edwards Vacuum Ltd.) was used.

A number of different combinations of two-step plasma treatments were carried out. For the first, prior to ammonia plasma treatment, an argon plasma treatment was performed. Argon (Pureshield Argon, 99.998% purity, size W, ISO 14175-I7-Ar, UN1006, EC 231-147-0, Barcode Number 2111174784788, BOC Ltd.) was introduced into the chamber from a cylinder through PVC 6.5 tubing and a Swagelok metering valve (part code SS-SS4, Swagelok Teeside Fluid Systems Technologies Ltd.). The chamber was purged for 5 min prior to plasma ignition (5–40 W, 120 s, 0.2 mbar). After argon plasma treatment, the chamber was pumped down to base pressure before ammonia (ammonia anhydrous, 99.99+% purity, CAS no. 7664-41-7, Catalogue no. 29,499-3, Lot no. 01919E2, Aldrich Chemical Co.) was introduced into the chamber as before. The chamber was purged for 10 mins with ammonia before the pressure was stabilised at 0.2 mbar, and plasma ignited (5–40 W, 120 s). After plasma treatment, the plasma was extinguished, and the chamber purged for 5 mins, before being pumped back down to base pressure.

In the same manner, oxygen plasma treatment (50 W, 600 s, 0.2 mbar, same equipment arrangement as previously described) was coupled with an argon plasma treatment (5–50 W, 120–180 s, 0.2 mbar). A modification to this was to flow the argon through a bubbler containing either distilled water or ammonia water (ammonium hydroxide, 28% purity, CAS no. 1336-21-6, Lot no. 04819JA, Aldrich Chemical Co.) prior to being admitted to the plasma chamber and plasma being ignited (1–50 W, 120–600 s, 0.2 mbar).

Oxygen plasma treatment (50 W, 600 s, 0.2 mbar) was also coupled with ammonia plasma treatment (2–20 W, 20–300 s, 0.2 mbar) in a two-step process.

3.4.2 Contact Angle

Static water contact angles (WCA) were measured using the sessile drop method (VCA 2500XE instrument, AST Products Inc., 1 µL ultra-high purity (UHP) water

droplets, ISO 3696 Grade 1). Three droplets were placed on each sample and the WCA recorded for each. The WCA of the samples was measured immediately after plasma treatment, and after washing in propan-2-ol and cyclohexane (1:1 v/v solution) (10 s or 2 min) in a 1:1 v/v solution of propan-2-ol (purity 99.5%, Fisher Scientific UK Ltd.) and cyclohexane (purity 99%, Fisher Scientific UK Ltd.)), followed by air drying (60 min). In the same manner, the hexadecane (*ReagentPlus*®, purity 99%, CAS no. 544-76-3, Lot no. STBF4225V, Sigma-Aldrich Company Ltd.), and ethanol (HPLC grade, CAS no. 24-25-7, Catalogue no. E/0665DF/17, Fisher Scientific UK Ltd.) contact angles were also measured, termed HCA and ECA respectively.

3.4.3 Optical Emission Spectroscopy

Optical emission spectroscopy of the plasma was carried out using OOIBASE software (Ocean Optics Inc.) running on Windows 3.1 computer (OPUS). The fibre used was 100 µm (Ocean Optics Inc., Cat. No. QP100-2-UV-BX, OOS-0038505-02), and was measuring the wavelength range 200–1200 nm using the Master OOS 2 port. The integration time was 585 ms, and the summation was set to 10 scans.

The ammonia plasma was run at 50 W after a 10 min purge time, and at a pressure of 0.2 mbar. The measurements were continued until the presence and intensity of peaks were constant (5 min). The fibre was placed looking at the glow region of the plasma, positioned 3 cm from the chamber.

3.4.4 Surface Tension Measurement

Surface tensions of the wash liquor were measured after washing (2 min) plasma-treated PTFE samples in 1 mL of either UHP water, or propan-2-ol and cyclohexane solution (1:1 v/v). Static surface tensions were measured using a tensiometer (FTA200, First Ten Ångstroms Inc.). Drop shape analysis was carried out on a pendant drop which had been ejected from a syringe (Hamilton, 250 µl) to the point just before break off. The shape of the drop was fitted to the Young-Laplace equation (Equation 3.1) to give the equilibrated surface tension of the solution.[199,200]

$$\Delta p = \gamma \left(\frac{1}{R_1} + \frac{1}{R_2}\right)$$

Equation 3.1

where Δp is the pressure difference across the air/fluid interface (N m^{-2}), γ is the surface tension (N m^{-1}), and R_1 and R_2 are the princpropan-2-oll radii of curvature

(m). The Young-Laplace equation assumes the shape of the drop is entirely determined by gravity and surface tension.

Prior to measurement, the syringe was rinsed 40 times with UHP water, and then 10 times with the sample solution. In order to reduce the effect of pixel size on the accuracy of the measurments, it was ensured that the pendant drop occupied at least 75% of the vertical height of the image.[200] The tensiometer was calibrated using the known external diameter of 3 mm standard sphere (received with tensiometer, First Ten Ångstroms Inc.), and UHP water surface tension measurements. Static surface tensions were measured for each solution until three successive readings within ±0.1 mN m^{-1} had been recorded.

3.4.5 Scanning Electron Microscopy

SEM was carried out using FEI Helios Nanolab Mk2 microscope operating in secondary electron mode, and running at 5 kV. Samples were coated with 20 nm of gold palladium prior to analysis, and images taken at 4 magnifications (1000x, 2500x, 10000x, and 20000x). Plasma-treated samples were analysed both before and after solvent washing (2 min, propan-2-ol and cyclohexane 1:1 v/v solution, dried vertically in dry nitrogen stream for 10 s).

3.4.6 ATR-FTIR

FTIR spectra were obtained using a PerkinElmer Frontier IR, using a U-ATIR accessory, a Diamond element (Diamond/KRS-5, serial no. 27281) and CsI windows. Spectra were obtained between 4000–400 cm^{-1}, at a resolution of 1 cm^{-1}, and averaged over 32 scans. Plasma-treated samples were analysed both before and after solvent washing (2 min, propan-2-ol and cyclohexane 1:1 v/v solution, dried vertically in dry nitrogen stream for 10 s).

3.4.7 AFM

AFM measurements were taken using a Nanoscope V (Bruker, Model RTESPA, Part no. MPP-11120-10) with Multimode 8, and using ScanAsyst technology. The measurements were taken using both in tapping mode in air, and in ScanAsyst mode using Feedback autocontrol settings with parameters as follows; scan size = 0.5–50 μm, scan rate = 0.977 Hz, 512 samples/line, feedback gain 10.66–11.87, PeakForce setpoint 1.891 V, aspect ratio = 1.0, capture direction = down, amplitude setpoint = 250.00 mV, and drive amplitude = 1499.94 mV.

3.4.7.1 Tip Specification:

Geometry: Rotated (symmetric)

Tip height: 15–20 µm

Front Angle (FA): 15° ± 2 °

Back Angle (BA): 25° ± 2 °

Side Angle (SA): 17.5° ± 2 °

Tip Radius: 8 nm

Tip SetBack (TSB): 15 µm

3.4.7.2 Cantilever Specification:

Material = 0.01–0.025 Ω cm Antimony (n) doped Si,

Wafer = A047/20, Coating Front side = none, Coating back side = 50 ± 10 nm Al.

Thickness: 3.75 µm

Geometry: Rectangular

Table 5: Nominal, minimum, and maximum values for resonant frequency, spring constant, and dimensions of cantilever

	Nom.	**Min.**	**Max.**
Resonant Frequency / kHz	300	200	400
Spring Constant / Nm^{-1}	40	20	80
Length / µm	125	115	135
Width / µm	35	30	40

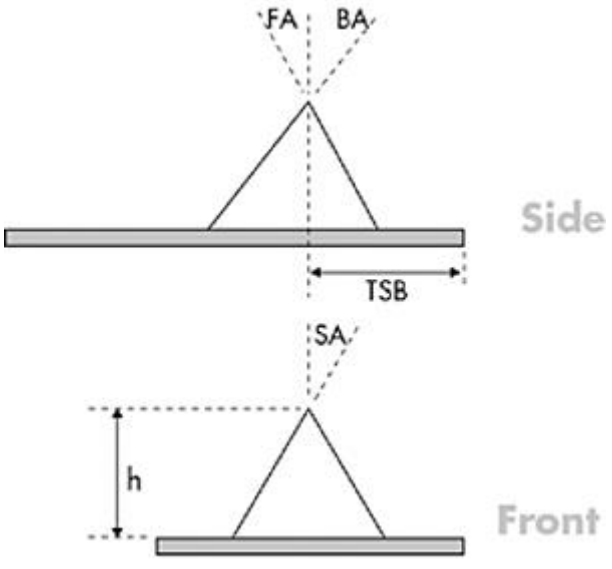

Figure 20: Schematic of cantilever and tip set up including relevant angles and height.

3.4.8 X-Ray Photoelectron Spectroscopy

XPS analysis of untreated and plasma-treated PTFE were carried out both prior to and after solvent washing (propan-2-ol and cyclohexane 1:1 v/v solution). Each sample was analysed in three separate locations on each sample. XPS was performed using a K-Alpha instrument (Thermo Scientific UK Ltd.) using microfused monochromatic AlKa X-ray source (1486.6 eV, 12 kV, 3 mA, and 36 W). Survey spectra used a pass energy of 150 eV, a step size of 0.4 eV, and a dwell time of 10 ms. High resolution spectra for C(1s), F(1s), N(1s) and O(1s) were also taken using a pass energy of 40 eV, a step size of 0.1 eV, and a dwell time of 100 ms. All the samples were mounted on a clean stainless steel plate and immobilised with copper clips. The largest X-Ray spot available in this instrument (nominal 400 micron diameter) was used on all the measurements. Charge compensation was used throughout the measurements. XPS was carried out by Dr Jose Portoles at NEXUS Newcastle University. XPS instrument files were exported in VAMAS format, and subsequently analysed using CasaXPS software version 2.3.18. Spectra were fitted with a Shirley background, and then the peaks fitted using a number of Gaussian-Lorentizian functions. The sensitivity factors associated with F, N, and O were set automatically relative to C by the CasaXPS software.

3.4.9 GC-MS

PTFE samples were solvent washed after plasma treatments (120 s, 1 mL, propan-2-ol and cyclohexane 1:1 v/v solution). Wash liquors and standard controls (propan-2-ol alone, cyclohexane alone, and propan-2-ol and cyclohexane 1:1 v/v solution) were analysed using GC-MS (Shimadzu QP2010-Ultra, 70 eV, mass range 35–650 u, carrier gas Helium at a rate of 0.41 mL min^{-1}, and injection volume 0.5 µL).

The samples were analysed using both an EI-GC non-polar molecule and an EI-GC polar molecule methodology. For the non-polar method, the column used was Rxi-5Sil MS with dimensions 0.15 µm x 10 m x 0.15 mm. For the polar method, the column used was Rxi-17Sil MS with dimensions 0.15 µm x 10 m x 0.15 mm. Instrument files were exported in .swx format, and analysed using MestreNova (version 7.1.2-10008) software.

3.5 RESULTS – Coupling Hydrophilizing Plasma Treatments

Initially work was carried out looking at single-step hydrophilizing plasma treatments. As each plasma chamber and equipment set-up would yield different plasma conditions and therefore different results, it was important to map the results space for this equipment.

Different plasma powers and duration times were compared for hydrophilization efficacy using the change induced in the static water contact angle with respect to the untreated PTFE substrate (129 ± 3°).

The sessile drop method of measuring the WCA angle of the plasma modified surfaces is a facile and cheap way of determining the hydrophilic nature of the surface produced by the plasma treatment. This was therefore used as a method of determining the best plasma treatment to produce a stable hydrophilic PTFE surface.

3.5.1 Single-step Argon Plasma

From the literature, it was evident that an argon plasma treatment was a method which results in significant defluorination of the polymer surface, and therefore a large decrease in WCA.

Table 6: Summary of results obtained for the water contact angle (WCA) before and after washing samples that had been subjected to an argon plasma treatment (5–20 W, 120 s, 0.2 mbar). SWR describes the standing wave ratio, and is a measure of the balance of plasma. These samples were created prior to use of a new RF generator. All samples were washed in propan-2-ol and cyclohexane mixture (1:1 by volume) for 10 s and air dried for at least 60 min prior to analysis.

Power /W	**SWR**	**WCA (unwashed) / °**	**WCA (unwashed) / °**	**WCA (washed) / °**	**WCA (washed) / °**
		Glow	**Remote**	**Glow**	**Remote**
0	-	-	-	129 ± 3	129 ± 3
5	1.1–2.5	48 ± 9	49 ± 9	49 ± 4	52 ± 5
20	1.6–2.5	51 ± 8	50 ± 13	58 ± 5	59 ± 8

3.5.2 Single-Step Ammonia Plasma

Ammonia plasma has been reported in the literature to cause a significant decrease in WCA, N. Inagaki *et al.* reported adv. WCA as low as 16° immediately after plasma treatment.[139] The process of washing the surface after plasma treatment removes any particulates from the surface, and has widely been reported to cause hydrophobic recovery similar to that observed after surfaces are aged in ambient conditions. The method by which hydrophobic recovery occurs is contested in the literature, and discussed in Table 2, Section 3.2.1. Solvent washed samples

(Soxhlet extraction in methanol for 1 h) were reported by J.P Badey *et al.* were measured to have an adv. WCA of 53° and a rec. angle of 15°.[141]

3.5.2.1 Wettability

This section encompasses the results from a power study of the effect on WCA of ammonia plasma-treated PTFE. In the literature it is reported that the degree of defluorination and amine group grafting onto polymer surface is strongly dependent on the plasma conditions. Conditions that resulted in lower ion energies or high concentrations of NH_3^+ resulted in higher degrees of defluorination.[201] In this work, with the aim of inducing hydrophilicity in the surface, defluorination is important, but also the stable grafting of hydrophilic groups onto the surface. If the only aim is defluorination, then the use of an inert plasma such as argon would be most effective, Section 3.5.1. In the case of ammonia plasma, the aim is to defluorinate the surface in order to make space on the polymer chain for the nitrogen containing groups within the plasma to be grafted.

Data is included for the unwashed samples immediately after plasma treatment, and the same samples after washing in propan-2-ol and cyclohexane (1:1 v/v solution), and air drying for 60 min prior to sessile drop analysis.

The largest decrease in WCA (final WCA of 22°) was achieved with the samples placed in the glow region of a 20 W ammonia plasma. Washing the surface (with 1:1 v/v solution of propan-2-ol and cyclohexane) for 10 s caused hydrophobic recovery to 50°.

In the prior art, the lowest reported aged sample had a WCA of 60° and this was using a mixture of water and argon as the feed gas.[144]

Table 7: Summary of results obtained for the water contact angle (WCA) before and after washing samples that had been subjected to an ammonia plasma treatment (5–40 W, 120 s, 0.2 mbar). All samples were washed in propan-2-ol and cyclohexane mixture (1:1 by volume) for 10 s and air dried for at least 60 min prior to analysis. Presented is the average WCA and the standard deviation of the sample.

Approx. Power / W	SWR	Time / s	WCA (unwashed) / °		WCA (washed) / °	
			Glow	Remote	Glow	Remote
0	-	-	-	-	129 ± 3	129 ± 3
6	1.4–3.0	120	43 ± 9	54 ± 10	61 ± 7	73 ± 10
10	1.0–1.6	120	54 ± 6	55 ± 11	68 ± 6	67 ± 9
20	1.2–1.5	120	22 ± 9	33 ± 10	50 ± 13	56 ± 8
30	1.1–1.4	120	65 ± 12	66 ± 8	79 ± 7	79 ± 7
40	1.0–1.2	120	68 ± 5	74 ± 6	74 ± 7	78 ± 10

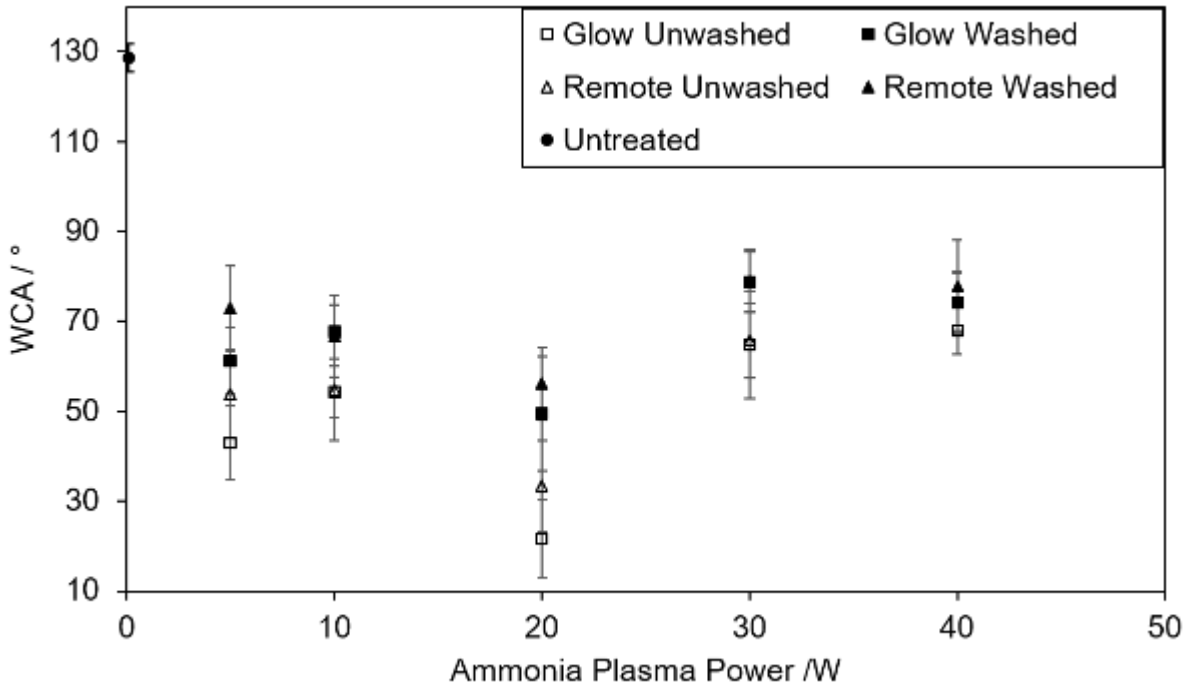

Figure 21: Effect of washing process (1:1 v/v solution of propan-2-ol:cyclohexane, 10 s) on Goodfellows PTFE samples treated with ammonia plasma on WCA achieved (5–40 W, 120 s, 0.2 mbar). Each power was repeated 3 times. The markers show the average WCA achieved, and the error bars denote the standard deviation of the sample.

From these results (Figure 21 and Table 7), it can be seen that the lowest WCA (50° ± 13° in the glow plasma region, and 56° ± 8° in the remote plasma region) is achieved after NH_3 plasma treatment for 120 s at 20 W (0.2 mbar). The lowest WCA achieved in this study after solvent washing for 10 s is 50 ± 13°, which

is similar to that reported in the literature immediately after plasma treatment (the lowest reported solvent washed samples had a adv. WCA of 53°, and rec. WCA of 15°, but this surface recovers to 70° after 10 h).[141] Note that the method by which static WCAs are measured is comparable to adv. WCAs as there is no prolonged equilibrium process carried out prior to measurement. Studies using solvent washing for 2 min are reported in section 3.5.3.4. It is possible that further hydrophilization of the surface could be achieved by optimizing the plasma treatment time.

3.5.2.2 OES

One of the difficulties of low-pressure plasma is that the leak rate can have a significant effect on the character of the plasma. In some cases, the air can improve the modification effects of the plasma, but equally it can have an adverse effect on the process. In this work, the leak rate of the system was always kept at better than 9.2 $x10^{-9}$ mol s^{-1}, and so the ingress of air over these relatively short plasma treatment times should not have a significant effect. OES can be used as a tool to ensure that there is no air causing the observed modification processes.

As the brightness of an ammonia plasma is less intense than its air or fluorinated counterparts, higher plasma powers (50 W) had to be used in order to obtain sufficient intensity on the OES spectrum. As the breakdown processes within a plasma, especially the decomposition reaction rates, are affected by the plasma power, the species observed in an OES at a higher power will not be the same as those in a lower power plasma, but any unexpected species will be more easily observable when the intensity of the peaks is increased. In this work, the radical concentrations will not be assessed as the analysis of the substrate upon removal from the system allows for the modification to be investigated without particular attention to the exact composition of the plasma to be determined.

From the literature, plasma decomposition of NH_3 results in primarily the formation of NH, NH_2, H and H_2, however some secondary species are also produced by secondary reactions. These include N_2, N_2H_2, and N_2H as well as more of the primary species. The concentration of these secondary species will be significantly lower than that of the primary species.[202]

Primary decomposition of ammonia gas within a plasma is into NH_2 and H or NH and H_2, and subsequent decomposition of NH_2, are the major reactions present in the plasma, Equations 3.2.1–3.2.3.[203,204]

$NH_3 \rightarrow NH_2 + H$ Equation 3.2.1

$NH_2 \rightarrow NH + H$ Equation 3.2.2

$NH_3 \rightarrow NH + H + H$ Equation 3.2.3

These decomposition reactions are occurring simultaneously with radical processes, Equations 3.2.4–3.2.10, although there is a little agreement in the literature as exactly which radical reactions are occurring and at what rate.[203]

$2NH_2 \rightarrow N_2H_4$ Equation 3.2.4

$2NH_2 \rightarrow NH_3 + NH$ Equation 3.2.5

$2NH \rightarrow N_2H_2$ Equation 3.2.6

$2NH \rightarrow N_2 + H_2$ Equation 3.2.7

$H + NH_2 \rightarrow NH_3$ Equation 3.2.8

$H + NH_3 \rightarrow H_2 + NH_2$ Equation 3.2.9

$NH + NH_3 \rightarrow N_2H_4$ Equation 3.2.10 [203,205]

The OES spectrum recorded in for this work, Figure 22, matches closely what is theoretically expected, and that which was reported by S.J. Kang *et al.*[202] This indicates that the observed changes in WCA are due to the ammonia plasma rather than any air that could be present in the system, hence any oxygen groups which are present on the ammonia treated surfaces must have come from the atmosphere upon removal from the vacuum system. In the literature, ammonia plasma has been reported to result in the grafting of groups such as CN, NH_2, COOH, and $CONH_2$ on the surface.[201] XPS of these surfaces produced in this work will indicate whether the subsequent exposure to air influences the surface.

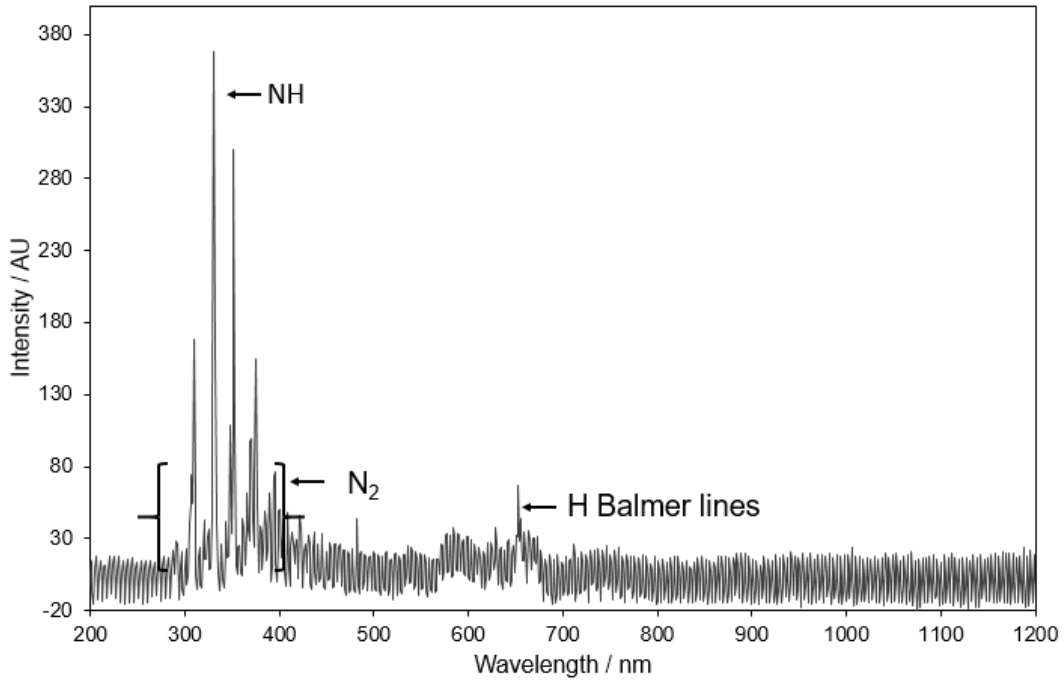

Figure 22: OES of NH_3 plasma (50 W, 5 mins, 0.2 mbar). Labelled are the significant peaks as labelled in NH_3 OES by S. Kang *et al.*[202]

3.5.3 Two-Step Argon then Ammonia Plasma

It is postulated that the argon step causes crosslinking of the surface prior to the incorporation of nitrogen moieties by the ammonia plasma, using a similar approach to as previously reported for plasma oxidation of polyolefins using an argon first step followed by an oxygen containing gas second step.[206]

3.5.3.1 Power Simplex Optimization

Following initial screening of the parameter space, simplex optimization of the plasma power conditions was employed to achieve the best possible surface modification.[207] The highest overall WCA was achieved after a 40 W Ar and 20 W NH_3 plasma treatment (120 s Ar plasma then 120 s NH_3 plasma, 0.2 mbar). The lowest overall WCA was measured after a 20 W Ar and 5 W NH_3 plasma treatment (120 s Ar plasma then 120 s NH_3 plasma, 0.2 mbar). These measurements were taken after solvent washing (1:1 v/v propan-2-ol:cyclohexane solution), when the samples were stable. In the literature, the lowest reported washed sample had a WCA of 60°, the 20 W Ar and 5 W NH_3 plasma treatment resulted in a lower WCA of 50°.[144]

It should also be noted that the calculated standard deviation on the average values obtained is quite high. It is postulated that this is due to the nonuniformity of the surface morphology induced by plasma treatment. This change in surface morphology is exacerbated as the plasma power is increased. Further work using AFM and optical microscopy would be necessary to prove this hypothesis. Further information on the simplex methodology can be found in the Supporting Information, Section 7.2.

Table 8: WCA achieved using different power combinations of argon and ammonia plasma treatment (5–40 W, 120 s Ar then 120 s NH_3, 0.2 mbar). Entries shaded in green correspond to lowest values. All samples were washed in propan-2-ol and cyclohexane mixture (1:1 by volume) for 10 s and air dried for at least 60 min prior to analysis. Highlighted in green is the lowest WCA achieved for a solvent washed substrate.

Argon Power / W	**SWR Argon**	**Ammonia Power / W**	**SWR Ammonia**	**WCA (unwashed) / °**	**WCA (unwashed) / °**	**WCA (washed) / °**	**WCA (washed) / °**
				Glow	**Remote**	**Glow**	**Remote**
(untreated)	-	(untreated)	**-**	**-**	**-**	129 ± 3	129 ± 3
0	-	5	1.4–3.0	54 ± 10	43 ± 8	73 ± 9	61 ± 7
0	-	10	1.0–1.6	55 ± 11	54 ± 6	67 ± 9	68 ± 6
0	-	20	1.2–1.4	22 ± 9	33 ± 10	50 ± 13	56 ± 8
0	-	30	1.0–1.4	66 ± 8	65 ± 12	79 ± 7	79 ± 7
0	-	40	1.0–1.2	74 ± 6	68 ± 5	78 ± 10	74 ± 7
5	1.1–2.5	0	-	48 ± 9	49 ± 9	49 ± 4	52 ± 5
20	1.6–2.5	0	-	51 ± 8	50 ± 13	58 ± 5	59 ± 8
5	1.0	5	1.0–1.2	42 ± 12	47 ± 5	59 ± 14	61 ± 5
5	1.0–1.4	20	1.1–1.5	29 ± 5	38 ± 14	67 ± 8	50 ± 4
20	1.0–1.4	5	1.0–1.8	30 ± 15	24 ± 16	51 ± 14	48 ± 9
20	1.0–1.2	20	1.2–1.8	24 ± 18	29 ± 22	55 ± 15	55 ± 9
40	1.0–1.5	20	1.1–1.4	93 ± 9	69 ± 25	93 ± 7	87 ± 17
40	1.4–1.8	5	1.1–1.8	52 ± 27	62 ± 22	71 ± 21	72 ± 25
10	1.0–1.4	10	1.0–1.4	70 ± 13	54 ± 10	77 ± 11	60 ± 10
30	1.0–1.7	10	1.0	43 ± 15	37 ± 7	65 ± 10	60 ± 11
30	1.0–1.5	15	1.0–1.4	82 ± 10	65 ± 10	87 ± 17	77 ± 11

(a)

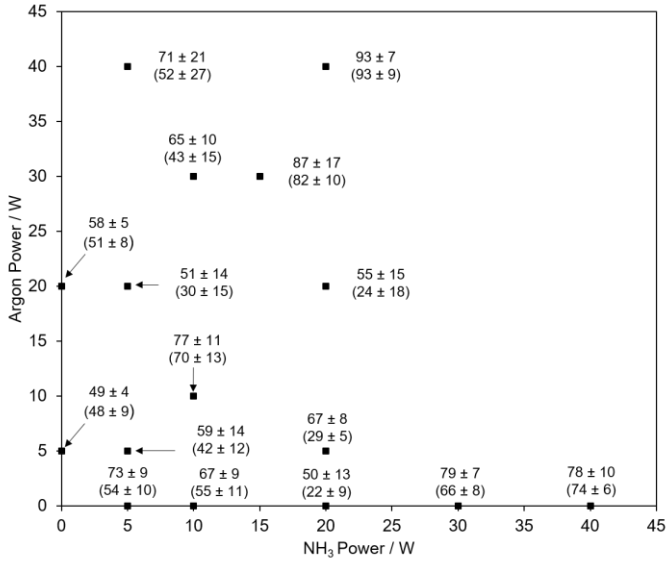

(b)

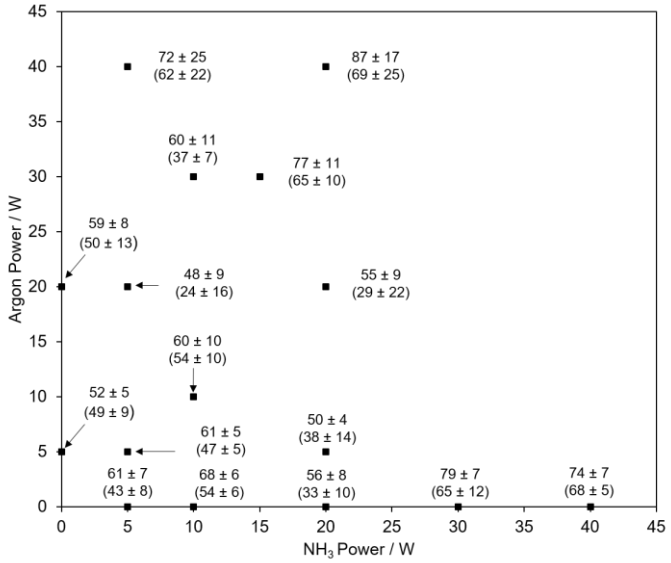

Figure 23: Average WCA achieved for samples in the (a) glow plasma region and (b) remote plasma region using different power combinations of argon and ammonia plasma treatment (5–40 W, 120 s Ar then 120 s NH_3, 0.2 mbar) after solvent washing (1:1 v/v propan-2-ol:cyclohexane solution, 10 s). Average WCA achieved for samples in the remote plasma region after single-step ammonia plasma treatment (5–40 W, 120 s, 0.2 mbar), and single-step argon plasma treatment (5–20 W, 120 s, 0.2 mbar), are also shown. Numbers in brackets correspond to the average WCA achieved prior to solvent washing. Errors shown are the standard deviation of the sample.

3.5.3.2 Time Simplex Optimization

Once the optimum power conditions were determined (20 W argon plasma followed by 5 W ammonia plasma treatment), the treatment time was optimized using the simplex method, Table 9.

Table 9: WCA achieved using different treatment time combinations of argon and ammonia plasma treatment (20 W Ar then 5 W NH_3, 30–120 s, 0.2 mbar). All samples were washed in propan-2-ol and cyclohexane mixture (1:1 by volume) for 10 s and air dried for at least 60 min prior to analysis. Errors shown are the standard deviation of the sample.

Argon Treatment time / s	**SWR Argon**	**Ammonia Treatment time / s**	**SWR Ammonia**	**WCA (unwashed) / °**	**WCA (unwashed) / °**	**WCA (washed) / °**	**WCA (washed) / °**
				Glow	**Remote**	**Glow**	**Remote**
120	1.0–1.4	120	1.0–1.8	30 ± 15	24 ± 16	51 ± 14	48 ± 9
30	1.0–1.4	120	1.0–1.1	32 ± 7	44 ± 5	60 ± 4	67 ± 3
120	1.0–1.5	30	1.0–1.2	94 ± 7	101 ± 9	100 ± 6	103± 5
210	1.0–1.1	120	1.0–1.4	46 ± 3	58 ± 5	75 ± 9	75 ± 14
120	1.1–1.2	210	1.0–1.1	26 ± 3	25 ± 6	59 ± 5	62 ± 8
165	1.1–2.0	165	1.0–1.5	30 ± 9	45 ± 7	78 ± 15	84 ± 10

(a)

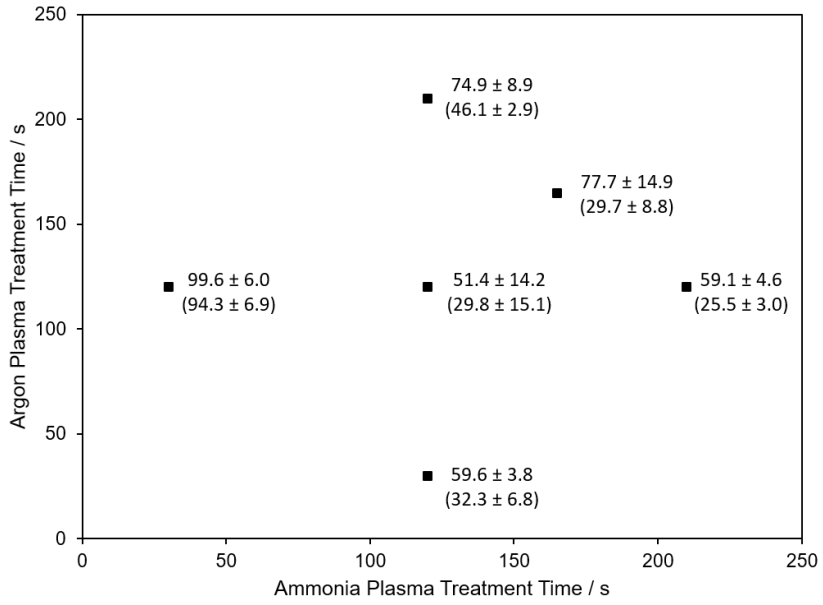

(b)

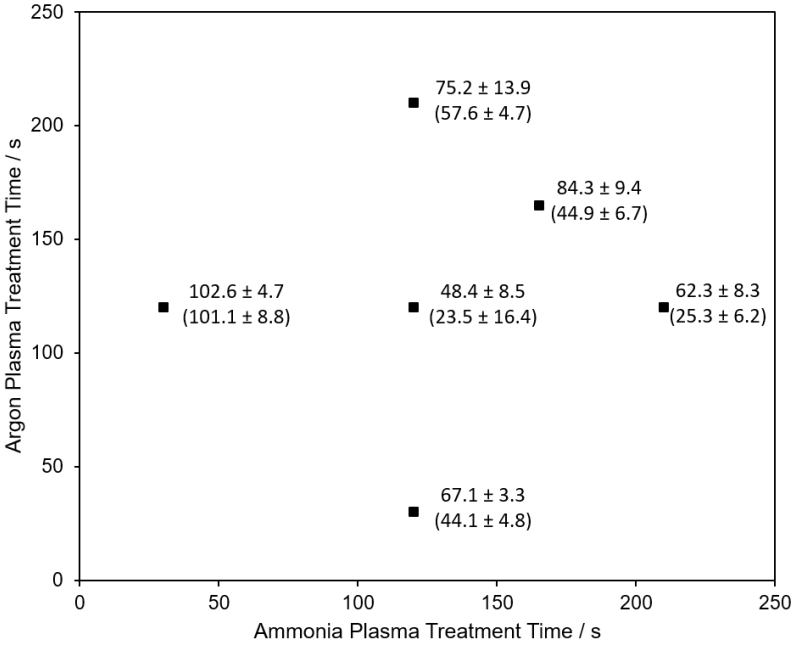

Figure 24: Average WCA achieved for samples in the (a) glow plasma region and (b) remote plasma region using different treatment time combinations of argon and ammonia plasma treatment (20 W, 30–210 s Ar plasma treatment, then 5 W, 30–210 s NH_3 plasma treatment, both at 0.2 mbar) after solvent washing (1:1 v/v solution propan-2-ol:cyclohexane, 10 s). Numbers in brackets correspond to the average WCA achieved prior to solvent washing. Errors shown are the standard deviation of the sample.

The lowest WCA achieved after two-step argon and ammonia plasma treatment and 10 s solvent washed was 51 ± 14° (unwashed 30 ± 15°) after glow plasma and 48 ± 9° (unwashed 24 ± 16°) after remote plasma treatment and 10 s solvent washed.

3.5.3.3 Summary 10 s solvent washing

Table 10: Summary of the best (lowest WCA) argon and ammonia single-step and two-step plasma treatments (0.2 mbar) of PTFE. All samples were washed in propan-2-ol and cyclohexane mixture (1:1 by volume) for 10 s and air dried for at least 60 min prior to analysis. Errors shown are the standard deviation of the sample.

Ar / W (Time / s)	Ammonia / W (Time / s)	Glow / Remote	WCA (unwashed) / °	WCA (washed) / °
5 (120)	0 (0)	Glow	48 ± 9	49 ± 4
5 (120)	0 (0)	Remote	49 ± 9	52 ± 5
0 (0)	20 (120)	Glow	22 ± 9	50 ± 13
0 (0)	20 (120)	Remote	33 ± 10	56 ± 8
20 (120)	20 (120)	Glow	24 ± 18	55 ± 15
20 (120)	20 (120)	Remote	29 ± 22	55 ± 9
20 (120)	5 (120)	Glow	30 ± 15	51 ± 14
20 (120)	5 (120)	Remote	24 ± 16	48 ± 9

The aim of this work was to achieve a low and stable WCA after solvent washing. It was hypothesised that the combination of argon and ammonia plasma treatment would limit the hydrophobic recovery observed since after a 5 W argon glow plasma, the solvent washed (10 s) WCA (49 ± 4°) was not different to that measured immediately after treatment (48 ± 9°).

Within experimental error:

- Before washing, the lowest WCA achieved in this study is 24 ± 18° for 2 step plasma treatment, and 22 ± 9° for single-step ammonia plasma treatment. These values are significantly higher than the best reported in the literature (less than 4° after argon and ammonia-water mixture plasma treatment).[147] Regardless, solvent washing shows that these surfaces are unstable and recover to higher WCA values.
- 5 W argon glow / remote plasma treatment provides a stable surface which is not affected by solvent washing (10 s) to give values of 49 ± 4° and 52 ± 5° respectively. Previously, argon plasma treatment has been reported to achieve a WCA of 30° immediately after plasma treatment.[135,136] These surfaces were not stable, as after 1 hour storage in air, the surfaces recovered to 65°.[136] There are no reported solvent washed argon plasma-treated samples.

- A WCA value of approx. 50° is also possible after washing (10 s) single-step 20 W ammonia plasma (glow).
- However, 20 W ammonia plasmas have significantly larger error ranges. Therefore, 5 W argon glow plasma to give a value of 49 ± 4° after solvent washing (10 s) is preferable.
- The best solvent washing (10 s) data after treatment with two-step argon (20 W, 120 s) and ammonia (5 W, 120 s) plasma is 48 ± 9°. However, this overlaps with just single-step argon glow plasma (49 ± 4°), and also with single-step glow ammonia plasma (50 ± 13°). Therefore there is no clear benefit can be drawn for the two-step process.
- In the literature, the lowest WCA achieved using any non-depositing plasma gas after solvent washing (methanol) was an adv. WCA of 53°, and rec. WCA of 15°, but this surface recovers to 70° after 10 h.[142]

3.5.3.4 Two Minute Wash Process

After changing the RF power generator, the plasmas created were now perfectly balanced, with an SWR of 1.0. Additionally it was necessary to determine how the plasma-treated surfaces recovered after a longer solvent wash process, Table 11. A two minute process was chosen based on Greenwood *et al.* (1997).[152] Each sample was placed in 10 mL of wash liquor (propan-2-ol and cyclohexane 1:1 v/v solution) in individual jars, and removed with tweezers and air dried.

Table 11: Summary of the WCA achieved after balanced ammonia and argon plasma, and washed for 2 min. Errors shown are the standard deviation of the sample. (Values in brackets are for 10 s solvent washing taken from Table 10.) Highlighted in green is the lowest WCA achieved for a solvent washed substrate.

Feed Gas	Power / W	SWR	Time / s	WCA (unwashed) / °		WCA (washed) / °	
				Glow	Remote	Glow	Remote
-	0	-	-	-	-	129 ± 3	129 ± 3
Ammonia	5	1.0	120	42 ± 1	53 ± 1	62 ± 1	69 ± 3
	20	1.0	120	38 ± 8 (22 ± 9)	53 ± 2 (33 ± 10)	64 ± 3 (50 ± 13)	66 ± 3 (56 ± 8)
Argon	5	1.0	120	112 ± 1 (48 ± 9)	107 ± 3 (49 ± 9)	109 ± 1 (49 ± 4)	112 ± 2 (52 ± 5)
	20	1.0	120	43 ± 4	31 ± 2	55 ± 4	47 ± 5

When compared with the data achieved using the previous RF generator, there is a significant difference in the data achieved for 5 W argon plasma treatment, Table 10 and Table 11. It is possible that the observed change in WCA

could also be due to the change in solvent wash time (10 s to 120 s), and so a wash duration study was carried out; Section 3.5.3.4.1

3.5.3.4.1 Wash Process Duration Study

In order to determine the effect of washing duration on the WCA of the sample, a wash time study was carried out. In order to exclude plasma to plasma variation from the study, 12 samples were placed into the chamber at once. The overall amount of PTFE present in the chamber must be the same as that previously in the chamber (4 samples) so the samples were made smaller. This also allowed the positioning of the samples in the remote and glow regions to be the same as in previous work, Figure 25. Samples were washed individually in a 1:1 v/v solution of propan-2-ol and cyclohexane for times ranging for 5 to 300 s, Table 12.

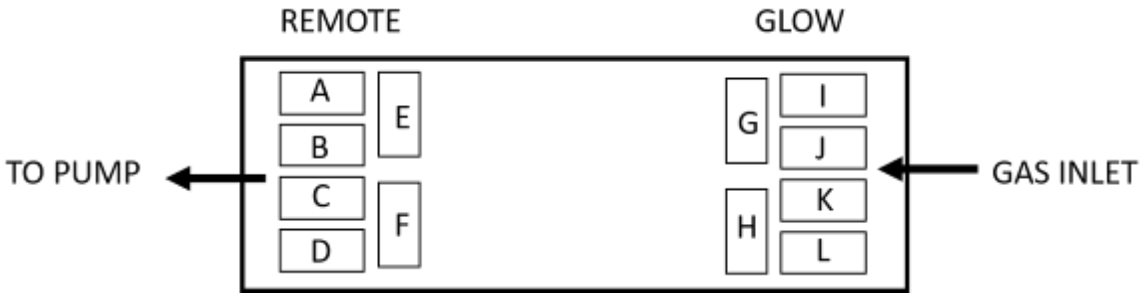

Figure 25: Chamber layout for 12 samples.

Table 12: Sample wash duration.

Samples	Wash Duration / s
A + G	5
B + H	10
C + I	30
D + J	60
E + K	120
F + L	300

Table 13: Effect of solvent washing duration (5–300 s, 1:1 v/v solution of propan-2-ol and cyclohexane) on argon plasma-treated samples (5 or 20 W, 120 s, 0.2 mbar). Reported is the mean WCA, and the standard deviation of the sample.

Power / W	Wash Duration / s	WCA Unwashed / °		WCA Washed / °	
		Glow	Remote	Glow	Remote
5	5	111 ± 5	106 ± 4	88 ± 11	99 ± 8
	10	111 ± 4	108 ± 3	104 ± 6	106 ± 2
	30	115 ± 2	104 ± 1	97 ± 24	98 ± 7
	60	116 ± 6	109 ± 3	105 ± 4	102 ± 3
	120	118 ± 2	107 ± 1	109 ± 3	106 ± 4

	300	112 ± 3	107 ± 3	89 ± 24	108 ± 3
20	5	113 ± 3	108 ± 4	107 ± 6	98 ± 8
	10	117 ± 3	109 ± 1	117 ± 2	108 ± 1
	30	115 ± 3	113 ± 3	115 ± 1	110 ± 2
	60	112 ± 1	113 ± 2	109 ± 1	110 ± 1
	120	111 ± 2	116 ± 4	112 ± 2	113 ± 2
	300	115 ± 3	112 ± 1	113 ± 2	113 ± 1

Due to the high WCA achieved using argon plasma treatment, it was not possible to see a distinct change between the varying washing times. This indicates that although previously it was thought that the 5 s washing time was to account for the differences between the data recorded using the old RF generator vs the data achieved using the new RF generator, it should be attributed to the change in the balance of the plasma. Previously the plasma was not as well balanced, which had a significant effect on the observed WCA (previously 49° for a 5 W plasma, using the balanced plasma it is in the region of 111°).

In order to accurately assess the effect of the solvent washing duration, it was necessary to use a plasma treatment which would cause the largest decrease in WCA, ammonia plasma treatment (5 W, 300 s, 0.2 mbar), Table 14.

Table 14: Effect of solvent washing duration on WCA (5–300 s, 1:1 v/v solution of propan-2-ol and cyclohexane) on ammonia plasma-treated PTFE samples (5 W, 300 s, 0.2 mbar, 3 external repeats, 1 internal repeat). Each plasma contains 12 samples (3 measurements for each washing time) and there are 3 plasmas (3 external repeats), totalling 9 measurements for each average value given. Reported is the mean WCA, and the standard deviation of the sample. The standard deviation of the mean is included in parentheses.

Wash Duration / s	WCA Unwashed / ° (standard deviation of the mean)		WCA Washed / ° (standard deviation of the mean)	
	Glow	Remote	Glow	Remote
5	37 ± 2 (1)	41 ± 2 (1)	62 ± 9 (3)	63 ± 7 (2)
10	37 ± 3 (1)	37 ± 2 (1)	63 ± 9 (3)	61 ± 3 (1)
30	38 ± 4 (1)	38 ± 3 (1)	63 ± 7 (2)	62 ± 8 (3)
60	36 ± 3 (1)	47 ± 3 (1)	66 ± 6 (2)	66 ± 7 (2)
120	36 ± 2 (1)	42 ± 2 (1)	67 ± 5 (2)	66 ± 4 (1)
300	36 ± 3 (1)	44 ± 3 (1)	68 ± 8 (3)	71 ± 5 (2)

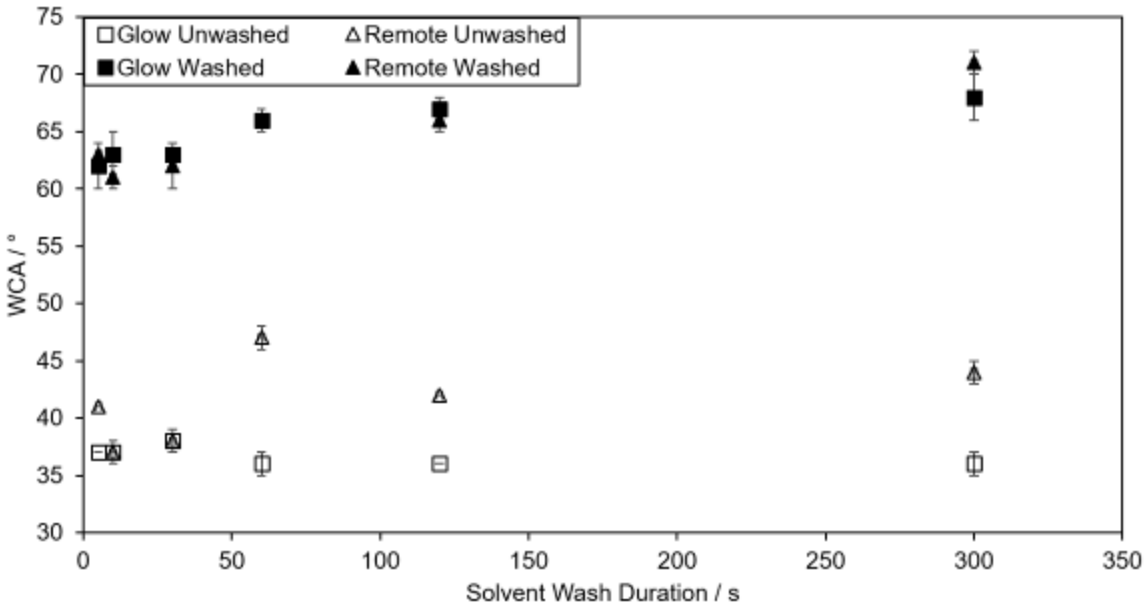

Figure 26: Effect of solvent washing duration on WCA (5–300 s, 1:1 v/v solution of propan-2-ol and cyclohexane) on ammonia plasma-treated PTFE samples (5 W, 300 s, 0.2 mbar, 3 separate repeats). WCA of untreated washed PTFE is 129°. The markers show the average WCA achieved, and the error bars denote the standard deviation of the mean. Each plasma contains 12 samples (3 measurements for each washing time) and there are 3 plasmas (3 external repeats), totalling 9 measurements for each average value given.

From this data (Figure 26 and Table 14), it can be seen that the ammonia plasma-treated surfaces are not stable to solvent washing, and after washing and drying under ambient conditions, there is a significant increase in the WCA. After longer washing durations, the mean WCA is higher on average (glow 68° and

remote 71° after 300 s wash, whereas after 5 s wash glow 62° and remote 63°). However, it should be noted that the when the standard deviation is taken into account, the difference is not significant.

The lowest WCA achieved for plasma-treated PTFE in the literature after solvent washing was an advancing angle of 53° immediately after Soxhlet extraction with methanol for 1 h, Table 1. There is a degree of inaccuracy associated with comparing static WCA such as those measured here with advancing and receding WCA such as those reported by J.P. Badey *et al.* It can be assumed that the static WCA lies between the advancing and receding angles, and so a direct comparison with the advancing angle is the most logical, although this is probably higher than that of the static WCA. Prior to washing, all the reported two-step surfaces are more hydrophilic than 53°, however, after solvent washing and air drying, all the surfaces are more hydrophobic than 53°. It should be noted however, that this surface was unstable, and recovered to advancing angle of 70° after 10 h.[141] The plasma-treated surfaces presented in this study (best 48 ± 9 after solvent washing) are more than 10 h old after solvent washing, and thus these surfaces are better than the best reported in the literature.

3.5.4 Summary

Single-step glow argon plasma resulted in a stable WCA of 52 ± 5° after solvent washing. When compared with the best (for any gas) reported in the literature, this is better than any samples that were aged – i.e. measured a significant amount of time after the plasma process. The lowest initial WCA reported after a single gas plasma was 30° without any solvent wash process, however it was noted that these exhibited significant hydrophobic recovery to 70° within 1 h.[136] Such an increase is not observed in the samples reported in this work.

Single-step glow ammonia plasma resulted in a surface with an initial WCA of 36°, but after solvent washing (2 min) and air drying this recovered to 66°. In the literature the lowest initial WCA reported was an advancing WCA of 16°, however this was using a hot plasma process and the samples were not solvent washed. The lowest solvent washed samples after ammonia plasma-treated were an advancing angle of 53° and a receding angle of 15°. These samples were reported to exhibit hydrophobic recovery to 70° after 10 h.[141]

The single-step plasma-treated data reported here when compared to all the solvent washed data is better than the literature, as the best solvent washed stable surfaces had a WCA of 70°. The initial WCA is not as good as that which is

reported in the literature, 4° reported after single-step argon and ammonia plasma treatment,[147] and 24° reported after single-step argon and water treatment.[144]

After the two-step argon and ammonia plasma treatment, the lowest WCA achieved was 24 ± 16°. This is lower than all of single-step data previously obtained, and after solvent washing, the WCA was stable at 48 ± 9° (argon 20 W, 120 s, followed by ammonia 5 W, 120 s). It is also lower than that which is reported in the literature, when comparing an advancing angle with a static angle.

It was shown that in order to remove the LMWOS successfully from plasma-treated surfaces, the wash process was required to be 120 s rather than any shorter. This removed some of the variability observed between successive runs under the same plasma conditions for the solvent washed results. This did not alter the initial plasma-treated WCA values.

3.6 RESULTS – Coupling Hydrophobizing and Hydrophilizing Plasma Treatments

Oxygen plasma treatments have been shown to increase the WCA of PTFE surfaces by roughening the surface sufficiently to induce a Cassie-Baxter wetting state. The hypothesis is that by introducing a second hydrophilizing plasma step, polar groups may be incorporated onto this roughened surface thus decreasing the observed WCA significantly, indeed below that observed after the single hydrophilizing plasma alone.

3.6.1 Single-Step Oxygen Plasma

The plasma conditions for single-step oxygen treatment were optimized for both power and treatment time simultaneously using the simplex method.

Table 15: WCA achieved using different power and time combinations of single-step oxygen plasma treatment of PTFE, (5–50 W, 30–315 s, 0.2 mbar). All samples were washed in propan-2-ol and cyclohexane mixture (1:1 by volume) for 10 s or 2 min and air dried for at least 60 min prior to analysis. Reported is the mean WCA, and the standard deviation of the sample. The standard deviation of the mean is included where appropriate in parentheses, and the solvent washing duration is included in angle brackets.

Power / W	Time / s	WCA (unwashed) / °		WCA (washed) /° <washing time / s>	
		Glow	Remote	Glow	Remote
0	0	-	-	129 ± 3 <120>	129 ± 3 <120>
2	600	135 ± 1	136 ± 1	130 ± 1 <120>	131 ± 2 <120>
2	1200	137 ± 2	138 ± 2	134 ± 2 <120>	117 ± 17 <120>
5	30	121 ± 3	123 ± 3	116 ± 4 (1) <10>	115 ± 4 (1) <10>
5	120	130 ± 2	130 ± 4	125 ± 2 (0) <10>	125 ± 3 (1) <10>
20	75	129 ± 3	130 ± 4	126 ± 2 (0) <10>	124 ± 5 (1) <10>
20	165	134 ± 3	135 ± 3	125 ± 8 (2) <10>	128 ± 6(1) <10>
5	240	134 ± 3	133 ± 8	127 ± 7 (2) <10>	124 ± 10 (2) <10>
20	240	138 ± 4	139 ± 1	130 ± 2 (0) <10>	135 ± 2 (0) <10>
20	315	138 ± 2	139 ± 4	134 ± 5 (1)	135 ± 4 (1)

				<10>	<10>
30	315	140 ± 1	140 ± 2	135 ± 4 (1) <10>	139 ± 2 (0) <10>
50	315	139 ± 3	143 ± 5	135 ± 2 (0) <10>	139 ± 2 (0) <10>
50	300	137 ± 2	165 ± 9	134 ± 3 (1) <120>	151 ± 15 (4) <120>
50	600	148 ± 13	168 ± 2	139 ± 6 (1) <120>	160 ± 13 (3) <120>

(a)

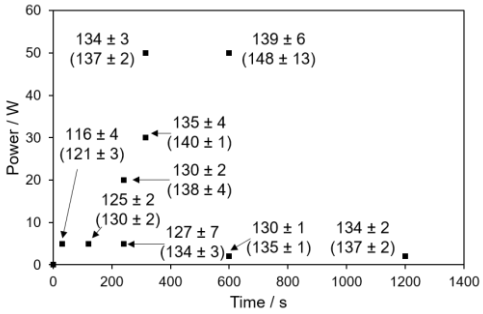

(b)

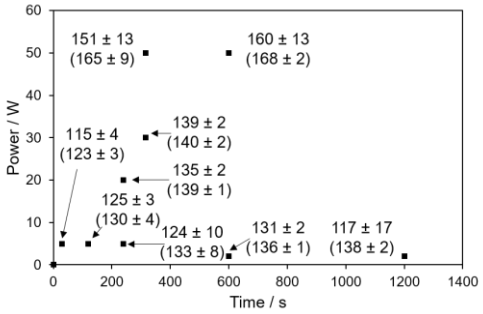

Figure 27: Average WCA achieved for samples in the (a) glow plasma region and (b) remote plasma region using different treatment time combinations of oxygen plasma treatment (2–50 W, 75–1200 s, 0.2 mbar) after solvent washing (1:1 v/v solution propan-2-ol:cyclohexane, 10 s or 2min). Numbers in brackets correspond to the average WCA achieved prior to solvent washing. Errors shown are the standard deviation of the sample.

3.6.2 Two-Step Oxygen then Argon Plasma

WCA as low as 10° were achieved in the literature using argon plasma treatments, Section 3.2.1, and as low as 47° in the previous work reported here, Table 11.

Table 16: WCA achieved using different power and time combinations of two-step oxygen and argon plasma treatment of PTFE, (oxygen plasma 30–50 W, 315–600 s, followed by argon 5–50 W, 30–315 s, all at 0.2 mbar). All samples were washed in propan-2-ol and cyclohexane mixture (1:1 by volume) for 2 min and air dried for at least 60 min prior to analysis. Reported is the mean WCA, and the standard deviation of the sample. The standard deviation of the mean is included where appropriate in parentheses, and the solvent washing duration is included in angle brackets.

Oxygen Power / W (Time / s)	**Argon Power / W (Time / s)**	**WCA (unwashed) / °**		**WCA (washed) /° <washing time / s>**	
		Glow	**Remote**	**Glow**	**Remote**
50 (600)	5 (120)	116 ± 2	130 ± 5	119 ± 4 <120>	113 ± 3 <120>
50 (600)	20 (120)	94 ± 2	105 ± 7	83 ± 5 <120>	100 ± 5 <120>
50 (600)	50 (120)	51 ± 6	127 ± 6	42 ± 5 (2) <120>	113 ± 6 (2) <120>
50 (600)	50 (180)	57 ± 19	124 ± 10	31 ± 25 (6) <120>	107 ± 11 (3) <120>
50 (600)	50 (300)	101 ± 8	113 ± 5	93 ± 16 (5) <120>	99 ± 8 (2) <120>
0	5 (120)	114 ± 3 (1)	108 ± 3 (1)	113 ± 3 (1) <120>	109 ± 3 (1) <120>
0	20 (120)	111 ± 2	116 ± 4	112 ± 2 <120>	113 ± 2 <120>
0	50 (120)	118 ± 1	112 ± 3	-	-

3.6.3 Two-Step Oxygen then Argon Bubbling through Ammonia Water Plasma

In previously reported literature, the incorporation of ammonia water into an argon feed stock resulted in significant reduction in the WCA of PTFE after plasma treatment (Section 3.2.1, Hai *et al.* reported 4°).[147] In light of this, the argon feed gas was bubbled through ammonia water prior to entry into the plasma chamber, Table 17.

Table 17: WCA achieved using different power and time combinations of two-step oxygen and argon bubbling through ammonia water plasma treatment of PTFE, (oxygen plasma 30–50 W, 315–600 s, followed by argon bubbling through ammonia water 5–50 W, 30–315 s, all at 0.2 mbar). All samples were washed in propan-2-ol and cyclohexane mixture (1:1 by volume) for 2 min and air dried for at least 60 min prior to analysis. Reported is the mean WCA, and the standard deviation of the sample. The standard deviation of the mean is included where appropriate in parentheses, and the solvent washing duration is included in angle brackets.

Oxygen Power / W (Time / s)	**Argon/Ammonia Water Power / W (Time / s)**	**WCA (unwashed) / °**		**WCA (washed) /°**	
		Glow	**Remote**	**Glow**	**Remote**
0	0	-	-	129 ± 3 <120>	129 ± 3 <120>
30 (315)	1 (600)	106 ± 5	112 ± 2	105 ± 3 <120>	107 ± 3 <120>
50 (600)	50 (120)	106 ± 6	117 ± 8	108 ± 4 <120>	110 ± 2 <120>
50 (600)	50 (180)	111 ± 1	114 ± 4	114 ± 3 <120>	107 ± 1 <120>
0	5 (120)	104 ± 4	98 ± 7	105 ± 2 <120>	104 ± 2 <120>
0	20 (120)	84 ± 9	100 ± 4	87 ± 15 <120>	104 ± 4 <120>
50 (300)	Argon bubbling through water 5 (120)	122 ± 2	128 ± 4	121 ± 2 <120>	122 ± 3 <120>
50 (300)	Argon bubbling through water 20 (120)	124 ± 0	126 ± 1	122 ± 1 <120>	121 ± 1 <120>
0	Argon bubbling through water 5 (120)	104 ± 4	98 ± 7	105 ± 2 <120>	104 ± 2 <120>
0	Argon bubbling through water 20 (120)	108 ± 5	107 ± 2	108 ± 2 <120>	105 ± 2 <120>

From the data presented here, it can be seen that the presence of the ammonia in the system has the effect of increasing the reduction of the WCA in comparison to argon bubbling through water alone, Table 17.

3.6.4 Two-Step Oxygen then Ammonia Plasma

As the findings from Section 3.6.3 indicated that the presence of ammonia in the feed gas stream reduced the observed WCA, and low WCA was achieved using single-step ammonia plasma (Section 3.5.2,) this was coupled with an oxygen treatment in a two-step treatment, Table 18.

Table 18: WCA achieved using different power and time combinations of two-step oxygen and argon bubbling through ammonia water plasma treatment of PTFE, (oxygen plasma 50 W, 600 s, followed by ammonia plasma 2–20 W, 30–300 s, all at 0.2 mbar). All samples were washed in propan-2-ol and cyclohexane mixture (1:1 by volume) for 2 min and air dried for at least 60 min prior to analysis. Reported is the mean WCA, and the standard deviation of the sample. The standard deviation of the mean is included where appropriate in parentheses, and the solvent washing duration is included in angle brackets. Highlighted in green are the lowest WCA achieved for a solvent washed single-step plasma process, and the lowest WCA achieved for washed and unwashed two-step plasma-treated PTFE.

Oxygen Power / W (Time / s)	**Ammonia Power / W (Time / s)**	**WCA (unwashed) / °**		**WCA (washed) /°, (standard deviation of the mean), <solvent wash duration / s>**	
		Glow	**Remote**	**Glow**	**Remote**
50 (600)	0	148 ± 13	168 ± 2	139 ± 6 (1)-<120>	160 ± 13 (3)-<120>
0	5 (300)	38 ± 3 (1)	43 ± 5 (1)	60 ± 6 (1) <120>	60 ± 5 (1) <120>
0	5 (120)	36 ± 2 (1)	42 ± 2 (1)	67 ± 5 (2) <120>	66 ± 4 (1) <120>
0	20 (120)	38 ± 8	53 ± 2	64 ± 3 <120>	66 ± 3 <120>
50 (600)	2 (300)	20 ± 6	105 ± 20	85 ± 2 <120>	121 ± 6 <120>
50 (600)	5 (30)	131 ± 1	140 ± 2	132 ± 1 <120>	138 ± 2 <120>
50 (600)	5 (120)	35 ± 8	98 ± 6	88 ± 2 <120>	122 ± 1 <120>
50 (600)	5 (300)	10 ± 0	14 ± 7 (1)	41 ± 10 (3) <120>	52 ± 15 (3) <120>
50 (600)	20 (300)	41 ± 5	78 ± 5	66 ± 3 <120>	78 ± 5 <120>

From the investigation, it can be seen that the solvent washed WCA data for single-step ammonia plasma-treated PTFE (approximately 66° for both plasma

regions) and that achieved after two-step oxygen then ammonia plasma treatment (56° for glow region, and 64° for remote plasma region) are not significantly different if the standard deviation of the sample is taken into account. When only the standard deviation of the mean is considered, the samples from the glow region after the two-step plasma treatment are significantly lower than those after the single-step ammonia treatment.

Additionally, in both the glow and remote regions, the unwashed samples have significantly different wettabilities depending on the treatment.

The presence of the oxygen step prior to the ammonia plasma results in a significant decrease in the WCA (<10°), such that it cannot be accurately measured by the sessile drop method. For this two-step process, the adv. WCA after solvent washing is 47 ± 6°, and the rec. WCA is 29 ± 3°. This is a lower adv. WCA than that reported in the literature (53°).[141]

3.6.5 Summary

Table 19: Summary of the best (lowest) WCA of PTFE achieved using oxygen multistep plasma treatments. Errors shown are the standard deviation of the sample. Highlighted in green is the highest WCA achieved for a single-step oxygen plasma after solvent washing, and the lowest WCA achieved for a two-step plasma-treated PTFE substrate after solvent washing.

O_2 / W (Time / s)	**Gas / W (Time / s)**	**Glow / Remote**	**WCA (unwashed) / °**	**WCA (washed) / ° <wash time / s>**
0	0	-	140 ± 1	129 ± 3 <120>
50 (600)	0	Glow	148 ± 13 <120>	139 ± 6 <120>
50 (600)	0	Remote	168 ± 2 <120>	160 ± 13 <120>
50 (600)	Argon / 50 (120)	Glow	51 ± 6	42 ± 5 <120>*
50 (600)	Argon / 20 (120)	Remote	105 ± 7	100 ± 5 <120>
30 (315)	Argon and Ammonia water / 2 (600)	Glow	69 ± 2	50 ± 1 <120>
30 (315)	Argon and Ammonia water / 2 (600)	Remote	85 ± 6	67 ± 14 <120>
50 (600)	Ammonia / 5 (300)	Glow	10 ± 0	41 ± 10 (3) <120>
50 (600)	Ammonia / 5 (300)	Remote	11 ± 1	52 ± 15 (3) <120>

* A lower value of 31 ± 25 also reported (180 s, 20 W argon treatment after oxygen plasma), but the large error value indicated a non-uniformity of the surface modification.

In the literature, the highest WCA achieved using oxygen plasma gas was 160°[174] and there was no reported data for WCA after solvent washing. The remote

plasma-treated (50 W, 600 s, 0.2 mbar) samples in this study (Table 19) are, within error, the same as these reported values after solvent washing.

The lowest WCA possible is achieved is using an oxygen plasma (50 W, 600 s) in tandem with an ammonia plasma (5 W, 300 s), which consistently gives a WCA of less than 10°. After solvent washing, hydrophobic recovery is observed. The glow plasma-treated samples recover to 41 ± 3°, and the remote treated samples recover to 53 ± 3°, where the errors quoted are the standard deviation of the sample.

In the literature, the lowest WCA achieved using any non-depositing plasma gas after solvent washing (methanol) was an adv. WCA of 53°, and rec. WCA of 15°, but this surface recovers to 70° after 10 h.[142] In this work, the oxygen and ammonia two-step process results in a lower adv. WCA of 47 ± 6° and a rec. angle of 29 ± 3°. The slightly higher rec. angle for these surfaces results in an overall lower hysteresis that that reported in the literature. Here θ_H is 18°, and in the literature θ_H was 38°.

3.7 RESULTS – Characterization of Plasma-treated Surfaces

3.7.1 Surface Roughness

Due to the granular method by which the PTFE is manufactured, there are distinct rolling hill features on the surface, which gives an overall high value for the surface roughness, even on the untreated PTFE.

Goodfellow PTFE film is manufactured by pressing PTFE powder into a press before heating it in an oven to fuse the granules together into a block. Even though PTFE is a thermoplastic, due to the high molecular weight, the melt viscosity is extremely high and so there is no flow during this process. Once the PTFE rod has been made, the film is produced using a "skiving" process, where a large blade is used to peel to film of the bulk rod. This skiving process is what causes the uniaxial striations on the surface of the film.[152,208]

3.7.1.1 SEM

SEM was used as a tool to determine the changes observed on the surface after oxygen and ammonia plasma treatments, Table 20. The images obtained for the untreated PTFE surfaces indicate that the surfaces appear uniform at the 100 micron scale, and have the linear striations caused by the manufacturing process. However at higher magnification, it is clear that there are a number of defects on the surface. Some appear as "holes" in the top layer where the component polymer strands from the bulk are visible. Others appear as simply indentations on the surface. Aside from these defects, the untreated PTFE is smooth and featureless, which is similar to that reported in the literature, and shown in Figure 18 and Figure 28.

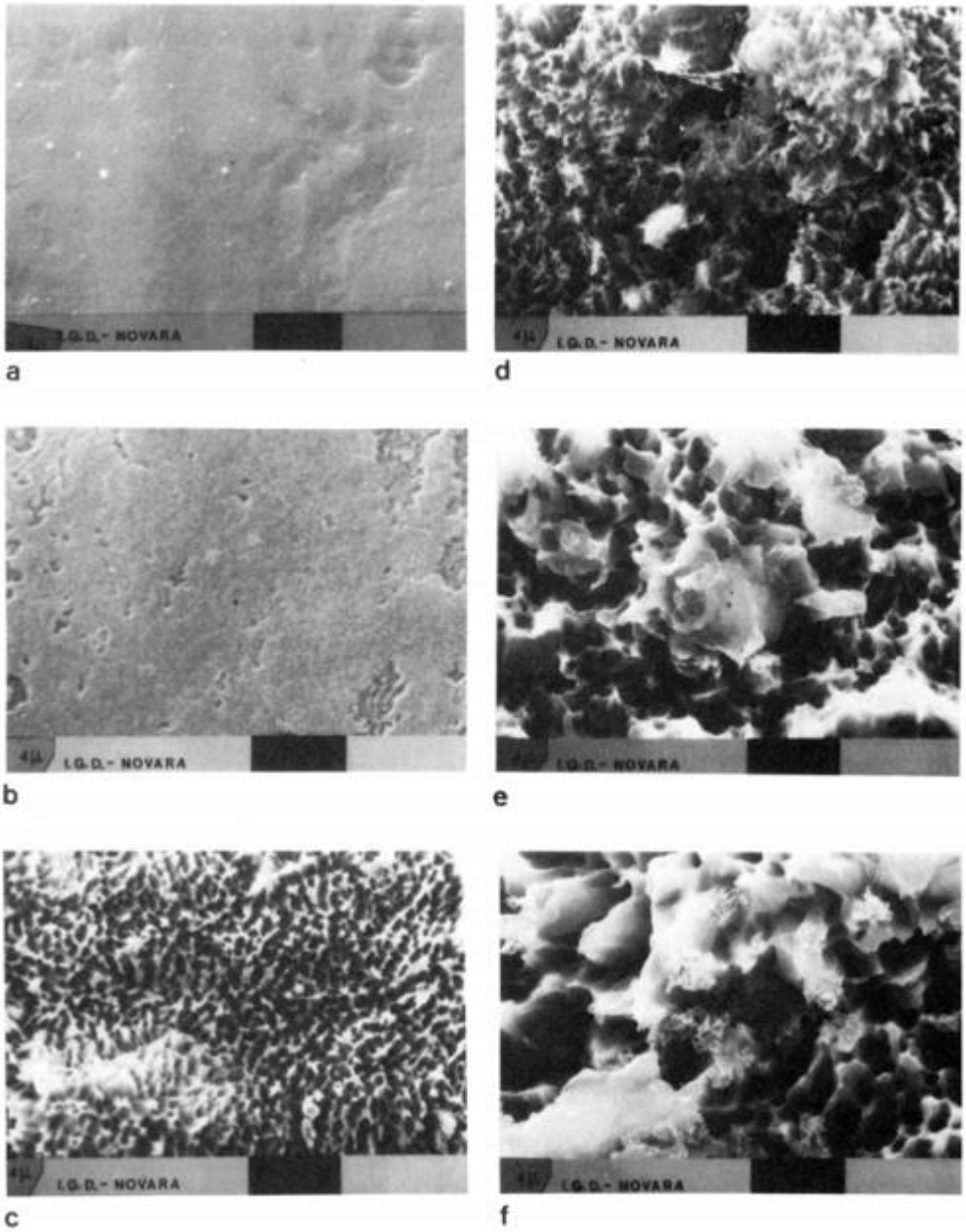

Figure 3. SEM results: (a) untreated sample; (b) after 1 min; (c) 2 min; (d) 5 min; (e) 10 min; (f) 15 min.

Figure 28: SEM results (a) untreated sample, (b) after 1 min oxygen plasma treatment (100 W, 0.02 mbar), (c) 2 min, (d) 5 min, (e) 10 min, and (f) 15 min. Scale bar represented is 4 µm, indicating an image size of approximately 40 µm.[209]

Table 20: Comparison of surface morphology of untreated and plasma-treated PTFE samples prior to solvent washing. SEM carried out using FEI Helios Nanolab Mk2 microscope using secondary electron mode, and running at 5 kV. Samples were coated with 20 nm of gold palladium prior to analysis. SEM carried out by Leon Bowen, Experimental Officer, Department of Physics, Durham University

	Untreated (washed)	**Ammonia, 5 W, 300 s (unwashed)**	**Oxygen, 50 W, 600 s (unwashed)**	**2 step: Oxygen, 50 W, 600 s, NH_3, 5 W 300 s (unwashed)**
100 µm		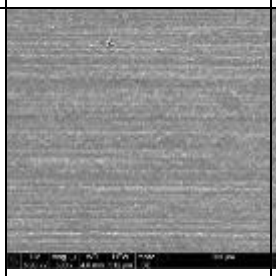	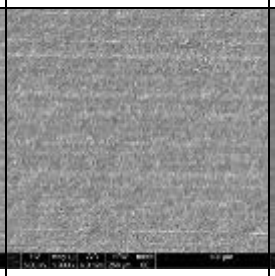	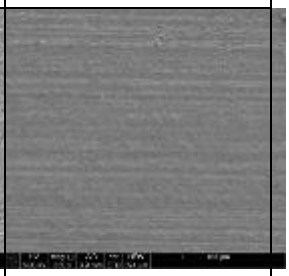
~40 µm	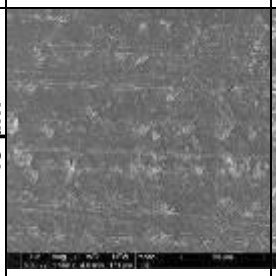	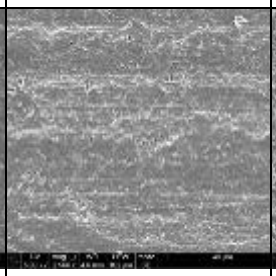	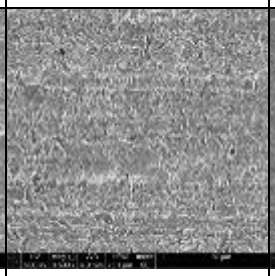	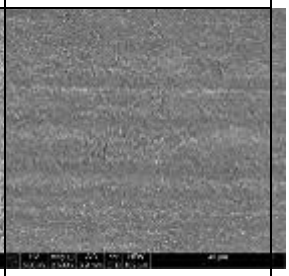
10 µm	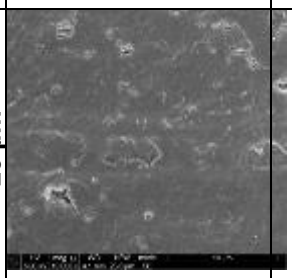		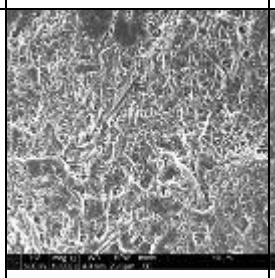	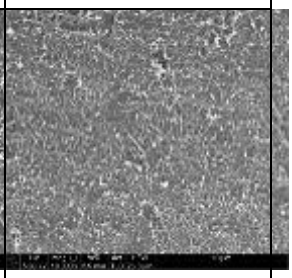
5 µm		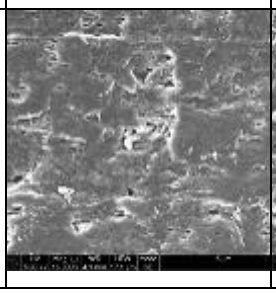	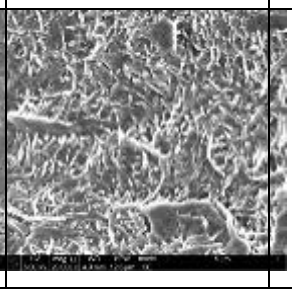	

The SEM images of the untreated PTFE samples indicate there are some indentations and surface defects even before plasma treatment. This indicates the importance of sampling the surface in a number of different regions and averaging the data. The problems that were incurred when using AFM for smaller scan sizes especially can be attributed to this non-uniformity. Any of those features could have caused the loss of contact between the tip and the surface.

The linear striations on the surface are vestigial of the manufacturing process, and are visible at low magnifications (1000x) in the untreated samples and all the plasma-treated samples. These ridges dominate the macrostructure of the PTFE surfaces, however the use of plasma treatment has significantly affected the microstructure of the PTFE, Table 20.

At higher magnifications, it is clear that the plasma processes cause some destruction of the surface, which is to be expected given the duration of the plasma treatments. The ammonia treated surface appears significantly altered with respect to the untreated sample at the 40 µm image size. At much higher magnification, the breaks in the surface to reveal the component strands underneath are visible. The oxygen plasma treatment of the surface is a lot more destructive than the ammonia plasma treatment. As previously discussed, this is an expected phenomenon. The effect of the 10 fold increase in power of the plasma and doubling of the plasma treatment duration is evident when the oxygen and ammonia plasma-treated samples are compared at the 5 µm scan size (approximately 20000x magnification). For the oxygen plasma treatment, it is possible that the long duration and high plasma power of the treatment has resulted in some melting of the component polymer strands together, resulting in regions that are less rough than others. Due to the differences in density of the plasma in the glow region and the remote regions of the chamber, this will be more present on the glow plasma-treated samples. These regions of reduced roughness can be assumed to be the cause of the lower WCA for the glow region samples in comparison to the remote plasma-treated samples (Table 18).

These findings regarding the oxygen plasma treatment are already well known in the literature, and a similar thing can be seen in work reported by Ryan *et al.*, and Morra *et al.* (Figure 28). Oxygen plasma treatments of 5 min or longer were reported to result in an adv. WCA of approx. 170°, and a rec. WCA of >150°.[209]

When the 2 step process is compared with the untreated surfaces, at low magnifications, there are few observable differences, the linear striations still dominate the macrostructure, and appear largely unaffected by the plasma treatment. However at high magnifications, the roughness that has been imparted into the surface is visible. There is some white debris present on the surface after the two-step treatment, which is not present on the untreated, or single-step treated samples. It would be expected that the amalgamation of the two single-step plasma treatments together would result in a surface which resembled a combination of the two surfaces. It appears from the SEM that the use of the ammonia plasma after the oxygen plasma results in a “softening” of the surface roughness. At the 10 µm

image size, the component strands of the PTFE are much smaller on the 2 step treated sample than they are on the single-step oxygen treated samples.

Table 21: Comparison of surface morphology of 2 step plasma-treated PTFE samples prior to solvent washing, and after washing and drying under nitrogen. SEM carried out using FEI Helios Nanolab Mk2 microscope using secondary electron mode, and running at 5 kV. Samples were coated with 20 nm of gold palladium prior to analysis. SEM carried out by Leon Bowen, Experimental Officer, Department of Physics, Durham University

Scale bar size	**2 step: Oxygen, 50 W, 600 s, NH_3, 5 W 300 s (unwashed)**	**2 step: Oxygen, 50 W, 600 s, NH_3, 5 W 300 s (washed)**
100 µm	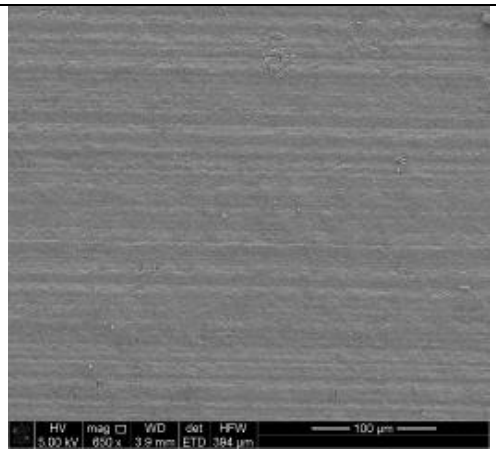	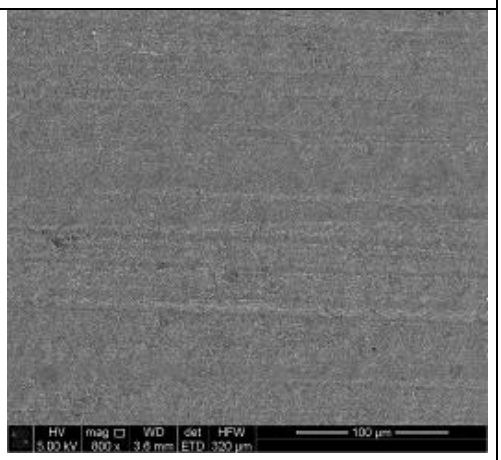
40 µm	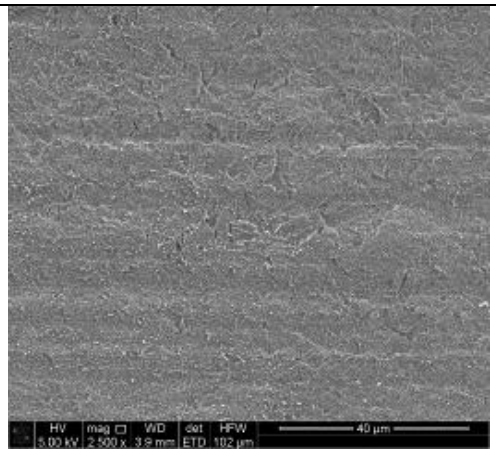	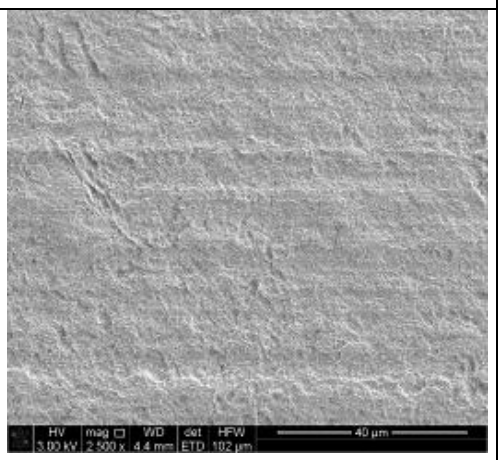
10 µm	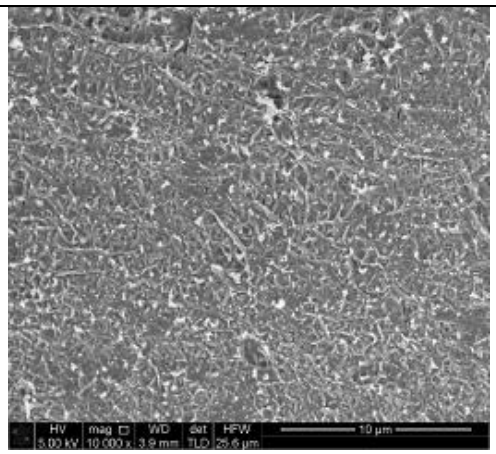	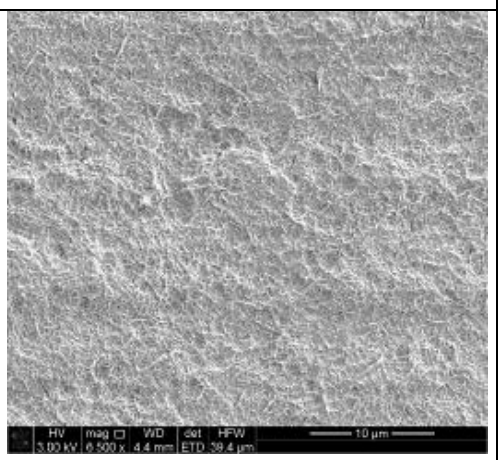

From Table 21, it is clear that the effect of solvent washing on the two-step plasma-treated surfaces is the removal of the submicron size white debris from the surface. This coupled with the observed increase in WCA (Table 18) after solvent washing would indicate that the effect of the solvent wash is to remove LMWOS species from the surface. Through the analysis of the wash liquor, the identity of these species may be further investigated.

3.7.1.2 Large scan size AFM using ScanAsyst Technology

In the SEM images, Section 3.7.1.1, the changes in roughness were visible, but the images did not allow for quantification of this change. In order to measure the change in the surface morphology, AFM was used.

In order to overcome the challenges associated with analysing such a rough surface with AFM, ScanAsyst mode was used. This mode allows for the feedback gain to be automatically controlled by the software, thus reducing the chance of losing contact with the surface.

Table 22: AFM of untreated and Two-step plasma-treated PTFE (oxygen 50 W, 600 s, followed by ammonia 5 W, 300 s, 0.2 mbar, back filled with nitrogen for 10 mins after plasma treatment). Plasma-treated samples were analysis both before and after solvent washing.

Plasma Treatment	**Scan Size / µm**	**2D image**	**3D image**	**RMS / nm**	**Image surface area difference /%**
Untreated	5	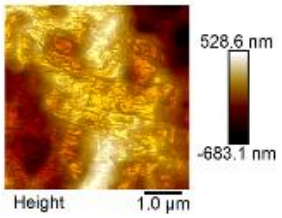	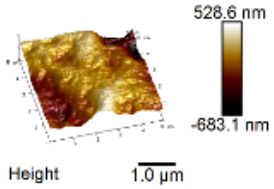	169	15.7
	50	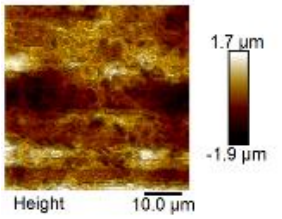	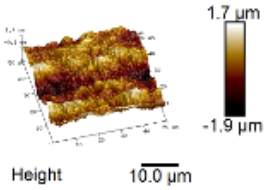	509	8.99
Two-step **Unwashed**	50	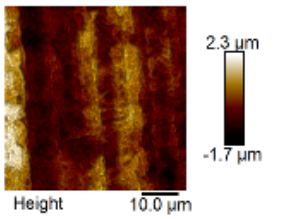	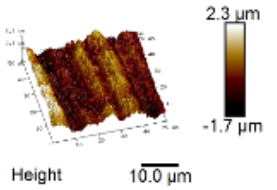	576	10.7
Two-step **Washed**	50	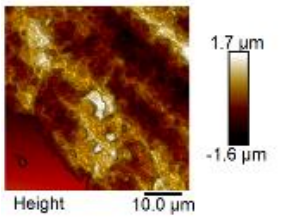	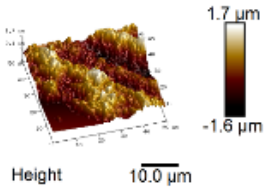	507	5.87
	20	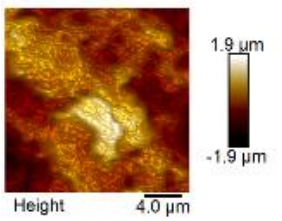	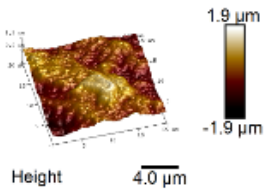	431	12.2

The AFM data shows the previously observed phenomenon of the plasma process causing an increase in the roughness of the surface (untreated RMS of 509 nm increases to 576 nm after Two-step plasma treatment) which is subsequently removed by the solvent wash process (decreases to RMS of 507 nm),

Table 22.

The image surface area difference is a descriptor of how the roughness affects the surface area, which is one of the terms in the Wenzel equation, Chapter 1. The image surface area difference is the increase in surface area caused by the morphology of the surface. For the untreated PTFE on a 5 μm scan, the actual surface area is 8.99% larger due to the roughness of the surface. After plasma treatment this increases to 10.7%, but after the wash process, this is reduced to 5.87%. This indicates a change in the surface which is not reflected in the RMS. The RMS returns to 507 nm, which is not dissimilar from the 509 nm of the untreated surface, but the images and the image surface area difference suggest a substantial change in the surface morphology.

3.7.2 FTIR

From the SEM and AFM data, it is clear that the oxygen plasma treatment is roughening the PTFE surface. There is the possibility that this is not the only change which is occurring at the surface. It can reasonably be expected that the oxygen plasma is also causing the incorporation of oxygen containing groups onto the surface. This could be due to the presence of LMWOS at the surface, which may be subsequently washed off, or due to the replacement of fluorine groups with OH or other oxygen containing groups. The use of FTIR-ATR (Fourier transformed infrared attenuated total reflection spectroscopy) may be able to see the incorporation of these groups, and the changes in the CF_2 stretch, Figure 29.[176] However, the sampling depth of the FTIR-ATR technique must be considered, it is not as surface specific as for example XPS, and must therefore be used in conjunction with other techniques in order to accurately depict changes at the surface. Due to the sampling depth of a few microns, the majority of the FTIR signal will be due to the bulk PTFE polymer, so the CF_2 stretches will dominate the spectra. However, small bands of oxygen containing species should be visible at much lower transmittance than that of the CF_2 stretches.

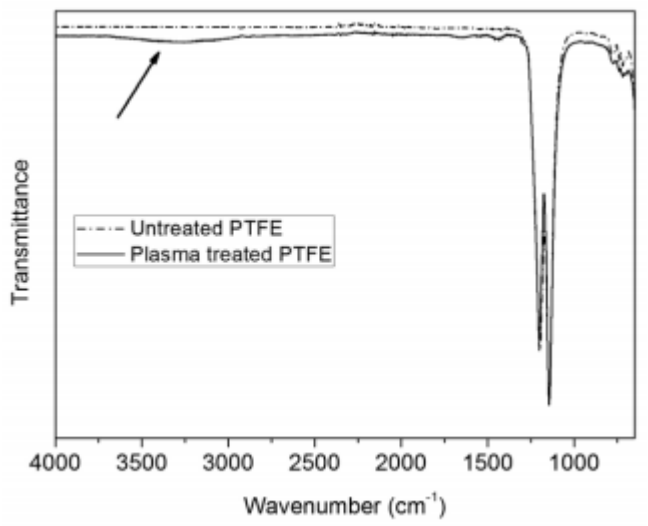

Figure 29: FTIR-ATR (Nicolet iS10, Thermo Scientific, fitted with ATR sampling accessory (Smart iTR), 32 scans and a resolution of 2 cm^{-1}) spectra of untreated and oxygen plasma-treated PTFE (200 W, 600 s, 0.09 mbar). Arrow points to region where the OH containing bands are present.[176]

Zanini *et al.* used FTIR-ATR to track the changes in oxygen incorporation in the surface, Figure 29. The untreated PTFE displays two main bands at 1150 cm^{-1} and 1204 cm^{-1} which are assigned respectively as the asymmetric and symmetric stretches of the CF_2 group. After oxygen plasma treatment (200 W, 600 s, 0.09 mbar), an additional broad low intensity band was observed at 3000–3700 cm^{-1}, which was attributed to the stretching of an OH group. They also reported two much smaller bands (not visible on Figure 29) at 1600–1730 cm^{-1} and 1390–1500 cm^{-1} which were assigned as the carbonyl stretching vibration in COOH and COO^- groups respectively.[176]

Subsequently, the OH and CF_2 bands were integrated and the OH/CF_2 band ratio calculated in order to quantitatively compare the effect of increasing plasma power on the incorporation of oxygen containing groups onto the surface.[176]

3.7.2.1 FTIR-ATR of Single-Step and Two-Step Plasma-treated *PTFE*

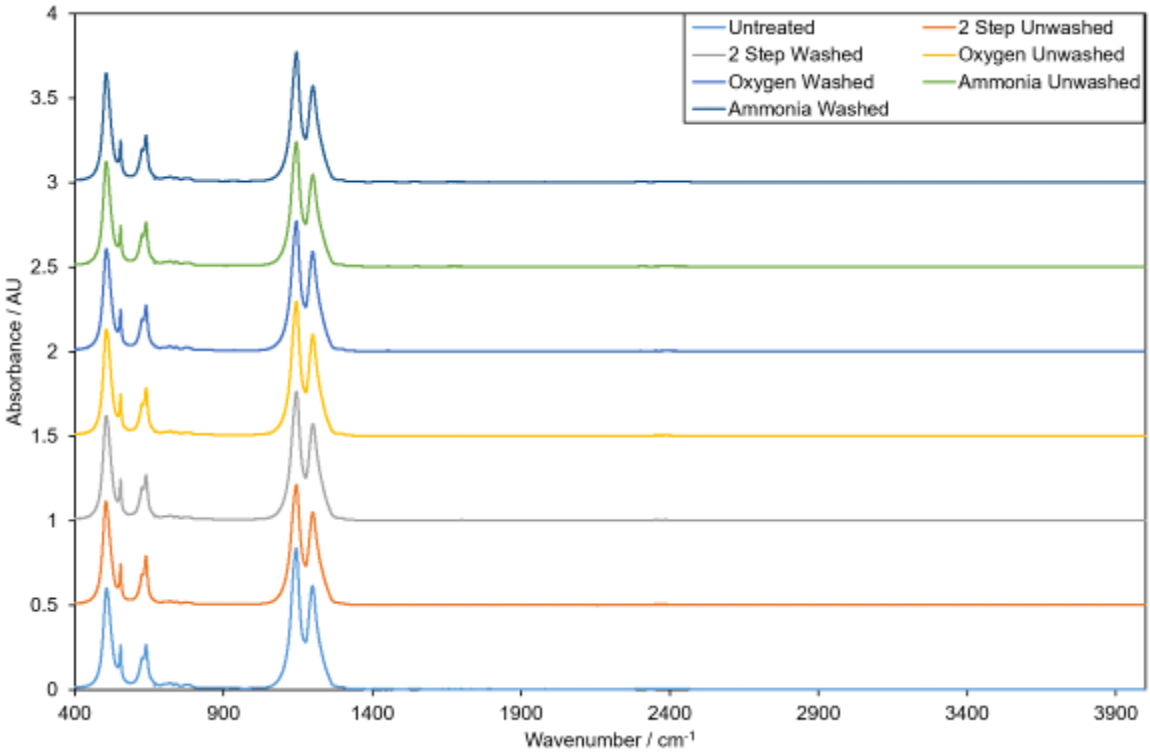

Figure 30: Stacked FTIR-ATR of untreated and plasma-treated PTFE.

2100–3000 cm^{-1}	**3000–3700 cm^{-1}**
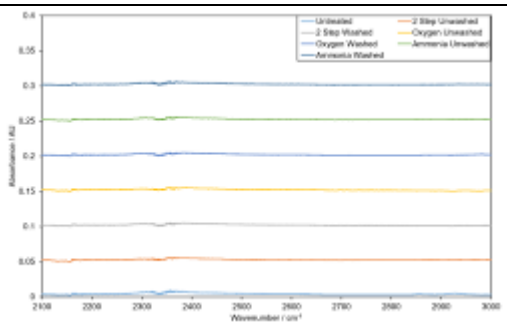	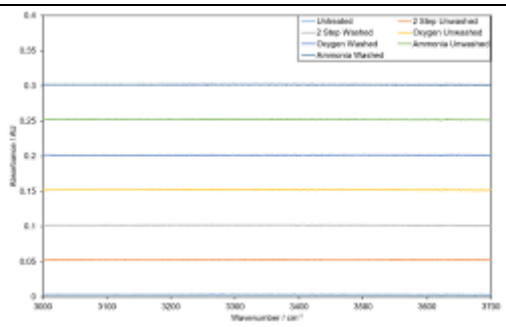

Figure 31: Zoom in on stacked FTIR of untreated and plasma-treated PTFE surfaces (2100–3000 cm^{-1} and 3000–3700 cm^{-1}).

The fluorocarbon peaks are well resolved and have by far the highest intensity, Figure 30. A sharp peak with medium intensity is observed which can be attributed to that of amorphous PTFE. In general the spectra of the untreated PTFE agrees well with that reported in the literature, Figure 32, and Table 23. Due to the polyhalogenated structure of PTFE, there are both symmetric and asymmetric stretching modes of the CF_2 group. This explains the doublet appearance at 1147 and 1200 cm^{-1}.[176,209] The C-F stretching modes complicate the FTIR spectrum by

coupling strongly to the other vibrational modes, especially the C-C stretches. This results is very intense slightly broadened peaks for the C-F stretches which dominate the spectrum.

(a)

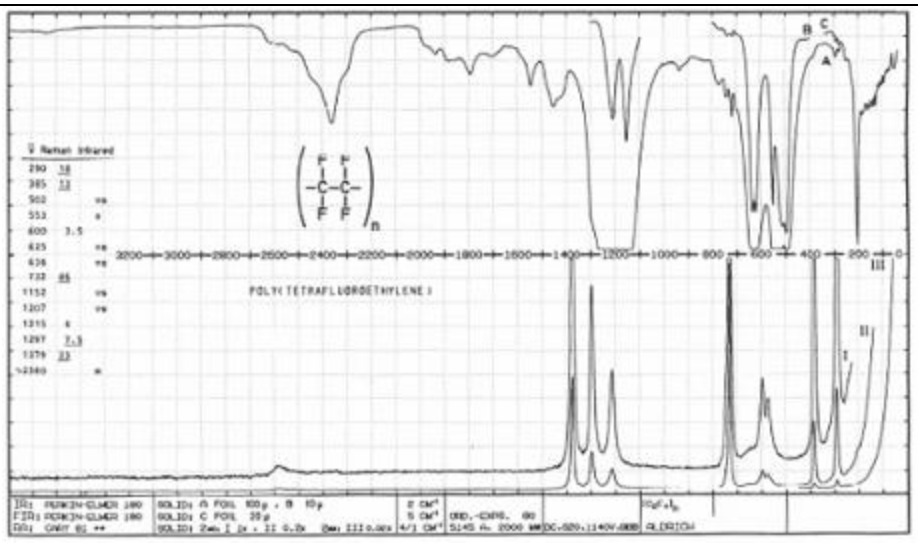

(b)

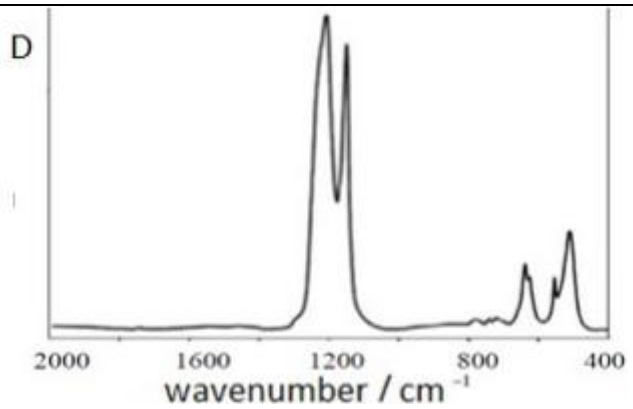

Figure 32: Literature FTIR spectra of PTFE. (a) FTIR and Raman spectra by D. Lin-Vien *et al.*[210] (b) FTIR absorbance spectrum by D.D. Fazullin *et al.*[211]

Table 23: Peak positions and assignments for untreated and plasma-treated PTFE.

Peak Position / cm^{-1}	**Description**	**Intensity**	**Assignment**	**Ref.**
508	Sharp	Very high	CF_2 deformation	211
555	Sharp	Very high	CF_2 oscillation	211
640	Sharp	Very high	Amorphous PTFE	2111,210
1147	Sharp	Very high	Symmetric CF_2 stretch	211,210
1200	Sharp	Very high	Asymmetric CF_2 stretch	211
1292	Shoulder	Low	CF_3	210
2351	Broad	Very low	Unknown	-
2373	Broad	Very low	Unknown	-
2943	Broad	Very low	Unknown	-

According to Cozad *et al.*, hydrocarbon contamination should be found in the region of 2850 cm^{-1}.[212] There is no obvious distinct peak present in this region, but a small amount of low intensity peaks can be seen when zoomed in.

Oxygen containing groups such as carbonyl stretches would be expected to be seen at 1730 cm^{-1},[212] there are no peaks in the FTIR that can be clearly attributed to oxygen containing groups.

The issue with FTIR is that the technique is not particularly surface specific; with a depth analysis in the region of a micron. As plasma is only modifying the top few nanometres of the surface, then any modification or incorporation of oxygen into the surface will only occur in the top few nm of the surface, and the bulk will remain unmodified. This means that any oxygen incorporation or defluorination will cause a very small change in the absorbance on the FTIR as it is only occurring in a 2–3% of that analysis. XPS on the other hand is very surface specific and can be used to see the changes in oxygen surface incorporation.

3.7.3 Wettability of Different Solvents

By measuring the contact angle of alternative solvents in addition to water, it is possible to learn more about the surface modification resulting from plasma treatment. It is well known and observed (Sections 3.2.3 and 3.6.1) that oxygen plasma treatment will result in a roughening of the PTFE surface,[140,175,176,180,194,209] but it may also induce an incorporation of oxygen containing moieties into the surface structure.[176] The presence of this oxygen was not shown in FTIR, but could be found using XPS, or qualitatively observed through the way different solvents contact with the surface.

As previously discussed (Chapter 1), the roughness of a surface will influence the observed contact angle such that it is no longer an accurate representation of the intrinsic wettability of the surface.[213] As a roughened substrate will exacerbate the intrinsic wetting/repellent nature of the surface in comparison to its smooth counterpart. It is important to understand whether the surface is in the Wenzel state, or is a composite surface; i.e. in the Cassie-Baxter state. In a Wenzel state, the droplet permeates into the roughness of the surface, whereas in the Cassie-Baxter state, there is air trapped between the droplet and the surface, hence the term composite surface.[214] If the surface does not obey the Wenzel equation, whereby an untreated CA of <90° will decrease after roughening and a

CA of >90° will increase after roughening, then it can be deduced that the surface is in the Cassie-Baxter state.

Through the comparison of how an oxygenated solvent such as ethanol contacts with the surface with a droplet of and an aliphatic solvent such as hexadecane, it is possible to observe whether there are dipolar interactions between the droplet and the surface.

Hexadecane has a higher surface tension (28.12 mN m^{-1})[215] than ethanol (22.31 mN m^{-1}),[216] and thus the value of γ_{la} will also be larger. In order for the same CA (within error) to be observed for both hexadecane and ethanol, then the numerator in the Young's equation will also have to change. As the solid surface and the atmospheric environment are kept constant, γ_{sa} will remain constant. Meaning that γ_{sl} is lower for hexadecane than it is for ethanol in order to account for the difference in surface tension. If dipolar interactions are influencing the observed CA of liquids on PTFE, it would expected that this is the other way around. Instead of dipolar interactions, the key interactions between the droplet and the surface are dispersive forces. The larger dispersion forces of hexadecane are shown by the refractive index. Hexadecane has a refractive index of 1.43,[217] and ethanol has a refractive index of 1.36.[218]

3.7.3.1 Results

Table 24: WCA, HCA, and ECA of untreated, single-step and the two-step plasma-treated GF PTFE, samples washed in 1:1 v/v solution of propan-2-ol and cyclohexane (120 s) and air dried for >60 min. Reported is the mean CA, and the standard deviation of the sample. The standard deviation of the mean is included in parentheses.

Feed Gas(es)	**Power / W**	**Treatment time / s**	**WCA Unwashed / °**		**WCA Washed / °**		**HCA Unwashed / °**		**HCA Washed / °**		**ECA Unwashed / °**		**ECA Washed / °**	
			Glow	**Remote**	**Glow**	**Remote**	**Glow**	**Remote**	**Glow**	**Remote**	**Glow**	**Remote**	**Glow**	**Remote**
Untreated	0	0	-	-	129 ± 3 (1)	129 ± 3 (1)	-	-	45 ± 2 (1)	45 ± 2 (1)	-	-	43 ± 1 (0)	43 ± 1 (0)
Argon	50	120	118 ± 1 (0)	112 ± 3 (1)			41 ± 8 (4)	44 ± 2 (1)			<10 total wetting	<10 total wetting		
Oxygen	50	600	153 ± 14 (3)	168 ± 2 (0)	142 ± 7 (2)	155 ± 15 (4)	79 ± 4 (1)	85 ± 3 2(1)	73 ± 5 (1)	73 ± 11 (3)	54 ± 5 (1)	64 ± 7 (2)	50 ± 4 (1)	57 ± 3 (1)
Ammonia	5	300	25 ± 13 (3)	36 ± 8 (2)	61 ± 9 (2)	68 ± 5 (1)	<10 total wetting	<10 total wetting	<10 total wetting	<10 total wetting	<10 total wetting	<10 total wetting	<10 total wetting	<10 total wetting
Step 1: Oxygen, Step 2: Ammonia	Step 1: 50, Step 2: 5	Step 1: 600, Step 2: 300	10 ± 0 (0)	11 ± 1 (0)	41 ± 10 (3)	52 ± 15 (3)	<10 total wetting	<10 total wetting	<10 total wetting	<10 total wetting	<10 total wetting	<10 total wetting	<10 total wetting	<10 total wetting

After roughening (oxygen plasma treatment, see section 3.7.1) the WCA significantly increases, this is expected as the WCA for untreated PTFE is >90°, so the surface obeys the Wenzel equation. However the untreated HCA and ECA are both <90° and thus if Wenzel wetting is occurring, these CAs would be expected to decrease after plasma treatment. As both the ECA and HCA increase, it can be deduced that the surface is in the Cassie-Baxter state, and there is air trapped between the droplet and the surface increasing the observed CA.

Hexadecane has a contact angle of around 73° after both glow and remote oxygen plasma treatments (50 W, 600 s, 0.2 mbar) after solvent washing (120 s, 1:1 v/v propan-2-ol and cyclohexane, air dried for at least 60 min), Table 24.

. Whereas ethanol has a much lower contact angle of 50° for glow oxygen plasma-treated and 57° for remote oxygen plasma-treated surfaces after solvent washing, Table 24.

The lower CA for the oxygenated solvent suggests that there is a reasonably high degree of oxygen incorporated into the surface by the plasma treatment. This can be confirmed using XPS, Section 3.7.4.

3.7.3.2 Calculations

It is possible using the Young's equation to determine the change in γ_{sl} when changing between water, hexadecane and ethanol, Table 25.

Table 25: Calculation of γ_{sl} using the Young's equation, reference values for γ_{la} and γ_{sa} and experimentally determined CA on untreated washed PTFE.

Liquid	**Solid surface free energy (γ_{sa}) / mN m^{-1}**	**Surface tension of liquid (γ_{la}) / mN m^{-1}**	**$\theta_{untreated}$ (experimentally determined) / °**	**Calculated surface-liquid interfacial tension (γ_{sl}) / mN m^{-1}**
Water	20[219]	72.5	129	65.63
Hexadecane	20[219]	28.12[215]	45	0.1162
Ethanol	20[219]	22.31[216]	43	3.683

3.7.3.3 Summary

After oxygen plasma treatment, the surface is in the Cassie-Baxter rather than the Wenzel state, indicated by the HCA and ECA data not obeying the Wenzel equation. After the two-step plasma treatment, the surface is totally wetting to both ethanol and hexadecane and stable to solvent washing, however some

hydrophobic recovery is observed for WCA after initially having a WCA of <10°. The lower CA for the oxygenated solvent in comparison with the oil CA suggests that there is a reasonably high degree of oxygen incorporated into the surface by oxygen plasma treatment.

3.7.4 XPS

One of the most commonly used and surface specific techniques for investigation of the modification of plasma-treated PTFE surfaces. In this section, the XPS were treated with a Shirley background, and fitted using a series of Gaussian-Lorentzian functions, see Chapter 2 Section 5. The sensitivity of the technique to different atoms can be accounted for using sensitivity multiplication factors with respect to carbon. When carbon is given a sensitivity factor of 1, fluorine has a sensitivity factor of 0.25, oxygen 0.35, and nitrogen 0.7.[220]

3.7.4.1 Untreated Washed PTFE

Initially the washed untreated surface was analysed, this gave a background from which changes caused by plasma modification could be quantified. Theoretically, the ratio between the amount of carbon and fluorine (F/C ratio) is 2.00, as each carbon atom is attached to two fluorine atoms, for the untreated sample assessed, the F/C ratio was calculated to be 2.04, Table 26. If the surface were contamination and defect free, there should be no adventitious carbon or carbon oxygen or carbon nitrogen environments, simply a CF_2 environment fitted with a single Gaussian-Lorentzian function, Chapter 2 Section 5. From the high resolution C 1s spectrum, the peak needs to be fitted by more than one Gaussian-Lorentzian function, indicating more than one carbon environment present, Figure 33. The fluorine spectrum displays a single peak, suggesting there is a single fluorine environment, CF_2, Figure 33. But C 1s scan indicates adventitious carbon (285.0 eV), and two further carbon environments, at 291.1 eV (CF_2) and a much lower intensity peak at 293.3 eV (CF_3).[220]

From the O 1s high resolution spectrum, one low intensity peak is observed which can be fitted with a single Gaussian-Lorentzian function, this could be a carbon-oxygen environment, and the very low intensity of the peak in comparison to the fluorine carbon environments prevents it from being clear in the C 1s. The position of the oxygen peak at 531.1 eV indicates either a hydroxide group or a carbonate group, both of with would likely come from aerial contamination.[220] As

there is no corresponding carbon peak, then it can be deduced that the oxygen present it hydroxide groups due to water contamination on the surface.

There is no nitrogen present in the N 1s high resolution scan, so any nitrogen that is subsequently incorporated is due to the plasma modification process, Figure 33.

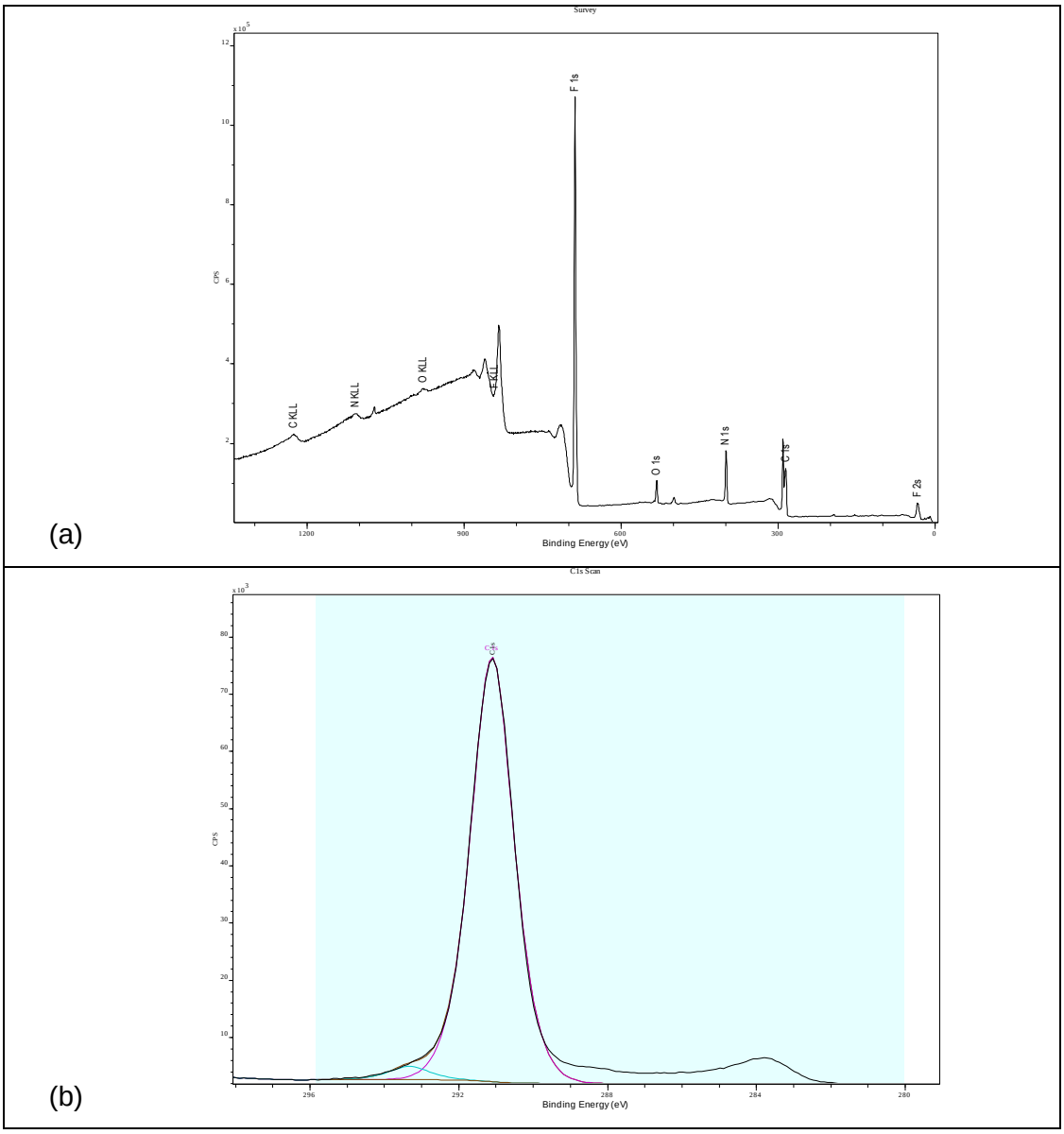

(a)

(b)

(c)

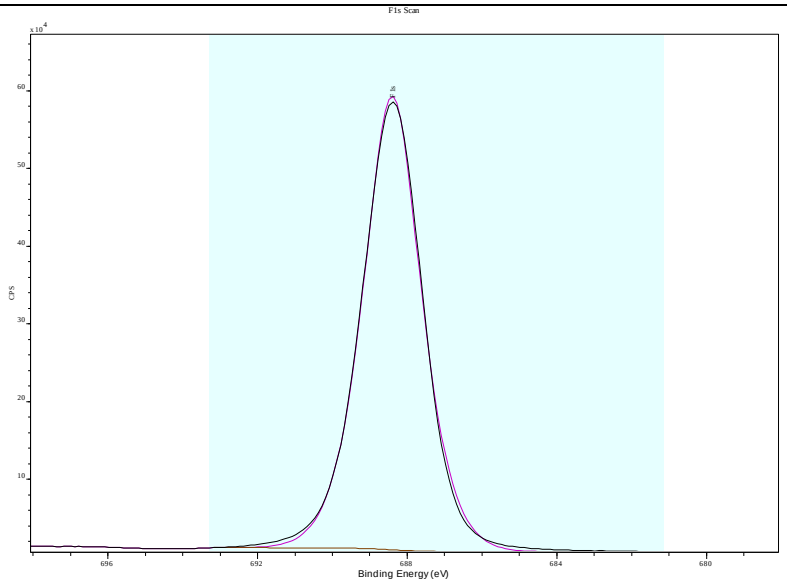
F1s Scan
x10^4
60
50
40
30
20
10
CPS
696
692
688
684
680
Binding Energy (eV)

(d)

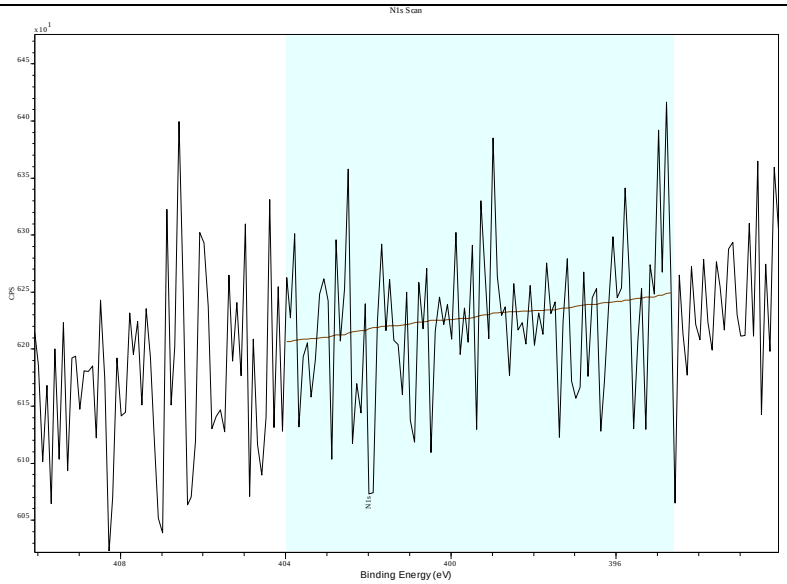
N1s Scan
x10^1
645
640
635
630
625
620
615
610
605
CPS
N1s
408
404
400
396
Binding Energy (eV)

(e)

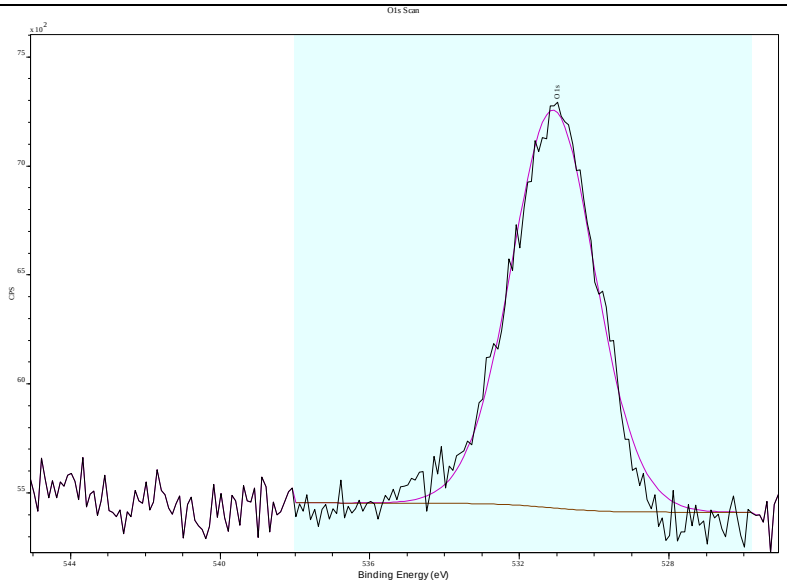
O1s Scan
x10^2
75
70
65
60
55
CPS
O1s
544
540
536
532
528
Binding Energy (eV)

Figure 33: XPS of untreated washed Goodfellow PTFE. (a) Survey spectra; (b) C 1s high resolution scan; (c) F 1s high resolution scan; (d) N 1s high resolution scan; and (e) O 1s high resolution scan.

Table 26: XPS of untreated PTFE. Peak positioning and area for Gaussian-Lorentzian fittings of XPS data collected by Dr Jose Portoles at NEXUS Newcastle University on Thermo K-Alpha. Peak assignments are determined using *Handbook of X-Ray Photoelectron Spectroscopy*.[220] Also calculated are the F/C, N/C and O/C ratios.

	Peak Position / eV	**Peak Area**	**Peak Assignment**	**F/C**	**N/C**	**O/C**
C 1s	291.1	118531	CF_2	-	-	-
	293.3	3612	CF_3			
F 1s	688.4	250215	CF_2	2.04	-	-
N 1s	-	-		-	0.00	-
O 1s	531.1	1813	Hydroxide	-	-	0.01

3.7.4.2 Ammonia Plasma-treated *PTFE*

The mechanism of hydrophilization imparted by the ammonia plasma is one of defluorination and incorporation of amine groups in the place of the fluorine atoms. This has been well investigated in the literature.[201] Although reporting significant incorporation of nitrogen (N/C ratio 0.24–2.68), and significant defluorination (F/C ratio of 0.85–0.5), Chevallier *et al.* did not investigate the wettability of their ammonia plasma-treated surfaces. The XPS data presented on the surfaces created using the low power and prolonged ammonia plasma reported in this work agrees with this. Additionally there is a significant incorporation of oxygen onto the surface as well, it is likely that this comes from the reaction after removal from the vacuum environment and exposure to air. The OES previously shown for ammonia plasma indicates that there is no oxygen present in the plasma (Section 3.5.2.2), so the oxygen must be from the air.

In comparison to the untreated substrates, there is a significant degree of defluorination observed, the F/C has decreased from 2.04 to 0.78 and 0.89 in the glow and remote plasma regions respectively. This has been accompanied by a significant incorporation of nitrogen into the surface, this can been seen in the increased N/C ratio – from 0.00 to 0.10, and the nitrogen peak at 398.6 eV and 399.1 eV(glow and remote respectively) can be attributed to a carbon with nitrogen group as a carbon peak at 286.0 eV is also seen. There is an increase in the O/C

ratio from 0.01 to 0.05, but as before this is not associated with an additional carbon peak, suggesting that the oxygen is on the surface as a hydroxide group.

In the literature, the concept of solvent washing is often overlooked, especially when investigating the surface using XPS. In this work, the plasma-treated surfaces have been shown to be significantly affected by the solvent washing process, Sections 3.5.2.1, 3.5.3.4, 3.6.2, and 3.6.4, and thus the samples were analysed by XPS both before and after solvent washing.

From these data, it appears that the solvent washing process serves to increase the N/C ratio (from 0.10 to 0.15 and 0.17 respectively for glow and remote samples), Table 27. In terms of fluorine content, for the glow plasma-treated surfaces the F/C ratio increases, but in the remote treated samples, the opposite is true. The observed increase for the washed sample is due to a decrease in the absolute amount of carbon rather than a change in the fluorine content of the surface. This is due to the LMWOS being removed from the surface being primarily composed of carbon species. The effect is not observed in the remote plasma-treated samples as the plasma is far less harsh in this region than in the glow.

Table 27: XPS of ammonia plasma-treated PTFE (5 W, 300 s, 0.2 mbar). Samples from both glow and remote regions of the plasma were analysed both prior to and after solvent washing (2 min, 1:1 v/v propan-2ol and cyclohexane solution). Peak positioning and area for Gaussian-Lorentzian fittings of XPS data collected by author and Dr Jose Portoles at NEXUS Newcastle University on Thermo K-Alpha. Peak assignments are determined using *Handbook of X-Ray Photoelectron Spectroscopy*.[220] Also calculated are the F/C, N/C and O/C ratios.

Solvent Washed	Plasma Position	Atom	Peak Position / eV	Peak Area	Peak Assignment	F/C	N/C	O/C
Washed	**Untreated**	**-**	-	-	-	2.04	0.00	0.01
Unwashed	**Glow**	**C 1s**	290.4	58435	CF_2	-	-	-
			284.1	49835	Adventitious carbon	-	-	-
			286.0	43962	C with N	-	-	-
		F 1s	687.7	119360	CF_2	0.78	-	-
			684.9	7272	CF_3		-	-
		N 1s	398.6	15752	C with N	-	0.10	-
		O 1s	531.2	7617	Hydroxide	-	-	0.05
	Remote	**C 1s**	291.0	59841	CF_2	-	-	-
			284.6	44090	Adventitious carbon	-	-	-
			286.6	38196	C with N	-	-	-
		F 1s	689.4	26491	CF_2	0.89	-	-
			688.2	73973	CF_3		-	-
			686.7	25912	CF		-	-
		N 1s	399.1	14900	C with N	-	0.10	-
		O 1s	531.7	5090	Hydroxide	-	-	0.04
Washed	**Glow**	**C 1s**	290.8	59027	CF_2	-	-	-
			284.5	41680	Adventitious carbon	-	-	-
			286.6	44063	C with N	-	-	-
		F 1s	687.8	117840	CF_2	0.88	-	-
			684.9	9608	CF_3		-	-
		N 1s	399.1	22232	C with N	-	0.15	-
		O 1s	531.4	8994	Hydroxide	-	-	0.06
	Remote	**C 1s**	290.7	51244	CF_2	-	-	-
			284.3	45430	Adventitious carbon	-	-	-
			286.3	45100	C with N	-	-	-
		F 1s	678.8	100043	CF_2	0.79	-	-

			685.0	11332	CF_3		-	-
		N 1s	399.0	24061	C with N	-	0.17	-
		O 1s	531.2	7928	Hydroxide	-	-	0.06

3.7.4.3 Oxygen Plasma-treated *PTFE*

From the SEM and AFM, Section 3.7.1, the effect of the oxygen plasma treatment is clearly roughening the surface, which is widely reported in the literature.[175,180] There is some disagreement in the literature as to whether there is significant oxygen incorporation associated with the oxygen plasma modification of PTFE surfaces. Some treatments were reported to have resulted in significant defluorination (F/C reduced from 2.0 to 0.9[221], and from 1.94 to 0.60[140]), but others did not report drastic defluorination.[136,174,178,222,223]

The data obtained here shows that there is no significant defluorination observed (F/C ratio decreased from 2.04 to 2.02 and 1.94 for glow and remote plasma treatment respectively), or indeed any incorporation of oxygen into the surface, Table 28. The oxygen plasma treatment purely has a roughening effect on the surface. This surface roughening and lack of overall defluorination explains the high WCA and increase in hydrophobicity observed. Although there is no overall decrease in the fluorine content of the surface, there is a marked increase in the proportion of the CF_3 with respect to CF_2 groups. This is likely due to the destructive nature of the plasma increasing the amount of CF_3 polymer end groups available. There is no incorporation of nitrogen at all, indicating that the surfaces are not reacting with the air after removal from the chamber, discussed further in Section 3.8.3.

The process of solvent washing resulted in a decrease in the fluorine content of the surface (shown by decreases in F/C ratio), and this has the effect of also decreasing the WCA of the surface, Section 3.6.1.

Table 28: XPS of oxygen plasma-treated PTFE (50 W, 600 s, 0.2 mbar). Samples from both glow and remote regions of the plasma were analysed both prior to and after solvent washing (2 min, 1:1 v/v propan-2ol and cyclohexane solution). Peak positioning and area for Gaussian-Lorentzian fittings of XPS data collected by author and Dr Jose Portoles at NEXUS Newcastle University on Thermo K-Alpha. Peak assignments are determined using *Handbook of X-Ray Photoelectron Spectroscopy*.[220] Also calculated are the F/C, N/C and O/C ratios.

Solvent Washed	Plasma Position	Atom	Peak Position / eV	Peak Area	Peak Assignment	F/C	N/C	O/C
Washed	**Untreated**	**-**	-	-	-	2.04	0.00	0.01
Unwashed	**Glow**	**C 1s**	291.2	99250	CF_2	-	-	-
			292.5	13177	CF_3	-	-	-
			288.3	8993	Carboxyl	-	-	-
		F 1s	688.5	245540	CF_2	2.02	-	-
		N 1s	-	-		-	-	-
		O 1s	532.0	115	Hydroxide or carboxyl	-	-	0.00
	Remote	**C 1s**	291.2	110357	CF_2	-	-	-
			292.9	13669	CF_3	-	-	-
			288.3	8697	Carboxyl	-	-	-
		F 1s	688.5	258009	CF_2	1.94	-	-
		N 1s	-	-		-	-	-
		O 1s	531.7	375	Hydroxide or carboxyl	-	-	0.00
Washed	**Glow**	**C 1s**	291.1	81804	CF_2	-	-	-
			292.2	26129	CF_3	-	-	-
			288.1	11507	Carboxyl	-	-	-
		F 1s	688.6	227478	CF_2	1.90	-	-
		N 1s	-	-		-	-	-
		O 1s	533.0	583	Hydroxide or carboxyl	-	-	0.00
			537.9	1722		-	-	
	Remote	**C 1s**	291.3	95686	CF_2	-	-	-
			292.4	24287	CF_3	-	-	-
			288.1	7610	Carboxyl	-	-	-
		F 1s	688.6	248178	CF_2	1.95	-	-
		N 1s	-	-		-	-	-
		O 1s	531.9	327	Hydroxide or carboxyl	-	-	0.00
			536.4	800		-	-	

3.7.4.4 Two-Step Oxygen then Ammonia Plasma-treated PTFE

Of the most interest is the two-step process. This plasma modification method has not been reported in the literature, and so there is no literature to compare directly. One would expect that treating the PTFE with this tandem two-step method would result in a middle ground between the surfaces reported for the single-step plasma treatments alone. As seen in the ammonia treated surfaces, Section 3.7.4.2, significant defluorination of the surface is observed, which can be seen with the WCA decreasing sharply. The defluorination which is observed is not as significant as that of the single-step ammonia treated samples, this is true for both the glow and the remote treated samples. More significant defluorination is occurring on the remote plasma-treated surfaces.

Unlike in the ammonia plasma-treated surfaces, Section 3.7.4.2, the N/C ratio decreases with solvent washing. Subsequently the F/C increases, this increase is larger for the remote plasma-treated surfaces, as this had a lower F/C ratio prior to solvent washing. There is no change in the O/C ratio observed, indicating the incorporated oxygen in the surface is not affected by the solvent washing process. The XPS analysis of these surfaces suggests that the mechanism by which the surface is the replacement of nitrogen containing groups with fluorine atoms. This would suggest that the major method by which hydrophobic recovery is occurring is due to surface reconstruction whereby the fluorine groups are re-presenting at the surface in order to reduce the surface energy.

Table 29: XPS of two-step plasma-treated PTFE (oxygen 50 W, 600 s, followed by ammonia 5 W, 300 s, both at 0.2 mbar). Samples from both glow and remote regions of the plasma were analysed both prior to and after solvent washing (2 min, 1:1 v/v propan-2ol and cyclohexane solution). Peak positioning and area for Gaussian-Lorentzian fittings of XPS data collected by author and Dr Jose Portoles at NEXUS Newcastle University on Thermo K-Alpha. Peak assignments are determined using *Handbook of X-Ray Photoelectron Spectroscopy*.[220] Also calculated are the F/C, N/C and O/C ratios.

Solvent Washed	Plasma Position	Atom	Peak Position / eV	Peak Area	Peak Assignment	F/C	N/C	O/C
Washed	**Untreated**	**-**	-	-	-	2.04	0.00	0.01
Unwashed	**Glow**	**C 1s**	290.7	49855	CF_2	-	-	-
			284.8	25694	Adventitious carbon	-	-	-
			287.0	42042	C with N	-	-	-
		F 1s	687.8	100422	CF_2	1.03	-	-
			685.4	20569	CF_3		-	-
		N 1s	399.3	28613	C with N	-	0.24	-
		O 1s	531.7	7488	Hydroxide	-	-	0.06
	Remote	**C 1s**	537.3	1050	CF_2	-	-	
			290.4	53597	Adventitious carbon	-	-	-
			284.4	29837	C with N	-	-	-
		F 1s	286.5	46188	CF_2	0.96	-	-
			687.6	111939	CF_3		-	-
			685.1	11863			-	-
		N 1s	398.9	24147	C with N	-	0.19	-
		O 1s	531.4	8975	Hydroxide	-	-	0.07
Washed	**Glow**	**C 1s**	290.5	57116	CF_2	-	-	-
			284.4	28933	Adventitious carbon	-	-	-
			286.6	33525	C with N	-	-	-
		F 1s	687.7	121798	CF_2	1.08	-	-
			684.9	7455	CF_3		-	-
		N 1s	398.9	16997	C with N	-	0.14	-
		O 1s	531.6	5891	Hydroxide	-	-	0.06
			537.6	1864		-	-	
	Remote	**C 1s**	290.7	63471	CF_2	-	-	-
			284.6	33428	Adventitious carbon	-	-	-
			286.8	35652	C with N	-	-	-

		F 1s	687.9	134458	CF_2	1.07	-	-
			685.3	6829	CF_3		-	-
		N 1s	399.0	15530	C with N	-	0.12	-
		O 1s	531.7	6379	Hydroxide	-	-	0.06
			537.4	1434		-	-	

3.7.5 Summary

Through the analysis of the different wetting behaviours of water, ethanol, and hexadecane, it was possible to determine that the oxygen plasma treatment induces a Cassie-Baxter wetting state, which is subsequently altered to the Wenzel wetting state by the ammonia plasma treatment, Section 3.7.3. This explains why such a hydrophilic surface is produced by the two-step treatment.

The untreated PTFE samples have some hydroxide groups present on the surface, but no nitrogen, and as expected the majority of the fluorine is present as CF_2, Section 3.7.4.1. Oxygen plasma treatment of the surface results in significant roughening of the surface, Section 3.7.1, no significant defluorination and no incorporation of oxygen onto the surface was observed in the XPS analysis, Section 3.7.4.3. Ammonia single-step plasma treatment did not significantly roughen the surface, however it did cause a large amount of defluorination, F/C reduced from 2.04 to 0.78 and 0.89 in the glow and remote plasma regions respectively. There was also significant incorporation of nitrogen into the surface (N/C ratio increases from 0.00 to 0.10), Section 3.7.4.2. The two-step plasma treatment resulted in a hybrid of the two constituent steps – increased roughness of the surface and significant defluorination and incorporation of nitrogen into the surface, Sections 3.7.1 and 3.7.4.4.

3.8 MECHANISTIC UNDERSTANDING: LMWOS Removal or Surface Reconstruction?

3.8.1 Investigation of efficacy of drying process

Initially, the method whereby the samples were solvent washed was to submerge the samples in the solvent wash solution for two min prior to drying in a petri dish at room temperature for approximately 18 h. Due to the flat nature of the surface, any contaminants on the surface will remain pinned to the surface as the solvent carriers evaporate. Additionally, it was noticed that the drying time in the petri dish was in the region of 60 min, which given the volatility of propan-2-ol and cyclohexane is longer than expected, suggesting a saturated environment within the petri dish, that was retarding the drying process. This may have given unreliable WCA data.

The method was therefore changed to incorporate a drying process in a nitrogen stream. The substrate was held at 90° to the bench, and dried under a nitrogen stream (5 bar squeezed out through compressed PVC 6.5 tubing). The samples were measured immediately after this drying process, and then rewashed and dried, and left in a petri dish for 18 h just like previously in order to assess whether there is any surface reconstruction.

It should be noted that as previously discussed, outside of UHV there is no way of completely preventing the deposition of a monolayer of adsorbed molecules onto the surface from the air; aerial contamination. This will occur in a few seconds, and so this contamination will be present on the all the samples measured, resulting in a systematic error across all measurements.

Table 30: WCA, HCA, and ECA of untreated, single-step (ammonia plasma 5 W, 300 s, 0.2 mbar, or oxygen plasma 50 W, 600 s, 0.2 mbar) and the two-step plasma-treated (ammonia plasma 5 W, 300 s, 0.2 mbar, followed by oxygen plasma 50 W, 600 s, 0.2 mbar) GF PTFE, samples washed in 1:1 v/v solution of propan-2-ol and cyclohexane (120 s) and dried in a nitrogen stream for 10 s. Subsequently, the samples were rewashed and dried in the same manner before being left in a petri dish for 18 h prior to CA analysis. Reported is the mean CA, and the standard deviation of the sample. The standard deviation of the mean is included in parentheses.

Plasma treatment	**WCA unwashed /°**		**WCA washed and dried under nitrogen /°**		**WCA washed and dried under nitrogen and left 18 h /°**		**HCA unwashed /°**		**HCA washed and dried under nitrogen /°**		**HCA washed and dried under nitrogen and left 18 h /°**		**ECA unwashed /°**		**ECA washed and dried under nitrogen /°**		**ECA washed and dried under nitrogen and left 18 h /°**	
	Glow	Remote	Glow	Remote	Glow	Remote	Glow	Remote	Glow	Remote	Glow	Remote	Glow	Remote	Glow	Remote	Glow	Remote
Untreated	-	-	129 ± 3 (1)	129 ± 3 (1)	129 ± 3 (1)	129 ± 3 (1)	-	-	45 ± 2 (1)	45 ± 2 (1)	45 ± 2 (1)	45 ± 2 (1)	-	-	43 ± 1 (0)	43 ± 1 (0)	43 ± 1 (0)	43 ± 1 (0)
Ammonia plasma 5 W, 300 s	35 ± 8 (2)	33 ± 14 (3)	49 ± 17 (4)	47 ± 19 (4)	69 ± 8 (2)	68 ± 10 (2)	14 ± 5 (1)	15 ± 5 (1)	<10 ± 0 (0)	<10 ± 0 (0)	<10 ± 0 (0)	<10 ± 0 (0)	<10 ± 0 (0)	<10 ± 0 (0)	<10 ± 0 (0)	<10 ± 0 (0)	<10 ± 0 (0)	<10 ± 0 (0)
Oxygen plasma 50 W, 600 s	144 ± 7 (2)	158 ± 13 (3)	137 ± 2 (0)	162 ± 9 (2)	138 ± 2 (0)	150 ± 15 (4)	81 ± 3 (1)	87 ± 4 (1)	54 ± 16 (4)	66 ± 8 (2)	69 ± 5 (1)	82 ± 5 (1)	54 ± 3 (1)	67 ± 6 (1)	44 ± 3 (1)	61 ± 7 (2)	44 ± 5 (1)	60 ± 9 (2)
2 step:	<10	<10 ±	41 ±	52 ±	64 ±	74 ±	<10	<10 ±	<10	<10 ±	<10	<10 ±	<10	<10 ±	<10	<10 ±	<10	<10 ±

ammonia 5 W, 300 s, followed by oxygen 50 W, 600 s	± 0 (0)	0 (0)	10 (3)	15 (3)	3 (1)	11 (4)	± 0 (0)	0 (0)	± 0 (0)	0 (0)	± 0 (0)	0 (0)	± 0 (0)	0 (0)	± 0 (0)	0 (0)	± 0 (0)	0 (0)

As previously seen, ammonia plasma treatment (single-step or two-step) results in total wetting of surface by hexadecane and by ethanol, which is unaffected by washing of the surface. In the case of the HCA, the unwashed surface has a slightly higher contact angle, however after solvent washing the surface becomes totally wetting again. This change is likely due to the presence of LMWOS on the surface which are washed off by the solvent.

After oxygen plasma treatment, the CA increases for all solvents, indicating a Cassie-Baxter state. After storage in air for 18 h, the WCA increases for ammonia single-step and two-step plasma-treated surfaces. For oxygen treated samples, there is no significant change after storage in air for 18 h for glow plasma-treated samples, however there is a decrease in WCA observed for remote plasma-treated samples. When the standard deviation of the mean is considered, this change is significant (162 ± 2° prior to storage, and 150 ± 4° after storage). As both of these samples have been solvent washed prior to analysis, this is not due to a morphological change, or the removal of LMWOS. This indicates that there is significant changes in the composition of this surface, this could be due to surface reconstruction, although at high WCA, this would raise the surface energy. As this change is not observed in the glow samples, it is unlikely that the change is due to aerial contamination/deposition. This phenomenon is also observed for the HCA, but not for the ECA which remains unaffected by storage in air.

3.8.2 Effect of storage in UHP water

In order to further understand the effect that aerial contamination on the observed wettability of the surface, some plasma-treated surfaces were stored in water and in air, and the WCA compared. It has previously been shown in the literature, that storage in a polar medium can retard the hydrophobic recovery of plasma-treated PTFE surfaces.

Table 31: WCA of solvent washed (120 s, 1:1 v/v solution of propan-2-ol and cyclohexane) ammonia plasma-treated GF PTFE (5 W, 300 s, 0.2 mbar) before and after storage for 48 h in air and in UHP water. Surface tension of storage medium after 48 h with solvent washed samples.

Plasma treatment	**WCA prior to immersion in UHP water /°**		**WCA after storage for 48 h in UHP water /°**		**WCA after storage for 48 h in air /°**		**Surface tension of UHP after storage of GF PTFE / mN m^{-1}**	
	Glow	**Remote**	**Glow**	**Remote**	**Glow**	**Remote**	**Glow**	**Remote**
Untreated	-	-	-	-	-	-	72.63 ± 0.05	72.63 ± 0.05
Ammonia plasma 5 W, 300 s	57 ± 3 (2)	72 ± 4 (2)	45 ± 5 (3)	61 ± 4 (3)	56 ± 0 (0)	67 ± 3 (2)	72.67 ± 0.02	72.75 ± 0.04

As the samples have already been solvent washed, there would be no expected significant hydrophobic recovery if the sole method of recovery is the removal of LMWOS as previously reported by M.E. Ryan.[180] Instead the fact that we observe decreases in the WCA when the surface is stored in both air and UHP water suggests that there is some surface reconstruction occurring.

Given one of the potential applications for these plasma-treated PTFE substrates is in the human body, and the increased hydrophilicity is to improve haemocompatabilty, if the surfaces are not adversely affected by storage in UHP water, then there should be no problems with retaining the PTFE substrates inside the body as for example stents or artificial ligaments. There is not a significant difference observed in the surface tension of the UHP which indicates that there is nothing being washed from the PTFE surface. There is a marked improvement in the WCA after submersion in UHP for 48 h in comparison with the samples stored in air. This indicates that the longevity of the modification of the surface would be increased when inside the body.

3.8.3 Varying the atmosphere it is exposed to after plasma treatment

As previously mentioned when looking at the OES of the ammonia plasma (Section 3.5.2.2), if there are unsaturated sites remaining on the surface when the substrate is returned to atmospheric-pressure prior to removal from the plasma chamber, then there can be increased incorporation of groups scavenged from the air. The effect of the exposure to air after the two-step process was assessed by instead

backfilling the chamber with dry oxygen free nitrogen. After samples were washed, they were dried in a nitrogen stream and stored under nitrogen.

Table 32: WCA of two-step plasma-treated (oxygen 50 W, 600 s, followed by ammonia 5 W, 300 s) PTFE substrates when the plasma chamber is backfilled with air, or with nitrogen. The samples are solvent washed and dried under a nitrogen stream. The error quoted is the standard deviation of the mean, this counteracts the slight variation in the number of samples used for the nitrogen backfilled and air backfilled samples.

	WCA Unwashed /°		**WCA Washed /°**	
	Glow	**Remote**	**Glow**	**Remote**
Air backfill	10 ± 0	14 ± 1	41 ± 3	52 ± 3
Nitrogen backfill	10 ± 0	19 ± 2	48 ± 4	67 ± 2

The results for the unwashed WCA after purging with nitrogen suggest that there is an effect on the remote plasma of backfilling with nitrogen rather than air (19 ± 2° when backfilled with nitrogen and 14 ± 1° when backfilled with air). This suggests that there are a small amount of sites on the surface that are not quenched by reaction within the plasma treatment. When the glow plasma-treated samples are assessed, there is no discernible difference, this is likely owing to the fact that the surfaces are too hydrophilic to be accurately measured by the sessile drop method.

When the nitrogen backfilled surfaces are solvent washed, the differences between these and the air backfilled samples is more apparent. The glow plasma-treated surfaces are 41 ± 3° when stored in air, and slightly higher at 48 ± 4° when the chamber is stored under nitrogen. This difference is more marked for the remote plasma-treated surfaces, 52 ± 3° when stored in air, and 67 ± 2° when stored in nitrogen. This suggests that there is some reaction of freshly solvent washed two-step plasma-treated samples with the air.

3.8.4 Summary

When plasma-treated samples are dried using nitrogen and the WCA measured immediately after this, the WCA is significantly lower than if the samples are left for 18 h, Section 3.8.1. This indicates that there is some change at the surface which is causing hydrophobic recovery, this could be due to aerial contamination or it could be due to surface reconstruction.

Just like the surfaces which were reported in the literature by T.K. Markkula *et al.*, if these two-step plasma-treated surfaces are kept in UHP water, the hydrophobic recovery of the surface is retarded. It can also reverse the process slightly for solvent washed samples, Section 3.8.2.

After solvent washing, the two-step plasma-treated samples have some active sites with subsequently react with the environment they are exposed to. If this is clean nitrogen, the observed WCA will be higher than if the environment is simply air, Section 3.8.3.

3.9 MECHANISTIC UNDERSTANDING: Wash Liquor Analysis

In the previous analysis described in this chapter, the surface itself has been analysed. Hydrophobic recovery is observed for all the plasma-treated samples – both those reported in this thesis, and that which is reported in the literature, and in light of this, the wash liquors were also analysed.

3.9.1 Surface Tension Analysis

PTFE was treated using the two-step oxygen and ammonia plasma method, and these samples were placed into clean glass vials containing 1 mL of UHP water for 2 min. The samples were then dried in a clean nitrogen stream, before being placed into 1 mL of the solvent wash (1:1 v/v solution of propan-2-ol and cyclohexane) for 2 min. The washed samples were subsequently placed into another vial containing 1 mL of solvent wash for a further 2 min. The surface tension of each of these wash liquors was measured, Table 33. The experiment was repeated but this time immersing two samples in each of the vials instead of one in order to increase the concentration of washed off species in the wash liquor.

Table 33: Effect of washing two-step plasma-treated surfaces in both UHP water and solvent mix (1:1 v/v solution of propan-2-ol and cyclohexane) for 2 min.

Samples immersed	**Surface Tension of UHP after immersion of unwashed PTFE / mN m^{-1}**	**Surface Tension of propan-2-ol and cyclohexane mix after immersion of unwashed PTFE / mN m^{-1}**	**Surface Tension of propan-2-ol and cyclohexane mix after immersion of washed PTFE / mN m^{-1}**
None	72.29 ± 0.06	28.46 ± 0.05	28.46 ± 0.05
1 sample	72.21 ± 0.06	28.45 ± 0.03	27.64 ± 0.04
1 sample	72.02 ± 0.04	28.36 ± 0.04	27.58 ± 0.01
2 samples	73.98 ± 0.06	28.50 ± 0.03	27.61 ± 0.02
2 samples	71.96 ± 0.05	27.81 ± 0.07	27.72 ± 0.04

The initial surface tension of UHP water is 72.29 ± 0.06 mN m^{-1}, and this is decreased by the addition of the plasma-treated PTFE samples. There is one

sample that increases in surface tension, the washing of LMWOS should work to decrease the surface tension of the UHP water at these concentrations, so it is likely that this increase is due to an experimental contamination. Excluding that sample, it is clear that although the wash liquors have lower surface tensions (as low as 72.02 ± 0.04 nM m^{-1} after one sample is washed, and as low as 71.96 ± 0.05 nM m^{-1} when two samples are washed) than the control UHP water sample, there is quite a large variation between the wash liquors. This variation is likely to indicate that the amount of LMWOS that are removed with UHP water washing is inconsistent, perhaps owing to inhomogeneous surface modification.

When plasma-treated PTFE samples were washed in the propan-2-ol and cyclohexane mixture, the change in surface tension is less significant. This is due to the fact that the surface tension of the control solvent mixture is low already, leaving less room for a significant decrease. The control sample had a surface tension of 28.46 ± 0.05 mN m^{-1}, which is reduced to 28.36 ± 0.03 mN m^{-1} when one sample is washed, and as low as 27.81 ± 0.07 mN m^{-1} when two samples are washed.

Once the samples are washed with the solvent and dried, it is generally considered in the literature, that the surface remaining is stable. From the data reported though, it suggests that there is aerial contamination that is deposited on the surface after the surface has been washed. And that species are being washed from the surface even after the initial solvent wash (reduction of surface tension to as low as 27.58 ± 0.01 mN m^{-1} from 28.46 ± 0.05 mN m^{-1}).

3.9.2 GC-MS

In light of the changes in the surface tension of the wash liquor that were observed, Section 3.9.1, GC-MS was carried out on the wash liquors with the aim of determining the types of molecules being washed from the surface by the solvent.

Before the wash liquors of interest were analysed, a background was determined by running the solvents (propan-2-ol and cyclohexane) individually and in the 1:1 v/v solution, Section 7.5.1. The GC-MS method does not start recording until two min after the sample has been injected, this means that the solvent does not flood the spectra, and low concentration species can be better seen.

There are a couple of contaminants present in the mass spectrum for the solvent backgrounds. These are chiefly silicon containing species that come from bleeding of the column, but there are also a few other common contaminants associated with an electron ionisation mass spectrometry technique, chiefly those associated with air; water, nitrogen, oxygen, and carbon dioxide.[224] In the case of

this data, the only one that can show up in the spectrum is carbon dioxide (m/z = 44), as the others have m/z values of <35 Da (the lowest m/z recorded in this data).

3.9.2.1 Wash Liquor of Plasma-treated PTFE Surfaces

Once the baseline from the solvent were determined, the wash liquors for the three plasma-treated surfaces (oxygen, 50 W, 600s; ammonia 5 W, 300 s; and these two treatments combined in the two-step process) were analysed, Table 34.

Table 34: GC-MS results for wash liquor of oxygen (50 W, 600 s, 0.2 mbar), ammonia (5 W, 300 s, 0.2 mbar), and Two-step (Oxygen 50 W, 600 s, 0.2mbar, followed by ammonia 5 W, 300 s, 0.2mbar) plasma-treated PTFE substrates (wash liquor is 1 mL of propan-2-ol and cyclohexane 1:1 v/v solution). Shown is (a) the graph showing the retention time of the solvent in the column, and both (b) average mass spectrum for retention times below 3.23 min (35–650 Da), and (c) average mass spectrum for retention times above 3.59 min (35–650 Da).

Remote Oxygen	(a) 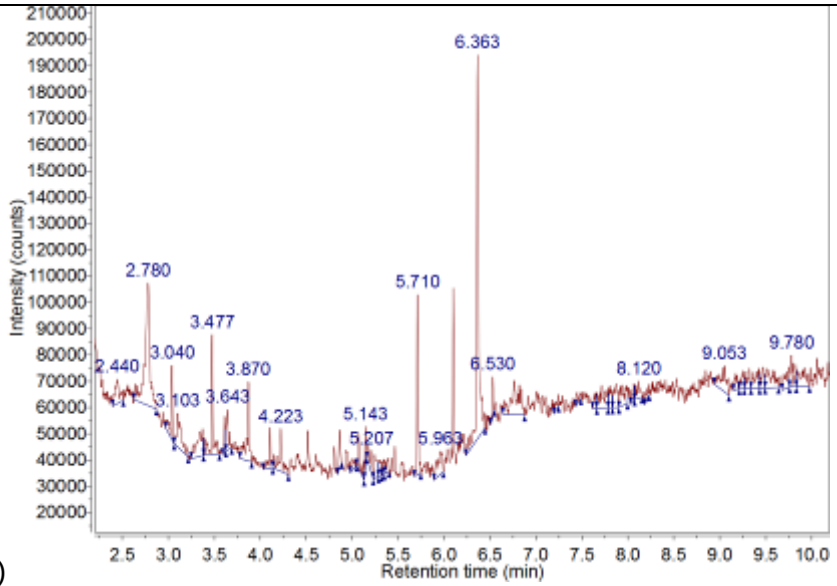 (b) <3.23 min 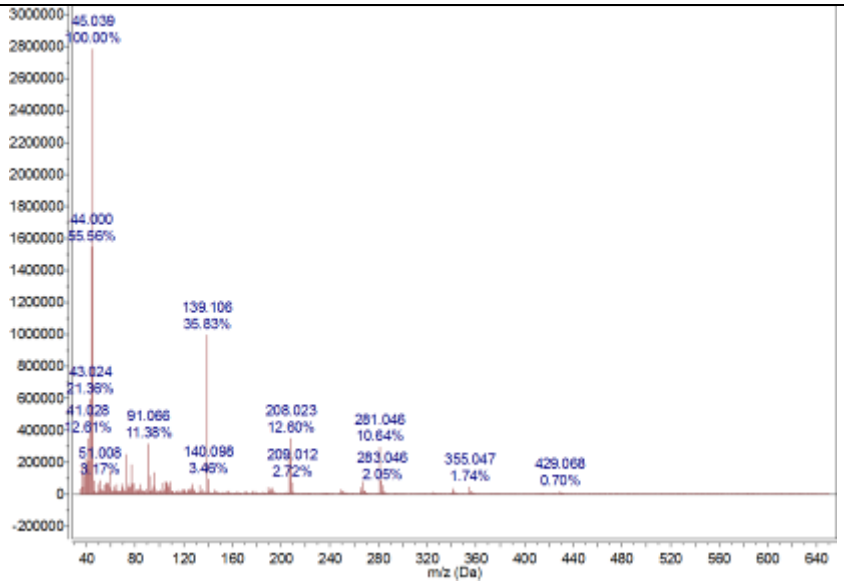

Glow Oxygen

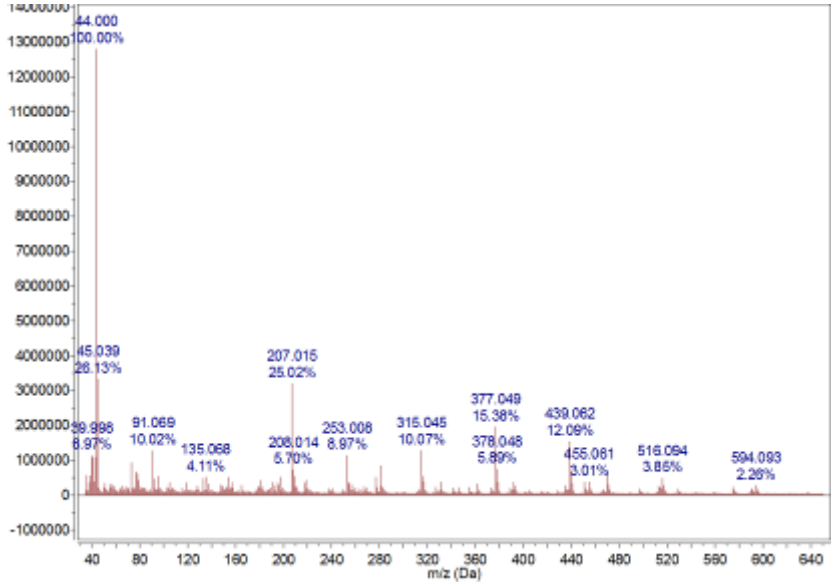

(c) >5.59 min

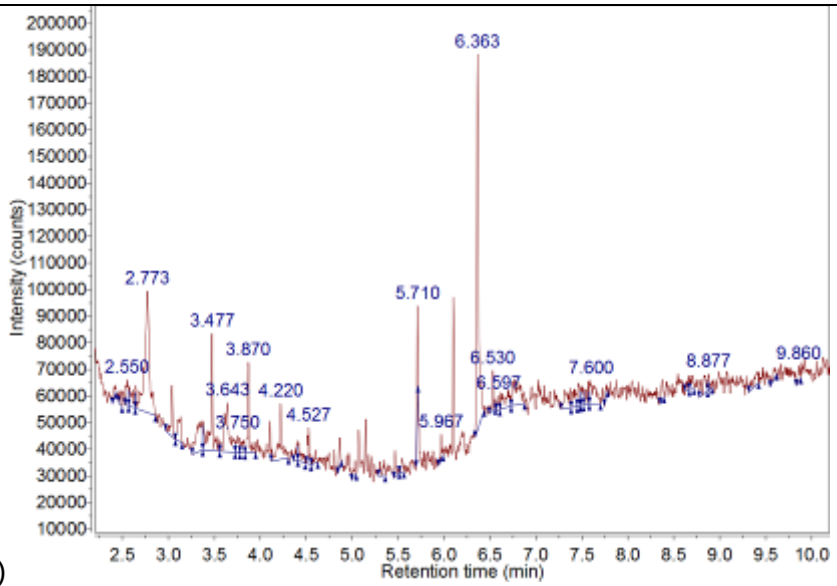

(a)

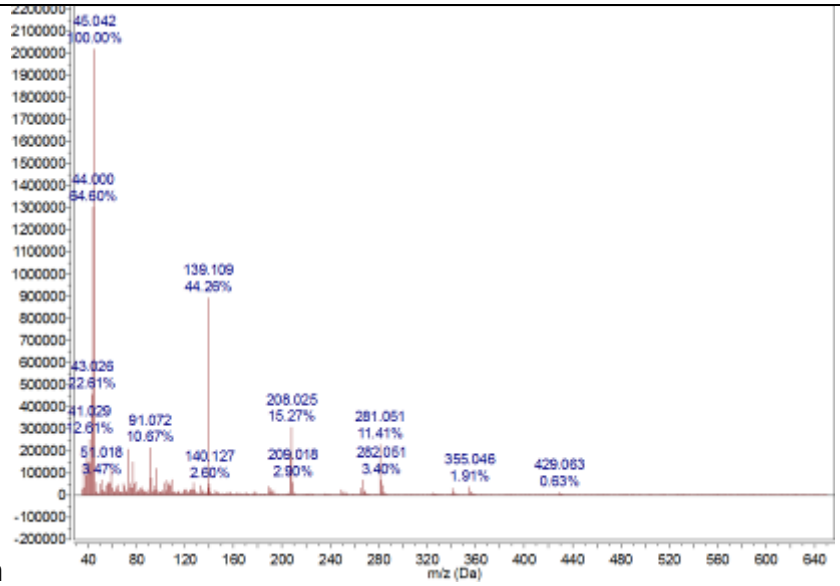

(b) <3.23 min

Remote Ammonia

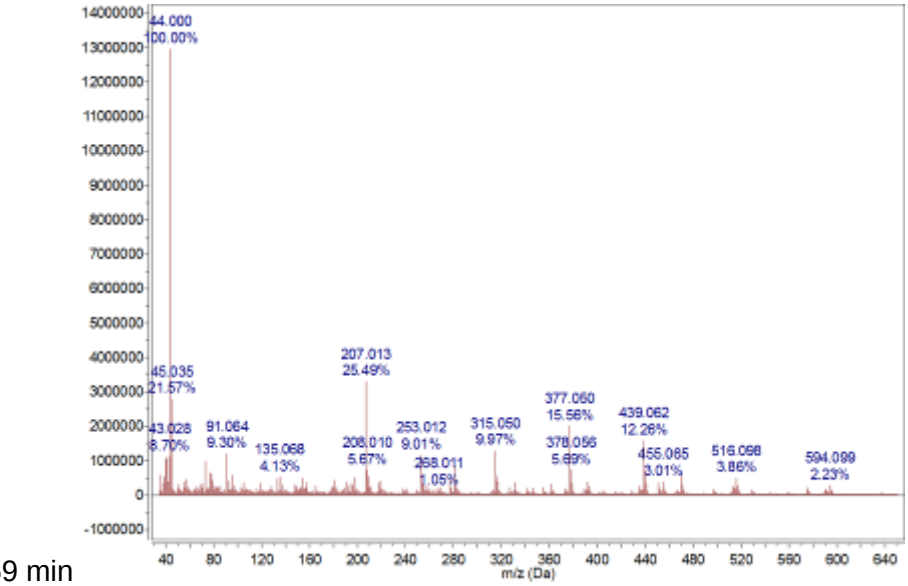

(c) >5.59 min

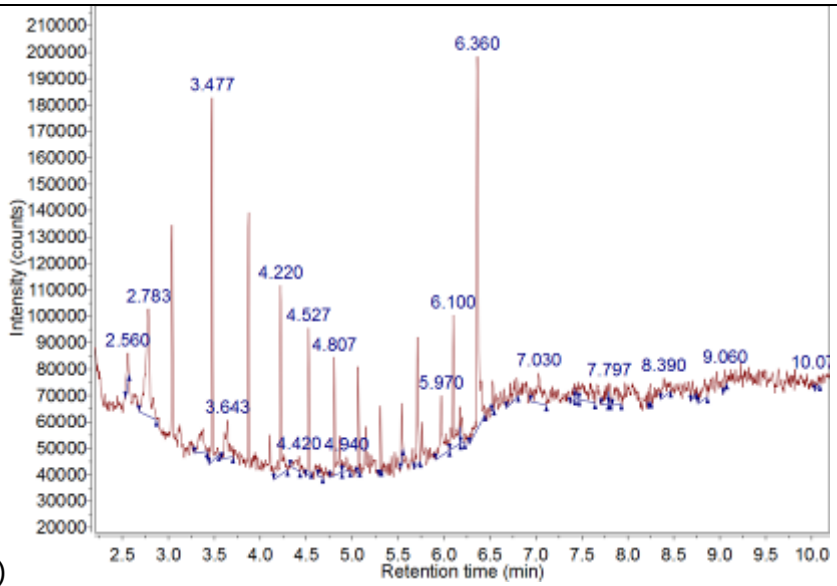

(a)

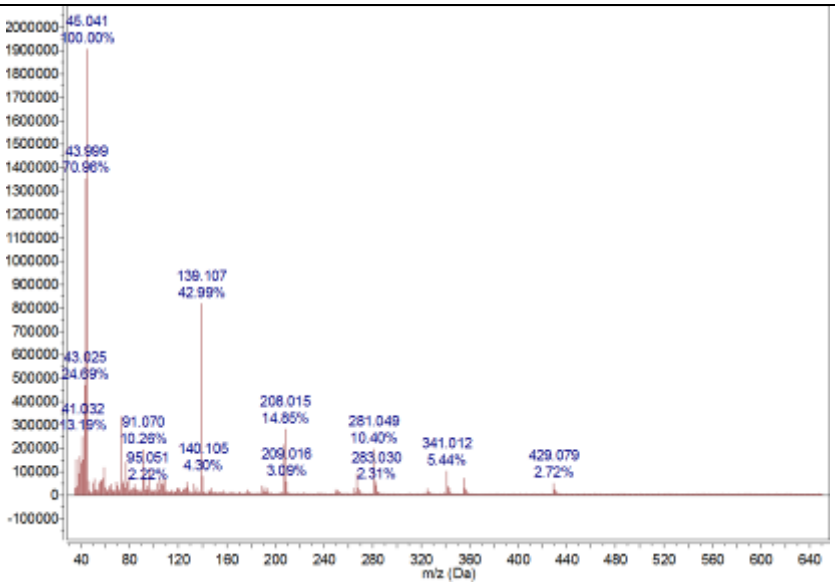

(b) <3.23 min

Glow Ammonia

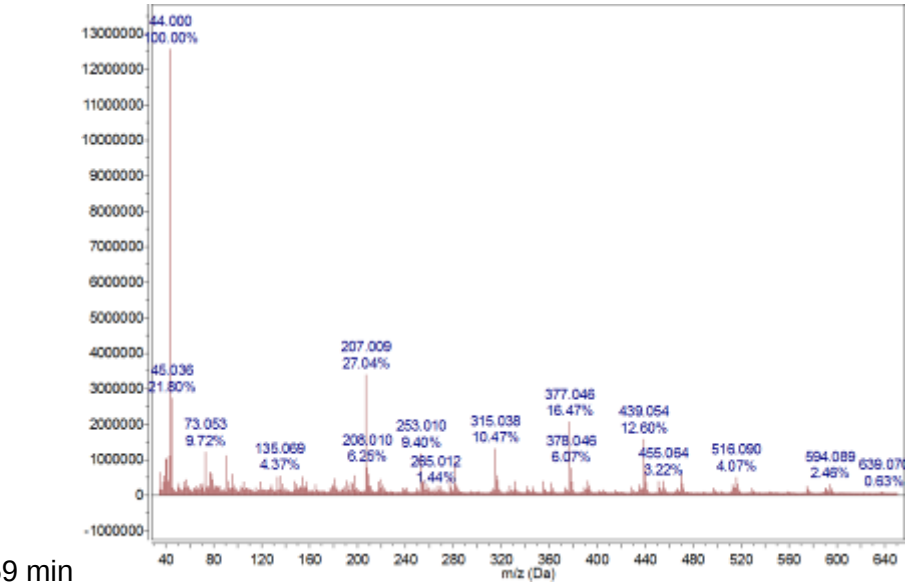

(c) >5.59 min

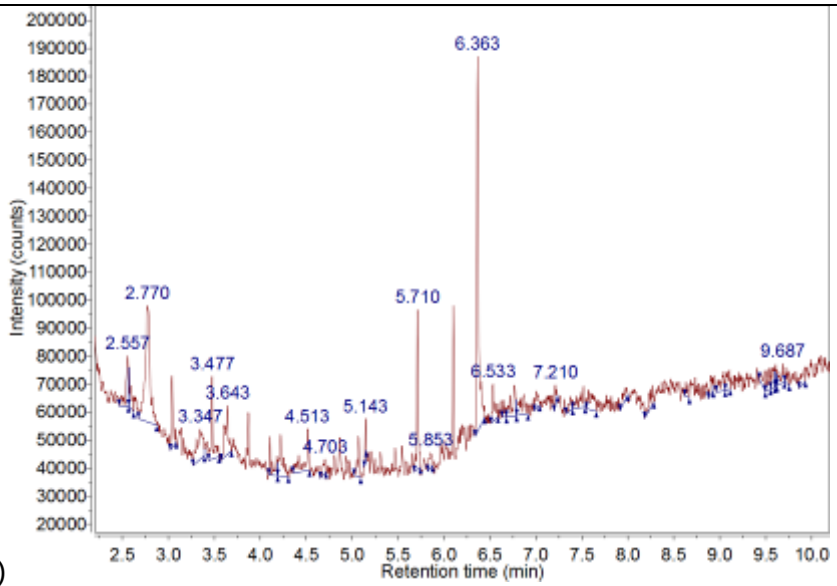

(a)

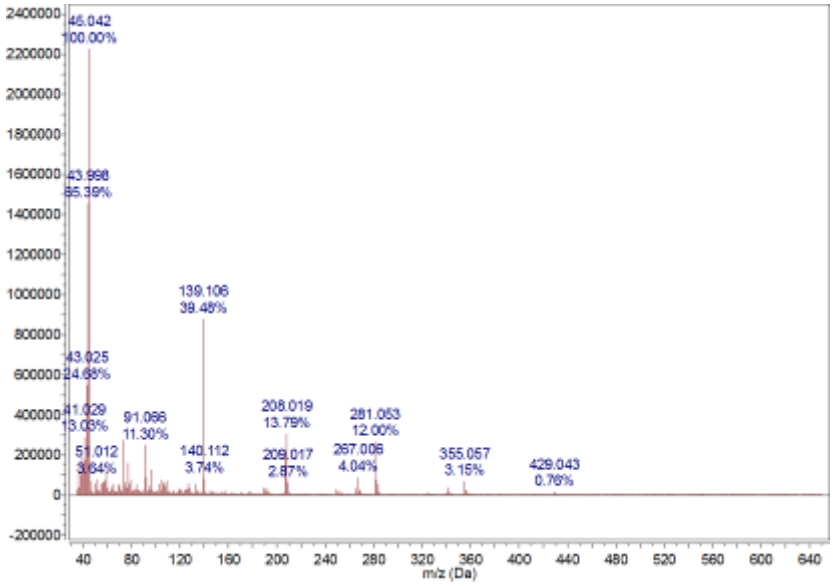

(b) <3.23 min

Remote Two-step Oxygen then Ammonia

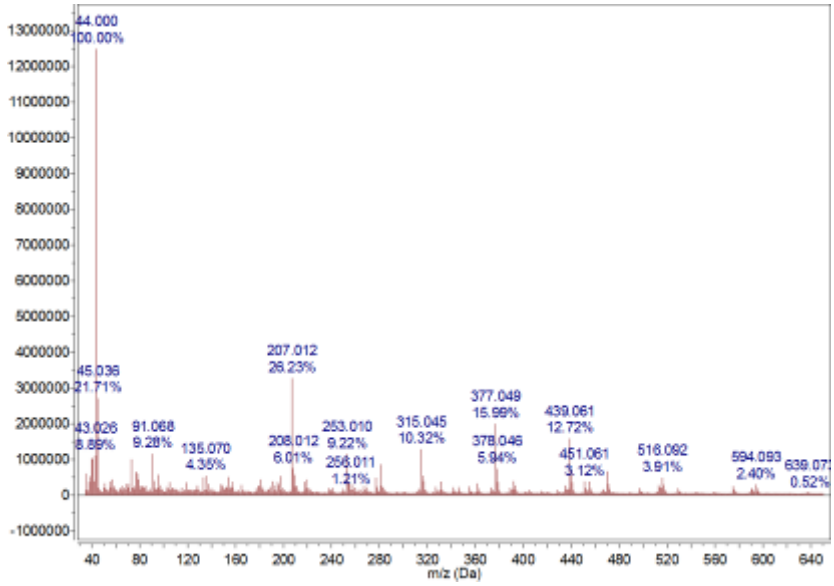

(c) >5.59 min

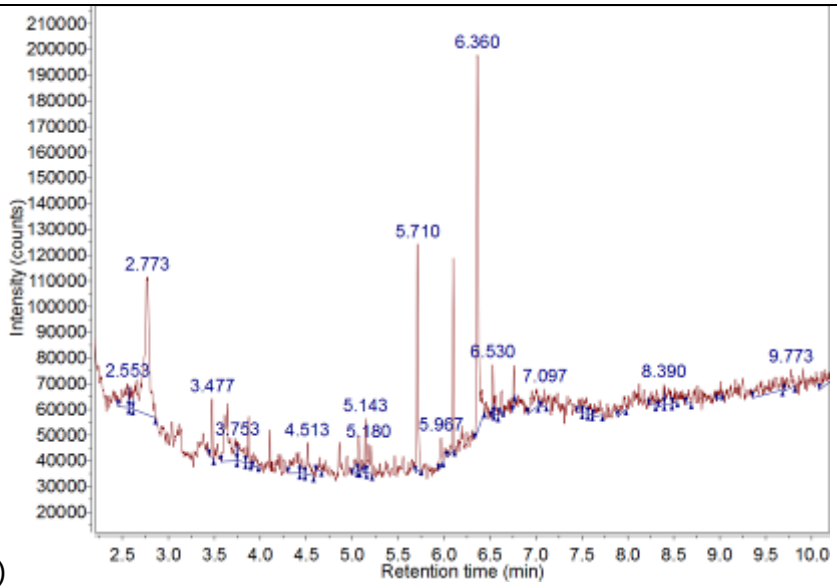

(a)

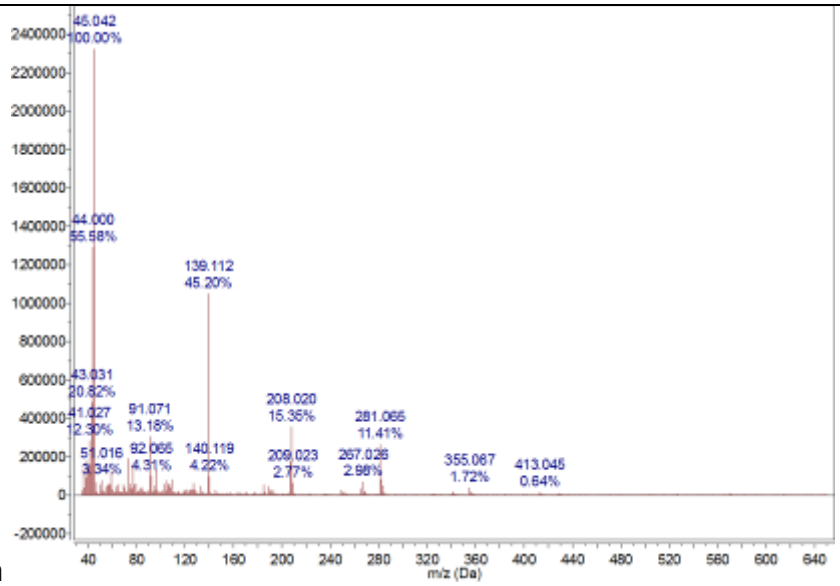

(b) <3.23 min

Glow Two-step Oxygen then Ammonia

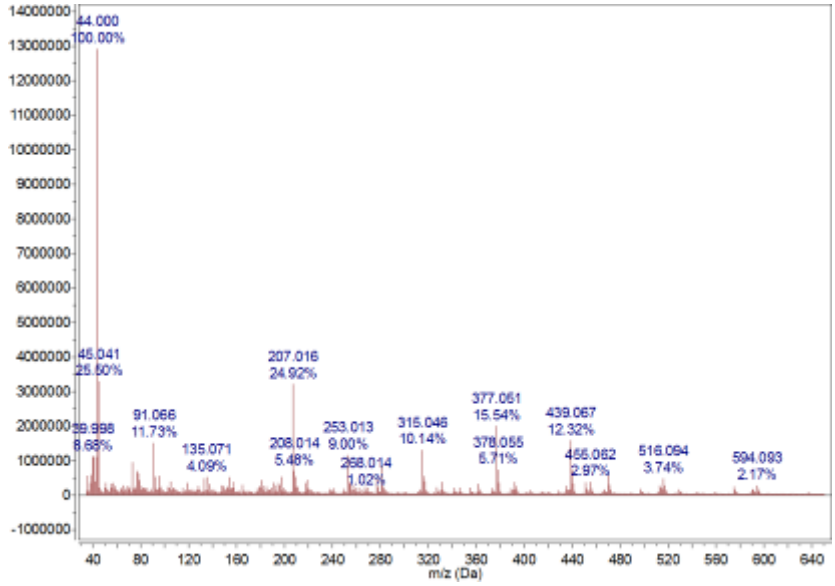

(c) >5.59 min

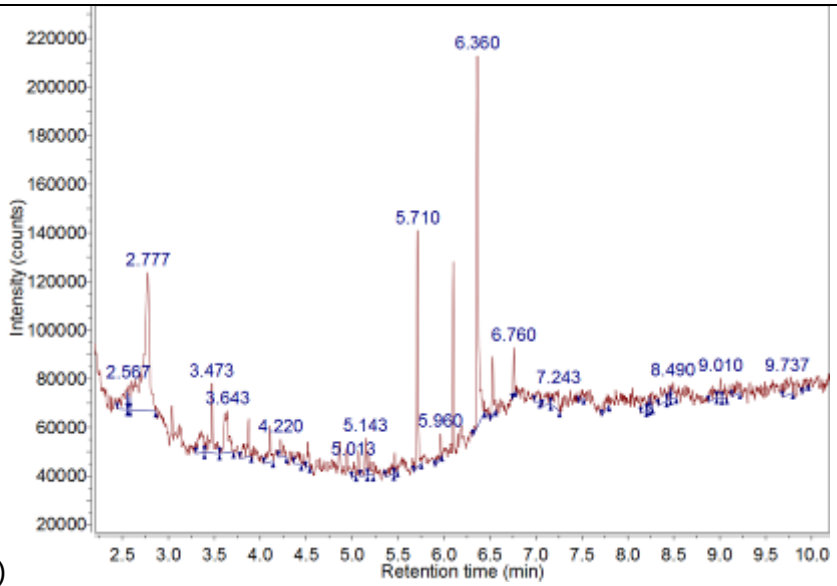

(a)

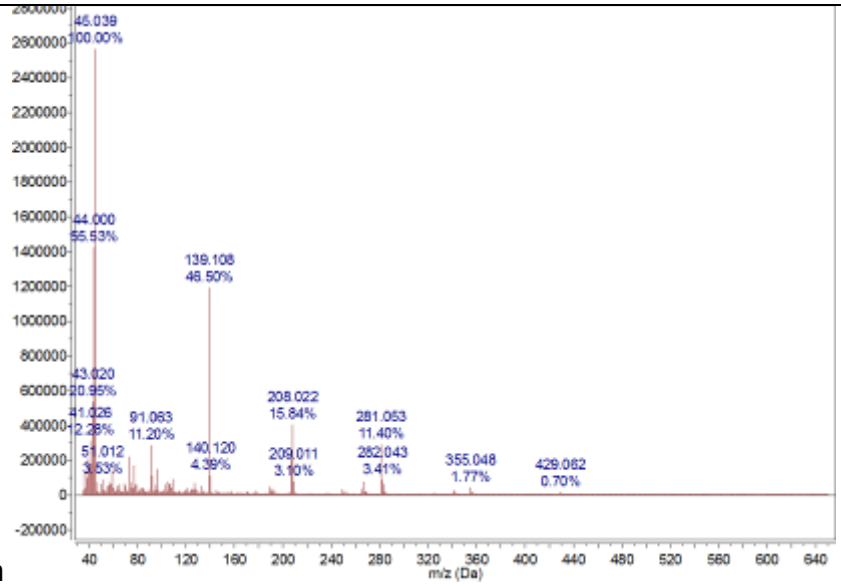

(b) <3.23 min

(c) >5.59 min

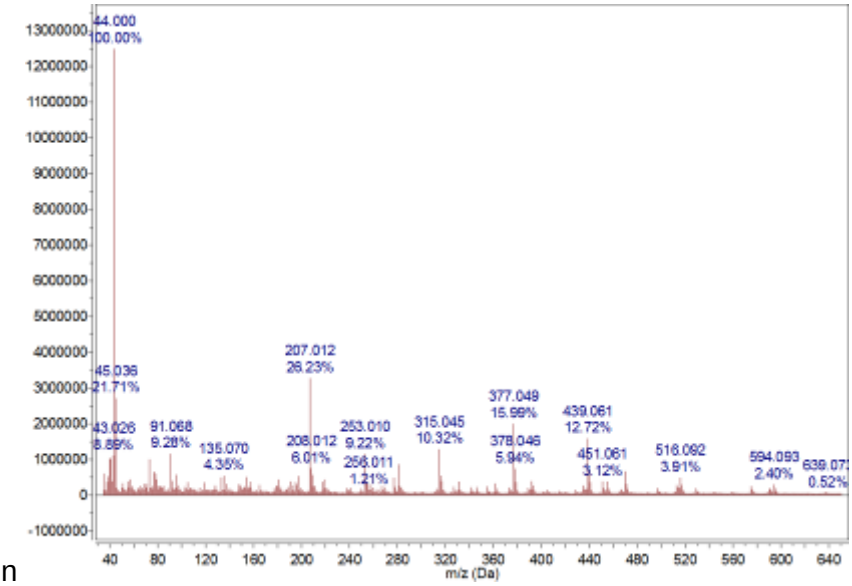

3.9.3 Summary

Although we were able to see a change in the surface tension of the wash liquor, giving an indication that there is a substantial concentration of LMWOS washed from the surface, in the GC-MS we simply see background contamination similar to that seen on the solvent alone, which can be attributed to column bleed and aerial contamination.

There are a few reasons that could explain why the species that are influencing the surface tension measurement are not appearing in the GC-MS spectra. First of these is that the concentration of these species of interest is below the limit of detection (LOD) of the detector. Alternatively, it could be that the species we are trying to detect, the identity of which is unknown, are not ionised by this method. Finally, the species may have eluted with the solvent before the two min data collection start point.

3.10 MECHANISTIC UNDERSTANDING: Investigating the Reversibility of the Hydrophobic Recovery

In tandem with the learnings from Section 3.8 about LMWOS removal, the hydrophobic recovery of WCA observed after solvent washing was investigated by observing the effect of sample storage in UHP water instead of air.

Table 35: Effect of storage conditions on solvent washed (120 s, 1:1 v/v solution of propan-2-ol and cyclohexane) ammonia plasma-treated (5 W, 300 s, 0.2 mbar) GF PTFE samples.

Storage Conditions	**Number of samples**	**WCA prior to storage /°**		**WCA after 24 h storage (blown dry with nitrogen after storage in UHP water) /°**		**WCA washed and dried under nitrogen /°**		**Surface Tension of wash liquor / mN m^{-1}**	
		Glow	Remote	Glow	Remote	Glow	Remote	Glow	Remote
UHP water at room temperature	1 glow and 1 remote	72 ± 3 (2)	67 ± 5 (3)	51 ± 8 (5)	48 ± 4 (2)	57 ± 6 (3)	51 ± 2 (1)	71.68 ± 0.05	71.83 ± 0.04
UHP water at 80 °C	1 glow and 1 remote	71 ± 2 (1)	72 ± 4 (2)	51 ± 16 (9)	89 ± 17 (10)	54 ± 8 (5)	88 ± 12 (7)	71.85 ± 0.05	91.92 ± 0.02
UHP water at 80 °C	2 glow and 2 remote	78 ± 4 (2)	71 ± 4 (2)	50 ± 13 (5)	50 ± 6 (2)	57 ± 12 (5)	61 ± 4 (2)	71.66 ± 0.06	71.83 ± 0.02
Air at 80 °C	2 glow and 2 remote	83 ± 3 (2)	70 ± 3 (1)	84 ± 6 (3)	77 ± 3 (1)	83 ± 0 (0)	73 ± 3 (1)	-	-

Storage in UHP water promoted the reversal of hydrophobic recovery in all samples apart from the remote plasma-treated sample that recovered to 89°, potentially this was too far gone. This phenomenon observed both at room temperature and at 80 °C. This reversal suggests that surface reconstruction is possible in the plasma-treated surfaces, and this is observable even after solvent washing.

Solvent washing after storage for 24 has no effect on the WCA for any samples apart from the remote plasma-treated UHP (80 °C) stored ones. Storage in hot air had no effect on the glow plasma-treated samples and a small increase in WCA was observed for the remote plasma-treated samples.

3.11 MECHANISTIC UNDERSTANDING: Mechanism of Two-Step Oxygen and Ammonia Plasma Modification

Explicitly, the mechanism by which the two-step process causes hydrophilization of the PTFE surface is similar to that which was initially proposed from the literature, Section 3.6. The high power (50 W) and long (600 s) oxygen plasma step increases the roughness of the surface, resulting in a very hydrophobic surface, but little changes in terms of the composition of the surface during this step. Subsequently an ammonia plasma at low power (5 W) and shorter duration (300 s) is responsible for incorporating nitrogen and oxygen containing groups into the surface in place of the fluorine which is removed.

The oxygen plasma induces a Cassie-Baxter wetting state, increasing the observed WCA significantly by the air trapped between the droplet and the surface. But after the second hydrophilizing process, due to the increased roughness and the surface compositional changes, Wenzel wetting is induced at the surface. This causes the significant decrease in the WCA which was not possible with a simple ammonia plasma. As well as a lower initial WCA, the two-step plasma treatment also retards some of the hydrophobic recovery observed in the literature and in single-step plasma treatments, this appears to be aided by the roughening step prior to hydrophilization.

The effect of solvent washing is marked, there is significant hydrophobic recovery for the ammonia single-step treatment and the two-step treatment. This can be attributed to LMWOS being washed from the surface. These species are formed because the harsh conditions of the plasma cause some surface destruction, but not all the particles are carried off in the plasma flow.

3.12 MECHANISTIC UNDERSTANDING: Understanding the Errors within the Plasma Modification Steps

One of the major issues with plasma modification is the fickle nature of plasma. A small change in the balance, leak rate, or pressure of a plasma can have a significant effect on the character of the plasma.

To this end, some of the data previously reported was statistically analysed to determine the significance of the internal and external errors of the plasma modification steps. In this case, an internal error is deemed to be the variation of measurements across a single sample. An external error is the variation between runs, i.e. between different plasma runs at the same plasma conditions.

Some of the errors that are associated with the plasma-treated samples can be attributed to the LMWOS upon the surface, as these are removed using the solvent wash process, so it would be expected that the washed samples will exhibit lower variation than that of the unwashed samples. However the data shown for ammonia plasma-treated samples shows a larger degree of variation for the solvent washed samples, Table 36.

Table 36: WCA for ammonia plasma-treated PTFE (5 W, 300 s, 0.2 mbar) both before and after solvent washing (120 s, 1:1 v/v solution of propan-2-ol and cyclohexane). Listed is the average and standard deviation for each sample or each run (3 measurements taken on each sample), and the overall average (9 measurements).

	Plasma Region	**WCA /°**			
		Run 1	**Run 2**	**Run 3**	**Overall Average**
Unwashed	**Glow**	37 ± 2	34 ± 2	36 ± 2	36 ± 2
	Remote	43 ± 1	41 ± 3	43 ± 1	42 ± 2
Washed	**Glow**	71 ± 4	62 ± 1	67 ± 3	67 ± 5
	Remote	65 ± 6	64 ± 2	69 ± 2	66 ± 4

3.13 CONCLUSIONS

In the work presented, the lowest WCA for a single-step plasma-treated surface after solvent washing (1:1 v/v solution of propan-2-ol and cyclohexane) was 47° (argon, 20 W, 120 s, 0.2 mbar, Table 11).

The lowest WCA possible is achieved is using an oxygen plasma (50 W, 600 s) in tandem with an ammonia plasma (5 W, 300 s), which consistently gives a WCA of less than 10°. Prior to solvent washing these two-step treated surfaces had WCA that were below the accurately measureable limit of the method. These are on par with the best reported surface of 4° from the literature.[147] After solvent washing, hydrophobic recovery is observed. The glow plasma-treated samples recover to 41 ± 3°, and the remote treated samples recover to 53 ± 3°, where the errors quoted are the standard deviation of the sample. The lowest WCA achieved for plasma-treated PTFE in the literature after solvent washing was an advancing angle of 53° immediately after Soxhlet extraction with methanol for 1 h, Table 1. It should be noted however, that this surface was unstable, and recovered to 70° after 10 h.[141] In light of this, all the best solvent washed samples from this work (both single-step and two-step) have a lower WCA than that reported in the literature.

The mechanism of the two-step oxygen and ammonia plasma modification process was determined to be that the oxygen plasma treatment induces a Cassie-Baxter wetting state, which is subsequently altered to the Wenzel wetting state by the ammonia plasma treatment, Section 3.7.3.

Through the use of characterization techniques such as SEM, AFM and XPS, the two-step plasma-treated surfaces were shown to result in a hybrid of the two constituent steps – increased roughness of the surface and significant defluorination and incorporation of nitrogen into the surface, Sections 3.7.1 and 3.7.4.4.

Just like the surfaces which were reported in the literature by T.K. Markkula *et al.*, if these two-step plasma-treated surfaces are kept in UHP water, the hydrophobic recovery of the surface is retarded. It can also reverse the process slightly for solvent washed samples, Section 3.8.2.

After solvent washing, the two-step plasma-treated samples have some active sites with subsequently react with the environment they are exposed to. If this is clean nitrogen, the observed WCA will be higher than if the environment is simply air, Section 3.8.3.

Although we were able to see a change in the surface tension of the wash liquors, giving an indication that there are some substantial LMWOS washed from

the surface, in the GC-MS we simply see background contamination similar to that seen on the solvent alone, which can be attributed to column bleed and aerial contamination.

In short, multiple gas plasma treatments can be used in tandem to create stable hydrophilic surfaces. The most wettable surface can be made by combining a harsh high power long duration destructive plasma with a subsequent more gentle shorter duration, lower power hydrophilizing gas plasma. The stability of plasma treated surfaces should be assessed after solvent washing to remove any LMWOS that are not strongly adhered to the surface, as these will cause falsely increased hydrophilicity when measure WCA.

Chapter 4: Atmospheric-Pressure Plasma Treatment of PTFE Surfaces

4 ATMOSPHERIC-PRESSURE PLASMA TREATMENT OF PTFE SURFACES

4.1 MOTIVATION

Previously the plasma modification processes described were carried out at low-pressures (previous work conducted at 0.2 mbar), but it is also possible to create plasmas at atmospheric-pressures. When up-scaling the processes described in Chapter 3, the need for low-pressure will incur significant cost implications.

There is a lot of 'down-time' associated with maintaining a good leak rate as well as the increased maintenance of pumps, vacuum chambers and connections and gas lines. All of these contribute to the cost of the process in an industrial setting. In addition to this, the need for the samples to be pumped down to base pressure prior to and after plasma treatment significantly increases the duration of the treatment. Low-pressure plasma processes are inherently batch rather than continuous processing methods. Batch processing is less desirable as it is significantly slower and therefore generally more expensive than a continuous process.

Furthermore, dielectric barrier discharge (DBD) plasma treatment of polymers has been used as a method to create electrets. The DBD process has been shown to impart charge onto the surface, and owing to the insulating nature of PTFE this charge is relatively stable. The area of electrowetting has been chiefly investigated for applications relating to electronics. However, the presence of an electric field upon a surface can promote an increase in wetting. In the same manner, it is postulated that the incorporation of charge into a PTFE surface can increase the hydrophilicity of the surface.

In view of these two points, the use of an atmospheric DBD system to produce a stable hydrophilic PTFE surface was investigated. The focus of this work was using a single, industrially viable (from a cost and safety viewpoint), atmospheric plasma treatment step.

4.2 LITERATURE REVIEW

4.2.1 Atmospheric Plasma Theory

The concept of atmospheric-pressure plasmas was discussed briefly in Chapters 1 and 2, however briefly most atmospheric plasmas are different from low-pressure plasmas in that they do not produce a glow discharge. Instead the plasma resembles small micro-discharges that jump from a 'live' electrode to an earthed electrode across an interelectrode gap. If the potential difference across the electrode gap is sufficiently high, the fixed electrode will emit electrons.[225] DBD plasma is self-limiting, and once the surface potential build up on the insulator electrode opposes the voltage across the plasma. This causes the plasma to self-extinguish unless the voltage supplied is augmented consistently.[315] When the sample is placed in the interelectrode gap, it is modified by the plasma micro-discharges as they strike the surface.

Cold plasmas are chiefly used in industrial applications as methods of decontaminating equipment or substrates, plasma cleaning processes are common practice in laboratory and medical settings.[226] Generally ozone-fed plasma cleaners are the most commonly used, and these are usually atmospheric-pressure devices. Laroussi first demonstrated the sterilization properties of non-thermal plasmas in 1996, and since then there has been a large variety of microorganisms and spores that have proven to be killed by cold plasma methods.[226,227] Through the use of an inert gas as a feed stock for the sterilizing plasma, it is also possible to create short and long lived radicals which are particularly effective for porous surfaces or substrates with cracks and crevices. By using a flow-through method, where a carrier gas is constantly passing over the surface, the decomposition products and debris from the plasma treatment are removed. Additionally, the flow will also act to cool the substrate, therefore minimizing damage to the surface. Inert gases also produce a more uniform plasma compared to air plasmas, resulting in an equal decontamination effect across the whole surface, and the inert gases also produce ultraviolet emissions which has an additional sterilizing effect.[226]

Additionally, organic and polymeric materials can be damaged under harsh plasma conditions, as shown by the long oxygen plasma described in Chapter 3. High-temperature plasmas, or those with a long duration or high power conditions can promote degradation of the material.[226,260] The reason that cold plasmas are not as aggressive as their low-pressure counterparts comes from the fact that the amount of gas molecules that are ionized in the plasma is comparatively low. Therefore, the majority of the energy of the discharge is carried by the electrons,

resulting in the bulk of the gas molecules remaining at close to room temperature. Under thermal plasma conditions, a much larger fraction of the gas molecules are ionized (>10^{-3} molecules), and so the bulk gas temperature can reach over 2000 °C.[226]

4.2.2 DBD Plasma Treatment of PTFE

In the work presented in this thesis, a DBD plasma apparatus is used to modify PTFE surfaces. This is often referred to as “parallel plate discharge” as the two electrodes are large plates, one live and one earthed, that are separated by a small interelectrode gap (typically 2–3 mm although can be as large as 8 mm depending on the voltage to the electrodes and the feed gas).

4.2.2.1 DBD – Dielectric Barrier Discharge

DBD (or silent discharge) is a non-equilibrium plasma characterized by the presence of a dielectric between two electrodes. When a high voltage is applied to the system, current is carried across the interelectrode gap via numerous micro-discharges. Micro-discharges occur when the potential difference across the interelectrode gap, then the electrode will emit electrons, the charge build-up on the sample surface will cause the plasma to self-extinguish. Because these micro-discharges are so short-lived, little sputtering of the electrodes occurs, even at high gas pressures.

The presence of the dielectric between the electrodes prevents the transition from a silent discharge to an arc discharge. This is both through promoting a random spatial distribution of the micro-discharges, and by facilitating the extinction of the micro-discharges. As a streamer reaches the electrode, there is a build-up of charge in that region of the dielectric which produces an electric field orientated against the applied field. This results in a reduction of the total field in that area until the current drops to zero, extinguishing the micro-discharge. Additionally, other streamers will preferentially hit the electrode surface away from this zero current region, hence encouraging better distribution of micro-discharges across the dielectric.[228,229]

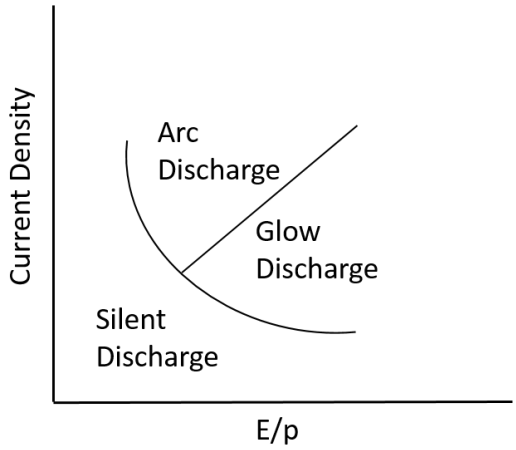

Figure 34: Schematic plot of how current density, electric field strength, and gas pressure determine the discharge type. Where E is electric field strength and p is gas pressure. Adapted from H.F. Beer thesis.[230]

By arcing across two electrodes, it is possible to ignite a DBD plasma at atmospheric-pressure without the introduction of heat into the system. Thus, the surface of temperature sensitive substrates can be modified, such as materials which are thermolabile, or biological surfaces.[231] Although the voltage required for ignition of the plasma is high, the current of the system is low, and thus a living thing can be used as the opposing grounded electrode to that supplied with the voltage. In this way, DBD plasma has been used for therapeutic uses in the treatment of dermatological conditions. Due to the complex morphology, differing electrical conductivities, and variable moisture content of the human skin over an area, it is possible to induce different plasma treatments in these areas during direct DBD treatment.[231]

There are two major categories of DBD plasma when experiments are carried out at atmospheric-pressures; filamentary and homogenous. Inhomogeneous, or filamentary, discharges are characterised by short-lived and transient micro-discharges that are randomly distributed.[231] The ignition location and duration cannot easily be predicted or controlled, and hence the resulting surface is often unevenly modified. Uniform surface treatment is much more likely to be achieved using a homogenous DBD plasma, where the plasma can be controlled spatially and temporally far more effectively.[231] A homogenous plasma is most likely with a defect free glass substrate as the dielectric (positioned on top of the earthed electrode).[231] Filamentary plasma can be induced using a point-to-plane electrode setup, whereby a thin metal electrode is supplied with the voltage, and the grounded electrode is metal with a dielectric such as an aluminium plate or a phosphate buffered saline solution over it.[231]

The steps by which an atmospheric plasma discharge is ignited can be broken down into a few steps; initially an electron avalanche propagates towards the anode. Subsequently the total number of electrons increases exponentially. These electrons generate their own electric field. The space charge field at the head of the avalanche is distorted by the electric field from the electrons. Once the electric field reaches a critical value, the avalanche will become a streamer, this only occurs if the interelectrode gap is sufficiently large (>50 mm) otherwise the plasma will resemble more of a glow discharge character.[231]

The differences between the two discharge types can understood further by analysing the behaviour of the electrons in the gas in the interelectrode gap. If the anode (earthed electrode or dielectric) is non-conductive, the electrons will not be lost from the air in the interelectrode gap and instead the negative charge from the dielectric will compensate for this. If the anode is conductive then electrons will be lost from the gas in the interelectrode gap instead of from the anode surface.[231]

4.2.2.1.1 DBD Plasma Treatment of PTFE Reported Literature

In the literature, DBD discharges have been used to modify the properties of PTFE using a wide range of different feed gases. The reported static water contact angle (WCA) of PTFE substrates after treatment in a DBD discharge range from very hydrophilic (25°) to hydrophobic (155°) depending on the atmosphere in which the discharge is ignited, Table 37.

The lowest WCA achieved using atmospheric DBD plasma to treat PTFE surfaces was approximately 25° after treatment by FDBD. This treatment was using a mixed nitrogen and hydrogen feed gas (65% N_2 and 35% H_2, 13 kV, 180 s treatment duration).[232,233] There was significant defluorination observed with this treatment (F/C ratio of 0.45 determined using XPS), which would explain the significant decrease in WCA. These samples were not washed or aged. Filamentary DBD in this case describes a plasma where the nature of the electrode setup results in the production of a single point filamentary discharge. This affects only a very small surface area rather than treating a whole film, as the discharge is ignited in the same position.[234] Using a set up similar to this, it would take a long time to treat a large surface area, especially given the relatively long treatment time of 180 s.

After a similar nitrogen and hydrogen atmospheric-pressure plasma treatment by the same group, using a DBD treatment method (0.25 W cm^{-2}, 60 s), a WCA of 40° was achieved (F/C ratio of approximately 0.5). However after storage

for 10 days in air, these samples exhibited hydrophobic recovery to 80°.[235] As this is without any solvent washing, it is not known whether the observed increase in WCA is due to aerial contamination from the surrounding environment or if it is due to a change in the surface composition.

The lowest WCA reported after storage in air was 75°, this was achieved after DBD plasma treatment in air. Z. Fang *et al.* reported an initial WCA of 56° after homogenous DBD plasma treatment (65 W, 40 s), and recovery to 75° after storage for 24 h.[236] They observed defluorination (F/C of 1.24), but not as severe as that which was previously mentioned for the lower WCA surfaces described by C. Sarra-Bournet *et al.* D. Pavlinak *et al.* reported what they described as a "permanently hydrophilized" plasma-treated surface on the inside of PTFE tubes. Their DBD plasma used air plasma feed gas, but the air was passed over a 5% oxalic acid aqueous solution. After 100 days stored in air, recovery from 65° to approximately 75°.[237]

In terms of solvent washed plasma-treated samples, as previously seen with low-pressure plasma-treated samples, there are very few papers reporting the results of solvent washing on the hydrophilicity of the treated PTFE substrates. One of the few that do is S. Ishikawa *et al.*, who washed their DBD treated samples with water after submersion in various aqueous solutions. They reported a decrease in the WCA of PTFE surfaces treated with an air DBD plasma after submersion in both H_2O, H_3BO_3, and H_2O_2.[238] After air filamentary DBD plasma treatment, a WCA of 93° was observed, and almost no defluorination was seen in the XPS analysis (F/C of 1.86). Immediately after plasma treatment, samples were immersed in distilled water and ethanol, as well as in aqueous solutions of H_3BO_3 (boric acid, 3 wt.%) and H_2O_2 (hydrogen peroxide, 3 wt%) for 3–5 s. After being removed from the solutions, the samples were dried in air, before being rewashed with distilled water and dried completely in air (no duration given).

After immersion in H_2O, the WCA was 69°, and the reported F/C was drastically decreased to 0.42. There was also reported an incorporation of oxygen into the surface after immersion, after plasma treatment the O/C ratio was 0.03, and after immersion in H_2O it was reported to be 0.12.[238] This suggests that the water could be quenching active sites on the surface left by the plasma treatment. A similar trend was observed after immersion in H_3BO_3; a WCA of 56°, F/C ratio of 0.76, and an O/C ratio of 0.17. After immersion in H_2O_2, the WCA was 55°, the F/C was 0.69, and the O/C was 0.15.[238] These changes in the F/C and O/C ratios after submersion in aqueous solutions suggest a significant change in the composition of the surface. It is possible that this is due to the washing process removing some

LMWOS from the surface, however it is also possible that the changes are observed due to surface reconstruction. Ishikawa *et al.* hypothesise that the change in F/C ratio is due to the removal of fluorine from the surface as hydrogen fluoride or as boron fluoride (when submerged in boric acid). They suggest that the immersion of the plasma-treated surfaces in aqueous solutions results in the reaction of trapped free radicals in the surface with the H_2O, H_3BO_3 and H_2O_2 molecules resulting in the formation of carboxylic acid end groups at the surface which render the surface significantly more hydrophilic.[238]

Table 37: Summary of prior art on DBD surface modification of PTFE. Entries ordered from lowest achieved WCA to highest.

Substrate	**Type of atmospheric plasma**	**Feed Gas**	**Plasma Conditions**	**F/C**	**WCA / °**	**Ageing study?**	**Reference**
PTFE sheet, Goodfellow, thickness 250 µm	FDBD	65% N_2, 35% H_2	13 kV, 180 s	Approx. 0.45	Approx. 25	Not given.	239,240
PTFE sheet, Xi'an Yuanhang Fluoroplastic Nylon Products Company Ltd., thickness 1 mm	DBD	Argon	3.25 kV, 90 s	0.57	34.9	Not given.	241
PTFE, Goodfellow, thickness 250 µm	DBD	H_2/N_2	0.25 W cm^{-2}, 60 s	Approx. 0.5	Approx. 40	Recovery to approx. 80° after 10 days.	242
PTFE film, thickness 0.15 mm, no details given as majority of paper in Chinese. Details taken from figures and abstract.	DBD	Air	30.83 W cm^{-2}, 60 s	Not given	50	Not given.	243
Commercial 0.2 mm PTFE films	DBD (homogenous)	Air	65 W, 40 s	1.24	56	Recovery to approx. 75° after 1 day.	244
Commercial PTFE, thickness 20 µm, 2.2 g cm^{-3}	DBD	Oxygen	1680 W, 40 s	Not given	58	Not given.	245
PTFE sheet, Nippon Valqua Industries Ltd., thickness 1.0 mm	DBD	He	15 W, 13.56 kHz, 30 s	Not given	Approx. 60	Little hydrophobic recovery seen on samples.	246
PTFE tubes (inner and outer tubes modified, curvature corrections required for WCA analysis)	DBD	Air (above the surface of the 5% solution of oxalic acid in distilled water)	AC current 15–20 kV, no treatment time given	Significant defluorination evident in C (1s), no F/C given	Approx. 65	Hydrophobic recovery seen. After 100 days samples had recovered approx. 10°. Deemed 'permanent hydrophilization'.	247
Commercial PTFE, thickness	DBD	Air	30 kV, 30 s	Not given	67.7	Not given.	248

0.1 mm							
Commercial PTFE, thickness 0.2 mm	DBD (filamentary)	Air	65 W, 40 s	1.23	70	Recovery to 85° after 1 day.	244
PTFE, no details given as majority of paper in Chinese. Details taken from figures and abstract.	DBD	Air	Power not given, 40 s	1.10	70	Not given.	249
Commercial PTFE sheet, thickness 0.1 mm	DBD	Air	6 kV, 40–150 s	1.10	70	Ages to 85°.	260
PTFE film, thickness 50 µm	DBD (filamentary)	Air	8.5 kV, 20 s	Not given	70	Not given.	256
Commercial PTFE, thickness 20 µm, 2.2 g cm^{-3}	DBD	Air	1260 W, 100 s	Not given	71.3	Not given.	245
Commercial grade PTFE, Goodfellow, thickness 20 µm, 2.2 g cm^{-3}	DBD	Air	600, 1300, 2000 W, time not given	Not given	102 at 600 W, 81 at 1300 W, and 81 at 2000 W. Note: a lower WCA was obtained after multiple cycles of DBD treatment. Lowest is 71	Not given.	250
Commercial PTFE sheet	DBD	H_2	27.12 MHz, 3 mm s^{-1}	1.4	86	Not given.	251
PTFE, Goodfellow, thickness 100 µm	DBD, Sigma Technologies (Tuscon AZ) model APC	He/O_2	1200 W, 2.5 s and 25 s	3.4 after 2.5 s, 2.8 after 25 s	88 after 2.5 s, 82 after 25 s	Not given.	252

	2000						
PTFE, Goodfellow, thickness 0.05 mm	DBD	Air	5.0 mJ, 5 s	Not given	89.4	Approx. 93° after 14 days.	253,254
Amorphous PTFE sheet, no details given.	DSCBD	Air, N_2/H_2O	400 W, 30 s	Only survey spectra given	Approx. 90 after air treatment, Approx. 90 after N_2/H_2O treatment	Minimal recovery observed.	255
PTFE sheet, no manufacturer details given, thickness 50 μm	DBD (filamentary) with rollers rotating at 240 rev min^{-1}	Air	8–13 kV, 10 μs cycle length, 40–90 cycles performed and 20 s total process time	1.86, decreased to 0.42 after immersion in H_2O, and 0.69 after immersion in H_2O_2	93, decreased further to 69 after immersion in H_2O, and to 55 by immersion in H_2O_2	Storage in air recovers to 119°. Surface modification by immersion in H_2O and H_2O_2 is temporary, and hydrophobic recovery observed (111° after removal from H_2O, and 86° after removal from H_2O_2).	238,256
PTFE, Goodfellow, thickness 0.05 mm	DBD	Air	3.5 mJ, 5 s	Not given	94.6	Not given.	253,254
Commercial PTFE sheet	DBD	Ar	27.12 MHz, 3 mm s^{-1}	Not given	100	Not given.	251
Commercial PTFE sheet	DBD	O_2	27.12 MHz, 3 mm s^{-1}	1.5	105	Not given.	251
PTFE sheet, no details given	Appears to be dielectric, no specific details given	98% He 2% O_2	150 W, 5 min	2.04	125	Not given.	257
PTFE sheet, no details given	DBD with shower head electrode.	B_2H_6/He	100–200 W, 5 min	0.4	Not given	Not given.	258

4.2.2.2 APGD – Atmospheric-pressure Glow Discharge

Glow discharge is often considered to be a more uniform type of cold plasma. Glow plasma conditions can easily be created in low-pressure environment, but in an atmospheric and continuous processing environment, it is usually necessary to use a plasma jet.[259,261] It is possible however to create a glow plasma, non-filamentary and radially homogenous over the whole electrode, using two electrodes and a DBD equipment setup.[260] Z. Fang *et al.* reported that the plasma character can be changed from filamentary to glow plasma by controlling the number of current pulses per half-cycle. In the case of DBD there are a number of discharge current pulses per half-cycle and this results in filamentary micro-discharges. APGD is characterized by a singular current pulse in each half-cycle, Figure 35. In order to get a homogenous discharge, Z. Fang also placed a fine wire mesh (#325) over the electrode, although the method by which this works is not understood.[260]

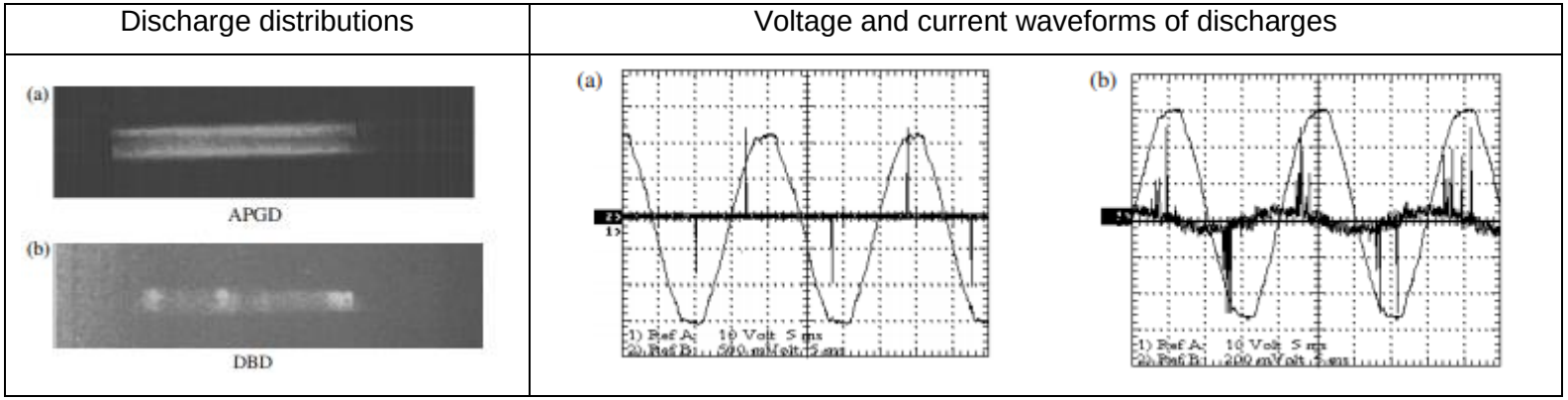

Figure 35: Shown is the (a) homogenous APGD discharge and (b) the non-homogenous filamentary DBD discharge with a 2 mm air gap between electrodes and an applied voltage of 6.5 kV.[260]

Table 38: Summary of prior art on APGD surface modification of PTFE. Entries ordered from lowest achieved WCA to highest.

	Type of atmospheric plasma	**Feed Gas**	**Plasma Conditions**	**F/C**	**WCA / °**	**Ageing study?**	**Reference**
PTFE film, thickness 50 µm	APGD	He	60 W, 30 s	1.18	46	After 10 days, recovery of 10° seen.	259
Commercial PTFE, thickness 0.1 mm	APGD	Air	6 kV, 40–150 s	1.07	53	Recovery to 70°.	260
PTFE, no details given as majority of paper in Chinese. Details taken from figures and abstract.	APGD	Air	Power not given, 40 s	1.05	55	Not given.	249
PTFE particles, I.E. du Pont de Nemours and Company, thickness 25 µm	APGD	Air	20 kHz, 230 V, 300 W, particles transported through plasma at 2 g min^{-1}	1.5	Not given	Not given.	261

The lowest reported WCA using an APGD helium plasma jet (60 W, 30 s) was 46°, which was not stable, and recovered to 56° after 10 days storage under ambient conditions.[259] There were no reported wash processes carried out on the APGD treated samples. The method described by Z. Fang which does not use a plasma jet as a method of creating a glow discharge (6.5 kV, 40 s) reported an F/C ratio of 1.07, and a WCA of 53° which recovered to approximately 70° after storage for 6 days in ambient conditions. There was also no reported washing process. When the same plasma conditions were used, but the pulse cycle was such that a non-homogenous plasma was created, Fang *et al.* observed a WCA of 70° rising to approximately 80° after storage. This change can be attributed to the lower increase in oxygen incorporation observed in the XPS spectra of the DBD treated samples.[260]

4.2.2.3 Corona Discharge

Corona discharge is similar to DBD in that it is filamentary in nature, however it is a point-to-plane method. The lowest reported WCA as 36° after treatment with helium plasma (20–60 W, 1–60 s), however there was no investigation into the stability of this modified surface to storage in air, or to solvent washing processes.[262]

Table 39: Summary of prior art on corona discharge surface modification of PTFE. Entries ordered from lowest achieved WCA to highest.

Substrate	**Type of atmospheric plasma**	**Feed Gas**	**Plasma Conditions**	**F/C**	**WCA / °**	**Ageing study?**	**Reference**
PTFE, no details given	Corona discharge	He	20–60 W, 1–60 s	Not given	36.0	Not given.	262
Teflon resin, thickness 0.05 mm	Corona discharge	N_2 with 1% NH_3	2500 W, 4.2 cm s^{-1}	0.71	Adv. 69, rec. 10	Not given.	263
Teflon resin, thickness 0.05 mm	Corona discharge	N_2 with 1% H_2	2500 W, 4.2 cm s^{-1}	0.89	Adv. 74, rec. 12	Not given.	263

4.2.2.4 Alternative Atmospheric Plasma Methods

Some of the plasma methods reported in the literature do not fit easily into the main categories, and oftentimes the nature of the plasma (glow or filamentary) is not investigated. The lowest WCA achieved was 28°, however the exact nature of the plasma that created this is unknown as an argon jet was used to induce a helium plasma. These surfaces were not stable, and recovered to 50° after ambient storage for 6 months, there was no investigation into solvent wash stability.[264]

For the most part, plasma jet treatments of PTFE substrates are not very successful in producing hydrophilic surfaces.[268,269,271,272,273]

Table 40: Summary of prior art on alternative types of plasma surface modification of PTFE. Entries ordered from lowest achieved WCA to highest.

Substrate	**Type of atmospheric plasma**	**Feed Gas**	**Plasma Conditions**	**F/C**	**WCA / °**	**Ageing study?**	**Reference**
Transparent PTFE tube with inner diameter of 0.5	TAPP. Atmospheric helium plasma induced in	Helium	Argon plasma 60	XPS performed	28	Yes. Recovery	264

mm, Shanghai Huafang Rubber and Plastic Co. Ltd.	a PTFE tube by an argon plasma jet inside a quartz tube.		Hz, variable voltage. Details of helium plasma not given.	but no F/C given		to approx. 50 after 6 months.	
PTFE sheet, Goodfellow, thickness 250 µm	APTD	N_2 + 2000 ppm H_2	10 kV, 180 s	Approx. 1.0	Approx. 25	Not given.	239,240
PTFE sheet, Goodfellow, thickness 250 µm	APTD	N_2 + 100 ppm NH_3	10 kV, 180 s	Approx. 1.2	Approx. 25	Not given.	239,240
PTFE NILACO Co. Ltd., thickness 0.125 mm	Capacitively coupled, 5 mm between electrodes.	He and trimethoxyborane(TMB)/H_2/He	50 W, 10 min	Approx 0.0 after TMB/H_2/He (complete defluorination suggests that a film is being deposited rather than the surface modified), 1.0 after He	50 after TMB/H_2/He, 60 after He	Not given.	265
PTFE foil, thickness 0.5 mm	SLAN	Ar/O_2	1 kW, 5 s	Not given	55	Not given.	266
PTFE sheet, Goodfellow, thickness 0.1 mm	APC2000 computer system used, no further information given.	He as work gas, O_2 as reactive gas	6.2–12.4 kW m^{-2}, no time given	C (1s) and F (1s) not shown	85	Not given.	267
PTFE sheet, DuPont, thickness 127 µm	Cold plasma source jet	Ar	14 W, 2 s mm^{-2}	Not given	85	Not given.	268
PTFE sheet, Goodfellow, thickness 1 mm	APPJ	Ar, Ar/CO_2	2.31 W, 20 s	1.79 for Ar, 1.59 for Ar/CO_2	Approx. 88 for both gas streams	Not given.	269
PTFE sheet, Goodfellow,	APC 200 computer	He/H_2O	0.861–2.58	0.5 after all	101 after	No	270

thickness 1 mm	system used, no further information given.		W cm^{-2}, 0.4–40 s	treatment times	0.4 s, 90 after 1.3 s, 77 after 40 s	significant ageing effects seen, WCA increased by approx. 1.4%.	
Goodfellow, thickness 1 mm, Ref FP303050	RF Plasma Torch, Atomflo-250D using 2 multiperforated parallel plate electrodes.	Ar and Ar/O_2	80 W, 10 min	2.09 after Ar/O_2, 1.98 after Ar	3 µL, 130 after Ar/O_2, 110 after Ar	Not given.	271
Goodfellow, thickness 1 mm,	RF atmospheric plasma torch, Atomflo 400L-Series	He/O_2	90 W, no time given	Approx 2, no significant change observed	140	Not given.	272
PTFE sheet, Goodfellow, no further details	RF Plasma Torch, Atomflo 400L-Series	He/O_2	60–150 W, 46.8 min	Approx 2, no significant change observed	155	No significant change observed.	273

4.2.2.5 Summary

From the literature search, the best treatment was atmospheric plasma using a mixture of nitrogen and hydrogen as the feed gas. Using this feed gas, multiple literature sources report a WCA of approximately 25° immediately after plasma treatment, using both FDBD and APTD methods.[239,240]

Using DBD treatment, the lowest WCA reported after air treatment was 50°,[243] the lowest reported aged sample recovered to 80° (from 40°) after 3 days.[242] When the stability of the treated samples is assessed, the lowest stable PTFE surface had a WCA of 50° after helium TAPP treatment.[264]

The only samples that were washed after plasma treatment were those that were immersed in H_2O and H_2O_2 after treatment by air DBD plasma (Section 4.2.2.1.1). Prior to immersion, the WCA was 93°, and after storage in air this recovered to 119°. After immersion in H_2O, the observed WCA was 69°, but this recovered to 111° after storage in air. An increased effect was seen after immersion in H_2O_2; the WCA was 55°, rising to 86° after removal from the solution and storage in air.[238,256]

4.2.3 PTFE Charged Surfaces

Although fluoropolymers are electrically insulating, they have also been shown to store injected electrical charges for prolonged periods of time even at high temperatures.[274] An early review by Van Turnhout in 1975 described fluorocarbon polymers as materials with excellent charge-storage properties.[291] Charge can be imparted into a PTFE rod easily. In GCSE science, rubbing a duster briefly over a PTFE rod is used to demonstrate how a negatively charged surface can be used to "bend" a stream of water from a tap.

4.2.3.1 Incorporation of Charge into Surfaces

Charge can be incorporated into a surface through corona plasma charging, tribocharging, and electrostatic fibre spinning.[275] The type of charging is dependent on the nature of the polymer. For example, tribocharging, whereby charge is imparted into the polymer via direct contact like rubbing, is only suitable for fibres which have varying electrical properties. Contact charging is the method by which toner particles are charged in order to be used in photocopying applications.[276]

Polymers can have regions where the mobility of charge is reduced to the point where the site can be described as a non-radiative quenching site, or more

commonly known as a charge trap.[277] The transport of charge through an insulating material is studied using voltage decay studies, and was initially modelled by Many and Rakavy.[278] P.W. Chudleigh reported a model based on three main parameters; the mobility of charge through the polymer, the mean free time of a carrier between charge traps, and the mean time a carrier spends in the trap. When the electric field strength was less than 4 x10^5 V cm^{-1}, the duration of time electrons spend in traps, and the mean free-carrier mobility within the polymer are independent of the strength of the electric field.[279] This means that the power of the DBD plasma used will have no effect on these parameters in terms of the charging of PTFE.

Charge is trapped on the surface through the simultaneous occurrence of 4 process; electron trapping, electron releasing, hole trapping, and hole releasing. This occurs at the bottom energy level of the conduction band and the top energy level of the valence band in an insulating solid, Figure 36.[283] As an ion from the surroundings approaches the surface, an electron from the surface can be involved in an Auger neutralisation reaction which results in a hole at the surface. As these holes are at the surface, they will interact strongly with the electrons in the surface region, and recombining and thus are “trapped” in the surface state. These holes are therefore unable to move into the bulk of the material without a significant amount of energy.[280]

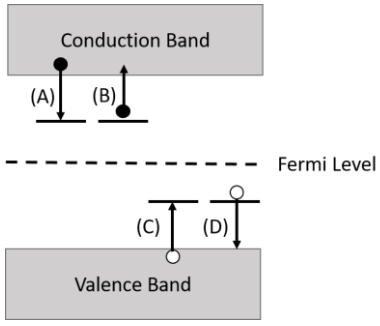

Figure 36: The processes by which charge is incorporated into an insulating surface. (A) An electron drops from the bottom energy level of the conduction band, known as electron trapping. (B) An electron is promoted into the conduction band, termed electron releasing. (C) Hole promoted from the top energy level of the valence band, known as hole trapping. (D) Hole drops down to the top level of the valence band, termed hole releasing.[283]

For PTFE, band theory is less applicable as the LUMO σ^* C-C orbital is above the vacuum level, and so will cost energy to put an electron into PTFE. The width of the bands is dependent on the overlap of orbitals, so is perhaps more accurately represented as localised bonds. K. Seki *et al.* using UPS and *ab initio* calculations, reported the energy band structure of PTFE, Figure 37.[281] They reported that the

top region of the valence band was comprised of the C and F *2p* orbitals, including both the C-C and C-F antibonding contributions.[281]

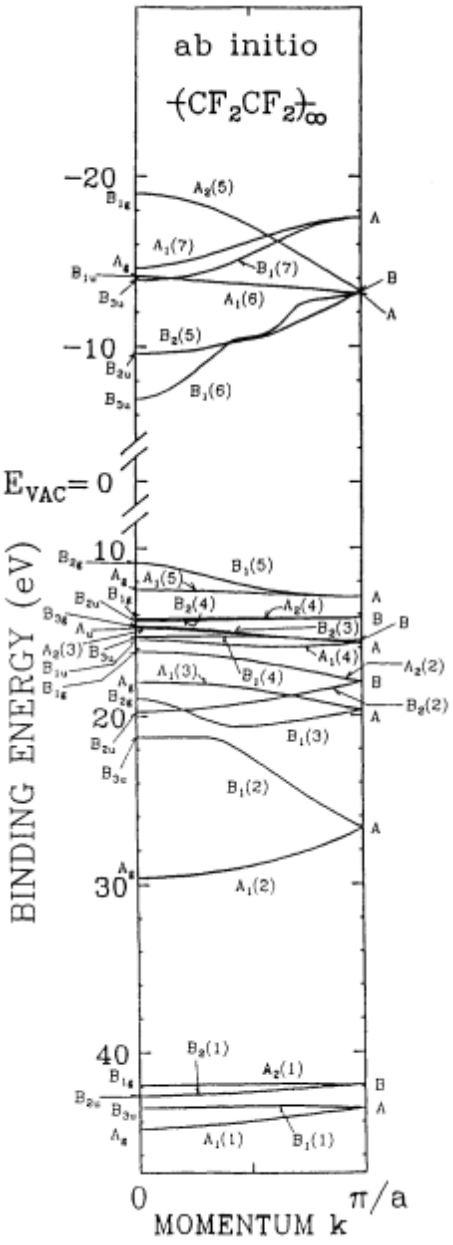

Figure 37: Energy band structure of PTFE chain in planar zig-zag formation (not helical) as reported by K. Seki *et al.*.[281]

By looking at the band structure reported by K. Seki *et al.*, it can be seen that the conduction band is 8 eV below the vacuum level, although in the abstract it is quoted as 2.9 eV. It is possible that electrons could be held in the conduction band during charge trapping. Work by A. Atta *et al.* indicated that the conduction of electrons through a PTFE substrate increases as the voltage on the surface increases.[282] In the work presented by this group, an Ar^+ beam was used to irradiate

PTFE surfaces in order to improve the conductivity of PTFE, and significant improvements were found for the stability of the substrate as a dielectric.[282]

The nature of the surface as the place where polymer chains end intrinsically results in some unsaturated bonds.[283] Additionally there is the presence of a layer of contamination, from both chemisorption and physisorption from the surrounding atmosphere.[284] Both of these result in a region of imperfections which give rise to different surface states. These act as charge traps for electrons, and are more prevalent at the surface than in the bulk.[283] It therefore follows that the surface microstructure will affect the degree of charge trapping present at the surface; for example a rough surface will have more surface potential traps, and therefore should hold a higher degree of charge when exposed to an electric field.[283] The use of SEM and AFM will determine whether there is significant physical defects present on the surface for there to be electron trapping after plasma treatment.

At the surface, PTFE chains align such that the there is a spiral with fluorine atoms on the outside and the carbon atoms in the centre. This helps the surface to maintain the lowest possible molecular potential energy, and results in a higher concentration of fluorine atoms at the surface than in the bulk.[283] As fluorine is a strongly electronegative atom, it can act as a site for electron trapping. As previously stated though, it will require energy in order to insert an electron into a pure PTFE substrate due to the high lying LUMO.

An alternative is electron insertion at chemical defect sites, for example, hole traps are located where there are impurities adsorbed on the surface. These adsorbed impurities on the surface can act as trap centres for electrons and holes, and mean there are far more traps at the surface than in the bulk.[283] The electron affinity of these impurities will indicate which functional groups have sufficiently low lying orbitals for electron insertion. For example, $O_2 \rightarrow O_2^-$ first electron affinity is -142 kJ mol^{-1}, which is significantly less than that of fluorine (-328 kJ mol^{-1}).[285]

Additionally, if the surface chemical structure of a polymer is distinctly different from the bulk, it can induce flashover phenomena. This describes the process of voltage breakdown along the surface of insulators, and is common in PTFE when subjected to low applied voltage.[283]

Early work by D.K. Davies investigated the work function of different polymer films (thickness 50 µm) through the dielectric surface potential after metallic contact under vacuum.[286] The expression that was used to calculate charge density, postulated by A.J. Dekker, is shown below.

$$\sigma = 1.77x10^{-13}\,\epsilon\left(\frac{\phi_M - \phi_D}{\lambda}\right)$$ Equation 4.1[286,287]

where σ is the surface potential density measured in C cm^{-2}, ϵ is the dielectric constant of the insulator (polymer), $\emptyset_M$ is the work function of the metal that is contacting the polymer, and the $\emptyset_D$ is the dielectric work function, and λ is the depth of injection of the charge. The work function for PTFE was calculated to be 4.26 ± 0.05 eV.[286]

Corona charging however is not so substrate specific. The plasma streamers formed from the charged electrode to the substrate during corona plasma contact the surface and impart charge into charge traps. Due to the insulating nature of these polymers, the charge is not completely conducted through the polymer and thus chiefly remains at the surface. As the plasma is not uniform in density, the charge remains uneven across the surface, creating pockets of higher charge where the streamers contact the surface.

4.2.3.2 Electrets

Electrets, first coined as a phrase in 1920, are often described as the electrical version of a magnet – i.e. they are dielectrics that are stably electrically charged.[288,289,290] These are useful as electrostatic components that can maintain a high electric field reliably even under severe temperature and humidity conditions.[291] The first electret was made from carnauba and resin by Eguchi, which were melted together with beeswax in a strong electric field. These were initially negatively charged, and over time these negative charges were replaced with positive permanent charges.[292]

There are a number of structural factors which can affect the efficacy of a polymer as a charge storage electret.[293] Firstly the WCA of a surface: as polymers with a thermally stable hydrophobic bulk charge trapping layer will have slower charge disspropan-2-oltion.[293] Additionally the length of the side chain form the polymer carbon backbone can also have an influence, those with longer conjugation length in side-chain moieties have more efficient charge trapping, therefore are better electrets. Conjugation, specifically π-conjugation, in the side chains of a polymer increases the stability of the electret formed.[293]

The surface charging characteristics of polymers have been mainly investigated with respect to their potential for application as electrets. Boisseau *et al.* were able to create an electret using a Teflon sheet with a metallic backing using a positive corona discharge with a point voltage of 10 kV.[294]

4.2.3.3 How to Measure Charge on Surfaces

There are a number of different methods of measuring charging of surfaces. In this report, the charge is measured using an electrostatic voltmeter, measuring the surface potential in volts. An alternative measure of the charging can be to use Lissajous figures to investigate changes in charging properties in polymer surfaces.[295] The Lissajous method measures the discharge energy by measuring the voltage pulse on the capacitor, and plotting the charge (nC) against the applied voltage (kV).[248]

Yovcheva *et al.* completed work that analysed charged polypropylene surfaces by XPS, which indicated that different polarity coronas lead to the formation of what he described as different surface local levels through changes in the oxygen content of the surface.[296]

Non-contact AFM can be used in order to map the surface potential of the substrate. The cantilever is oscillating already, in tapping mode, and the effect of the surface potential upon this oscillation can be measured in order to map the surface potential.

An alternative method by which the surface potential can be visualised is that described by Yagishita *et al.* Samples of spherulitic polypropylene were positively charged using a positive corona discharge in air biased at 700 V. Negatively charged Sudan-blue dye particles were introduced into the narrow space above the polypropylene sample, and adhered to the positively charged parts of the polypropylene surface. The distribution of the dye particles across the surface was analysed using optical microscopy. Their findings indicate that deep charge traps were found in the central parts of the samples, and shallow traps were found in the peripheral regions.[297] It should be noted however that although this study was undertaken on an insulating polymer, the surface was constructed of spherulitic polypropylene structures rather than the uniform film structure of the Goodfellows PTFE.

4.2.3.4 Mechanism of Charge Storage

As a non-polar polymer, PTFE has the capability of storing charge over a long period of time due to its intrinsic high electrical resistance.[298] In early work into the mechanism of charge trapping into polymers, it was shown that the low conductivity (i.e. insulating nature) of polymers was due to the low degree of mobility of charge

carriers in the bulk.[299] For the most part, charge carriers were located in charge traps.[299]

Due to the total fluorine substitution of the carbon backbone, PTFE forms one of the most thermally stable electrets of all the polymers. R.A. Creswell *et al.* found that total discharge of a corona charged electret did not occur until 230°C.[300] The temperature at which the electret is formed can have an influence on its long term stability. Electrets that acquire charge at higher temperatures have low charge mobility once they are returned to room temperature.[291,301]

Charge stability in bulk PTFE can be explained by the low charge mobility in the polymer due to its semi-crystalline nature. PTFE molecules align in fibres rather than spherulite structures.[302] The crystalline regions, and the interfaces between amorphous and crystalline regions in PTFE are reported to form charge traps, whereas the amorphous regions allow for charge mobility.[302] Due to the long fibrous formation, these amorphous sections are separated by crystalline regions which slows the disspropan-2-oltion of charge. Additionally, the presence of crosslinking on the surface can reduce still further the charge mobility of a charge surface, and increase the charge stability.[303]

The investigation of charge trap sites can be carried out using a number of techniques; the most commonly used is the thermally stimulated current (TSC) technique. In TSC, thermal diffusion is used to generate electrical signals, and the charge distribution is obtained from the electrical response from the surface.[304.305] Acoustic analysis techniques use laser-induced pressure pulse, pulsed electroacoustic methods or piezoelectrically generated pressure steps in order to map the charge distribution on the substrate surface.[305] AFM can also be used in both contact and non-contact modes in order to map the charge trap sites on the surface.[305,306] There is some contention over exactly how deep the traps are that hold the charge on the surface, and indeed whether these result in significant surface restructuring. Mellinger states that for PTFE, traps with a binding energy as high as 6 eV can be found on the surface.[274]

Previous work by Guan-Jun Zhang *et al.* have reported the maximum density of electron traps and hole traps in the surface layer of PTFE of 2.7 $x10^{17}$ eV^{-1} m^{-3} (measured after corona charging, 30 min, ±5 kV). They also calculated using isothermal current theory that the energy level of its electron charge traps was 0.85–1.0 eV, and that of the hole charge traps was 0.80–0.90 eV.[283]

It is previously been reported (A.A. Rychkov *et al.* (1996)), that the incorporation of polar moieties into the surface of a fluoropolymer can improve the

charge storage properties. This was achieved by storage in water prior to corona charging.[307]

Later work by the same group into the production of charge stabilised corona charged PTFE surfaces showed that it was possible to increase the amount of deep charge traps present at the surface by exposing PTFE surfaces to phosphorous trichloride vapours. The “phosphorous containing nano-sized groups” on the surface increased the stability of the positive charge on the surface.[308] This was further developed using three wet chemical treatments (orthophosphoric acid, tetrabutyl titanate, and tetraethoxysilane) prior to corona charging to enhance the charge stability of PTFE films. The effect of charge stabilization was hypothesised to be due to a combination of the formation of deeper charge traps, and the decrease in molecular mobility caused by the additional functional groups attached to the surface from the wet chemical treatments.[308]

Perlman *et al.* reported in the early 1970s that the stability of PTFE electrets could be attributed to ion trapping rather than electron trapping in the material.309 Through the comparison of TSC measurements of corona-charged surfaces with that of samples treated with ion irradiation under vacuum, it can be seen that the modification of the PTFE surface by the plasma results in a different kind of charge trapping.[309] The incorporation of oxygen containing species onto the surface both by the plasma treatment and by adsorption from the surrounding environment is therefore deemed by Perlman *et al.* to be responsible for and dominate the mechanism of charge trapping.

One way of thinking about a charge trap is as a ‘particle in a box’. The size of the ‘hole’ in PTFE needed to bind an electron can be estimated mathematically. The classical binding energy of an electron in a PTFE hole can be calculated using the Born equation, Equation 4.2, and varies with 1/r.

$$\Delta G = \frac{e^2}{8\pi\varepsilon_0 r}\left(1 - \frac{1}{\varepsilon_r}\right)$$

Equation 4.2[310]

where e is the charge of the electron (1.602 x10^{-19} C), r is the radius of the hole, ε_0 is the vacuum permittivity (8.854 x10^{-12} F m^{-1}), and ε_r is the relative permittivity of the substrate (2.1).

Quantum mechanics give a zero point energy (z.p.e) for a particle in a spherical box given in Equation 4.3, which varies according to $1/r^2$.

$$E_{1,0} = 3.142^2 \left(\frac{\hbar^2}{2mr^2} \right)$$

Equation 4.3

where m is the mass of an electron (9.109 x10^{-31} kg), ħ is Planck's constant/2π (1.055 x10^{-34} J s^{-1}), and 3.142 is the first zero of the first-order Bessel function.

The energy of the electron in the box lies below the vacuum level when the Born energy exceeds the z.p.e.. The cross-over radius of the hole is found by equating the Born energy with the z.p.e. to yield a radius r = 1.0 nm. It is therefore expected that the electron would only be trapped in a hole with a diameter > 2 nm, which is very large compared to the gaps between molecules in a non-porous solid. This simple calculation suggests that electrons cannot be trapped in crystalline or amorphous PTFE without the presence of some other element or functional group to stabilise the electron.

4.2.3.5 DBD and Corona Plasma Charging of PTFE

Surfaces can be charged using a DBD or corona plasma, whereby the negative charges in the plasma move towards the surface when an electric field is applied, i.e. the plasma is ignited.[283] During the plasma charging process, the ions generated within the plasma discharge exchange charges with the PTFE surface in an Auger neutralisation mechanism forming a homo-charged electret.[311,312] The difference between corona and DBD is that DBD uses horizontal parallel plates, at least one of which is covered by a dielectric.[313] A corona apparatus consists of two different kinds of electrodes, typically a plate and a point, or a coaxial wire and a tube. This apparatus gives rise to a non-homogeneous filamentary glow discharge.[314]

4.2.3.5.1 DBD Charging

If the potential difference across the electrode gap is sufficiently high, the fixed electrode will emit electrons.[315] DBD plasma is self-limiting, and once the surface potential build up on the insulator electrode opposes the voltage across the plasma. This causes the plasma to self-extinguish unless the voltage supplied is augmented consistently.[315] Through the use of an AC voltage, the polarity of the supplied voltage is continuously switching and thus the DBD plasma lifetime can be extended and a constant plasma can be maintained. However it is also possible to create a plasma using a non-alternating power supply, which is most commonly

used for pulsed systems where the extended lifetime of a plasma is of less concern. In this work a pulsed system is used, and the AC voltage is converted to DC using transistors, see Section 4.3.1, Figure 40.

Theoretically, the charge that is imparted onto the insulator during DBD plasma treatment is determined by the stability of the micro-discharges in the plasma. The properties of the micro-discharge are dependent on the interelectrode gap, the treatment pressure and the gas composition.[316] The key variables that effect the efficacy of atmospheric DBD plasma treatment of PTFE are; the feed gas, plate voltage, pulse frequency, interelectrode gap, and treatment time. At large interelectrode gaps (>3 mm), the plasma formed is less homogenous, and more filamentary in nature, resulting in non-uniform surface modification, and at higher powers, surface damage.[295] This non-uniformity contributes to the phenomenon of charge traps rather than uniform surface potential distribution. The temperature of the plasma charging was shown by Xia *et al.* to have a significant effect on the overall surface charging of ePTFE (expanded PTFE).[317]

It is well known, that the feed gas for the plasma treatment has a significant effect on the surface modification observed. For example, feed gases that are chiefly made up of unreactive gases, like noble gases and nitrogen, will not easily form negative ions. This will result in a plasma with electropositive character, where the number of positive ions is almost exactly equal to the number of electrons. Conversely, more electronegative atoms will combine with free electrons in the plasma to form negative ions meaning that the number of electrons is a lot less than that of the positive ions. The negative ions formed maintain charge neutrality.[318] Indeed, Rychkov *et al.* reported increased charging for polymer surfaces with polar moieties present, indicating that oxygen and nitrogen containing plasmas may have increased charging capabilities over their non-polar counterparts.[307] Additionally Zaghloul *et al.* presented results that indicated that charging of PTFE surfaces was reduced in a nitrogen environment in comparison to when samples were plasma-treated in an air environment.[337]

4.2.3.5.2 Effect of Charged Surface on DBD Plasma

Charge trapping on sample surfaces has previously been shown to have an effect on the character of the discharge produced by DBD apparatus.[312] Seed electrons necessary for uniform discharge may be produced by desorption of the electrons stored in a shallow trap on the surface. It was found that this could occur if the energy level of the trap were lower than 1 eV. This was because the intrinsic

electrons of the dielectric had a higher binding energy and therefore the trapped electrons are far more easily removed than those within the dielectric.[324]

It may also be noted that the charge build up on the dielectric surface will cause a back voltage which will switch off the plasma. The total charge which may be accepted into the surface is limited by this back voltage. Once the voltage has reversed, in the case of AC systems, the current flow also ceases, and the charge is removed from the capacitor until the voltage across the electrode gap is insufficient to produce a plasma.

Work was completed by P.S. Brown *et al.* on charging the surfaces of PTFE using a piezoelectric gun. The aim of this work was create a charged polymer surface that would cause water droplet "jumping".[329] This work focussed on hydrophobic PTFE surfaces and how they could cause droplets to bounce. In this work, the DBD modified PTFE surfaces are more hydrophilic, and so droplet bouncing is not something observed. It is however postulated that as the surface roughness is increased, this is something which may be observed.

S. Morsch *et al.* used an SPM probe to achieve localised charge on polymer surfaces using a corona type discharge, termed "nanopatterning".[306] PTFE was not studied in this work, however polyvinylidene fluoride (PVDF) was. Hydrophobic polymers achieved surface charging, however for the more hydrophilic polymers (WCA <60°), no surface charging was possible.

4.2.3.5.3 Corona Charging of PTFE

PTFE electrets were charged to ±1000 V using point-to-plane corona discharge, and the surface potential decay was measured using an electrostatic probe (Model 244, Monroe Electronics Ltd.). They reported that there was almost no surface potential decay when porous PTFE was charged using negative corona discharge, even after several hours at 200 °C. However when the substrate was positively charged, there was a much faster rate of surface potential decay.[319]

More recently, Rychkov *et al.* charged PTFE electrets to between 144 V and 1950 V using positive corona discharges at low-pressure (10 Pa).[320] Other work by the same group reported stable PTFE electrets charged at -500 V.[321]

Previous work by Guan-Jun Zhang *et al.* have reported the maximum density of electron traps and hole traps in the surface layer of PTFE of 2.7 $x10^{17}$ eV^{-1} m^{-3}. They also calculated using isothermal current theory that the energy level of its electron charge traps was 0.85–1.0 eV, and that of the hole charge traps was 0.80–0.90 eV.[283]

It is previously been reported (Rychkov *et al.* (1996)), that the incorporation of polar moieties into the surface of a fluoropolymer can improve the charge storage properties. This was achieved by storage in water prior to corona charging.[307]

Surface potential density is an alternative measurement of the charge imparted onto PTFE surfaces, and is measured in C m^{-2}. Nifuku *et al.* reported a maximum charge of 10 µC m^{-2} for PTFE treated with corona discharge (both DC and pulsed).[322]

In terms of modifying the PTFE surface prior to charging of PTFE surfaces, Haridoss *et al.* showed that defluorination of the PTFE prior to charging promoted stable electret formation. This group chemically defluorinated the surface using a Na-Naphthalene complex solution.[323]

Table 41: Summary of prior art on atmospheric DBD and corona charging of PTFE.

Gas	Conditions	Charge	Type of Discharge	Ref.
Air	30 kV, 40 ns, 1kHz	20 nC mm^{-2}	DBD	248
Air	10 kV, no treatment time given	+/- 1000 V	DBD	319
Air	+/- 5 kV, 30 min	+800 V	Corona	283
Air (pretreated by placing in water prior to plasma treatment)	100 s, 1 Hz	+200 V	Corona	307
Air	5 kV, 10 s	8 pC mm^{-2}	DBD	324
Air	5 kV	+/- 350 V, +/- 500 V, +/- 650 V, +/- 800 V, +/- 950 V	Corona	325
Air, heated to 150 °C	-2.5 kV, 24 h.	-1.6 kV	Corona	326
Air	-8 kV, 100 s, 1 kHz	Exact surface potential only given in arbitrary units	Corona	327

4.3 EXPERIMENTAL

PTFE substrates (15 mm x 10 mm samples, Goodfellow Cambridge Ltd., thickness 0.25 mm, FR301350/20, Batch number 300291002) were washed in 1:1 solution by volume of propan-2-ol (PROPAN-2-OL, 99.5%, Fisher Scientific UK Ltd.), and cyclohexane (99% purity, Fisher Scientific UK Ltd.) solution, and air dried (60 min).

4.3.1 Dielectric Barrier Discharge Reactor

Plasma treatment was carried out in a parallel plate silent discharge apparatus built in-house, Figure 38.

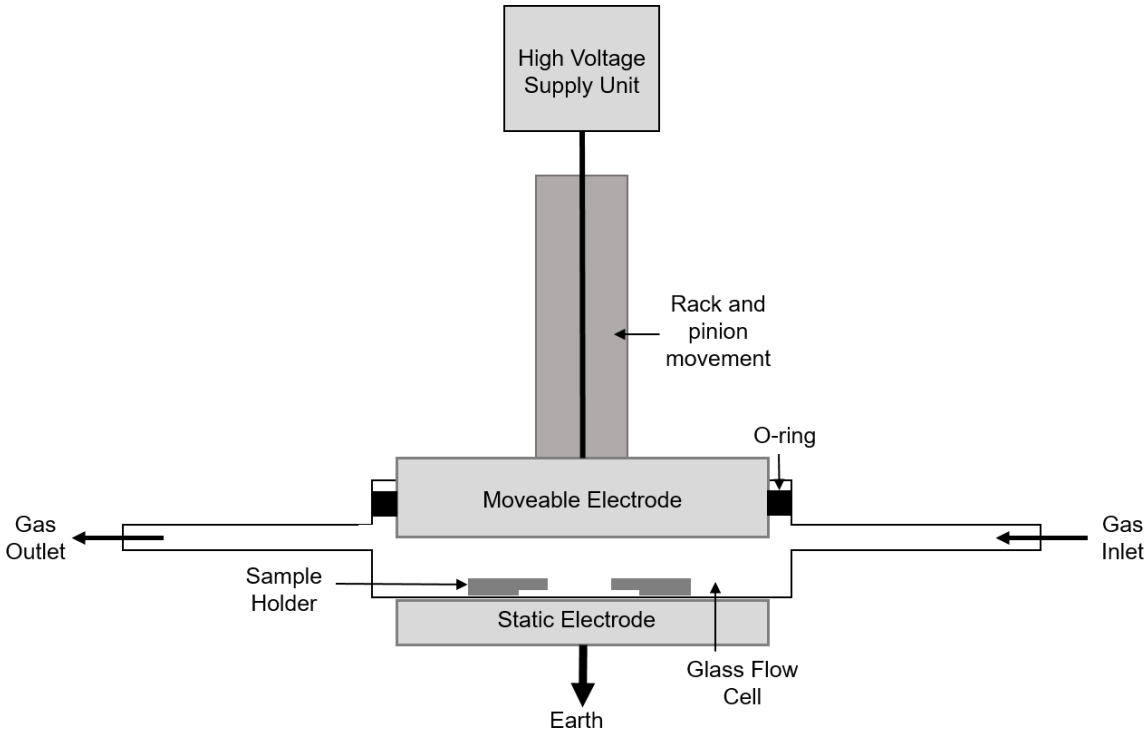

Figure 38: Schematic representation of in-house built DBD silent discharge apparatus.

Dampened sinusoidal pulses (14 kV, 3 kHz, 100 µs on, 4 ms off) were generated using a thyristor switched high-voltage power supply. The DBD output is sinusoidal pulses, Figure 39. The peak voltage of the pulse is 17.5 kV (this is the *applied* voltage to the electrode†). The applied 17.5 kV voltage pulse is measured to be on for 100 µs (excluding the ringing component), and the total period time is 4 ms, and the repetition rate is 250 Hz. In this work, the settings mean that the peak voltage is 14 kV. The shape of the voltage output for the DBD unit is an initial forward going (positive) voltage pulse which then goes negative before 'ringing' ensues (images A and B in Figure 39). This 'ringing' is a part of the pulse, and is a

series of dampened oscillations until the voltage gradually reduces to zero. Although the power supplied to the DBD unit is mains AC, this is converted to DC prior to entering the electrode containing circuit, Figure 40.

† *Note: This is not the actual voltage across the electrode whilst the plasma is ignited. Measuring this was considered too dangerous by the electrical workshop.*

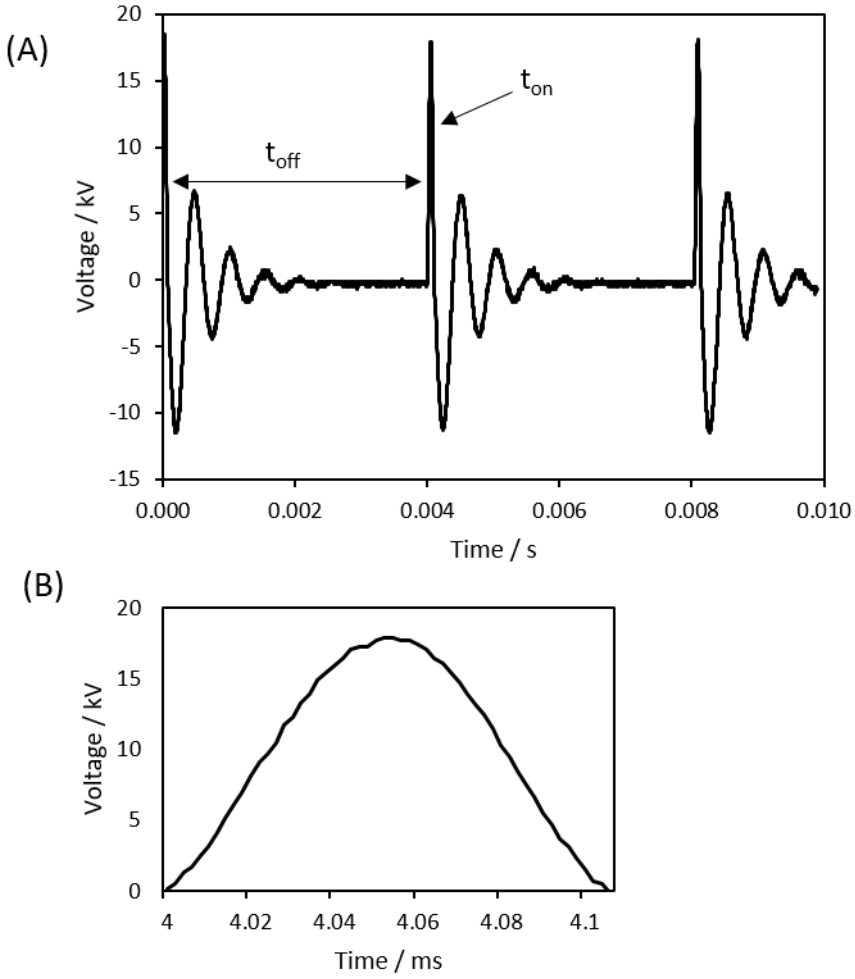

Figure 39: Characteristics of standard pulse of DBD rig. (A) was measured by Kelvin Appleby using Tektronix Ltd. MDO4104-3 oscilloscope, March 2016. (B) is a close up of the pulse shape, showing the applied 17.5 kV pulse time duration is 100 µs (prior to ringing). This is measured using a separate circuit connect in parallel to the electrodes. The measured voltage is the applied voltage to the moveable electrode when there is no plasma ignited, see (C) in Figure 40.

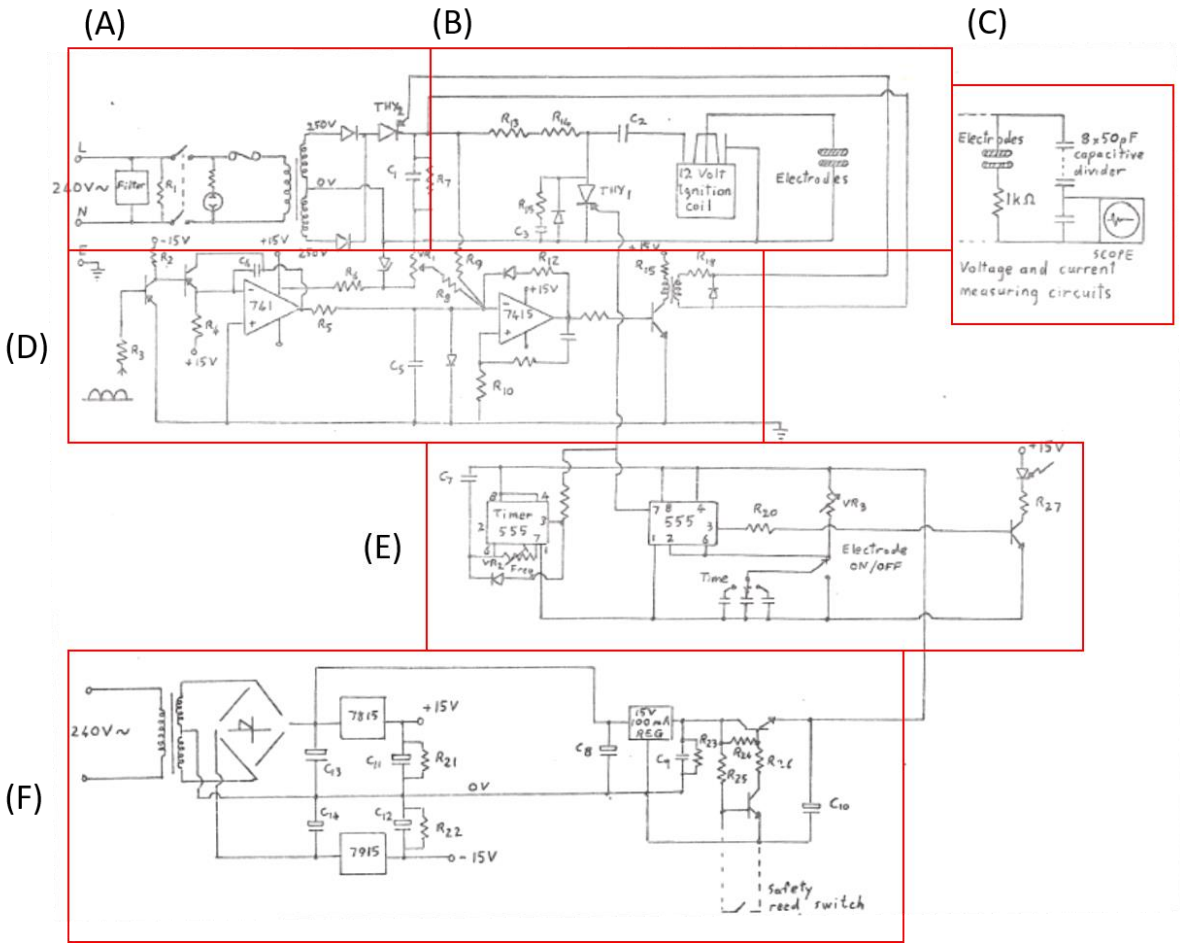

Figure 40: Circuit diagram of DBD equipment.[230] (A) Converts mains AC into DC voltage using two parallel transformers. Max peak voltage is 500 V at junction after thyristor (labelled THY_2). Filter protects mains and other equipment from a surge from ignition coil. (B) The capacitors are charged to 500 V whilst the thyristor (THY_1) is off. When the thyristor turns on, there is a sudden drop to 0 V, causing a sudden spike (high voltage) from the ignition coil. The falling edge of the input creates the output from the coil. Once the thyristor turns off, the voltage goes back up to 500 V. Although the coil is supplied with DC voltage, because of the pulse and the ringing effect, the voltage is pseudo-AC, Figure 39. (C) External voltage and current measurement circuit, this is disconnected for safety. (D) Power level and pulse control circuit. In these experiments, the power level is set to 4/5 of max power, and the pulse is set to 100 µs and 4 ms off, Figure 39. (E) Timing control circuit, in these experiments this is manually overridden and a stopwatch is used to measure treatment times. (F) Separate power circuit to control timing circuit.

The aluminium electrodes were degreased using propan-2-ol prior to use. The glass flow cell was placed on the earthed electrode, and acted as a dielectric, Figure 38. The glass flow cell was constructed from borosilicate glass and PVC 6.5 tubing is attached using quick-release Keck adaptors (Scientific Glass Laboratories Ltd., part codes; JS29/2 GL14 thread, GL14/C cap, and GL14/N connector). The PTFE samples were placed into the sample holder (custom built, constructed using two glass microscope cover slips (borosilicate glass, thickness No. 1, 18 mm x 18 mm, VWR International Ltd., Catalogue number 631-0120) glued on top of each

other, and then attached underneath a microscope slide (Clear glass, thickness 1.0–1.2 mm, Academy Science Ltd., Catalogue number N/A141)), Figure 41. The powered electrode was lowered until the interelectrode gap was 3 mm, and the o-ring had sealed. The discharge was ignited for varying times (3–300 s), which was measured and controlled manually using a stopwatch.

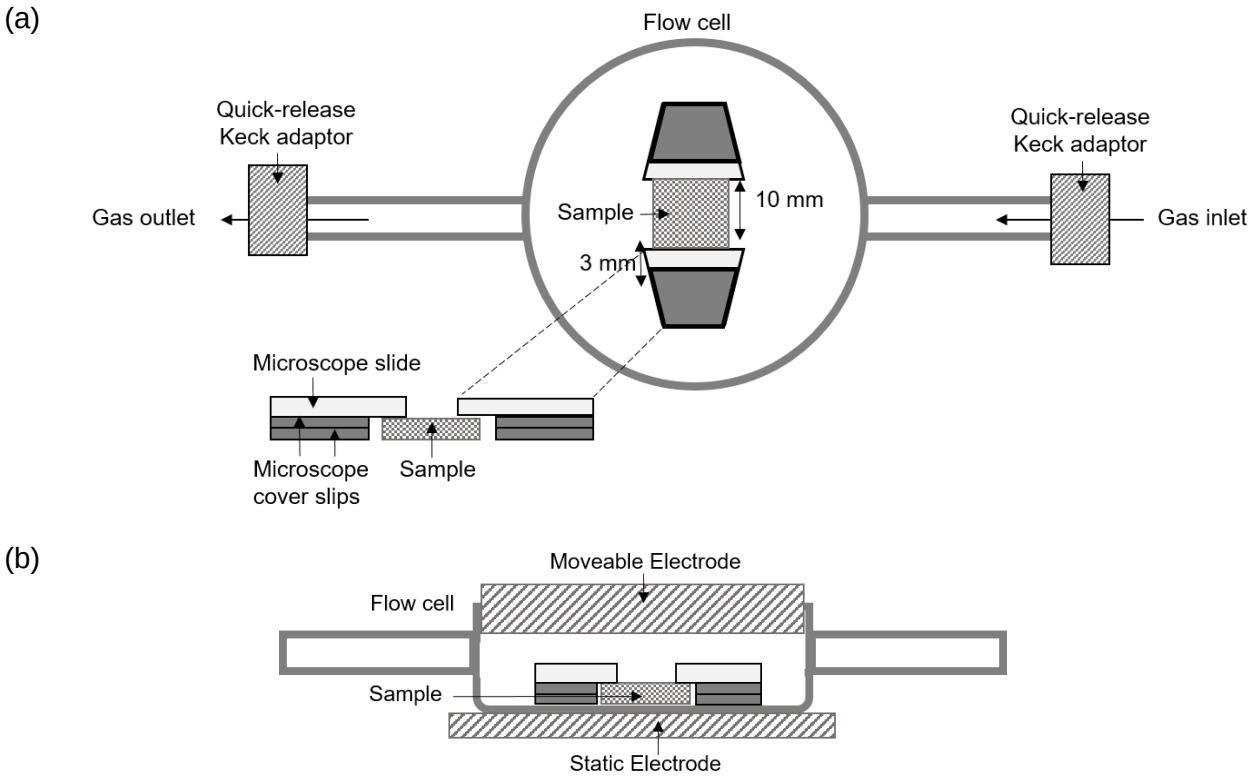

Figure 41: Sample holder and glass flow cell. (a) Top-down view and sample holder blow-out. (b) Side view of flow cell. The moveable electrode had no dielectric material.

4.3.1.1 Static Gas

Initially, the substrate was secured in the flow cell which was placed onto the static electrode. The quick release adaptors were not attached to anything, and the plasma was ignited with no flow of gas across the substrate. This was deemed a 'static air' treatment, Figure 38.

4.3.1.2 Flowing Gas

Due to the potential presence of secondary species on the surface during plasma treatment when there is no flow of air across the surface, a flow meter was used to push gas over the surface, Figure 42. A bubbler was attached to the gas outlet in order to monitor the exit of gas from the system and ensure regular flow. The gas

was fed from a cylinder through the flow cell of 20 cm^3 min^{-1} (Flow meter, Argon, max flow 80 cm^3 min^{-1}, Product 20C95, ¼" connections, connected to FloStat, type MNC1, both CT Platon SAS), Figure 42.

Gases were introduced through PVC 6.5 tubing and the line purged using two Keck Tubing Adaptors (WZ-06841-50, Cole-Parmer Instrument Company LLC), and a Keck Tubing Coupling Adaptor (WZ-06841-54, Cole-Parmer Instrument Company LLC). The gases used were air (UN1002, Barcode number 21012130640223, BOC Ltd.), nitrogen (oxygen free nitrogen, UN1066, EC 231-783-9, Barcode number 21044172747052, BOC Ltd.), argon (Pureshield Argon, UN1006EC231-147-0, 21011173891114, BOC Ltd.), and helium (UN1046, EC231-168-5, 21720110956331, BOC Ltd.).

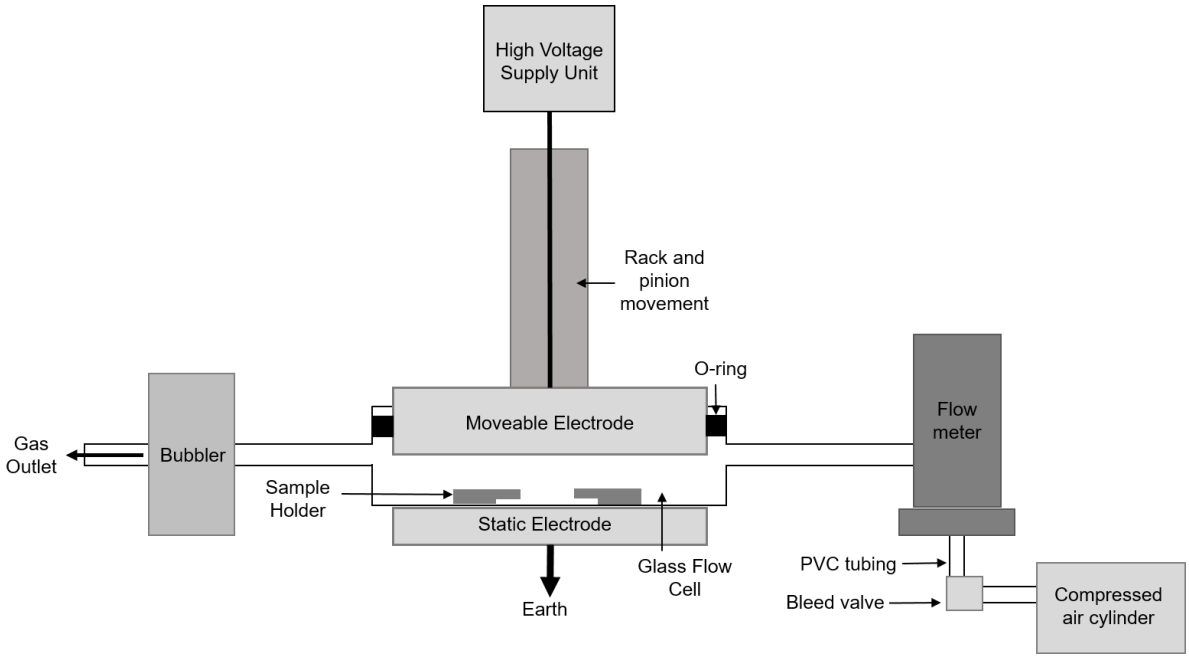

Figure 42: Schematic representation of DBD apparatus with flow meter allowing for constant flow of air through the flow cell.

4.3.1.3 Bubbler

In order to incorporate polar moieties into the plasma environment, a bubbler was placed in series after the flow meter. This was connected to the PVC tubing using two quick-release Keck barbed adapters (Part codes JS29/2 GL14 thread, GL/14 cap, and GL14/N Connector, Scientific Glass Laboratories Ltd.)

4.3.2 Contact Angle

The WCA was measured immediately after plasma treatment and after washing in propan-2-ol/cyclohexane solution (2 min, 1:1 solution by volume) and air drying (60 min). Static water contact angles (WCA) were measured using the sessile drop method (VCA 2500XE instrument, AST Products Inc., 1 µL ultra-high purity water droplets, ISO 3696 Grade 1).

4.3.3 Surface Potential

The surface potential was measured using an electrostatic voltmeter (Isoprobe model 244, Monroe Electronics Ltd., fitted with probe model 1017, Monroe Electronics Ltd.) with a surface-to-probe spacing of 2 mm. This small spacing decreases the influence of outside electric fields.328 The system was fitted with an air pump (Second Nature Whisper 400, 115 V A.C., 60 Hz, 3 W, Willinger Bros Inc.) that allowed purging of the system for 2 h prior to use. This decreased the drift on the measurements (manufacturer's suggestion). If insufficient air purging is carried out prior to the analysis of a surface, the charge measurement displayed will not stabilise within 5 min. If it continues to fluctuate for more than 5 min, this suggests that there has been insufficient air purging of the system carried out prior to analysis.

Due to the non-uniform character of the DBD plasma, there will be non-uniform charging of the insulator surface,[318] for this reason an average of 5 measurements across the surface was taken on each sample.

4.3.4 SEM

SEM was carried out using FEI Helios Nanolab 600 microscope operating in secondary electron mode, and running at 3 kV. Samples were coated with 12 nm of gold prior to analysis, and images taken at 4 magnifications (1000x, 2500x, 10000x, and 20000x). Samples were images prior to and after solvent washing (2 min, 1:1 solution by volume of propan-2-ol and cyclohexane).

4.3.5 High Speed Camera Capture

Frame by frame capture of DBD plasma (static air, 14 kV, 3kHz) was recorded using FASTCAM-APX RS Model 250 k. The record rate was 36000 fps, and the shutter speed was 2.8 $x10^{-5}$ s.

4.4 RESULTS – FEED GASES

Initially, the aim was to try and achieve a stable and low WCA PTFE surface using a simple single-step atmospheric plasma treatment. As seen in Chapter 3, the identity of the feed gas has a significant effect on the wettability of the surface produced. In DBD plasma, this has not been investigated as thoroughly as it has in for low-pressure plasmas, the majority of DBD plasma processes are carried out in air rather than any other feed gas.

A combination of inert (argon and helium) and reactive gases (air and nitrogen) were chosen as feed sources, all those chosen were considered to be cheap and harmless and could be easily implemented into an industrial process.

4.4.1 Static Air

The most simple plasma treatment is where there is no flow through, the air is simply 'static'. In order to achieve this, the flow cell was simply not attached to anything, and the plasma ignited. This is how the majority of reported air plasma-treated samples are made in the literature.

Using the same approach as taken in Chapter 3, a time study was used to initially map the results space. In the case of the DBD plasma treatments, there is less importance attached to a change in the power (supplied voltage in the case of DBD plasma apparatus) as the system is pulsed.

The untreated washed PTFE had a static WCA of 129 ± 3°, and a surface potential of +10 V ± 65 V. Treatment of the PTFE substrates by static air DBD discharges using the flow cell resulted in increased hydrophilicity of the surface, Table 42 (Section 4.5.4) and Figure 43.

The lowest WCA achieved was 76 ± 14° immediately after plasma treatment (10 s), however this recovered to 116 ± 3° after washing propan-2-ol/cyclohexane solution (1:1 solution by volume). The smallest amount of hydrophobic recovery (an observed increase of 13°) was observed for samples treated for 20 and 30 s. This hydrophobic recovery phenomenon has been well documented, Chapter 1. It should be noted that there is a build-up of secondary species due to the static nature of the gas (no flow through). This has been previously reported to cause degradation to polymer surfaces, and a build up debris on the surface without a carrier gas to remove this.[226]

(a) (b)

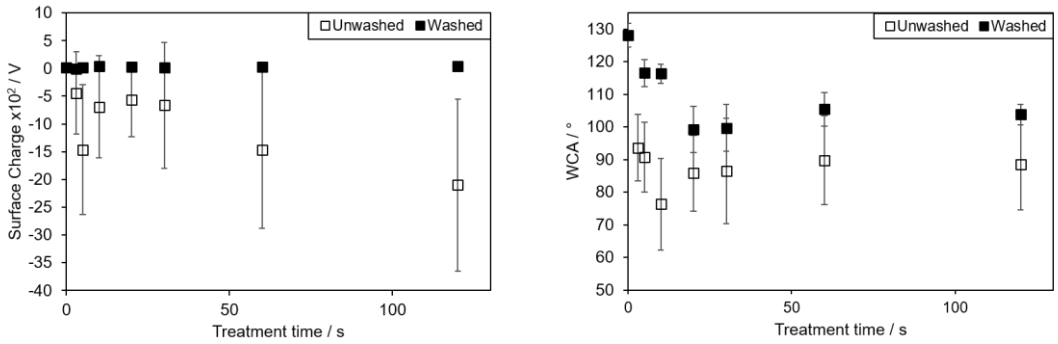

Figure 43: Effect of treatment time on (a) surface potential, and (b) WCA after DBD plasma air (14 kV, 3 kHz, 5–120 s), under static air conditions. Measurements made immediately after treatment (☐), and after washing in propan-2-ol/cyclohexane (1:1 solution by volume, 10 s) and air drying (60 min, (■)). Error bars denote standard deviation of the sample.

Table 42: WCA and surface potential achieved after varying length static air DBD treatments of PTFE substrates (14 kV, 3 kHz, 3–120 s). WCA and charge were measured immediately after plasma treatment and after washing in propan-2-ol/cyclohexane solution (10 s, 1:1 solution by volume) and air drying (60 min). Errors quotes are standard deviation of the sample.

Time / s	Exp #	No. Repeats	WCA Unwashed / °	Charge Unwashed / V	WCA Washed / °	Charge Washed / V
0	HB365, HB1009	4	-	-	129 ± 3	10 ± 65
3	HB701	4	94 ± 10	-442 ± 747	Not measured	-6 ± 42
5	HB932	4	91 ± 11	-1464 ± 1168	117 ± 4	20 ± 24
10	HB927	4	76 ± 14	-694 ± 921	116 ± 3	37 ± 6
20	HB737	4	86 ± 12	-571 ± 655	99 ± 7	29 ± 22
30	HB843	4	87 ± 16	-665 ± 1136	100 ± 7	13 ± 81
60	HB722	4	90 ± 14	-1469 ± 1415	105 ± 5	29 ± 15
120	HB728	4	88 ± 14	-2100 ± 1547	104 ± 3	36 ± 14

There is a large standard deviation in the measured WCA as the droplets were observed “jumping” from the syringe to the surface. This happens regardless of the treatment time. It is postulated that this is due to charging of the PTFE substrate surface. The phenomenon of charging of insulator surfaces after DBD or Corona discharge has been well documented, Section 4.2.3. After washing in propan-2-ol/cyclohexane (1:1 solution by volume) and air drying, the droplets no longer “jumped” to the surface. The solvent wash step removes the charge on the surface

Using an electrostatic voltmeter (Isoprobe 244, Monroe Electronics Ltd.), it is possible to measure the charge on the surface, Section 4.3.3.[329] Charge trapping on polymer surfaces is often not consistent, as often the micro-discharges from

DBD plasmas are not uniform or completely stable.[330] Deep and shallow charge traps have been observed by others on PTFE surfaces charged using DBD plasma treatments.[331] The combination of different depths of charge trapping sites is reflected in the large standard deviation seen for the average charge of the treated surfaces, Figure 43 and Table 42. It was previously shown by Toomer *et al.* in 1980 that surfaces that have a higher surface potential show a more rapid decay in surface potential than those which are initially less charged.[331]

The largest average potential was observed on the surface after a 120 s DBD static air treatment. Generally, very short treatment times (3–5 s) resulted in a lower average potential across the surface. This is supported by the findings reported in the literature.[321,320,330,331]

After washing with propan-2-ol/cyclohexane (1:1 solution by volume) and air drying, the observed surface potential was close to zero, and the same as that of an untreated PTFE surface (approx. +50 V). This indicates that the charge deposited on the surface is removed by solvent washing, and is therefore not a stable electret that holds its charge through wash processes.

4.4.2 Flowing Air

The results using flowing air do not show the previously observed lowest WCA at a treatment time of 10 s, Figure 44 and Table 6. The lowest WCA achieved was 68 ± 14° (after treatment time of 60 s), but there is no significant difference between any of the treatment times. All are within error of each other. As previously seen, the washing step causes a significant recovery of the WCA and reduction of the standard deviation due to the lack of “droplet jumping”.

As observed previously (Section 4.4.1), the DBD treatment created both deep and shallow negative charge traps on the surface. The treatment time has no significant effect on the degree of charge measured on the surface.

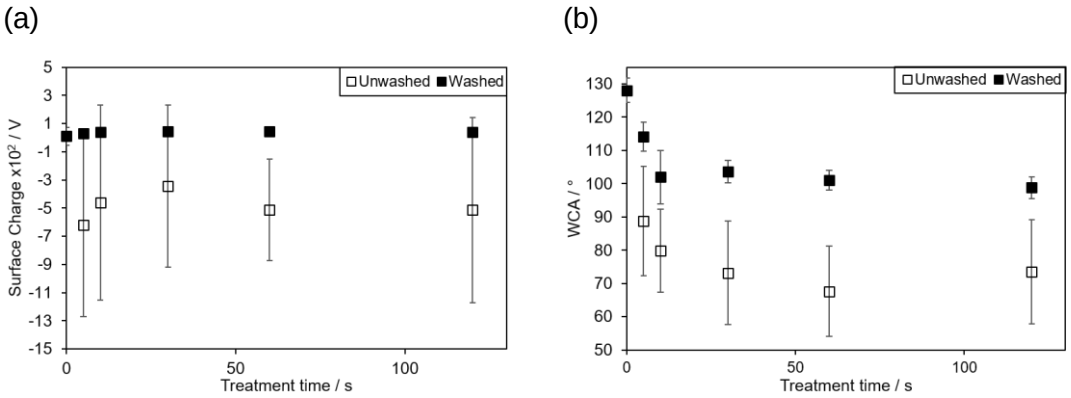

Figure 44: Effect of treatment time on (a) surface potential, and (b) WCA achieved after DBD plasma using flowing air (14 kV, 3 kHz, 5–120 s, 20 $cm^3\,min^{-1}$), immediately after treatment (□), and after washing in propan-2-ol/cyclohexane (1:1 solution by volume, 10 s) and air drying (60 min, (■)). Error bars denote standard deviation of the sample.

Table 43: WCA and surface potential achieved after varying length DBD treatments of PTFE substrates in flowing air (14 kV, 3 kHz, 5–120 s, 20 $cm^3\,min^{-1}$). WCA and charge were measured immediately after plasma treatment and after washing in propan-2-ol/cyclohexane solution (10 s, 1:1 solution by volume) and air drying (60 min). Errors quotes are standard deviation of the sample.

Time / s	Exp #	No. Repeats	WCA Unwashed / °	Charge Unwashed / V	WCA Washed / °	Charge Washed / V
0	HB365, HB1009	4	-	-	129 ± 3	10 ± 65
5	HB583, HB752	4	89 ± 16	-619 ± 653	114 ± 4	31 ± 22
10	HB577, HB749	4	80 ± 13	-462 ± 693	102 ± 8	42 ± 8
30	HB586, HB746	4	73 ± 16	-344 ± 575	104 ± 3	45 ± 3
60	HB594, HB743	4	68 ± 14	-512 ± 361	101 ± 3	42 ± 12
120	HB589, HB740	4	74 ± 16	-513 ± 657	99 ± 3	42 ± 4

4.4.2.1 Comparison Static Vs Flowing Air

It was hypothesised that there would be a significant difference between the static treatments and those where there was a continuous flow of air across the surface. When comparing the WCA achieved using static and flowing conditions immediately after treatment, the flowing air generally produces a lower WCA, Figure 43 and Table 47. It is likely that this difference is due to the presence of secondary ionized species around the surface when the air above the surface is static.

The difference between the WCA achieved for surfaces treated with static and flowing air increases as the treatment time increases. The ignition of a plasma is affected largely by the nature of the feed gas, and as the plasma duration

increases, the availability of free species in the static air above the substrate decreases. This results in a less effective plasma treatment as the formation of streamers is hampered by the secondary ionized species being present.

The exception to this is the low WCA achieved after 10 s static air treatment (prior to solvent washing), where the presence of secondary species above the surface has resulted in a large reduction in WCA. As the treatment time is increased however, this benefit is no longer seen, which suggests that as the amount of secondary species is increased, the benefit is diminished.

4.4.2.2 Comparison with Literature

The lowest reported WCA after DBD plasma treatment using air was 50° immediately after treatment.[243] After ageing, the lowest reported WCA was 75°,[247] however this was using curved tubes rather than flat samples, so there is some discrepancy as to whether this has been correctly accounted for. The lowest reported contact angle for a flat sample treated with air DBD was 85°.[260] The average WCA obtained for both static and flowing air treatments were similar to this, Figure 43 and Figure 44.

Inherently, the potential difference applied to the fixed electrode in DBD treatment will determine the surface potential, as the surface potential should always oppose the fixed electrode.[315] The absolute charging of a surface is dependent on the feed gas, the voltage of the discharge and the plasma treatment duration.[331] In this case, the static and flowing air plasmas produce a different amount of surface charging. In the flowing case, there are constantly more ions and electrons being fed into the system. In the prior art, there have been many references to charging surfaces with positive or negative voltages, and these result in either positive or negatively charged surfaces. In the literature, the voltage supplied to the electrode in the surface determines the charge trapped on the surface, not the nature of the plasma.[332]

4.4.3 Flowing Nitrogen

Due to the unsealed nature of the DBD apparatus, it was not possible to carry out DBD treatments under static conditions for any other gases, and so only flowing conditions (20 $cm^3 min^{-1}$) were investigated.

At treatment times of 30 s and higher, the WCA of the surfaces produced was hydrophilic, and as low as 68 ± 15° were achieved prior to solvent washing after nitrogen treatment (14 kV, 3 kHz, 60 s), Figure 45. After solvent washing all the surfaces were no longer hydrophilic (WCA greater than 90°).

Prior to solvent washing all surfaces were negatively charged, this implies that electrons were trapped at the surface from the plasma region. As seen before, these surfaces were not stable to solvent washing, and all charge was removed by immersion in propan-2-ol/cyclohexane solution (1:1 v/v, 120 s). It is not clear how these electrons are trapped at the surface, as there is a large amount of contention about the method in the literature, Section 4.2.3.4.

(a) (b)

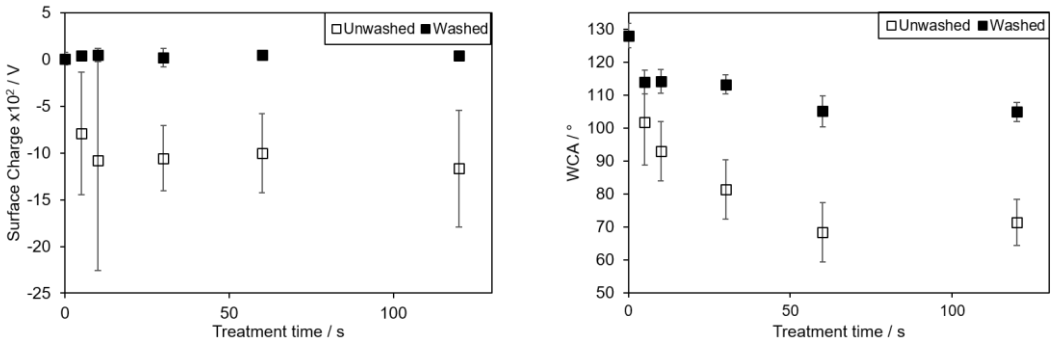

Figure 45: Effect of treatment time on (a) surface potential, and (b) WCA achieved after DBD plasma using flowing nitrogen (14 kV, 3 kHz, 5–120 s, 20 $cm^3 min^{-1}$), immediately after treatment (☐), and after washing in propan-2-ol/cyclohexane (1:1 solution by volume, 10 s) and air drying (60 min, (■)). Error bars denote standard deviation of the sample.

Table 44: WCA and surface potential achieved after varying length DBD treatments of PTFE substrates in flowing nitrogen (14 kV, 3 kHz, 5–120 s, 20 $cm^3 min^{-1}$). WCA and charge were measured immediately after plasma treatment and after washing in propan-2-ol/cyclohexane solution (10 s, 1:1 solution by volume) and air drying (60 min). Errors quotes are standard deviation of the sample.

Time / s	Exp #	No. Repeats	WCA Unwashed / °	Charge Unwashed / V	WCA Washed / °	Charge Washed / V
0	HB365, HB1009	4	-	-	129 ± 3	10 ± 65
5	HB799	4	102 ± 12	-790 ± 659	114 ± 4	44 ± 6
10	HB794	4	93 ± 15	-1077 ± 1178	114 ± 4	50 ± 69
30	HB789	4	81 ± 9	-1057 ± 350	113 ± 3	22 ± 98
60	HB784	4	68 ± 15	-999 ± 424	105 ± 5	49 ± 31
120	HB776	4	71 ± 15	-1166 ± 626	105 ± 3	43 ± 6

4.4.3.1 Comparison with Literature

As nitrogen is generally non-reactive, it is usually not used as a feed gas without being 'spiked' with other gases like ammonia and hydrogen.[239,240,242] Therefore there can be no direct comparison with the data obtained here. The lowest reported WCA using DBD with a nitrogen containing feed gas was 25° when using 65% nitrogen and 35% hydrogen.[239,240] Using atmospheric-pressure Townsend discharge (APTD), a WCA of approximately 25° was achieved when nitrogen gas was dosed with 100 ppm of ammonia gas.[239,240] There is no charging of PTFE using nitrogen reported in the literature, those reported in Section 4.2 (using mixtures of nitrogen and hydrogen, and nitrogen and water) do not analyse any deposited charge, or indeed note that there was any.

4.4.4 Flowing Argon

In comparison to the reactive air and nitrogen feed stocks, it would be expected that an argon fed plasma would be less effective at hydrophilizing the surface. There are no polar functional groups present in an argon feed gas, and in the low-pressure work it was discussed that the incorporation of polar groups happened by active sites scavenging from the air after removal from the chamber rather than during the plasma treatment. Additionally, the lack of available electrons in the plasma region will result in the plasma taking on a more electropositive character, resulting in an overall positively charged surface.

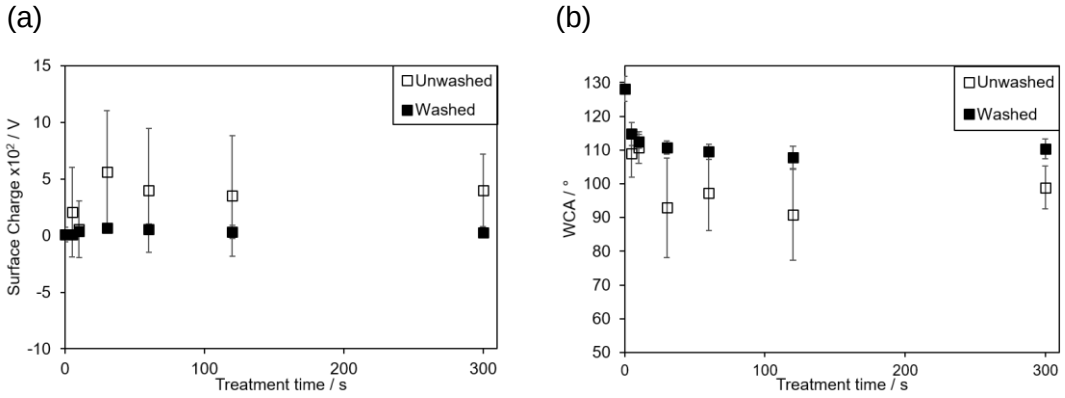

Figure 46: Effect of treatment time on (a) surface potential, and (b) WCA achieved after DBD plasma using flowing argon (14 kV, 3 kHz, 5–300 s, 20 cm^3 min^{-1}), immediately after treatment (☐), and after washing in propan-2-ol/cyclohexane (1:1 solution by volume, 10 s) and air drying (60 min, (■)). Error bars denote standard deviation of the sample.

Table 45: WCA and surface potential achieved after varying length DBD treatments of PTFE substrates in flowing argon (14 kV, 3 kHz, 5–300 s, 20 cm^3 min^{-1}). WCA and charge were measured immediately after plasma treatment and after washing in propan-2-ol/cyclohexane solution (10 s, 1:1 solution by volume) and air drying (60 min). Errors quotes are standard deviation of the sample.

Time / s	Exp #	No. Repeats	WCA Unwashed / °	Charge Unwashed / V	WCA Washed / °	Charge Washed / V
0	HB365, HB1009	4	-	-	129 ± 3	10 ± 65
5	HB1038	4	109 ± 7	207 ± 398	115 ± 3	7 ± 41
10	HB1045	4	111 ± 5	58 ± 250	113 ± 2	40 ± 8
30	HB1151	4	93 ± 15	563 ± 540	111 ± 2	67 ± 21
60	HB1148	4	97 ± 11	402 ± 547	110 ± 2	57 ± 45
120	HB1145	4	91 ± 14	351 ± 532	108 ± 3	32 ± 59
300	HB1164	4	99 ± 6	399 ± 320	110 ± 3	26 ± 32

4.4.4.1 Comparison with Literature

The data presented here lies within the wide range of WCA that have been reported in the literature (34.9–110°).[241,251,268,269,270,271] Shao *et al.* reported the lowest WCA of 34.9° achieved after argon DBD plasma treatment (3.25 kV, 90 s). This surface had an F/C ratio of 0.57 (also the lowest reported in literature, the range was 0.57–1.98). There was no investigation into the stability of these surfaces, and they were not washed prior to analysis.[241]

4.4.5 Flowing Helium

In a similar manner to argon, using helium as a feed gas should cause no significant compositional changes to the surface, and so would not be expected to cause a significant change in WCA. Additionally, the resultant surface would be expected to have a positive surface potential owing to the lack of available electrons present in the helium plasma (compared to air or nitrogen).

(a) (b)

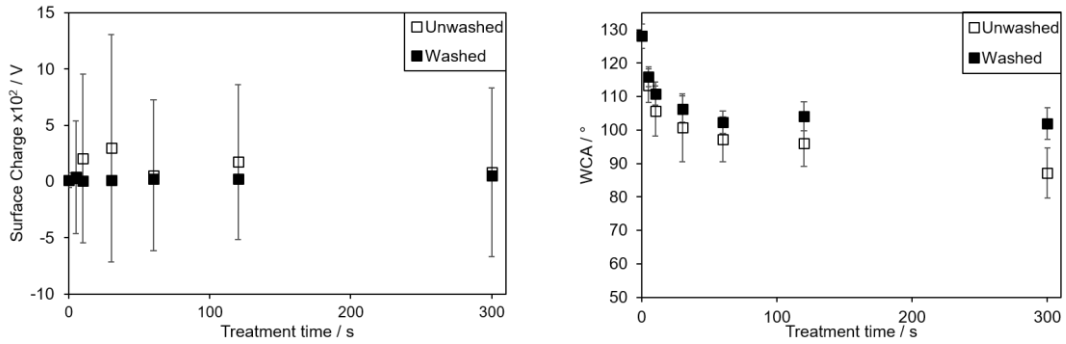

Figure 47: Effect of treatment time on (a) surface potential, and (b) WCA achieved after DBD plasma using flowing helium (14 kV, 3 kHz, 5–300 s, 20 cm^3 min^{-1}), immediately after treatment (☐), and after washing in propan-2-ol/cyclohexane (1:1 solution by volume, 10 s) and air drying (60 min, (■)). Error bars denote standard deviation of the sample.

Table 46: WCA and surface potential achieved after varying length DBD treatments of PTFE substrates in flowing helium (14 kV, 3 kHz, 5–300 s, 20 cm^3 min^{-1}). WCA and charge were measured immediately after plasma treatment and after washing in propan-2-ol/cyclohexane solution (10 s, 1:1 solution by volume) and air drying (60 min). Errors quotes are standard deviation of the sample.

Time / s	Exp #	No. Repeats	WCA Unwashed / °	Charge Unwashed / V	WCA Washed / °	Charge Washed / V
0	HB365, HB1009	4	-	-	129 ± 3	10 ± 65
5	HB1081	4	113 ± 5	40 ± 149	116 ± 3	32 ± 40
10	HB1087	4	106 ± 8	207 ± 171	111 ± 4	3 ± 47
30	HB1095	4	101 ± 10	297 ± 356	106 ± 4	12 ± 30
60	HB1098	4	97 ± 7	55 ± 205	102 ± 3	25 ± 28
120	HB1107	4	96 ± 7	174 ± 160	104 ± 4	22 ± 21
300	HB1111	4	87 ± 8	82 ± 382	102 ± 5	51 ± 21

Overall the charging of the surface after helium treatment oscillated around the +200 V mark, the magnitude of the positive charging was less than that previously observed for other feed gases. The highest surface potential was achieved after 30 s (+297 ± 356 V), Table 46. The lowest WCA achieved was after 300 s (87 ± 8°) which after washing was measured as 102 ± 5°.

4.4.5.1 Comparison with Literature

The lowest reported WCA was 28° immediately after plasma treatment (no plasma details given), which recovered to 50° after 6 months.[264] Zettsu *et al.* reported a surface where “little hydrophobic recovery was seen”, however this surface had a WCA of 60° (15 W, 30 s).[246] All of these reported surfaces are significantly more hydrophilic than the best that was achieved in this study.

4.4.6 Effect of Surface Potential on WCA

As previously mentioned, the theory of electrowetting is being applied in this case to decrease the observed WCA of the surface, thus increasing the hydrophilicity of the PTFE surface. The Young-Lippman equation (Equation 4.4) can be used to determine what the intrinsic WCA (θ_i) would be if the charge were not present on the surface. In this manner, the efficacy of electrowetting can be determined.

$$cos\theta_V = cos\theta_i \frac{\varepsilon_0 \varepsilon_r V_p^2}{2\gamma_{lg} d}$$

Equation 4.4[333]

where V_p is the measured surface potential, d is the thickness of the dielectric, ε_o is the vacuum permittivity (8.854 F m^{-1}), ε_r is the permittivity of the dielectric (2.1 F m^{-1}), γ_{lg} is the surface tension of UHP water in air (72.29 mN m^{-1}), and θ_V is the observed WCA of the charged surface.

Using this equation, and thickness of the dielectric as the PTFE, the overall electrowetting effect on the WCA was investigated. The value of θ_i for the static air treatment (120 s), which had the largest magnitude of surface potential imparted on the surface was calculated to be 88°, the same as the measured WCA. This indicates that the surface potential does not significantly affect the wettability of the surface, which given the droplets jumping form the needle to the surface, we know not to be true.

Thus the method by which the equation is used must be changed, the thickness of the dielectric instead could refer to the thickness of the double layer of the water. In which case, the Debye length will need to be well defined. In order to do this, a salt solution could be used instead of water.

4.4.7 High Speed Camera Capture

In order to determine during which part of the voltage cycle (Figure 39), the plasma was ignited, a high speed camera was used to film the DBD plasma equipment, Figure 48. As both positive and negative surface potentials were measured on the plasma-treated surfaces, it was important to see if there was plasma ignited in both the positive and negative voltage regions. Using an oscilloscope, the voltage cycle was shown to include a short ‘spike’ of positive voltage that had a height of +20 V, and a breadth of 110 µs in total, followed by a ringing effect. The first negative voltage has a broader character than the first positive peak, with a height of -10 V, and a width of 270 µs. This is followed by an equally broad positive peak with a

height of +5 V, and width of 270 µs. The following negative peak is similar in width (260 µs) and voltage (-4.5 V).

The DBD discharge was filmed at a range of different rates; 10000, 20000, and 36000 fps. The highest frame rate correlated with a shutter speed of 28 µs, which is significantly less than the reported ignition time of 100 µs. At this speed, it was possible to see that above a certain voltage threshold plasma was ignited during both the first positive and first negative pulse, but not in the subsequent ringing pulses. As can be seen in the frame by frame snapshots, Figure 48, there are 2 frames for the first more intense plasma, corresponding to the positive plasma. As each frame corresponds to 28 µs, then the two frame plasma corresponds to approximately 56 µs. This is less than the width at the base of the first positive peak (110 µs), and corresponds more closely to the width of the peak at +5 V (40 µs). Then there is a single frame with no plasma ignition, which indicates that there has to be a particular threshold voltage before the plasma will ignite. The second negative plasma lasts 4 frames which corresponds to 111 µs. This is significantly less than the peak width (270 µs), indicating again that there is a threshold voltage below which plasma is ignited. There are no plasma ignitions for the subsequent positive and negative peaks, so the plasma must exceed +/- 5 V.

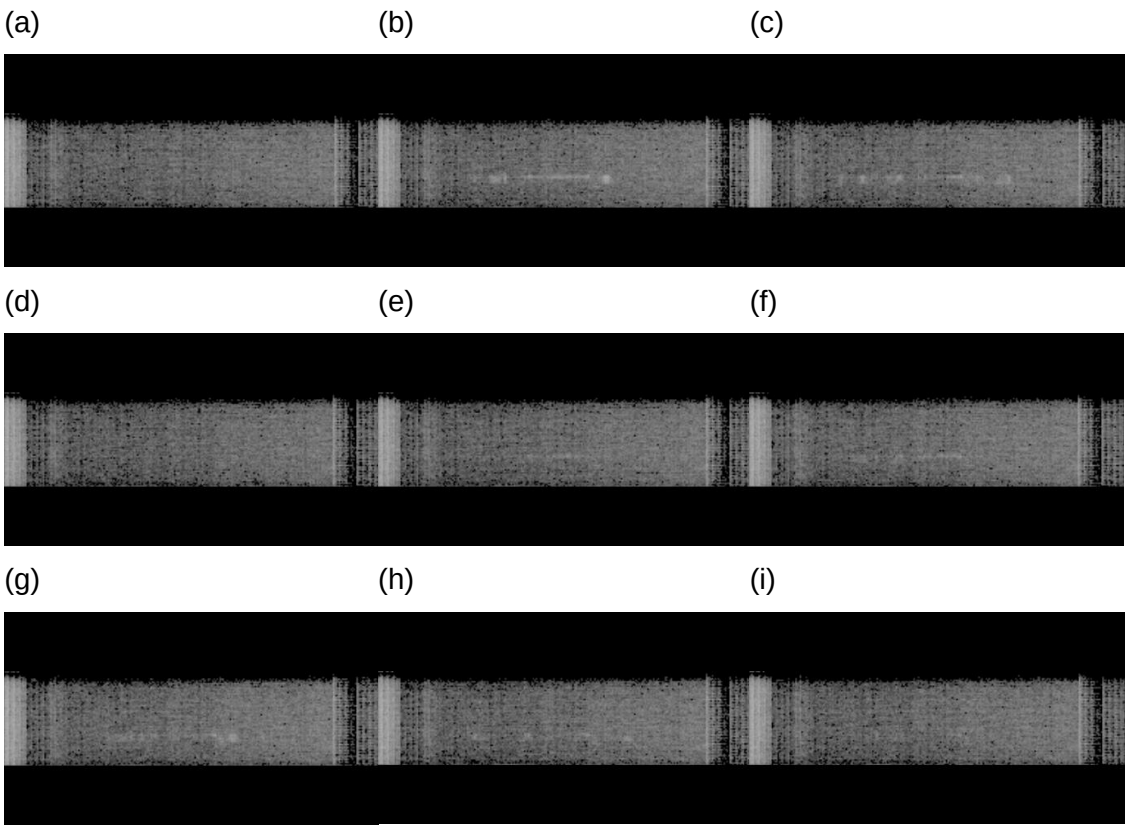

Figure 48: Frame by frame capture of DBD plasma (static air, 14 kV, 3kHz). Recorded using FASTCAM-APX RS Model 250 k. Record rate 36000 fps, and shutter speed 2.8 $x10^{-5}$ s. (a) no plasma; (b) and (c) positive voltage plasma; (d) no plasma; (e), (f), (g), and (h) lower intensity negative voltage "ringing" plasma; and (i) no plasma. Thanks go to Dr. Lisong Yang and Professor Colin Bain for their help in obtaining these images.

4.4.8 Conclusions

The absolute charging of a surface is dependent on the feed gas, the voltage of the discharge, and the plasma treatment duration.[331] These data investigate the effect of both plasma duration and feed gas on the wettability and surface potential of a PTFE substrate.

In terms of the aim of creating a stable wettable surface, these single feed gas DBD plasma treatments were not effective. The surfaces were not as hydrophilic as that which was reported in Chapter 3, and additionally, were not stable to solvent washing. The hypothesis that the increase in surface potential imparted by the DBD plasma would result in a decrease in WCA due to the electrowetting effect was shown to be true, as droplets "jumped" to the surface, and spread more when this happened. Although the charge was removed by the solvent wash process, if the samples were unwashed, the charge remained stable for a prolonged period of time (>6 months), like the previously reported electrets.[294]

In this study, inert (argon and helium) gas plasma treatments resulted in an average positive charge on the surface. This was expected owing to the lack of available electrons present in comparison to their reactive counterparts. However, there were both negative and positive measurements were taken on each surface indicating a non-uniform polarity of charge. This non-uniformity was due to the plasma igniting in both the negative and positive voltage cycles of the DBD equipment: the initial first positive voltage and then the corresponding negative ringing. In neither case was there a significant effect on the charging caused by an increase in plasma treatment duration.

4.5 RESULTS – INTRODUCING POLAR SPECIES INTO PLASMA FEED

It has previously been reported that the incorporation of polar species into the feed stock for a plasma process can increase the hydrophilizing effect observed on the resultant substrate. When H. Xu *et al.* bubbled argon through water prior to introduction into a low-pressure plasma modification system, a WCA of 24° was achieved immediately after plasma treatment, which recovered to 60° after storage in ambient conditions for 100 h. Without the introduction of water, the 30° WCA achieved exhibited hydrophobic recovery up to 70° in one case,[334] and 110° in the other.[335]

4.5.1 Bubbling through water

Previous work by S. Morsch *et al.* showed that an increased relative humidity around a corona discharge can cause enhanced spreading of charge in an insulator due to improved surface conductance.[336,337]

In light of this previous work, the humidity of the plasma environment within the flow cell was increased by placing a bubbler filled with deionised water in series with the flow meter, Section 4.3.1.3. The flow cell was purged for 10 mins with this 'wet' gas before the plasma was ignited.

It was expected that the presence of these polar groups in the plasma will cause a change in character just like changing the feed gas would. But additionally, the presence of water on the surface will provide a stock of electrons at the surface which could be influenced by the plasma and incorporated into the surface.

4.5.1.1 Flowing Air Bubbling Through Water

The 'wet air' treatment caused a smaller decrease in WCA than that previously observed. The largest decrease in WCA was achieved using 120 s treatment time, and the trend suggests that lower WCA could be achieved using longer treatment times. The effect of solvent washing is to significantly increase the WCA, the standard deviations of the sample overlap slightly in most cases. After solvent washing, as seen before, the charge on the surface is disspropan-2-olted and returns to approx. 0 V.

As seen with previous DBD treatments, there is a noticeable charge imparted to the surface after DBD treatment with wet air, Figure 49. Previously, the potential on the surface for flowing air was chiefly negative, however with the wet air treatment, the lower treatment times (5–30 s) resulted in a an average positive potential surface on average, whereas at longer treatment times, both negative and

positive charges are recorded on the surface giving an average closer to 0 V. This could be explained by reactive gases forming negative ions more easily than inert or non-reactive gases, thus resulting in the formation of a plasma which is more electronegative in character.[318] Additionally, the incorporation of the water into the plasma gas will allow for some of the electrons to be taken from the gas rather than the surface as the electron avalanche strikes the surface, Section 4.2.2.1. As the treatment duration increases, this effect appears to be less pronounced.

(a) (b)

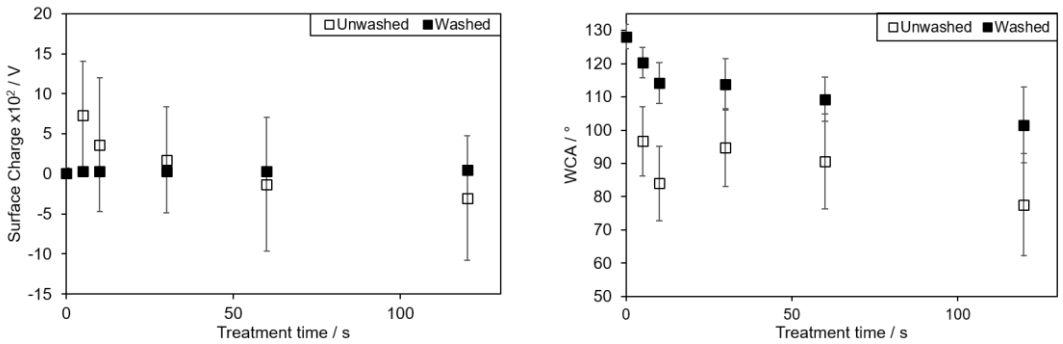

Figure 49: Effect of treatment time on (a) surface potential, and (b) WCA achieved after DBD plasma using air that has flowed through a water bubbler (14 kV, 3 kHz, 5–120 s, 20 $cm^3 min^{-1}$), immediately after treatment (☐), and after washing in propan-2-ol/cyclohexane (1:1 solution by volume, 10 s) and air drying (60 min, (■)). Error bars denote standard deviation of the sample.

Table 47: WCA and surface potential achieved after varying length DBD treatments of PTFE substrates in flowing 'wet air' (14 kV, 3 kHz, 5–120 s, 20 $cm^3 min^{-1}$). WCA and charge were measured immediately after plasma treatment and after washing in propan-2-ol/cyclohexane solution (10 s, 1:1 solution by volume) and air drying (60 min). Errors quotes are standard deviation of the sample.

Time / s	Exp #	No. Repeats	WCA Unwashed / °	Charge Unwashed / V	WCA Washed / °	Charge Washed / V
0	HB365, HB1009	4	-	-	129 ± 3	10 ± 65
5	HB658, HB770	4	97 ± 10	733 ± 672	120 ± 5	36 ± 18
10	HB655, HB767	4	84 ± 11	365 ± 838	114 ± 6	36 ± 15
30	HB652, HB764	4	95 ± 12	174 ± 661	114 ± 8	34 ± 22
60	HB649, HB758	4	91 ± 14	-128 ± 833	109 ± 7	30 ± 37
120	HB646, HB755	4	78 ± 15	-301 ± 777	102 ± 11	46 ± 4

4.5.1.2 Flowing Nitrogen Bubbling Through Water

In contrast to the data for the flowing nitrogen DBD treated surfaces, when water is introduced into the feed source, it results in positive charging of the PTFE surface,

rather than negative charging. The magnitude of the charging is similar, the highest charged surface was observed after 120 s plasma treatment (1099 ± 1027 V), Table 48. The lowest WCA prior to washing was achieved after 120 s (81 ± 10°), and after washing the lowest WCA was after 120 s (105 ± 5°).

(a) (b)

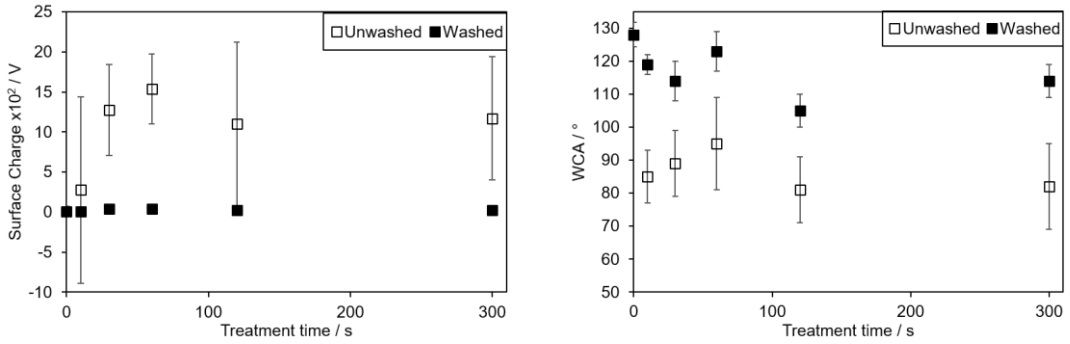

Figure 50: Effect of treatment time on (a) surface potential, and (b) WCA achieved after DBD plasma using nitrogen bubbling through water (14 kV, 3 kHz, 5–300 s, 20 cm^3 min^{-1}), immediately after treatment (☐), and after washing in propan-2-ol/cyclohexane (1:1 solution by volume, 2 min) and air drying (60 min, (■)). Error bars denote standard deviation of the sample.

Table 48: WCA and surface potential achieved after varying length DBD treatments of PTFE substrates in flowing nitrogen through distilled water (14 kV, 3 kHz, 10–300 s, 20 cm^3 min^{-1}). WCA and charge were measured immediately after plasma treatment and after washing in propan-2-ol/cyclohexane solution (2 min, 1:1 solution by volume) and air drying (60 min). Errors quotes are standard deviation of the sample.

Time / s	Exp #	No. Repeats	WCA Unwashed / °	Charge Unwashed / V	WCA Washed / °	Charge Washed / V
0	HB365, HB1009	4	-	-	129 ± 3	10 ± 65
10	HB1322	4	85 ± 8	277 ± 1166	119 ± 3	8 ± 31
30	HB1304	4	89 ± 10	1274 ± 567	114 ± 6	43 ± 13
60	HB1312	4	95 ± 14	1538 ± 440	123 ± 6	39 ± 7
120	HB1307	4	81 ± 10	1099 ± 1027	105 ± 5	28 ± 13
300	HB1380	4	82 ± 13	1171 ± 772	114 ± 5	25 ± 26

4.5.1.3 Flowing Argon Bubbling Through Water

After treatment with argon and water, the highest charge achieved was after 10 s (395 ± 324 V), although this was not significantly better than after any of the other treatment times. All were within a standard deviation of each other, Table 49. The lowest WCA achieved prior to washing was after 300 s (82 ± 7°), which after washing increased to 108 ± 2° (also the lowest achieved).

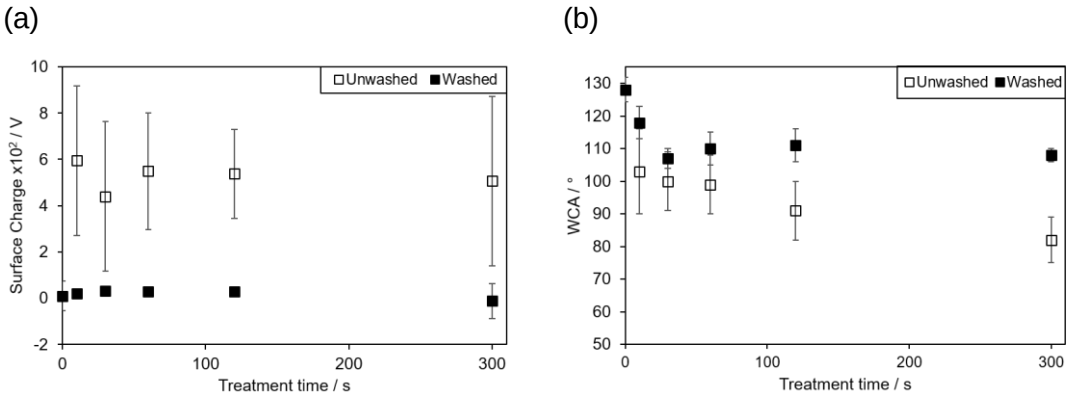

Figure 51: Effect of treatment time on (a) surface potential, and (b) WCA achieved after DBD plasma using flowing argon bubbling through water (14 kV, 3 kHz, 5–300 s, 20 cm^3 min^{-1}), immediately after treatment (□), and after washing in propan-2-ol/cyclohexane (1:1 solution by volume, 2 min) and air drying (60 min, (■)). Error bars denote standard deviation of the sample.

Table 49: WCA and surface potential achieved after varying length DBD treatments of PTFE substrates in flowing argon through distilled water (14 kV, 3 kHz, 10–300 s, 20 cm^3 min^{-1}). WCA and charge were measured immediately after plasma treatment and after washing in propan-2-ol/cyclohexane solution (2 min, 1:1 solution by volume) and air drying (60 min). Errors quotes are standard deviation of the sample.

Time / s	Exp #	No. Repeats	WCA Unwashed / °	Charge Unwashed / V	WCA Washed / °	Charge Washed / V
0	HB365, HB1009	4	-	-	129 ± 3	10 ± 65
10	HB1363	4	103 ± 13	595 ± 324	118 ± 5	20 ± 10
30	HB1371	4	100 ± 9	440 ± 324	107 ± 3	32 ± 11
60	HB1360	4	99 ± 9	549 ± 253	110 ± 5	30 ± 13
120	HB1355	4	91 ± 9	538 ± 193	111 ± 5	29 ± 14
300	HB1350	4	82 ± 7	506 ± 367	108 ± 2	-12 ± 75

4.5.1.4 Flowing Helium Bubbling Through Water

Contrary to that achieved from helium DBD plasma, the surfaces treated with helium and water DBD plasma all exhibited negative surface potential. The largest magnitude of these was after 300 s (-354 ± 291 V). Prior to washing, the lowest WCA achieved was 66 ± 8° (300 s), which after washing became 102 ± 6°, Table 50.

(a) (b)

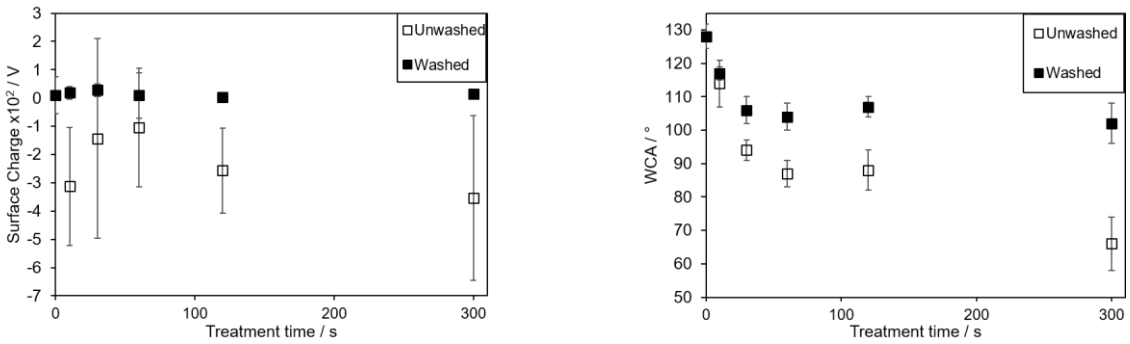

Figure 52: Effect of treatment time on (a) surface potential, and (b) WCA achieved after DBD plasma using helium bubbling through water (14 kV, 3 kHz, 5–300 s, 20 cm^3 min^{-1}), immediately after treatment (☐), and after washing in propan-2-ol/cyclohexane (1:1 solution by volume, 2 min) and air drying (60 min, (■)). Error bars denote standard deviation of the sample.

Table 50: WCA and surface potential achieved after varying length DBD treatments of PTFE substrates in flowing helium through distilled water (14 kV, 3 kHz, 10–300 s, 20 cm^3 min^{-1}). WCA and charge were measured immediately after plasma treatment and after washing in propan-2-ol/cyclohexane solution (2 min, 1:1 solution by volume) and air drying (60 min). Errors quotes are standard deviation of the sample.

Time / s	Exp #	No. Repeats	WCA Unwashed / °	Charge Unwashed / V	WCA Washed / °	Charge Washed / V
0	HB365, HB1009	4	-	-	129 ± 3	10 ± 65
10	HB1343	4	114 ± 7	-313 ± 209	117 ± 2	18 ± 22
30	HB1327	4	94 ± 3	-143 ± 353	106 ± 4	28 ± 22
60	HB1332	4	87 ± 4	-105 ± 210	104 ± 4	9 ± 81
120	HB1335	4	88 ± 6	-257 ± 151	107 ± 3	3 ± 17
300	HB1340	4	66 ± 8	-354 ± 291	102 ± 6	15 ± 11

4.5.1.5 Comparison with Literature

In the literature, it was reported that introducing water vapour into the plasma region post-discharge could have an effect on the surface properties. The work focussed on OES and mass spectrometry though rather than WCA and XPS.[338] The absolute charging of a surface is dependent on the feed gas, the voltage of the discharge and the plasma treatment duration.[331]

The lowest reported WCA in the literature was 28° immediately after helium plasma treatment (no plasma details given), which recovered to 50° after 6 months.[264] Compared to this, the best surfaces reported here are not as hydrophilic.

4.5.2 Bubbling through ammonia water

4.5.2.1 Flowing Air Bubbling Through Ammonia Water

In the literature, the lowest WCA value (4°) was achieved using argon and ammonia water as the feed gas (low-pressure plasma).339 In light of this, the mini-bubbler was used to introduce ammonia water into the system with air as the work gas.

The highest charge was achieved after 300 s (+947 ± 422 V), after treatment with water in the bubbler, the average charge on the surface became negative after longer treatment times, and after treatment with flowing air, the surface potential was also negative. The lowest WCA achieved after treatment with air and ammonia water was after 300 s prior to washing (95 ± 8°), and after 30 s after solvent washing (122 ± 1°).

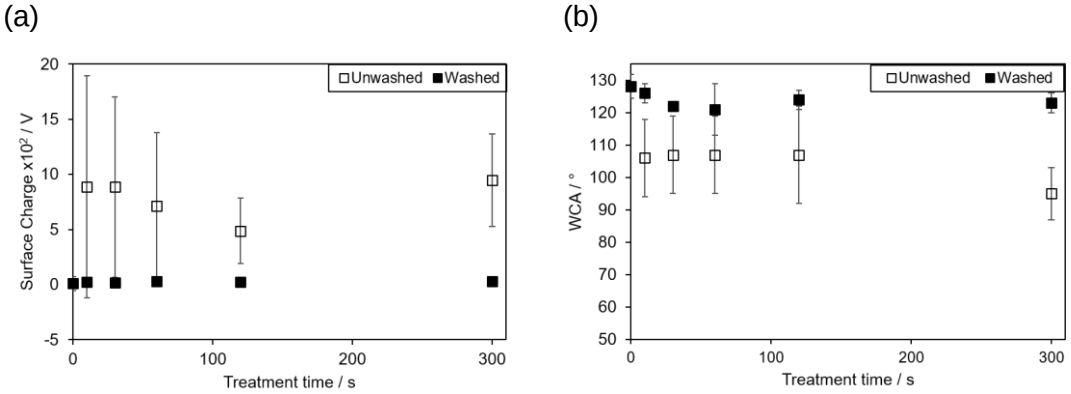

Figure 53: Effect of treatment time on (a) surface potential, and (b) WCA achieved after DBD plasma using air that has flowed through bubbler containing ammonia water (Ammonium hydroxide, 28% purity, CAS no. 1336-21-6, Lot no. 04819JA, Aldrich Chemical Co.) (14 kV, 3 kHz, 5–120 s, 20 cm^3 min^{-1}), immediately after treatment (□), and after washing in propan-2-ol/cyclohexane (1:1 solution by volume, 2 min) and air drying (60 min, (■)). Error bars denote standard deviation of the sample.

Table 51: WCA and surface potential achieved after varying length DBD treatments of PTFE substrates in flowing air through a bubbler containing ammonia water (14 kV, 3 kHz, 5–120 s, 20 cm^3 min^{-1}). WCA and charge were measured immediately after plasma treatment and after washing in propan-2-ol/cyclohexane solution (2 min, 1:1 solution by volume) and air drying (60 min). Errors quotes are standard deviation of the sample.

Time / s	Exp #	No. Repeats	WCA Unwashed / °	Charge Unwashed / V	WCA Washed / °	Charge Washed / V
0	HB365, HB1009	4	-	-	129 ± 3	10 ± 65
10	HB1383	4	106 ± 12	889 ± 1008	126 ± 3	22 ± 18
30	HB1386	4	107 ± 12	885 ± 819	122 ± 1	16 ± 16
60	HB1392	4	107 ± 12	713 ± 668	121 ± 8	3 ± 17
120	HB1398	4	107 ± 15	487 ± 297	124 ± 3	21 ± 16
300	HB1389	4	95 ± 8	947 ± 422	123 ± 3	31 ± 6

4.5.2.2 Flowing Nitrogen Bubbling Through Ammonia Water

The largest negative charging of the surface was observed after 60 s DBD plasma treatment. In the same manner as previously observed, the wash process removed the charge from the PTFE surface. As the treatment time increases, the observed WCA decreases, the lowest WCA observed was after 300 s (87 ± 14° after washing).

(a) (b)

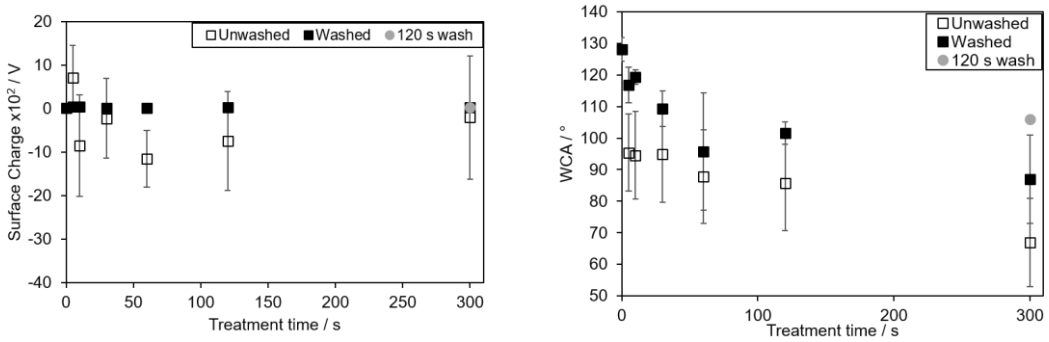

Figure 54: Effect of treatment time on (a) surface potential, and (b) WCA achieved after DBD plasma using nitrogen bubbling through ammonia water (Ammonium hydroxide, 28% purity, CAS no. 1336-21-6, Lot no. 04819JA, Aldrich Chemical Co.) (14 kV, 3 kHz, 5–300 s, 20 cm^3 min^{-1}), immediately after treatment (☐), and after washing in propan-2-ol/cyclohexane (1:1 solution by volume, 10 s) and air drying (60 min, (■)). Error bars denote standard deviation of the sample.

Table 52: WCA and surface potential achieved after varying length DBD treatments of PTFE substrates in flowing nitrogen through a bubbler containing ammonia water (14 kV, 3 kHz, 5–300 s, 20 cm^3 min^{-1}). WCA and charge were measured immediately after plasma treatment and after washing in propan-2-ol/cyclohexane solution (10 s, 1:1 solution by volume) and air drying (60 min). Errors quotes are standard deviation of the sample.

Time / s	Exp #	No. Repeats	WCA Unwashed / °	Charge Unwashed / V	WCA Washed / °	Charge Washed / V
0	HB365, HB1009	4	-	-	129 ± 3	10 ± 65
5	HB957	4	95 ± 12	712 ± 1108	117 ± 6	44 ± 11
10	HB960	4	95 ± 14	-850 ± 821	119 ± 2	40 ± 14
30	HB881	4	95 ± 15	-222 ± 765	109 ± 6	18 ± 8
60	HB884	4	88 ± 15	-1155 ± 729	96 ± 19	15 ± 21
120	HB874/HB878	8	86 ± 15	-745 ± 695	102 ± 4	28 ± 14
300	HB893	4	79 ± 10	-652 ± 488	87 ± 14	29 ± 9
300	HB1544	4	67 ± 14	-202 ± 621	106 ± 1 <120 s wash>	24 ± 18 <120 s wash>

4.5.2.3 Flowing Argon Bubbling Through Ammonia Water

In general, charging using argon as a feed gas resulted in a positively charge surface prior to washing, with the exception of the 120 s treatment which had an average negative surface potential.

The largest degree of positive surface charging was observed for 5 s treatment (397.5 ± 337.2 V), however, there was a similar magnitude of positive charging in the samples treated for 300 s (315.0 ± 310.5 V).

Much lower WCA were achieved using the longer plasma treatment times. This trend has previously been observed when using other feed gases, but not in such a pronounced manner. The lowest unwashed WCA observed was 72.4 ± 7.0° (300 s), and the lowest washed samples were 86.0 ± 7.1° (300 s).

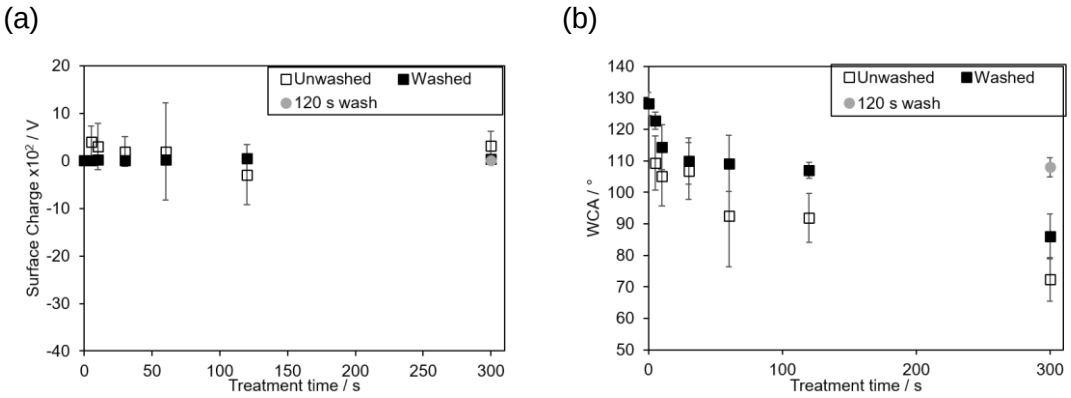

Figure 55: Effect of treatment time on (a) surface potential, and (b) WCA achieved after DBD plasma using flowing argon bubbling through ammonia water (Ammonium hydroxide, 28% purity, CAS no. 1336-21-6, Lot no. 04819JA, Aldrich Chemical Co.) (14 kV, 3 kHz, 5–300 s, 20 cm^3 min^{-1}), immediately after treatment (□), and after washing in propan-2-ol/cyclohexane (1:1 solution by volume, 10 s) and air drying (60 min, (■)). Error bars denote standard deviation of the sample.

Table 53: WCA and surface potential achieved after varying length DBD treatments of PTFE substrates in flowing argon through a bubbler containing ammonia water (14 kV, 3 kHz, 5–300 s, 20 cm^3 min^{-1}). WCA and charge were measured immediately after plasma treatment and after washing in propan-2-ol/cyclohexane solution (10 s, 1:1 solution by volume) and air drying (60 min). Errors quotes are standard deviation of the sample.

Time / s	Exp #	No. Repeats	WCA Unwashed / °	Charge Unwashed / V	WCA Washed / °	Charge Washed / V
0	HB365, HB1009	4	-	-	129 ± 3	10 ± 65
5	HB1010	4	109 ± 9	398 ± 337	123 ± 3	18 ± 20
10	HB1013	4	105 ± 9	298 ± 486	114 ± 7	24 ± 11
30	HB1016	4	107 ± 9	197 ± 312	110 ± 7	9 ± 102
60	HB1019	4	93 ± 16	193 ± 1020	109 ± 9	30 ± 22
120	HB1028	4	92 ± 8	-289 ± 637	107 ± 3	57 ± 13
300	HB1031	4	72 ± 7	315 ± 311	86 ± 7	41 ± 8
300	HB1547	4	83 ± 11	276 ± 237	108 ± 3 <120 s wash>	40 ± 4 <120 s wash>

4.5.2.4 Flowing Helium Bubbling Through Ammonia Water

There is a distinct correlation between WCA and treatment time for those surfaces treated using helium and ammonia water DBD plasma. The longer the treatment time, the lower both the washed and unwashed WCA values, Figure 56. The lowest WCA achieved was after 300 s plasma treatment (91.7 ± 3.2° after washing, 80.8 ± 4.5° prior to solvent washing).

As previously seen, the charge is removed by the process of solvent washing. The charge obtained for the surfaces, is initially very variable at low treatment times (5 s). An increase in surface potential is observed as the treatment time increases at low treatment times (5–60 s). After 300 s, the surface potential measured is negative again.

(a) (b)

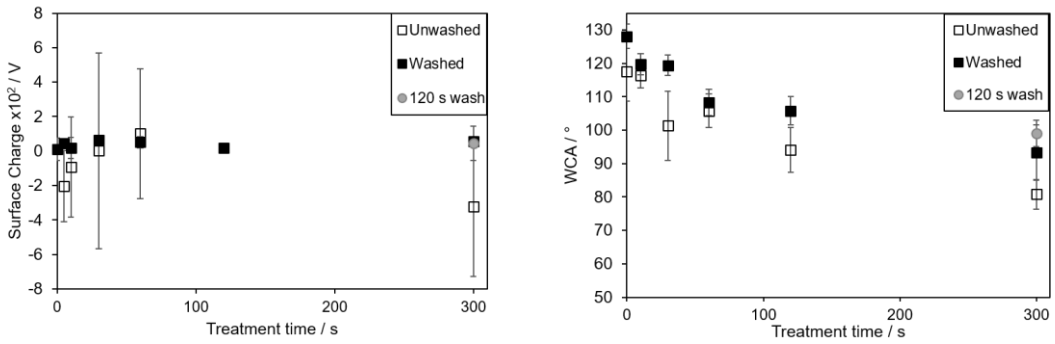

Figure 56: Effect of treatment time on (a) surface potential, and (b) WCA achieved after DBD plasma using helium bubbling through ammonia water (Ammonium hydroxide, 28% purity, CAS no. 1336-21-6, Lot no. 04819JA, Aldrich Chemical Co.) (14 kV, 3 kHz, 5–300 s, 20 cm^3 min^{-1}), immediately after treatment (□), and after washing in propan-2-ol/cyclohexane (1:1 solution by volume, 10 s) and air drying (60 min, (■)) and after washing in propan-2-ol/cyclohexane (1:1 solution by volume, 120 s) and air drying (60 min, (●)). Error bars denote standard deviation of the sample.

Table 54: WCA and surface potential achieved after varying length DBD treatments of PTFE substrates in flowing helium through ammonia water (14 kV, 3 kHz, 5–300 s, 20 cm^3 min^{-1}). WCA and charge were measured immediately after plasma treatment and after washing in propan-2-ol/cyclohexane solution (10 s, 1:1 solution by volume) and air drying (60 min). Errors quotes are standard deviation of the sample.

Time / s	Exp #	No. Repeats	WCA Unwashed / °	Charge Unwashed / V	WCA Washed / °	Charge Washed / V
0	HB365, HB1009	4	-	-	129 ± 3	10 ± 65
5	HB1131	4	118 ± 9	-204 ± 205	120 ± 3	46 ± 16
10	HB1127	4	116 ± 4	-94 ± 290	119 ± 3	18 ± 61
30	HB1124	4	101 ± 10	1 ± 568	108 ± 4	64 ± 24
60	HB1121	4	106 ± 5	101 ± 376	106 ± 4	52 ± 33
120	HB1118	4	94 ± 7	-	93 ± 8	17 ± 20
300	HB1134	4	81 ± 5	-320 ± 405	92 ± 3	56 ± 17
300	HB1536	4	77 ± 7	-68 ± 142	99 ± 4 <120 s wash>	46 ± 7 <120 s wash>

4.5.2.5 Comparison with Literature

There have been no reported uses of doping ammonia water in DBD plasma for the treatment of PTFE. There have been two reported uses of NH_3 (gas) doped into nitrogen for treatment of PTFE. A WIPO patent in 1999 reported an adv. WCA of 69° and a rec. WCA of 10° after corona discharge treatment (N_2 with 1% NH_3, 2500 W, 4.2 cm s^{-1}) of Teflon resin.[263] C. Sarra-Bournet *et al.* reported a WCA of approx. 25° for PTFE sheet (Goodfellow Ltd., thickness 250 µm)after APTD treatment (N_2 +

100 ppm NH_3, 10 kVm 180 s).[239,240] In comparison to these reported values, the best WCA (67°) achieved in this work is significantly less hydrophilic.

There have also been reports of doping reactive species into a more inert work gas, for example V. Rodriguez-Santiago *et al.* and E.A.D. Carbone *et al.* used argon doped with oxygen as a feed gas. Carbone *et al.* reported an increase in WCA to 130°, and an increase in the F/C ratio to 2.09 (80 W, 10 min).[271] Whereas Rodriguez-Santiago *et al.* reported a decrease in WCA to 55°.[270] It is likely that the composition of the feed gas is responsible for these differing effects. Work by V. Rodriguez-Santiago *et al.* reported a WCA of 77° after atmospheric plasma treatment (0.861–2.58 W cm^{-2}, 40 s) of PTFE using He/H_2O as the feed gas. Hydrophobic recovery was reported to be 1.4% (78.1°).[270] The WCA achieved prior to solvent washing for helium (77°) and argon (72°) is comparable to that achieved in the literature. There are no reported solven washed samples to compare these with.

4.5.3 SEM

Just like in the low-pressure work, the effect of the plasma treatment on the surface morphology was investigated using SEM methods. The secondary electron images, Table 55, show that the DBD plasma treatment has a much less significant effect on roughening the surface in comparison to the low-pressure treatments. The pulsed nature of the plasma means that far less surface destruction is seen, and we would expect less LMWOS to be present on the surface because of this. There is very little visible difference between the washed and unwashed surfaces at any of the magnifications, and no huge differences in comparison to the untreated PTFE substrates either.

Table 55: Comparison of surface morphology of untreated and DBD plasma-treated (flowing nitrogen bubbling through ammonia water, 300 s, 14 kV, 3 kHz, 100 µs and 4 ms off) PTFE samples prior to and after solvent washing (2 min, 1:1 v/v solution of propan-2-ol and cyclohexane). Samples were coated with 12 nm of gold prior to analysis. Secondary electron images collected on FEI Helios Nanolab 600, operating at 3 kV. Images collected by Stuart Goldie, PhD Researcher, Durham University.

	Untreated (Washed)	**Flowing Nitrogen Bubbling Ammonia Water, 300 s (Unwashed)**	**Flowing Nitrogen Bubbling Ammonia Water, 300 s (Washed)**
300 µm	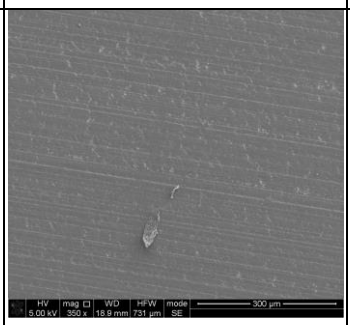	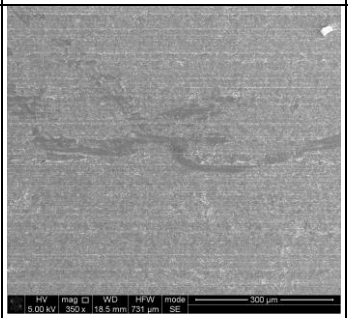	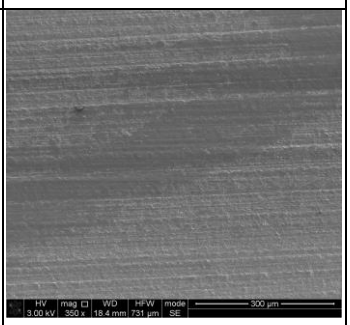
~40 µm	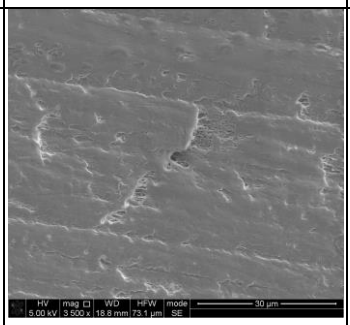	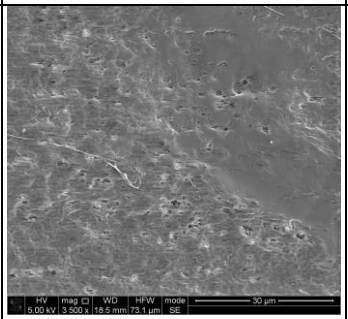	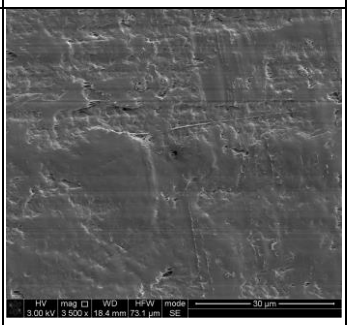
~10 µm	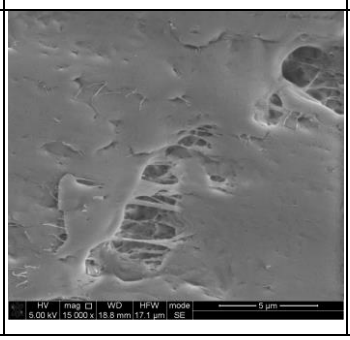		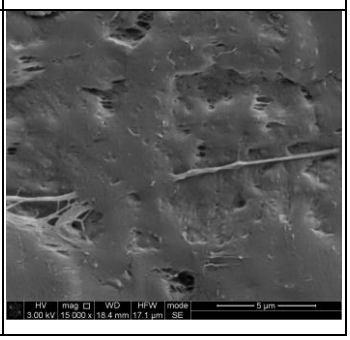

4.5.4 Summary of WCA and Surface potential

Overall the lowest WCA of 99° ± 4° after 120 s solvent washing was achieved using long treatment times (300 s) and helium flowing through ammonia water bubbler as the feed source. The overall low degree of change in WCA indicates that the surface of the PTFE is not being heavily modified by the atmospheric plasma treatments, this is in contrast with that achieved using low-pressure plasma with the same feed gases. Prior to solvent washing, significantly lower WCA were achieved

for all the plasma-treated samples, it is likely that this is due to the charging of the surface. This charging could be mapped using AFM.

Some of the gas plasma treatments resulted in average positive charging of the surface, and some resulted in negative charging of the surface. All the treatments which used argon, helium, air and ammonia water, and nitrogen and ammonia water as the feed gas resulted in surfaces which had an average positive surface potential. However the addition of water or ammonia water into the feed gas resulted in the initially positively charged surfaces from the “pure” gas becoming negatively charged as a consequence of doping. This can be attributed to an increase in the polar species present in the gas meaning that there is an abundance of available electrons.

There is no real trend across all treatments in terms of treatment time and the observed charge afterwards, it is dependent on the nature of the feed gas. A much larger degree of surface charging is observed after the static air treatment, this is likely due to the lack of flow through causing debris to remain on the surface, as previously discussed (Section 4.4.1).

Table 56: Summary of DBD gas treatments (no charge remains after washing). Some samples are washed for 10 s, and some for the longer duration of 120 s. This does not affect the unwashed data, and the best 10 s washed data points were repeated with 120 s wash time. Highlighted in orange is the best solvent washed WCA after 10 wash time, and highlighted in green is the best WCA after 120 s solvent wash. The values reported are the average of the sample, and the errors denote the standard deviation of the sample.

Feed Gas	**WCA / ° (DBD Time / s) <Washing Time / s>**		**Best Average Charge Before Washing / V (Time / s)** †
	Best	**Best After Wash**	
Untreated	-	129 ± 3	+10 ± 65
Static Air	76 ± 14 (10)	99 ± 7 (20) <10>	-2100 ± 1547 (120)
Flowing Air	68 ± 14 (60)	101 ± 3 (60) <10>	-619 ± 653 (5)
Flowing Air + Water	78 ± 15 (120)	102 ± 11 (120) <10>	-301 ± 777 (120)
Flowing Air + Ammonia Water	95 ± 8 (300)	122 ± 1 (30) <120>	+947 ± 422 (300)
Flowing Nitrogen	71 ± 15 (120)	105 ± 3 (120) <10>	-1166 ± 626 (120)
Flowing Nitrogen + Water	81 ± 10 (120)	105 ± 5 (120) <120>	+1099 ± 1027 (120)
Flowing Nitrogen + Ammonia Water	67 ± 14 (300)	87 ± 14 (300) <10>	-1155 ± 729 (60)
		106 ± 1 (300) < 120>	
Flowing Argon	91 ± 14 (120)	108 ± 3 (120) <10>	+563 ± 540 (30)
Flowing Argon + Water	82 ± 7 (300)	108 ± 2 (300) <120>	+595 ± 324 (10)
Flowing Argon + Ammonia Water	72 ± 7 (300)	86 ± 7 (300) <10>	+398 ± 337 (5)
		108 ± 3 (300) <120>	
Flowing Helium	87 ± 8 (300)	102 ± 5 (300) <10>	+297 ± 356 (30)
Flowing Helium + Water	66 ± 8 (300)	102 ± 6 (300) <120>	-354 ± 291 (300)
Flowing Helium + Ammonia Water	77 ± 7 (300)	92 ± 3 (300) <10>	-320 ± 405 (300)‡
		99 ± 4 (300) <120>	

† Best charge is the highest average magnitude (regardless of if it is positive or negative) of surface potential.

‡ Not easy to draw a clear best charge here.

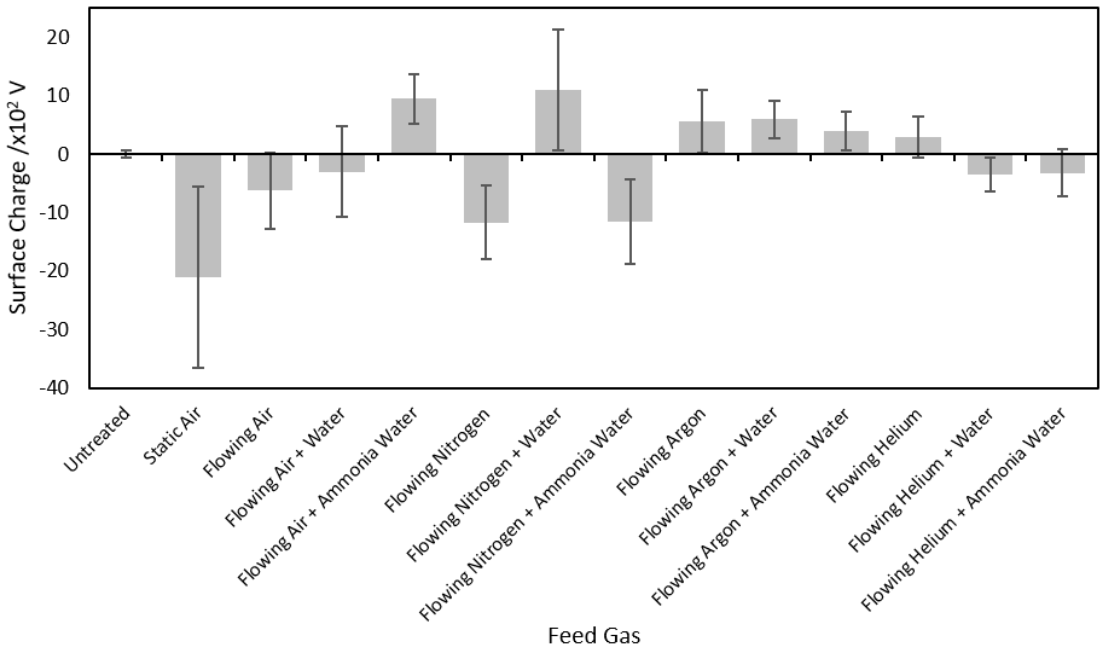

Figure 57: Summary of the best unwashed charge achieved according to feed gas.

4.6 CONCLUSIONS

Overall, the atmospheric-pressure plasma conditions investigated in this chapter were not as effective at producing a stable hydrophilic surface as those reported in Chapter 3 using low-pressure plasma methods. The idea of electrowetting did result in the droplet jumping from the needle to the surface during DSA, however as the surface was not uniformly charged, not every droplet spread to the same degree. The lowest WCA achieved prior to solvent washing was 67 ± 14° (nitrogen bubbling through ammonia water, 14 kV, 3 kHz, 300 s) and 66 ± 8° (helium bubbling through water, 14 kV, 3 kHz, 300 s). However both of these surface returned to a hydrophobic nature (WCA greater than 90°) after solvent washing and drying under nitrogen. There is very little change observed in the surface roughness of the DBD plasma-treated surfaces in comparison to the untreated PTFE substrates, and this lack of topography changes contributes to the minimal change in hydrophilicity observed.

Charge was consistently imparted onto the surface using DBD plasma treatment regardless of the feed gas. This potential remained stable on the surface unless the surface was solvent washed, when all charge was removed. It is this charge storage property that allows PTFE to be used as an electret. It was shown using high speed camera capture that the DBD plasma was ignited about a threshold value of approximately ± 5 V, which corresponded to the first initial sharp positive voltage and the subsequent first negative ring.

The incorporation of polar species into the plasma feed stream resulted in a small decrease in the observed WCA, however after washing the surface was still above 90°. Additionally, the average surface potential of the treated PTFE surfaces was affected by the presence of the polar molecules in the plasma. For reactive gases such as air and nitrogen, the effect was less obvious. This is likely to the reactive nature of the base gas, there are already sufficient electrons available in the plasma, and so resultant the charge of the surface is dominated more by the duration of the plasma treatment than by the feed gas. There is a more significant effect observed for the inert gases, especially helium. Helium alone produced a positively charged surface, meaning that electrons were harvested from the surface by the plasma. When water or ammonia water were doped into the feed stream, the resulting surface was negatively charged. This indicates that electrons are incorporated into the surface by the plasma. The presence of the polar molecules in the plasma stream means that there is an abundance of electrons available, and none are harvested from the surface.

Chapter 5: Post Plasma Modification of PTFE – *Using atmospheric plasma as an activation step for subsequent monomer grafting*

5 POST-PLASMA MODIFICATION OF PTFE – *USING ATMOSPHERIC-PRESSURE PLASMA AS AN ACTIVATION STEP FOR SUBESQUENT MOLECULE GRAFTING*

5.1 MOTIVATION

In Chapter 4, atmospheric DBD plasma was used to modify PTFE surfaces with the initial aim of decreasing the WCA. As previously mentioned, in an industrial setting, a DBD plasma is a far more facile method of modifying PTFE on a large scale than a low-pressure plasma treatment. There is no vacuum environment to maintain, no pumps, and no need for continuous checking for leaks to ensure the correct plasma conditions can be repeatedly achieved.

The findings from Chapter 4 showed that as a method of decreasing the WCA of PTFE, the DBD method was not as effective as the low-pressure method detailed in Chapter 3. However, due to the slight change in WCA observed even after washing, there appears to have been some incorporation of some polar functional groups into the surface. In a similar manner that an argon low-pressure plasma can be used as an activation step, it is postulated that the DBD plasma can be used as an activation step to allow for further chemical reaction on the surface. This may also be aided by the incorporation of charge into the surface.

The use of a post-plasma deposition is hypothesised to result in a significant and stable decrease in the WCA. The deposition of a polymer layer on top of the activated PTFE should also prevent the problem of hydrophobic recovery observed in the previous work reported in Chapter 3 and 4. The LMWOS removal and surface reconstruction will be hampered by the presence of another layer on top of the PTFE, and so providing that the deposited layer is stable, the samples should be more stable to solvent washing. However, it could also be argued that the presence of LMWOS still on the surface prior to deposition will mean that the surface is less robust as the LMWOS are being functionalised rather than the surface. In the case of the DBD plasma-treated surfaces reported in Chapter 4, there is not significant LMWOS observed in the SEM in comparison to the low-pressure plasma-treated surfaces, and so the surfaces were not washed prior to deposition.

In terms of industrial processing, an atmospheric plasma with a subsequent vapour or wet chemical deposition step is likely to be cheaper and quicker than a low-pressure plasma treatment.

5.2 LITERATURE REVIEW

5.2.1 Electric Field Assisted Deposition

Widely reported in the literature is the use of electric fields in order to assist deposition onto surfaces – this is used in inkjet printing.340 There has been reported the use of electric fields to assist the assembly of nanoparticle arrays, mainly for contact hole patterning.[341,342]

Electrohydrodynamic atomization, or electrospraying uses a ring-shaped electrode to charge the droplets of solution before being sprayed onto the surface to form a self-supported macroporous scaffold. S.N. Jayasinghe *et al.*, reported the use of an ethanolic siloxane sol made from alkoxysilanes that is polycondensed onto the surface to form “fir-tree like” structures.[343]

More complex surface structures can also be made by using an electric field to control a liquid deposition. Dickey *et al.* used electric fields to form pillars from a film deposited on a surface before photocuring using a mercury lamp.[344] By applying an electric field across a thin film, it is possible to destabilize the surface such that undulations will form and grow until they span the interelectrode gap.[344] The best film type for this kind of pillar formation was found to be thiol-ene film (17.5 wt% thiol (pentaerythritol tetrakis(3-mercaptopropionate)) and 17.5 wt% vinyl ether (Tris[4-(vinyloxy)-butyl] trimellitate)).[344]

A recent patent by Kettering University has suggested that atmospheric air/nitrogen plasma (in this case RF glow plasma not DBD) can be used to modify PTFE particles, which are then exposed to a monomer (example given is HEMA) in order to introduce hydrophilicity at the surface.[345]

5.2.2 Post Plasma Monomer Grafting Prior Art

Although there has been substantial previous work done using a plasma step as a pretreatment to grafting of monomers onto PTFE surfaces, Table 57, there is limited investigation into the use of atmospheric plasma as an activation treatment.

For example, Ch. Baquey *et al.* used low-pressure argon/oxygen plasma to activate an ePTFE (expanded PTFE, a very porous substrate) surface in order to graft acrylic acid from aqueous solution.[346] This was used as a precursor step to the grafting of and subsequent immobilization of peptides on the ePTFE for use as a vascular graft, Figure 58.

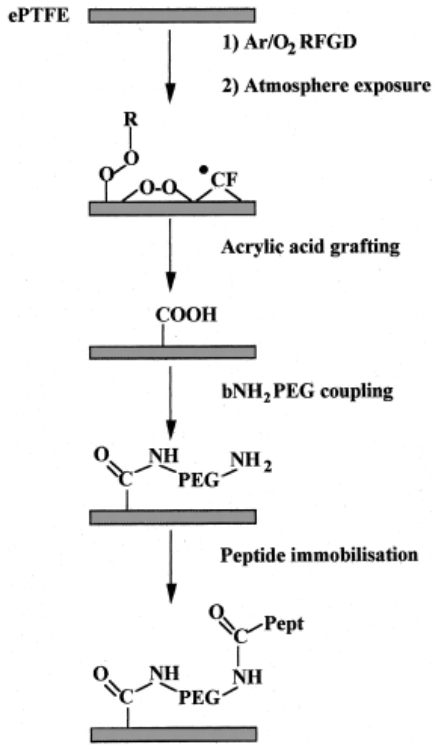

Figure 58: Schematic mechanism proposed by Ch. Baquey *et al.* of how a plasma step can be used in conjunction with a monomer grafting step for use in vascular graft applications.[346]

Turmanova *et al.* reported grafting vinyl monomers (acrylic acid, 4-vinylpyridine, and 1-vinylimidazole) on argon plasma (low-pressure) modified PTFE substrates. After grafting in an argon atmosphere at 80 °C for 2 h, the lowest WCA achieved was 56° using acrylic acid on PTFE treated with 1200 W Ar for 120 s.[347]

Work by Tu *et al.* investigated grafting acrylate monomers on PTFE substrates modified using hydrogen plasma (low-pressure) and ozone pretreatments (82°).[348] After the grafting of 2-(2-bromoisobutyryloxy)ethyl acylate (BIEA) monomer onto the surface of plasma-modified PTFE, sodium 4-styrenesulfonate (SSS) was polymerized via atom transfer radical polymerization (ATRP) onto the PTFE surface using the BIEA as an initiator. WCA as low as 26° was achieved when ATRP was performed on BIEA grafted PTFE.

Cho *et al.* reported the use of hydrogen and argon DBD plasma (low-pressure) as an activation step for the deposition of a hydrocarbon film (from acetylene and argon plasma) onto the PTFE surface.[349]

A recent patent (2016) claims that 2-hydroxyethyl methacrylate (HEMA), can be used to hydrophillize PTFE, but no details of results achieved on PTFE were given in the claims (which focussed on PMMA and PP).[350]

Table 57: Summary of prior art on post-plasma grafting of monomers onto PTFE.

Pressure	Monomer	Grafting process	Pre-treatment	WCA achieved /°	F/C achieved	Ref
Atmospheric-pressure	Acrylic acid (AA) and sodium 4-styrenesulfonate (SSS) at ratio of 4:1.	Immersed in AA/SSS solution and kept in oxygen free sealed environment at 70 °C for 20 h. Afterwards samples were washed in ethanol, extracted in water for 10 h using Soxhlet extractor and dried overnight at 40° under vacuum.	DBD treatment using atmospheric air (8 mm interelectrode gap, air flow 10 L min^{-1}, 10 kHz, 3 min).	36 after 25 s, initially 55	Not given.	351
	4-vinylpyridine and copper acetate monohydrate 4VP/CuAc	Spin coated from 300 µL of ethanol solution (CuAc: 3.92 $x10^{-2}$ M) with 1:2 ratio of CuAc to 4VP.	Atmospheric-pressure helium DBD plasma (15 W, 760 Torr, 15 s).	60 after plasma treatment, not analysed after grafting.	XPS carried out but no F/C ratio given.	352, 353.
	2-acrylamido-2-methyl-propyl-sulfoacid (AMPS)	Immersed in aqueous solution with dissolved photosentizer benzophenone, acetone and AMPS monomer. Reaction initiated by UV lamp 1 kW under nitrogen atmosphere (no treatment time given). After reaction, PTFE was cleaned with deionized water, treated with acetone and soaked in water for 24 h. Samples are finally dried at 70 °C for 30 min using an electrical	Atmospheric-pressure air DBD plasma (220V, 50 Hz, 760 Torr, no treatment time given). Samples exposed to air for 8–10 min after plasma treatment.	Not measured.	Not measured.	354

		thermostatic drier.				
Low-pressure	Glycidyl methacrylate (GMA)	Immersed in 30 mL of 30 vol.% 1,4-dioxane GMA sealed under argon and put under UV at 28 °C for 60 min. Samples washed in acetone and dioxane at 50° C for 24 h.	Argon plasma treatment (35 W, 0.6 Torr, 60 s).	142	XPS carried out but no F/C ratio given.	355
	AA	Graft copolymerization carried out at 80 °C for 4 h, with 2 h post polymerization after under an inert argon atmosphere. To suppress homopolymerization, 0.25 wt% $FeCl_3$ was added.	Argon plasma (1200 W, 0.2 Torr, 30–360 s). Samples exposed to atmosphere for 15 min after plasma treatment.	56	XPS carried out but no F/C ratio given.	347
	4VP			80		
	1-vinylimidazole (1VI)			68		
	Poly(GMA)	Argon treated PTFE added to BPO, GMA, and CTA solution in DMF.	Argon RF plasma (35 W, 0.5 Torr, 90 s) followed by air exposure (20 min).	60	0.18	356
	AA	Immersed in AA aqueous solution (25 v/v%, 65 °C, 5 h) Washed by Soxhlet extraction in ethanol (24 h).	Low-pressure glow argon and oxygen plasma (20 sscm, 100 w, 0.1 Torr, 60 s).	82	1.0	346
	Acrylamide (AAm)	Activated PTFE samples immersed in 50 mL of monomers in PROPAN-2-OL. 20 wt% for AAm, AA and GMA, and 10 wt% for BIEA.	Sequential hydrogen plasma (50 W, 0.1 Torr, 180 s) and ozone (15 min) treatments. Samples	Not given.	Not given.	348
	AA			Not given.	Not given.	

	GMA		washed in propan-2-ol and dried under vacuum at room temp.	Not given.	Not given.	
	BIEA			82	Not given.	
	BIEA with subsequent ATRP of SSS			26	Not given.	
	Methoxy-poly(ethylene glycol) (MPEG)	Immediately after plasma treatment, PTFE immersed in 15 mM phosphate buffer at pH 6, MPEG-NHS derivative added to give 2.5% (w/v) solution.	Ammonia RF plasma (20 W, 0.3 Torr, 50 s).	55	0.5	357
	Cysteamine	Immediately after plasma treatment the samples were inserted into either 2 wt% cysteamine or 2-aminoethanol in water.	Argon plasma (8.3 W, 0.08 Torr, 120–480 s).	90	1.6	358
	2-aminoethanol			87	1.1	358

The lowest WCA (36°) achieved when grafting a monomer onto an atmospheric plasma-treated surface was when AA/SSS (4:1 ratio) were grafted onto a DBD (air, 3 min, 10 kHz) treated PTFE surface.[351] SSS has an SO_3^- group at one end, and a CH_2 group at the other. AA also has an unsaturated CH_2 and a polar pendant group when the monomer is polymerized. Z-Y Xi *et al.* investigated the mechanism by which this monomer mixture reacted with the plasma-treated PTFE substrate using ATR-FTIR, XPS, FSEM, AFM, and droplet wettability and permeation analysis. From the SEM, it is evident that there is a significant degree of pores or defects on the surface, which as shown in the previous work shown in this thesis has a marked effect on the observed CA of the surface. It should be noted that this 36° reported was the WCA measured after 25 s on the surface, not the immediate WCA which was 55°, suggesting that the porous nature of the PTFE has a significant effect on the observed wetting. No investigation into the type of wetting state achieved by this process was reported. As previously shown in Chapter 3, if the change in the functional groups is detectable by ATR-FTIR, then it can assumed that the thickness of the layer deposited on the surface is significantly large. This is shown in the changes in the AFM images reported, where significant smoothing of the surface is observed after deposition.

Their findings indicated that the presence of the large amount of AA monomer in the solution promoted a grafting a layer of AA onto the PTFE surface before subsequent reaction with the SSS. This layer was stable to a 10 h Soxhlet extraction in water, although no solvent washing like that previously employed in this thesis was carried out. Previously, it has been shown that storage or washing of a plasma-treated PTFE sample in water can increase the hydrophilicity of the surface rather than induce hydrophobic recovery that is seen when washing in propan-2-ol and cyclohexane solution.

They reported that the longer the duration of the DBD plasma treatment, the higher the degree of grafting of AA/SSS on the polymer surface, although the highest amount of grafting achieved was 4.3% coverage from solution after 20 h incubation at 70 °C. As far as commercial industrial viability goes, this is a prolonged treatment requiring a plasma treatment, a 20 h oven incubation in solution and then a significant Soxhlet extraction (10 h) and drying stage (overnight) afterwards. A much shorter and quicker process would be more beneficial in terms of cost.

5.2.2.1 Lowest Reported WCA

The lowest WCA (36° after 25 s, 55° immediately after droplet impact) that was reported in the literature was for atmospheric-pressure, air-plasma-treated PTFE subsequently immersed in acrylic acid (AA) and sodium 4-styrenesulfonate (SSS) solution.[351] A WCA as low as 26° was reported after sequential low-pressure hydrogen and ozone-treated PTFE surfaces were grafted with BIEA and subsequent ATRP of SSS.[348]

5.2.3 Zwitterionic Polymer Deposition

A zwitterionic polymer is made up of monomers with a positive pendant group and a negative pendant group, which when the monomers are joined together in a chain occupy a separate region in space, thus retaining the zwitterionic character. As zwitterionic polymers can interact with water through electrostatically induced hydration resulting from the negatively and positively charged groups of the polymer.[359] The grafting of a zwitterionic polymer onto the DBD plasma-treated PTFE surface reported in Chapter 3 is thought to be a method to produce a sufficiently low WCA, and an improvement on the work produced via DBD plasma treatment alone.

In the literature, there has been a lot of work into the grafting of dopamine (DOPA) catechol based monomers onto polymer surfaces, these are bioinspired mussel-mimetic surfaces.[360,361,362]

Hydrophobic polymers (PS, PVC, PP, PMMA, PDMS and nylon) were dip-coated using sulfobetaine solution by H.S. Sundaram *et al.*.[359] This was in order to create an anti-fouling surface (testing using fluorescently labelled BSA-FITC). This was successful on DOPA-PSB-100 (a high molecular weight biomimetic catechol chain end poly(sulfobetaine methacrylate) (PSBMA) monomer) coated nylon, PP and PVC fibres.[359] After sulfobetaine deposition, there was at least an 80% reduction in the IgG fouling of the polymeric surfaces in comparison to the control sample.[359]

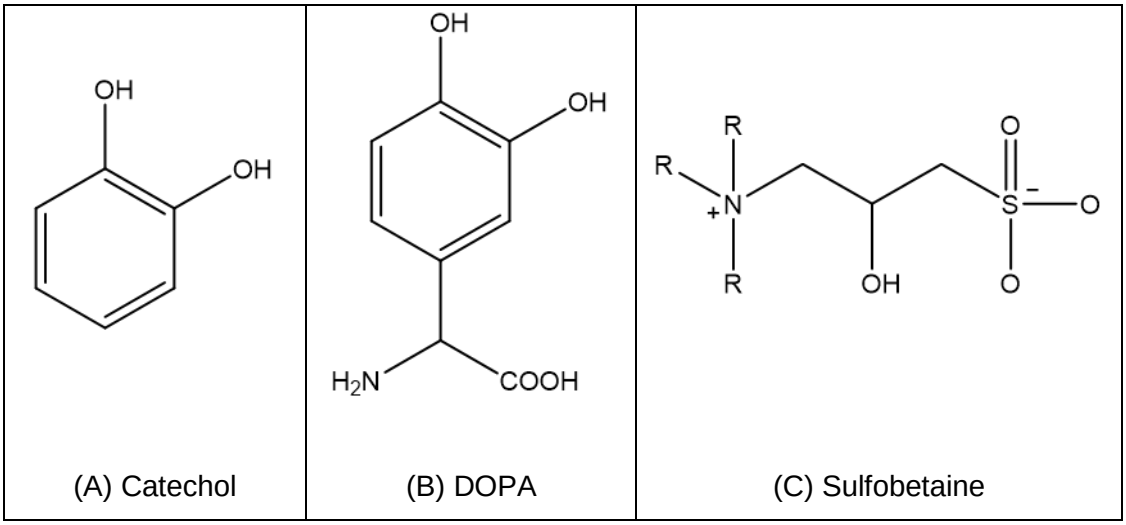

(A) Catechol (B) DOPA (C) Sulfobetaine

Figure 59: Basic structures of grafting monomers. (A) Catechol functional group, (B) DOPA molecule. (C) Basic sulfobetaine zwitterionic molecule.

Atmospheric plasma was used by Venault *et al.* to promote crosslinking of PEGMA monomer on ePTFE.[363] The ePTFE membranes were incubated in PEGMA solution (10 wt% in propan-2-ol) before being treated with argon plasma (5–120 s, 150 W, 13.56 MHz, 10 L min^{-1}, 1.01 bar).[363] After plasma treatment the samples were ultrasonically washed sequentially in methanol and deionised water for 60 mins each, and kept in a vacuum oven under reduced pressure for 3 days.[363] After this plasma assisted PEGylation treatment (120 s), the ePTFE surfaces had very low WCA (9° ± 1°, untreated 105° ± 1°) and increased surface roughness (319 ± 10 nm, untreated 248 ± 7 nm).[363] There was no investigation into how stable these surfaces were, or how they aged.

In similar work reported by J.-F. Jhong *et al.* in 2014, ePTFE was shown to be modified using low-pressure hydrogen plasma prior to atmospheric argon plasma controlled copolymerization of the surface with PSBMA and poly(ethylene glycol) methacrylate (PEGMA).[364]

5.3 EXPERIMENTAL

PTFE substrates (15 mm x 10 mm samples, Goodfellow Cambridge Ltd., thickness 0.25 mm, FR301350/20, Batch number 300291002) were washed in 1:1 solution by volume of propan-2-ol (PROPAN-2-OL, 99.5%, Fisher Scientific UK Ltd.), and cyclohexane (99% purity, Fisher Scientific UK Ltd.) solution, and air dried (60 min).

The DBD plasma treatment is carried out in the same manner as previously described (static air, 30 s treatment, and nitrogen bubbling through ammonia water, 60–300 s). Dampened sinusoidal pulses (14 kV, 3 kHz, 100 µs on, 4 ms off, actual voltage on time discussed in Chapter 4) were generated using a thyristor switched high-voltage power supply.

5.3.1 Post-Plasma Exposure to Monomers

A 'mini-bubbler' has been designed that allows for the introduction of a small amount of monomer into the unit after plasma treatment. The bypass is placed in series with the flow meter prior to the flow cell, and connected via PVC 6.5 tubing.

The bubbler bypass system consists of a small bubbler, two Rotaflo taps (6 mm GP Rotaflo stopcock, GP6RA/7, SciLabware Ltd.), two quick-release Keck barbed adapters (Part codes JS29/2 GL14 thread, GL/14 cap, and GL14/N Connector, Scientific Glass Laboratories Ltd.), and connected via ½" glass tubing, Figure 60.

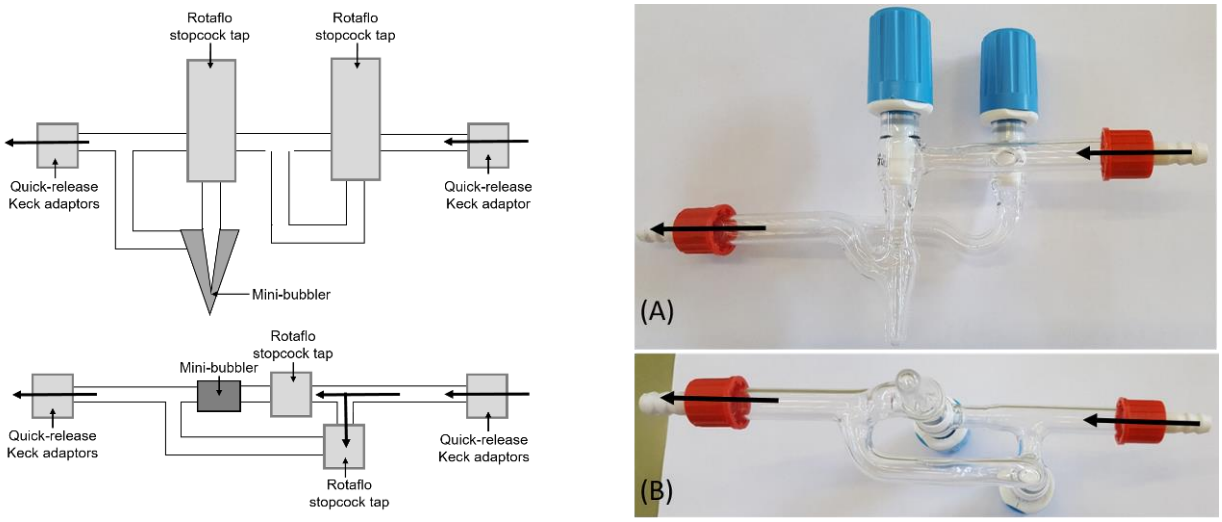

Figure 60: Mini-bubbler bypass system: (A) side-on view; and (B) bottom-up view.

The mini-bubbler bypass system is designed to be more compact and robust than previous systems, and does not include Quick-fit glassware, thus eliminating the potential need for vacuum grease. Quick-release Keck adaptors are incorporated to allow the bubbler bypass system to be easily dismantled without the potential for glass breakage when trying to remove tubing. The Rotaflo tap is positioned directly above the bubbler to allow the monomer to be easily pipetted into the bubbler well. This new bubbler system includes a tapered bubbler, and therefore requires less than 1 mL of monomer. This allows for more expensive monomers to be sparingly used.

In this work, a number of different methods for monomer deposition were used. The first of these was vapour deposition, whereby a droplet was placed next to the charged PTFE sample in a small glass petri dish (borosilicate glass, diameter 30 mm, height 12 mm, flat plate borosilicate glass lid). The monomers used in this way were 2-hydroxyethyl methacrylate (HEMA, 97% purity, CAS no. 868-77-6, Lot no. S21959-484, Aldrich Chemical Co.), acrylic acid (AA, 99% purity, CAS no. 79-10-7, Lot no. 7127022), Glycidyl methacrylate (GMA, 97% purity, CAS no. 106-91-2, Lot no. MKBBG6062V, Aldrich Chemical Co.), 1-allyl imidazole (1-AI, 97% purity, CAS no. 31410-01-2, Barcode 335170250, Acros Organics; Fisher Scientific UK Ltd.), allyl mercaptan (AM, 80.0% purity, CAS no. 870-23-5, TCI Europe; Tokyo Chemical Industry Co. Ltd.), and 4-vinyl pyridine (4-VP, 95% purity, CAS no. 100-43-6, Lot no. 05916HC, Aldrich Chemical Co.). Tetramethylsilane (TMS, 99.99% purity, CAS no. 75-76-3, Alfa Aesar; ThermoFisher Scientific Ltd.) was also used to see if deposition using a reactive molecule with a silicon linker group could be performed. The same vapour deposition method was also used for two dilute solutions; one solution of AA dissolved in cyclohexane (1% v/v solution), and an aqueous sulfobetaine (Figure 61, [3-(methylacryloylamino)propyl]dimethyl(3-sulfopropyl)ammonium hydroxide inner salt, CAS no 5205-95-8, Lot no 473170, Aldrich Chemical Co.) solution (1 wt% solution with deionised water). The WCA and surface potential of these vapour-deposited samples were measured prior to the samples being washed in solvent solution (1:1 v/v solution of cyclohexane and propan-2-ol) and dried vertically in a nitrogen stream.

Charged PTFE surfaces were also dipped into the same aqueous sulfobetaine solution, and into the AA in cyclohexane solution. These samples were dried vertically in a nitrogen stream to prevent any pooling of solution on the surface prior to measuring the WCA. As before, the samples were washed and dried vertically before being analysed again.

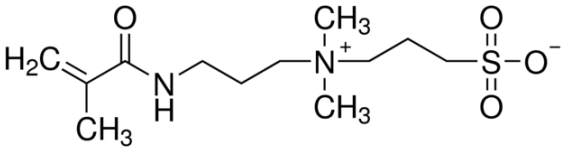

Figure 61: Structure of [3-(methylacryloylamino)propyl]dimethyl(3-sulfopropyl)ammonium.[365]

5.3.2 Contact Angle

The WCA was measured immediately after plasma treatment and after washing in propan-2-ol/cyclohexane solution (2 min, 1:1 solution by volume) and air drying (60 min). Static water contact angles (WCA) were measured using the sessile drop method (VCA 2500XE instrument, AST Products Inc., 1 µL ultra-high purity water droplets, ISO 3696 Grade 1).

5.3.3 Surface Potential

The surface potential was measured using an electrostatic voltmeter (Isoprobe model 244, Monroe Electronics Ltd., fitted with probe model 1017, Monroe Electronics Ltd.) with a surface-to-probe spacing of 2 mm. This small spacing decreases the influence of outside electric fields.[366] The system was fitted with an air pump (Second Nature Whisper 400, 115 V A.C., 60 Hz, 3 W, Willinger Bros Inc.) that allowed purging of the system for 2 h prior to use. This decreased the drift on the measurements (manufacturer's suggestion). If insufficient air purging is carried out prior to the analysis of a surface, the charge measurement displayed will not stabilise within 5 min. If it continues to fluctuate for more than 5 min, this suggests that there has been insufficient air purging of the system carried out prior to analysis.

Due to the non-uniform character of the DBD plasma, there will be non-uniform charging of the insulator surface,[367] for this reason an average of 5 measurements across the surface was taken on each sample.

5.3.4 ATR-FTIR

FTIR spectra were obtained using a PerkinElmer Frontier IR, using a U-ATIR accessory, a Diamond element (Diamond/KRS-5, serial no. 27281) and CsI windows. Spectra were obtained between 4000–400 cm^{-1}, at a resolution of 1 cm^{-1}, and averaged over 32 scans.

5.4 RESULTS – Vapour Deposition

The charging of PTFE surfaces could mean it is possible to deposit a polymeric film on the surface simply by passing vapours of the monomer over the surface, from here on termed vapour deposition. The presence of radicals and residual charge on the surface, incorporated by the DBD plasma treatment, can act as an initiator for polymerization. The advantages of vapour deposition over traditional wet chemical methods is that the need for solvents and drying stages after deposition are vastly reduced, which has a cost advantage when looking at scale-up of the process.

After DBD charging, the surfaces were placed in small glass petri dishes (borosilicate glass, diameter 30 mm, and height 12mm, volume 8.5 cm^3, flat plate borosilicate glass lid) and a droplet of monomer placed next to the sample. These were then covered with a flat plate glass lid to prevent evaporation and left overnight.

Monomers were chosen that contained at least one unsaturated carbon-carbon bond, and contained hydrophilic elements such as oxygen, nitrogen and sulfur, Table 58. The presence of an unsaturated bond should facilitate deposition onto the charged surface. Additionally, it was postulated that the O, N, and S moieties would increase the overall hydrophilicity of the surface.

Table 58: Monomer abbreviations and structures for vapour deposition onto charged PTFE surfaces.

Monomer	Abbreviation / price per mL	Product details	Structure	Comments
2-Hydroxyethyl methacrylate	HEMA £0.06	97% purity, CAS no. 868-77-6, Lot no. S21959-484, Aldrich Chemical Co.	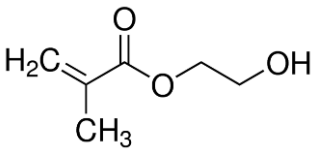	Vapour pressure 0.01 mmHg (25 °C).
Glycidyl methacrylate	GMA £0.24	97%, CAS no. 106-91-2, Lot no. MKBG6062V, Aldrich Chemical Co.	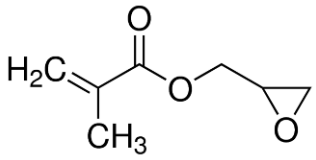	Vapour pressure 3.15 mmHg (25°C).

1-Allyl imidazole	1-AI £0.64	97% purity, CAS no. 31410-01-2, Barcode 335170250, Acros Organics; Fisher Scientific UK Ltd.	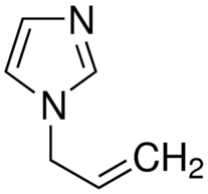	Vapour pressure not available.
Allyl mercaptan	AM £1.84	80.0% putiry, CAS no. 870-23-5, TCI Europe; Tokyo Chemical Industry Co. Ltd.	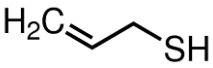	Vapour pressure not available.
Acrylic acid	AA £0.04	99% purity, CAS no. 79-10-7, Lot no. 71217022, Aldrich Chemical Co.	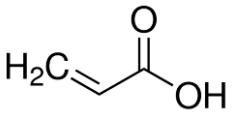	Vapour pressure 4.0 mmHg (20 °C).
4-Vinyl pyridine	4VP £0.30	95% purity, CAS no. 100-43-6, Lot no. 05916HC, Aldrich Chemical Co.	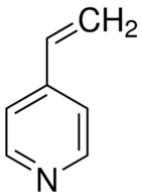	Vapour pressure data not available.
Tetramethylsilane ††	TMS £0.33	99.99% purity, CAS no. 75-76-3, Alfa Aesar; Thermo Fisher Scientific Ltd.	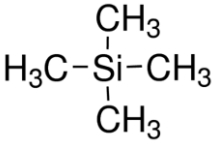	Very volatile. Vapour pressure 603.0 mmHg (20 °C).

†† This molecule does not have a double bond, but is very volatile.

5.4.1 Vapour Deposition of HEMA onto Static Air DBD Charged PTFE

Monomer deposition onto PTFE has been previously achieved by dipping into monomer solution,[346,351,354,355,357,358] spin coated,[352,353,]368 or graft copolymerised at 80 °C.[347] In this work, the monomer was deposited using vapour deposition, whereby a droplet was placed next to the charged PTFE sample in a small glass petri dish (borosilicate glass, diameter 30 mm, height 12 mm, volume 8.5 cm^3, flat plate borosilicate glass lid). As one of the cheapest monomers, HEMA was used as a quick read on whether there was potential that this hypothesis of a DBD activation step as a precursor to vapour monomer deposition could work.

Table 59: WCA and surface potential achieved after static air DBD treatment of PTFE (14 kV, 3 kHz, 30 s) and subsequent HEMA vapour deposition (1 droplet, 3 days). No solvent washing for this data.

Plasma Treatment	**WCA prior to deposition / °**	**Surface potential prior to deposition / V**	**WCA after deposition / °**	**Surface potential after deposition / V**
Static air, 30 s	74 ± 9	-982 ± 1036	92 ± 14	-604 ± 634

This process has caused a change in the WCA (small and not statistically significant), however the deposition has caused an undesirable increase in the WCA. The changes in WCA and charge on the surface indicate that the deposition of the HEMA onto the surface has been successful. The increase in WCA and reduction in surface potential indicates that the DBD activation step is successful. HEMA is not a suitable monomer to promote a significant decrease in WCA though.

5.4.2 Vapour Deposition of Monomers onto Nitrogen and Ammonia Water DBD Charged PTFE

Samples that had been plasma-treated with nitrogen bubbling through ammonia water (14 kV, 3 kHz, 60 s), were placed next to a droplet of neat monomer, and sealed in a small glass petri dish. In a scaled up version of this method, the monomer vapour could easily be passed over the sample after plasma treatment in situ. However, using this small scale equipment, the opportunity for significant contamination of the equipment meant it was better to keep the monomer away from the flow cell and electrodes.

5.4.2.1 Surface Potential and Wettability

If there has been a deposition onto the surface, this will be evident by a significant change in the surface potential and WCA, Table 60. The stability of the coating was analysed for the coatings which showed the most significant changes in WCA and surface potential: AM and AA.

Table 60: WCA and surface potential achieved after vapour deposition of different monomers onto PTFE surfaces charged using nitrogen flowing through ammonia water DBD (14 kV, 3 kHz, 60 s, 20 $cm^3 min^{-1}$). Samples washed in propan-2-ol/cyclohexane (1:1 by volume solution, 2 min).

Monomer	Plasma Treatment	No. repeats	WCA prior to deposition / °	Charge prior to deposition / V	WCA after deposition Unwashed / °	Charge after deposition Unwashed / V	WCA after deposition Washed / °	Charge after deposition Washed / V
AM	None	4	129 ± 3	10 ± 65	124 ± 2	-15 ± 95	-	-
HEMA	Nitrogen flowing through ammonia water, 14 kV, 3kHz, 60 s	8	88 ± 15	-1155 ± 729	86 ± 14	21 ± 786	-	-
1-AI		12	88 ± 15	-1155 ± 729	103 ± 7	-72 ± 377	-	-
TMS		8	88 ± 15	-1155 ± 729	81 ± 22	-469 ± 1145	-	-
GMA		16	88 ± 15	-1155 ± 729	97 ± 15	204 ± 778	-	-
AM		8	88 ± 15	-1155 ± 729	82 ± 12	-637 ± 723	-	-
		4	88 ± 15	-1155 ± 729	-	+210 ± 921	105 ± 4	29 ± 12
AA		8	88 ± 15	-1155 ± 729	86 ± 14	121 ± 1029	-	-
		4	88 ± 15	-1155 ± 729	-	-317 ± 645	104 ± 5	35 ± 12
4VP		8	88 ± 15	-1155 ± 729	102 ± 9	132 ± 395	-	-

The lowest WCA were achieved when acrylic acid and allyl mercaptan were used as monomers, Table 60. However, there is no improvement in water contact angle compared to the control (nitrogen flowing through ammonia water DBD treatment, i.e. no monomer). TMS also results in a low WCA, but the variation in the WCA was significantly larger than for AM and AA.

The importance of the plasma step is demonstrated by attempting to cause vapour deposition on an untreated PTFE surface. Without the plasma step, there is no significant decrease in the WCA of the surface. As expected, there is no change in the surface potential of the surface without the plasma treatment.

There is no significant change between the WCA after vapour deposition in either the untreated or treated cases. There is no significant change in the charge of the surface of the untreated samples after vapour deposition. It should also be noted that the samples that had not been charged smelt far less than those which had been charged prior to deposition.

In terms of the stability of the deposited surface to solvent washing, the coating is affected by the wash process, and hydrophobic recovery is observed (to 104° from 86° for AA, and to 105° from 82° for AM). This could be due to the coating not being uniform or sufficiently thick, or it could simply be caused by the surface adhesion not being strong enough to withstand solvent washing processes.

5.4.2.2 ATR-FTIR

Due to the high cost and bad odour of the AM monomer, the AA monomer was deemed the most industrially friendly option for vapour deposition. Therefore further analysis was carried out on DBD-treated PTFE surfaces that had been exposed to AA vapour. FTIR was carried out as described in Section 5.3.4.

If the AA layer deposited on the PTFE surface is sufficiently thick, it should be visible on the FTIR. The OH and carbonyl stretches will be the most intense peaks that will be visible in the FTIR spectra. The carbonyl stretch for carboxylic acid will be expected to show between 1780–1710 cm^{-1}, Figure 62.[369] The other functional group that should be visible if a sufficient layer of AA has been deposited would be the carboxylic acid OH stretch which appears between 2500–3000 cm^{-1}.[369]

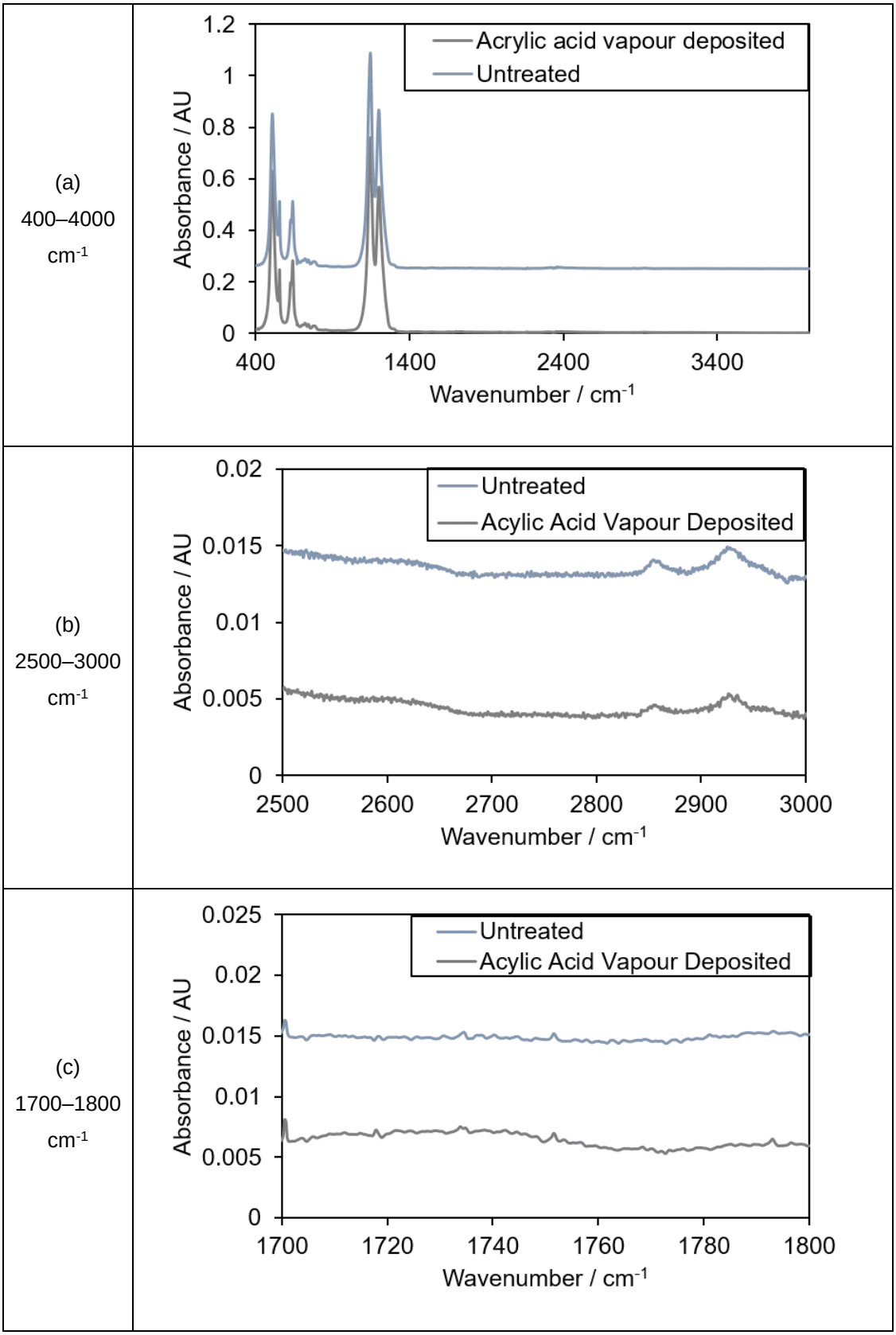

Figure 62: FTIR of untreated washed PTFE and DBD plasma-treated (nitrogen flowing through ammonia water, 20 cm^3 min^{-1}, 14 kV, 3 kHz, 300 s) PTFE after 24 h exposure to AA monomer vapour. (a) full spectra; 400–4000 cm^{-1}, (b) carboxylic acid OH stretch region; 2500–3000 cm^{-1}, (c) carbonyl stretch, 1700–1800 cm^{-1}.

From Figure 62, it can be seen that the layer of AA deposited on the surface was not sufficiently thick to provide a strong enough signal for distinct peaks to be observed on the FTIR spectrum. A more surface sensitive technique such as XPS is required to determine the manner by which the AA monomer is adhered to this surface, and in what quantity. The surface potential change, Table 60, indicates that either vapour deposition has occurred, or that the surface has discharged. Previously, the DBD-treated surfaces were seen to be stable for prolonged amounts of time, however without the accompanying FTIR stretches associated with deposition being observed, it cannot be confirmed that any physisorption has occurred.

5.4.2.3 Summary

Although there was a change in the WCA and/or surface potential after these treatments, there is not sufficient evidence to suggest that the monomers were adhered to the surface and subsequently polymerized. The lowest WCA was achieved using AA and AM, both of which retained a WCA in the region of 80–90°, but deposition was indicated by significant change in the surface potential of the surfaces. None of the surfaces produced were more hydrophilic than the control plasma-treated surface.

5.4.3 Vapour Deposition of Sulfobetaine

In work published by Y. Yuan *et al.*, sulfobetaine monomer was grafted onto ozone pretreated silicon surfaces in order to improve haemocompatability.[370] A graft yield of 12.7 $x10^{-5}$ g cm^{-2} (WCA of 31°) was achieved with a solution of DMMSA (*N*,*N*'-Dimethyl-*N*-methacryloyloxyethyl-*N*(3-sulfopropyl)ammonium) concentration of 10.0 wt% and Fe^{2+} ions (2.6–3.0 mol L^{-1}). Samples were placed in this solution for 24 h in a sealed-tube. After polymerization, samples were washed in saline solution at 50°C for 24 h with continuous stirring and washed with water until constant weight. The deposited layer reported by Y. Yuan *et al.*, is very thick, and would not allow for preservation of any surface structure of the PTFE substrate.

Vapour deposition of a sulfobetaine based molecule (Figure 61, [3-(methylacryloamino)propyl]dimethyl(3-sulfopropyl)ammonium hydroxide inner salt), was carried out on untreated and plasma activated PTFE surfaces. The basic structure of the sulfobetaine group of molecules is zwitterionic, with a positively charge amino group at one end and at the other end of the carbon backbone is the

negatively charge SO_3^- group. Unlike the previous work, this does not have a clear carbon-carbon bond from which to polymerize. Instead, it is postulated that in a similar manner to ALD, the sulfur acts as an anchor group to the surface, and the nitrogen group is the protruding pendant group. As the sulfobetaine is a solid chemical, a 1 wt.% aqueous solution was prepared to allow for vapour deposition.

The 24 h deposition time resulted in a significant increase in the WCA of the surface (from 67° after plasma treatment to 90° after deposition), Table 61. Although there was a slight change in the WCA observed after solvent washing (99°), the surfaces did not revert back to the untreated WCA of 129°. This suggests that some of the deposited coating remains on the surface after washing. There is a decrease in the hysteresis of the sulfobetaine deposited surface upon solvent washing, this suggests that the film deposited in non-uniform in nature, and the solvent washing combats this.

5.4.3.1 Surface Wettability

Table 61: Static and dynamic WCA measured after vapour deposition of aqueous sulfobetaine solution (1 wt%) for 24 h in glass petri dishes sealed with parafilm, and after washing in propan-2-ol/cyclohexane (2 min, 1:1 solution by volume). After removal form solution, samples were blown dry using dry nitrogen stream (10 s).

Plasma Treatment	**Sulfobetaine Deposition Duration**	**Static WCA prior to washing / °**	**Adv. WCA prior to washing / °**	**Rec. WCA prior to washing / °**	**CA hysteresis prior to washing / °**	**Static WCA after washing in propan-2-ol/cyclohexane / ° <120 s>**	**Adv. WCA after washing in propan-2-ol/cyclohexane / ° <120 s>**	**Rec. WCA after washing in propan-2-ol/cyclohexane / ° <120 s>**	**CA hysteresis after washing in propan-2-ol/cyclohexane / °**
None	None	-	-	-	-	129 ± 3	136 ± 1	116 ± 7	20 ± 7
Nitrogen bubbling ammonia water, 14 kV, 3kHz, 300 s	None	67 ± 14	97 ± 12	66 ± 8	31 ± 4	106 ± 1	110 ± 30	87 ± 33	30 ± 18
Nitrogen bubbling ammonia water, 14 kV, 3kHz, 300 s	24 h	90 ± 4	98 ± 3	72 ± 6	20 ± 4	99 ± 2	110 ± 2	92 ± 5	13 ± 3

5.4.3.2 ATR-FTIR

The deposition of a sulfobetaine layer onto the PTFE sample will increase the amount of C-H groups on the surface as the sulfobetaine molecule has a carbon backbone. The C-H stretch appears between 2850–2950 cm^{-1},[369] and although a change in this region is observed between the untreated and sulfobetaine deposited surface, it indicates there is more C-H on the untreated rather than treated sample, Figure 63. This indicates that there is no adhesion of a sulfobetaine layer on the surface that is observable by ATR-FTIR.

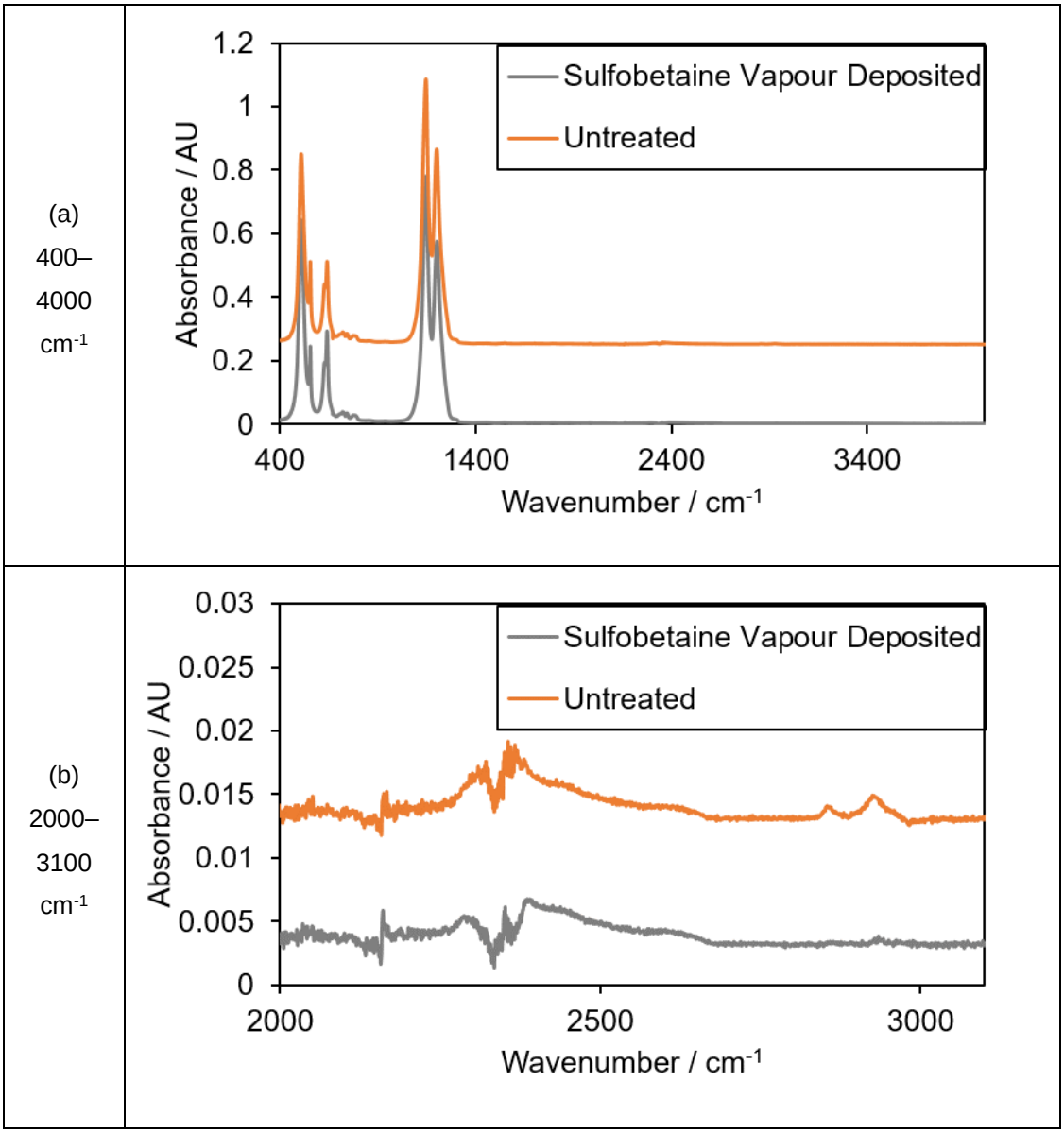

Figure 63: ATR-FTIR of untreated washed PTFE and DBD plasma-treated (nitrogen flowing through ammonia water, 20 cm^3 min^{-1}, 14 kV, 3 kHz, 300 s) PTFE after 24 h exposure to aqueous sulfobetaine solution (1 wt%) vapour. (a) Full spectrum; 400–4000 cm^{-1}, and (b) C-H stretch region; 2000–3100 cm^{-1}.[369]

5.4.3.3 Summary

There is a decrease in WCA observed when charged PTFE samples are exposed to sulfobetaine vapour. The presence of sulfobetaine molecules on the surface is not shown on ATR-FTIR of the surface, which indicates that if there has been some adhesion to the PTFE, the layer is too thin to show up on FTIR. The surface that is produced is not hydrophilic enough when compared to other data presented in this thesis. It is likely that owing to the low vapour pressure of the sulfobetaine solution, minimal reaction will occur with the surface. The change in WCA could be due to deposition of impurities.

5.5 RESULTS – Straight Dipping into Solution

Although some improvement was observed when depositing monomers via vapour deposition onto DBD treated surfaces, the surfaces were not as hydrophilic as desired, and so the traditional method of dipping the samples into solution was also investigated.

5.5.1 Acrylic Acid in Cyclohexane

As the most successful monomer in the vapour deposition stage, AA was investigated in a wet solution chemistry grafting step. There has been previous success (WCA of 56° achieved) with this reported in the literature after low-pressure argon treatment (1200 W, 120 s).[347]

The immersion of the untreated PTFE samples in the AA solution had very little effect on the WCA (reduction to static WCA of 111 ± 3°), Table 62. After solvent washing, the WCA was not significantly different to that observed for the untreated washed PTFE substrates. This indicates that without the plasma "activation" step, the AA does not adhere to the surface, and washes off.

Plasma-treated surfaces that were immersed in the AA solution had a lower WCA than without the dipping stage. However this was not statistically different when the standard deviation of the sample is considered. The large error overlap due to droplet jumping on the charged surfaces means that the values have to be much further apart for statistical significance.

5.5.1.1 Surface Wettability

Table 62: Static and dynamic WCA measured after immersing PTFE surfaces in acrylic acid solution (1% v/v in cyclohexane) for 24 h, and after washing in propan-2-ol/cyclohexane (2 min, 1:1 solution by volume). After removal form solution, samples were blown dry using dry nitrogen stream (10 s).

Plasma Treatment	**Acrylic Acid Deposition Duration**	**Static WCA prior to washing / °**	**Adv. WCA prior to washing / °**	**Rec. WCA prior to washing / °**	**Static WCA after washing in propan-2-ol/cyclohexane / ° <120 s>**	**Adv. WCA after washing in propan-2-ol/cyclohexane / ° <120 s>**	**Rec. WCA after washing in propan-2-ol/cyclohexane / ° <120 s>**
None	None	-	-	-	129 ± 3	136 ± 1	116 ± 7
None	24 h	111 ± 3	118 ± 4	108 ± 2	121 ± 7	127 ± 7	119 ± 7
Nitrogen bubbling ammonia water, 14 kV, 3kHz, 300 s	None	67 ± 14	97 ± 12	66 ± 8	106 ± 1	110 ± 30	87 ± 33
Nitrogen bubbling ammonia water, 14 kV, 3kHz, 300 s	24 h	57 ± 8	65 ± 7	50 ± 6	97 ± 11	107 ± 12	83 ± 13

5.5.2 Aqueous Sulfobetaine Solution

5.5.2.1 Surface Wettability

Samples (charged and uncharged) were placed into the 1 wt% aqueous sulfobetaine solution (1 h or 24 h) and subsequently dried in a petri dish (24 h). The surface potential and WCA were measured both before washing and after solvent washing and air drying (1:1 v/v solution of propan-2-ol and cyclohexane), Table 63.

From these results, it can be seen that the plasma pre-treatment prevents all of the sulfobetaine solution from being washed from the surface, and you are left with a hydrophilic surface. There is no charge on the surface after washing suggesting that any charge sites are either disspropan-2-olted or been coated with a sulfobetaine layer.

Although as previously seen, the WCA is significantly affected by the solvent washing process, the surface that remains is still hydrophilic.

.

Table 63: Surface potential and WCA measured after dipping in aqueous sulfobetaine solution and after washing in propan-2-ol/cyclohexane (10 s or 2 min, 1:1 solution by volume) and deionised water (2 min).

Plasma Treatment	**Aqueous Sulfobetaine Solution Deposition Duration**	**WCA prior to washing / °**	**Charge prior to washing in propan-2-ol/cyclohexane / V**	**WCA after washing in propan-2-ol/cyclohexane / ° <Washing duration / s>**	**Charge after washing in propan-2-ol/cyclohexane / V <Washing duration / s>**	**WCA after washing in deionised water/ ° <Washing duration / s>**	**Charge after washing in deionised water / V <Washing duration / s>**
None	None	-	-	129 ± 3 <120>	10 ± 65 <120>	-	-
None	24 h	<10	39 ± 9	112 ± 7 <10>	44 ± 11 <10>	-	-
Nitrogen bubbling ammonia water, 14 kV, 3kHz, 60 s	None	88 ± 15	-1155 ± 729	96 ± 19 <10>	15 ± 21 <10>	-	-
Nitrogen bubbling ammonia water, 14 kV, 3kHz, 60 s	1 h	<10	60 ± 16	39 ± 9 <10>	6 ± 15 <10>	-	-
		<10	60 ± 16	-	-	67 ± 7 <120>	46 ± 73 <120>
Nitrogen bubbling ammonia water, 14 kV, 3kHz, 60 s	24 h	<10	36 ± 14	42 ± 17 <10>	15 ± 12 <10>	-	-

5.5.3 RESULTS – Nitrogen Bubbling Through Sulfobetaine Solution Plasma Treatment

After the success of dipping the samples into the sulfobetaine solution, but the lack of success when using the most industrially friendly vapour deposition method, an attempt was made to produce a hydrophilic surface using a one-step method. In this manner, sulfobetaine solution was placed in the mini-bubbler, and nitrogen passed through this prior to plasma ignition. A number of different plasma treatment durations were investigated.

Table 64: Surface potential and WCA measured after nitrogen was bubbled through sulfobetaine solution (14 kV, 3 kHz, 30–600 s), and after washing in propan-2-ol/cyclohexane (10 s, 1:1 solution by volume).

Plasma Treatment Duration / s	WCA prior to washing / °	Charge prior to washing / V	WCA after washing in propan-2-ol/cyclohexane / °	Charge after washing in propan-2-ol/cyclohexane / V
0	-	-	129 ± 3	10 ± 65
30	83 ± 15	-320 ± 1438	-	-
120	75 ± 15	-252 ± 1346	107 ± 8	39 ± 25
300	72 ± 22	-272 ± 1368	110 ± 2	11 ± 51
600	69 ± 21	533 ± 1114	-	-

Just as with the other plasma treatments, significant charge was imparted on the surface during the plasma treatment. There was also a significant decrease in the WCA observed after plasma treatment. This did not appear to be dependent on the plasma duration, as there is no significant difference between the short and long plasma treatment times owing to the charge causing large variation in the WCA measured.

The introduction of the sulfobetaine molecule into the bubbler has decreased the WCA more (69 ± 21°) in comparison to nitrogen bubbling through water (82 ± 13°, Chapter 4, Section 5.1.2), but due to the large errors caused by charging, it cannot be said that these are statistically different. Quoted here is the standard deviation of the sample. When the standard deviation of the mean is used instead, then the samples are statistically different. But with a sample size of 4 repeats and 3 measurements on each sample, the standard deviation of the mean is not accurate.

This method did not produced a stable hydrophilic surface regardless of the plasma treatment time, and the WCA values obtained after washing are the same as for just nitrogen bubbling through water DBD treatment. This is due to the low

vapour pressure of the sulfobetaine molecule, so any deposition was likely contamination or water.

5.6 CONCLUSIONS

In terms of creating a stable hydrophilic surface, the vapour deposition monomer grafting processes assessed in this chapter were not overly successful. Surfaces with an average WCA in the 82–86° region were created using vapour deposition of AM and AA monomers. However these surfaces were not stable to solvent washing. They were also not significant improvements on that which was reported in Chapter 4. Using sulfobetaine molecules instead for vapour deposition was also unsuccessful (average WCA of 99°), likely due to the low vapour pressure.

Since electric field assisted vapour deposition was unsuccessful, wet chemistry methods were employed, and charged samples were dipped into AA and sulfobetaine solutions. Dipping into AA and cyclohexane solution (1 vol.%) produced a hydrophilic surface (57°), but this was also not stable to solvent washing, exhibiting hydrophobic recovery to 97°.

The most hydrophilic surface was achieved by dipping into sulfobetaine solution, producing a WCA of <10° prior to washing. After washing in cyclohexane and propan-2-ol (1:1 v/v solution), a WCA of 39° was achieved indicating that although not completely stable to the wash process, the surface that remained was still hydrophilic. This was an improvement on the surfaces reported in Chapter 4, and on par with those achieved using the low-pressure two-step process reported in Chapter 3. In the literature, the lowest WCA reported for sulfobetaine dipped PTFE samples was 31°.[370] When the solvent washed samples were subsequently washed in deionised water, further hydrophobic recovery was observed (67°). This suggests that the longevity of the samples if employed as filters or medical implants in an aqueous environment would be compromised slightly. This is likely owing to the fact that the sulfobetaine molecule is so readily dissolvable in water.

Attempts to combine the sulfobetaine introduction and plasma treatment steps into a one-step process were unsuccessful. A sulfobetaine solution doped nitrogen plasma did not produce a surface that was as hydrophilic as the sulfobetaine dipped samples.

Chapter 6: Conclusions and Future Work

6 CONCLUSIONS AND FUTURE WORK

6.1 CONCLUSIONS

The aim of this work was to create a hydrophilic surface that was stable to solvent washing, using plasma process methods. The use of low-pressure sequential plasma treatments (oxygen 50 W, 600 s, followed by ammonia 5 W, 300 s, both at 0.2 mbar) was shown to be the most effective in creating a stable hydrophilic surface. Prior to solvent washing, this plasma treatment method consistently produced surfaces with a WCA of less than 10° (below the limit of the analysis method). After washing in propan-2-ol and cyclohexane solution (2 min, 1:1 v/v solution) and drying under a nitrogen stream, the glow plasma-treated samples exhibited hydrophobic recovery to 41 ± 3°, and the remote plasma-treated samples to 52 ± 3°. This was as good as, and better than, the best reported in the literature (adv. angle of 53° after methanol washing, but recovered to 70° after 10 h).[371] Using a number of characterization techniques, the mechanism by which this hydrophilic surface was achieved was determined. The oxygen plasma created a Cassie-Baxter surface through significant roughening of the substrate, but caused no significant defluorination or oxygen incorporation into the sample. The surface was subsequently converted to a Wenzel surface by the ammonia plasma treatment, which caused significant defluorination and incorporation of nitrogen into the surface, likely in amino type functional groups.

In terms of economics, a less expensive plasma processing method could be achieved by employing atmospheric-pressure plasma methods rather than the low-pressure gas plasma. Although the idea of electrowetting did result in the droplets jumping to the surface from the needle in the DSA characterization technique, the surface potential was not uniform, and so the droplets did not spread uniformly. Charge was consistently imparted on the surface by DBD plasma treatments, and was stable on the surface unless the substrates were solvent washed when all charge was removed. The SEM images suggest that there is limited roughness changes associated with the DBD treatment, but some LMWOS species are observed prior to solvent washing, although significantly less than were observed on the low-pressure plasma-treated surfaces. Further work using XPS could be used to determine the exact compositional surface changes that are associated with the DBD plasma treatments reported.

For inert feed gases, the surface produced had a positive potential. Often noble gases are used to ‘stabilize’ reactive gas plasmas, as their longer mean free path results in the electrons in a helium or argon having higher energy than their

reactive counterparts. As in a DBD plasma, the electron avalanche propagating towards the anode is responsible for the generation of a streamer, the energy of the electrons in the plasma will have a significant effect on the character of the plasma. In this way, the change in feed gas was observed to have a significant effect on the polarity of surface potential of the resultant PTFE substrates, even though a significant difference in the wettability of the surfaces was not observed.

When polar species were doped into the inert feed gases, the surfaces produced had a negative rather than a positive potential. This was due to the increase in abundance of electrons present in the plasma region. It was shown using high-speed camera capture that the plasma was ignited during more the negative and positive voltage regions of the pulse.

In terms of post-plasma modification, the most hydrophilic surface was achieved by dipping DBD plasma activated (nitrogen bubbling through ammonia water, 14 kV, 3 kHz, 300 s) PTFE surfaces into sulfobetaine solution, producing a WCA of <10° prior to washing. After washing in cyclohexane and propan-2-ol (1:1 v/v solution), a WCA of 39° was achieved indicating that although not completely stable to the wash process, the surface that remained was still hydrophilic, and on par with those achieved using the low-pressure two-step process reported in this thesis. In the literature, the lowest WCA reported for sulfobetaine dipped PTFE samples was 31°.[372]

Attempts to combine the sulfobetaine introduction and plasma treatment steps into a one-step process were unsuccessful. A sulfobetaine solution doped nitrogen plasma did not produce a surface that was as hydrophilic as the sulfobetaine dipped samples. Further work to optimize this method is required in order to reduce the duration and ease of the production of these stable sulfobetaine surfaces.

6.2 FUTURE WORK

6.2.1 Suitability for Medical Applications

The major potential use of the stable hydrophilic surfaces produced is for use in the body as replacement ligaments and heart stents. In order to assess the suitability of these surfaces for this application, it would be necessary to conduct a stability study in blood at constant body temperature. The heat stability of PTFE is known to be very good, but the incorporation of polar groups onto the surface may alter the surface thermal stability.

6.2.2 Multistep plasma processes

The low-pressure work presented in this thesis indicated that multi-step processes could achieve lower WCA than longer single-step counterparts. This was most effective where the surface roughness was increased by a harsh destructive plasma step prior to a gentler hydrophilizing plasma treatment. A similar approach could be used with the atmospheric plasma processes. The methods employed in this thesis are relatively gentle processes, causing very little roughening of the surface. Chiefly this is due to the pulsed nature of the plasma, which is necessary in order to allow self-extinguishing of the plasma streamers, but also means that the duration of the plasma would need to be significantly longer in order to achieve a similar effect to that of the low-pressure oxygen plasma.

A further improvement to the observed charge trapping in the surface could be achieved by combining the low-pressure roughening oxygen plasma with the charge imparting single-step DBD gas plasmas. The increase in degree of roughness on the surface should increase the amount of physical charge traps available for electrons, and thus increase the electrowetting effect observed for charge PTFE substrates.

6.2.3 Electrostatic Air Filtration

Due to the nature of the charged surfaces produced by this DBD charging method, it is possible to use these surfaces as electrostatic filters for air filtration. The use of electrostatic charged surfaces to filter out particulates in air has been industrially implemented over the past few years as a method of decreasing the size of the particulates which can be captured by a filter. Charge attraction as part of the filter provides a workaround to the physical difficulty of making nanoscale porous materials for filtering nanoscale particulates.

K.M. Sim *et al.* published work on using a corona discharge to electrostatically activate the substrate for air filtration.[373] This work does not focus on the production of a filter, instead using a commercial filter and coating it with nanoparticles of *S. flavescens* roots for antimicrobial properties. However, the work does indicate that the creation of electrostatic filters is possible using corona discharge.[373]

P.C. Raynor *et al.* compared uncharged fiberglass filters with charged polypropylene filters in a hospital air filtration system.[374] Their data showed that the efficacy of the charged filter decreased for 7 weeks (of 13 weeks testing) before reaching a steady state, at which point it was assumed it has reached the mechanical efficiency of the media.[374] Charging of the filters meant that particles of opposite charge was attracted to the filter, and also neutral particles experienced image forces that accelerated them toward the filter.[375]

There is potential for these charged surfaces produced via different feed gases, and hence of different polarity (positive or negative) to be used as electrostatic filters. PTFE is an ideal substrate for air filtration applications due to its low cost, inertness, and physically robust properties.

6.2.4 Sequential DBD plasma and ALD treatment

Plasma treatment of the surface has been reported in the literature to be used as an ‘activation’ step for PTFE prior to subsequent deposition. Atomic layer deposition (ALD) has been around for the past 50 or so years in one form or another, and was previously known as atomic layer epitaxy (ALE). In the work reported in this thesis, the thickness of the film coating the PTFE was unknown, but the nature of the ALD process would allow for thin layers to be deposited consistently. ALD uses sequential self-limiting reactions to ‘grow’ a monolayer on the surface.[376,377] This monolayer is conformal, meaning it is the same thickness over the whole surface, and therefore the surface morphology is preserved. The conformal nature of the surface coating is due to the self-limiting nature of the chemical reactions.[378] This means that the surfaces produced in both the atmospheric-pressure treatments, but also the low-pressure processes (which significantly alter the surface topography), can be subsequently coated with an ALD process.

Advantages of ALD over other techniques chiefly revolve around the fact that there is precise control of the thickness of the deposited layer. The coating of the surface will always be conformal, and the number of ALD cycles performed will determine the thickness of the film. As the precursors for ALD are in the gaseous

phase, the size and shape of samples that can be coated are only limited by the size and shape of the reactor vessel, and no direct line of sight is required between surface and precursors. [376]

Due to the thermally fragile nature of polymer substrates, ALD methodologies have to be adapted from those used for silicon or glass substrates. Previous work coupling plasma treatment and ALD was performed by G. Lee *et al.*, reporting changes in the amount of pin-holing observed in an Al_2O_3 ALD coating after plasma pretreatment of HDPE surfaces. Analysis of the WCA after plasma treatment (no feed gas given, no power given, 10–60 s, no pressure given) showed that a WCA of 30° was achieved after plasma treatment of 60 s in comparison to a WCA of 93.5° prior to plasma treatment.[379]

Q. Xu *et al.* have reported significant effects on the hydrophilicity of polypropylene (PP) surfaces upon coupling plasma treatments with ALD cyclic treatments.[380] An air plasma (50 W, 20 s, 10 mbar) was coupled with 200 cycles of TiO_2 ALD under nitrogen (20 sscm). Using this sequential method, WCA of PP was reduced from 113° to 33°. Without the plasma activation stage, the WCA was barely reduced after 200 cycles, and after 800 cycles, the lowest WCA achieved was approximately 90°.

The same group also reported the effect of ALD on PTFE surfaces for enhanced hydrophilicity and separation properties.[381] Porous PTFE membranes (round chips, 25 mm diameter, 65 µm thickness, and mean poresize 0.2 µm) were treated with $Al(CH_3)_3$ (TMA) in an ALD cycle under nitrogen. After 100 ALD cycles, the WCA decreased from 131° to 126°, and after 200 cycles it reduced further to 62°. When the membrane had undergone 500 ALD cycles, the water droplet easily penetrated the membrane and disappeared within 10 s.

A.K. Roy *et al.* performed plasma-enhanced Al_2O_3 ALD (PE-ALD) on PTFE in order to increase ‘glueability’. This was achieved by alternating surface exposure to oxygen plasma and to TMA vapour. The untreated PTFE samples had a WCA of 103°, and after treatment with oxygen plasma, this increased to 111°. Using traditional thermal ALD, a WCA of 40° was reported after 800 cycles. In contrast, after PE-ALD, a WCA of 19° was achieved after 200 cycles.[382] It was postulated that the use of plasma in the ALD process caused defluorination on the surface, thus allowing strong covalent bonds to form with the metal oxide rather than the physical adsorption seen after thermal ALD.[382]

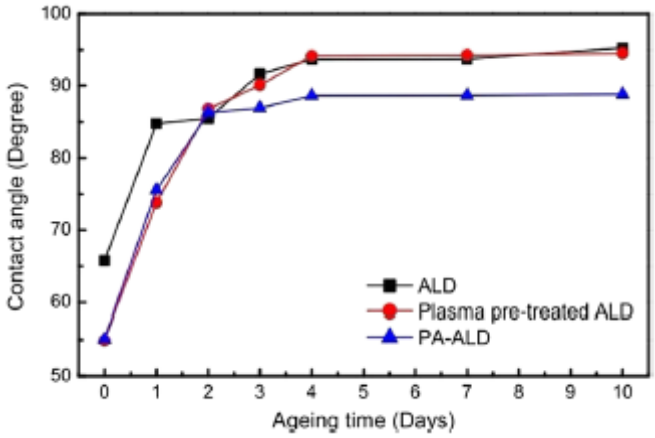

Figure 64: Effect of ageing time on plasma-treated ALD and ALD treated PET surfaces.[383]

One of the main obstacles to achieving hydrophilization of PTFE surfaces is the hydrophobic recovery associated with plasma-treated surfaces. There is conflicting evidence as to whether ALD deposition on polymer surfaces exhibits hydrophobic recovery in the same manner as that seen for plasma-treated surfaces. R. Edy *et al.* studied the effect of plasma treatment on PET surfaces and found hydrophobic recovery was still an issue, Figure 64.[383]

Conversely, work by A.K. Roy *et al.* suggested that PTFE surfaces which underwent either thermal, or oxygen plasma enhanced, Al_2O_3 ALD deposition, became hydrophilic (PE-ALD achieved WCA of 19°, thermal ALD achieved WCA of 40°). These surfaces were stable upon storage in ambient air for 6 months.[382]

Work by G.C. Correa *et al.* into the behaviour and properties of Al_2O_3 coated Si (100) samples after storage in various different environments indicated that alumina surfaces are not stable in pure water, acidic or basic environments for prolonged periods of time.[384] It was found that after storage in water the surface was considerably roughened (AFM, Figure 65, and SEM, Figure 66). They suggested that the platelet and hourglass shapes shown in the SEM were due to gibbsite and bayerite respectively.[384] These are both monoclinic forms of $Al(OH)_3$. The differences seen between the as deposited and thermally annealed surfaces was attributed to the thermal annealing causing a ‘densification’ of the amorphous alumina film, Crystallization does not occur until 800–900 °C, so it cannot be crystallization hence the term densification.[384] The TiO_2 samples prepared in the same way were more stable in neutral and acidic solutions, but much less stable in 1M KOH solution.[384]

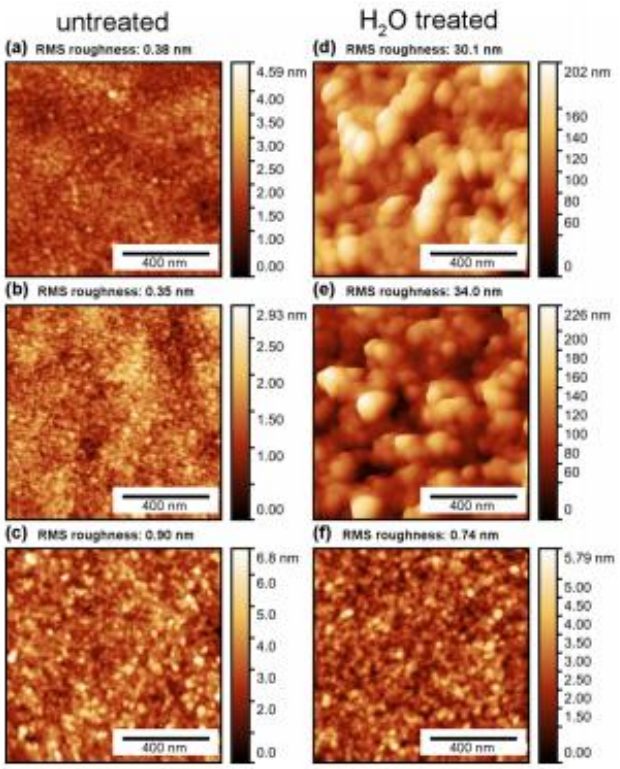

Figure 65: AFM images of untreated and H_2O stored Al_2O_3 coated Si (100) samples: (a) as synthesized; (b) 450 °C annealed; and (c) 900 °C annealed. (d-f) AFM images of the same samples as (a-c) after storage in 18 MΩ water for 47 days. Al_2O_3 deposited on Si (100) surface using ALD from TMA and H_2O at 150 °C.[384]

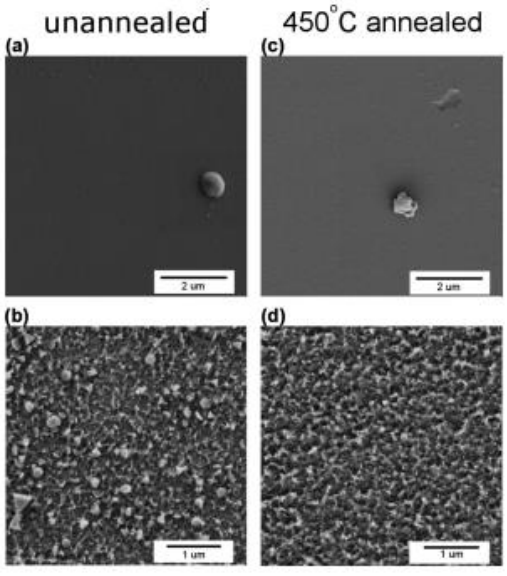

Figure 66: SEM images of unannealed (as deposited) and 450 °C annealed alumina surfaces: (a) as deposited; (b) as deposited after 63 days in water; (c) 450 °C annealed; and (d) 450 °C annealed after 63 days in water. Al_2O_3 deposited on Si (100) surface using ALD from TMA and H_2O at 150 °C.[384]

There is potential to use the charged DBD or low-pressure plasma-treated surfaces produced in the previous work in order to produce stable ALD surfaces which have improved hydrophilicity versus the plasma-treated surfaces. These surfaces would have improved hydrophobic recovery resistance than the gas plasma-treated surfaces owing to the formation of a film coating over the surface. This would prevent surface reconstruction as the polar groups are bound to the linker group of the ALD film. There would also be complete surface preservation as the method produces conformal monolayers, so the thickness of the coating is uniform.

7 SUPPORTING INFORMATION

7.1 Literature Review Tables

7.1.1 Inert Gases

7.1.1.1 Argon

PTFE type	Flow Rate / sscm	Time / s	Power / W	Pressure / bar	Untreated F/C	Treated F/C	Untreated Static WCA (°)	Treated Static WCA (°)	Untreated RMS (nm)	Treated RMS (nm)	Reference
PTFE 21µm, density 0.21 g/cm^3	Not given	60	100	20 x10^{-5}	2.97	2.802					385
PTFE fiber	Not given	1200	70	5 x10^{-5}	2.59	1.76					386
Ketersa PTFE	Not given	Not given	Not given	1.00	3.15	2.91	105				385
PTFE	Not given	1200	50	2 x10^{-4}	Not given	0.69					387
PTFE	1.0	1200	50	2.7 x10^{-4}	2.00	0.69					388
Goodfellow	1.0	300	20	2.7 x10^{-4}	2.00	1.53					389
Goodfellow PTFE film 0.01 cm thick	Not given	40	28	5.3 x10^{-5}	2.00	2.00					390
Goodfellow PTFE film 0.01 cm thick	Not given	200	30	6.7 x10^{-4}	1.98	1.70					391
Goodfellow PTFE 0.01 cm	Not given	40	28	5.3 x10^{-5}	2.0	1.0					392

thick											
Montefluos 1 mm thick	8	30	100	2×10^{-5}	1.52	0.54					393
Goodfellow 1 mm thick	85	60	Not given	$8.5–9 \times 10^{-5}$	1.98	0.57			14	28	158
Goodfellow foil 25 µm thick	5	0-600	Not given	1×10^{-6}	1.99	1.17					386
Goodfellow 1 mm thick	500	600	40		2.03	1.98			19.4	14.6	394
Goodfellow 1 mm thick	500	600	80						19.4	10.7	394
Goodfellow 1 mm thick	3000	20	2.31	1.013	1.8	1.4			25	60	145
Goodfellow 1 mm thick	20	20	120	1×10^{-3}	2.0	0.9					395
PTFE 20 µm	30	30	100	28×10^{-5}	3.27	2.47					396
PTFE 10mm thick	Not given	120	18.7	1.33×10^{-3}	1.94	1.99		120			196
Goodfellow PTFE 50µm foil	300	500	8.3	Not given			120	30			397
Norton PTFE	Not given	3600	30	2.7×10^{-5}	1.98		105	30*			398
PTFE	Not given	180	10	1×10^{-4}			105-110	30-45			399
Goodfellow	300	240	10	1×10^{-4}			108.7	45.6	18.8	23.3	186
PTFE 0.15 mm thick	Not given	20	Power density – 30.83 W/cm^3	Not given			105	50			396
PTFE 0.15 mm thick	Not given	30	Power density – 24.12 W/cm^3	Not given			105	50			396

PTFE 0.15 mm thick	Not given	30	Power density – 17.86 W/cm^3	Not given			105	50			396
Nitto Denko 1µm thick	2	30	7	1.33 x10^{-4}			120	50			400
Norton PTFE	Not given	1800	30	2.7 x10^{-5}	1.98	1.44	105	50*			398
AO Plaspolymer 50µm	Not given	60	Not given	10-20 x10^{-5}	1.95	1.57	111	51			394
PTFE 0.1mm thick	Not given	40	Not given	Not given	2.05	1.05	120	53			145
PTFE 0.15 mm thick	Not given	40	Power density – 11.62 W/cm^3	Not given			105	53			396
Nitto Denko 1 µm thick	2	10	7	1.33 x10^{-4}			120	55			400
Nitto Denko 1 µm thick	2	60	7	1.33 x10^{-4}			120	57			400
Fuxing Fluorin films	20	100	100	25.6 x10^{-5}	1.97	Remote 1.44	108	58.0			401
PTFE 450 µm	Not given	600	Not given	1 x10^{-4}	1.8	1.3	76	60	8.5	22.8	196
PTFE 0.5 mm thick	Not given	1200	180	Not given			108	62			395
Goodfellow	300	240	5	1 x10^{-4}			108.7	65			186
Goodfellow foil 25 µm thick	300	240	8.3	1 x10^{-4}	1.99	0.72	117	65	17.2	24.9	397
Fuxing Fluorin films	20	100	100	Not given	1.97	Direct 1.35	108	65.2			401
PTFE 0.5 mm	Not	1200	50	Not			108	73			395

thick	given			given							
PTFE sheet	Not given	60	10	8 x10^{-4}			115	75			401
PTFE 0.5 mm thick	Not given	300	180	Not given			108	79			395
PTFE 0.5 mm thick	Not given	300	50	Not given			108	83			395
Goodfellow	300	10	10	1 x10^{-4}			108.7	83.7			186
DuPont 127 µm	4500	10	14	1.013			104	85	6.6	7.5	399
PTFE 21µm thick, 0.21 g/cm^3	Not given	1800	90	Not given	2.50	2.03	126	90			397
PTFE 0.5 mm thick	Not given	1200	100	Not given			108	90			395
Goodfellow 1 mm thick	3000	20	2.31	1.013	1.8	1.8	110	90	25	50	145
PTFE 0.5 mm thick	Not given	300	100	Not given			108	94			395

7.1.1.2 Neon

PTFE type	Flow Rate / sscm	Time / s	Power / W	Pressure / bar	Untreated F/C	Treated F/C	Reference
Goodfellow	1.0	300	20	2.7 x10^{-4}	2.00	1.79	389

7.1.1.3 Helium

PTFE type	Flow Rate / sscm	Time / s	Power / W	Pressure / bar	Untreated F/C	Treated F/C	Untreated RMS (nm)	Treated RMS (nm)	Untreated Static WCA (°)	Treated Static WCA (°)	Reference

Goodfellow	1	300	20	Not given	2.0	1.44					389
PTFE 21 µm, density 0.21 g cm^{-3}	Not given	60	50	$20x10^{-5}$	2.968	1.577					385
PTFE 21 µm, density 0.21 g cm^{-3}	Not given	60	70	$20x10^{-5}$	2.968	1.305					385
PTFE 50 µm thick	Not given	15	60	1.0					114	46	402
PTFE 21µm, density 0.21 g cm^{-3}	Not given	60	100	$20x10^{-5}$	2.968	1.198			136.8	95.5	385

7.1.2 Non Inert Gases

7.1.2.1 Nitrogen

PTFE type	Flow Rate / sscm	Time / s	Power / W	Pressure / bar	Untreated F/C	Treated F/C	Untreated Static WCA (°)	Treated Static WCA (°)	Untreated RMS (nm)	Treated RMS (nm)	Reference
Goodfellow 1mm	85	60	Not given	$8.5\text{-}9 x10^{-5}$	1.98	0.89			14 (2.3)	25 (5.1)	395
PTFE foil	Not given	60	200	$7.5 x10^{-4}$	2.1	1.7					403
PTFE foil	Not given	600	200	$7.5 x10^{-4}$	2.1	1.6					403
Goodfellow	5	1800	20	$6.6 x10^{-5}$	1.94	0.46	103	34			140
Goodfellow	5	1200	20	$6.6 x10^{-5}$	1.94	0.68	103	58			140
Goodfellow	5	600	20	$6.6 x10^{-5}$	1.94	0.73	103	75			140

7.1.2.2 Ammonia

PTFE type	Flow Rate / sscm	Time / s	Power / W	Pressure / bar	Untreated F/C	Treated F/C	Untreated RMS (nm)	Treated RMS (nm)	Untreated Static WCA (°)	Treated Static WCA (°)	Reference
Goodfellow 1 mm	85	60	Not given	8.5-9x10^{-5}	1.98	0.78	14.3 (2.3)	21 (2.8)			404
Gaflon 4 mm	100	120	350	Not given	2.50	0.74					405
Gaflon 0.5 mm	30	120	350	Not given	2.45	0.6	19	19	115	53	406
Gaflon 0.5 mm	30	120	500	Not given	2.45	0.63			115	60	406
Gaflon 0.5 mm	30	120	200	Not given	2.45	0.7			115	61	406
Gaflon 0.5 mm	30	120	800	Not given	2.45	0.48			115	63	406
Gaflon 0.5 mm	30	300	200	Not given	2.45	0.75			115	72	406
Gaflon 0.5 mm	30	60	200	Not given	2.45	1.05			115	79	406
Gaflon 0.5 mm	110	120	350	Not given	2.45	0.72			115	82	406
Gaflon 0.5 mm	200	120	350	Not given	2.45	1.67			115	92	406

7.1.2.3 Oxygen

PTFE type	Flow Rate (sscm)	Time (s)	Power (W)	P (bar)	Untreated F/C	Treated F/C	Untreated Static WCA (°)	Treated Static WCA (°)	Untreated RMS (nm)	Treated RMS (nm)	Reference
Goodfellow 1 mm	85	60	Not given	8.5-9x10^{-5}	1.98	1.92			14 (2.3)	31 (4.5)	158
Goodfellow	1	300	Not given		2.0	1.98					389
Goodfellow 1 mm	20	20	120	1 x10^{-3}	2.0	0.9					395
Norton PTFE	Not given	1800	30	2.7 x10^{-5}	1.98	1.86					398
PTFE foil	Not given	60	Not given	7.5 x10^{-4}	2.1	2.1					403
PTFE foil	Not given	600	Not given	7.5 x10^{-4}	2.1	2.0					403
Goodfellow	5	600	20	6.6 x10^{-5}	1.94	0.61	103	111			140
Goodfellow	5	300	20	6.6 x10^{-5}	1.94	0.81	103	132			140
Goodfellow	5	1200	20	6.6 x10^{-5}	1.94	0.60	103	145			140
Goodfellow, 0.25 mm thick	6	0.002 pulses for 1 hr	1000	Not given	1.83	1.67	120	160.3 initially, 148 after ageing for 30 days			407
Goodfellow	5	30	20	6.6 x10^{-5}	2.00	1.09	Adv 118.3 Rec 114.7	Adv 120.9 Rec 85.7		Decrease in RMS observed	140
Goodfellow	5	300	20	6.6 x10^{-5}	2.00	1.21	Adv 118.3 Rec 114.7	Adv 121.8 Rec 104.7		Decrease in RMS observed	140

Goodfellow	5	900	20	6.6 x10^{-5}	2.00	1.19	Adv 118.3 Rec 114.7	Adv 143.3 Rec 131.7		Decrease in RMS observed	140
Goodfellow	5	120	70	6.6 x10^{-5}	2.00	1.36	Adv 118.3 Rec 114.7	Too hydrophobic to measure		Strong increase in RMS observed	140

7.1.2.4 Hydrogen

PTFE type	Flow Rate / sscm	Time / s	Power / W	Pressure / bar	Untreated F/C	Treated F/C	Untreated RMS / nm	Treated RMS / nm	Static WCA Untreated / °	Static WCA Treated / °	Reference
Goodfellow	1	600			2.0	0.67					389
Nitto Denko 1 µm	10	120	75	13.4 x10^{-5}	1.92	0.41 direct plasma					408
Nitto Denko 1 µm	10	120	75	13.4 x10^{-5}	1.92	0.60 remote plasma					408
PTFE 50 µm	10	120	100		1.90	0.41 remote					409
PTFE 50 µm	10	30	100		1.90	0.60 direct					409
Gaflon 4 mm	30	120	500		2.50	0.78					400
Nitto Denko 1 µm	10	120	75	13.3 x10^{-5}	1.9	0.6					410
Goodfellow 0.1 mm	20	20	120	1 x10^{-3}	2.0	0.3					395
Nitto Denko 80	Not	60	50	1.3 x10^{-4}			29.9	43.7			411

µm	given										
Dyenon powder	Not given	36000	270	8×10^{-4}	1.86	1.13					412
Dyenon powder	Not given	9000	270	8×10^{-4}	1.86	1.48					412
Nitto Denko 1 µm	10	10	100	13.3×10^{-5}					118	62	410
Nitto Denko 1 µm	10	40	100	13.3×10^{-5}					118	67	410
Nitto Denko 1 µm	10	90	100	13.3×10^{-5}					118	67	410
Nitto Denko 1 µm	10	120	100	13.3×10^{-5}					118	67	410
Nunchirtz GmbH	25	30	200	12×10^{-5}	1.9	0.75			110	69	413
Gaflon 0.5 mm	50	60	350	Not given	2.45	0.90			115	83	387
Gaflon 0.5 mm	50	120	350	Not given	2.45	0.76			115	85	387
Gaflon 0.5 mm	100	60	350	Not given	2.45	0.86			115	85	387
Gaflon 0.5 mm	30	60	800	Not given	2.45	0.98			115	86	387
Gaflon 0.5 mm	30	60	350	Not given	2.45	0.95			115	87	387
Gaflon 0.5 mm	30	60	500	Not given	2.45	0.85			115	88	387
Gaflon 0.5 mm	200	60	350	Not given	2.45	0.74			115	88	387
Gaflon 0.5 mm	100	120	350	Not	2.45	0.86	22.2	19.2	115	92	387

				given							
Gaflon 0.5 mm	200	120	350	Not given	2.45	0.86			115	92	387
Gaflon 0.5 mm	30	60	200	Not given	2.45	1.53			115	95	387
Nichias PTFE 50 mm thick	Not given	10	100	1.3×10^{-4}					118	Direct 62	414
Nichias PTFE 50 mm thick	Not given	60	100	1.3×10^{-4}					118	Direct 64	414
Nichias PTFE 50 mm thick	Not given	120	100	1.3×10^{-4}	1.8	1.1			118	Remote 77	414

7.1.2.5 CF_4

PTFE type	Flow Rate / sscm	Time / s	Power / W	Pressure / bar	Untreated F/C	Treated F/C	Reference
Goodfellow	1	300	Not given	Not given	2	2.05	389

7.1.3 Gas Mixtures

In addition to pure gases, mixtures of gases may also be used a feed sources.

7.1.3.1 Air

PTFE type	Time / s	Power / W	Pressure / bar	Untreated F/C	Treated F/C	Untreated Static WCA / °	Treated Static WCA / °	Roughness / nm	Roughness / nm	Reference
PTFE 21µm, density 0.21 g cm^{-3}	60	100	20×10^{-5}	2.968	2.802					385

PTFE fiber	1200	70	$5x10^{-5}$	2.59	1.76					415
Ketersa PTFE	Not given	Not given	1.00	3.15	2.91	105				416
Dupont 10 mm thick	120	18.7	$1.33\ x10^{-3}$	1.94	1.99	Not given	120			417
PTFE	30	400	1.013			107	<90	47.3	41.0	191
PTFE	180	10	$1\ x10^{-4}$			105-110	30-45			418
PTFE 0.15 mm thick	20	Power density – 30.83 W/cm^3	Not given			105	50			419
PTFE 0.15 mm thick	30	Power density – 24.12 W/cm^3	Not given			105	50			419
PTFE 0.15 mm thick	30	Power density – 17.86 W/cm^3	Not given			105	50			419
AO Plaspolymer 50 µm	60	Not given	$10–20\ x10^{-5}$	1.95	1.57	111	51			420
PTFE 0.1 mm thick	40	Not given	Not given	2.05	1.05	120	53			421
PTFE 0.15 mm thick	40	Power density – 11.62 W/cm^3	Not given			105	53			419
PTFE 0.5 mm thick	1200	180	Not given			108	62			422
PTFE 0.5 mm thick	1200	50	Not given			108	73			422
PTFE sheet	60	10	$8\ x10^{-4}$			115	75			423
PTFE 0.5 mm thick	300	180	Not given			108	79			422
PTFE 0.5 mm thick	300	50	Not given			108	83			422
PTFE 21µm thick, 0.21 g cm^{-3}	1800	90	Not given	2.50	2.03	126	90			424
PTFE 0.5 mm thick	1200	100	Not given			108	90			422
PTFE 0.5 mm thick	300	100	Not given			108	94			422

7.1.3.2 Water and Argon

NB: Exact composition unknown, water introduced into Ar plasma using a water bubbler held at 20 °C.

PTFE type	Flow Rate / sccm	Time / s	Power / W	Pressure / bar	Untreated F/C	Treated F/C	Untreated Static WCA / °	Treated Static WCA / °	Reference
PTFE 2mm, density 0.22 g cm^{-3}	5-10	120s	400	27-50 $x10^{-5}$	1.68	1.76	110	23.6	425

7.1.3.3 Argon and Carbon Dioxide

NB: Exact composition 3.3% CO_2, 96.7% Ar.

PTFE type	Flow Rate / sccm	Time / s	Power / W	Pressure / bar	Untreated F/C	Treated F/C	Untreated RMS (nm)	Treated RMS	Untreated Static WCA (°)	Treated Static WCA (°)	Reference
Goodfellow 1 mm	3000	20	2.31	1.013	1.8	1.6	25	42	110	89	145
Goodfellow 1 mm	3000	60	2.31	1.013	1.8	1.3					145

7.1.3.4 Methane and Nitrogen

NB: Exact composition was a 1:1 ratio of CH_4:N_2.

PTFE type	Flow Rate / sccm	Time / s	Power / W	Pressure / bar	Untreated Static WCA (°)	Treated Static WCA (°)	Reference
Nitto Denko Ltd 80 µm	8	60	50	1.6 $x10^{-4}$	131	52	146
Nitto Denko Ltd 80 µm	8	60	40	1.6 $x10^{-4}$	131	57	146

Nitto Denko Ltd 80 µm	8	60	30	1.6×10^{-4}	131	63	**146**
Nitto Denko Ltd 80 µm	8	60	20	1.6×10^{-4}	131	67	146
Nitto Denko Ltd 80 µm	8	60	10	1.6×10^{-4}	131	89	146

7.1.3.5 Helium and Oxygen

NB: Exact composition unknown.

PTFE type	Flow Rate / sscm	Time / s	Power / W	Pressure / bar	Untreated RMS (nm)	Treated RMS	Reference
Goodfellow 1 mm	15000 (He) 150 (O_2)	1000	90	Not given	17	58	426

7.1.3.6 Nitrogen and Hydrogen

NB: Exact composition was a 3:1 ratio of H_2:N_2.

PTFE type	Flow Rate / sscm	Time / s	Power / W	Pressure / bar	Untreated RMS (nm)	Treated RMS	Reference
ePTFE Yu-Min-Tai 75 µm	50 (N_2) 150 (H_2)	60	100	8.7×10^{-5}	Not given	49	427
ePTFE Yu-Min-Tai 75 µm	50 (N_2) 150 (H_2)	240	100	8.7×10^{-5}	Not given	56	427
ePTFE Yu-Min-Tai 75 µm	50 (N_2) 150 (H_2)	600	100	8.7×10^{-5}	Not given	74	427
ePTFE Yu-Min-Tai	50 (N_2) 150	420	100	8.7×10^{-5}	Not given	82	427

75 µm	(H2)						

7.1.3.7 Methanol and Hydrogen

PTFE type	Flow Rate / sscm	Time / s	Power / W	Pressure / bar	Untreated Roughness / nm	Treated Roughness / nm	Reference
Goretex ePTFE	Not given	Not given	Not given	Not given	0.45	13.0	428

7.2 Simplex Optimization of Two-Step Plasma Treatment

Simplex optimization is a quick method whereby the conditions of two or more continuous variables that affect an experiment can be optimized at the same time. As a step-wise method, the experiments are performed one-by-one, with the exception of the starting simplex where all three experiments are run first.

In this case, the optimized combination of the powers of both the argon and ammonia plasmas will be determined. As there are two factors being investigated, the simplex method uses a triangle (k+1 vertices, where k is the number of factors).[429] The three points used for the original simplex are summarised in Table 65, and the responses achieved ranked. The combination that produced the highest WCA was ranked worst (W), the "next-worst" ranked as medium response (M), and the treatment resulting in the lowest WCA was ranked as best (B).

Table 65: Summary of the power combinations used for the first simplex triangle.

	Argon Power / W	**Ammonia Power / W**	**Response**
1	5	5	W
2	20	5	B
3	20	20	M

In order to obtain the next combination of powers to be investigated, the "worst" point was reflected through the line which joins the other two points of the triangle. This will yield a new triangle, Simplex 2, Figure 67. This process is continued until the reflection yields a triangle already investigated, Simplexes 1 and 2 in Figure 67. At this point the simplex triangles are oscillating around the optimum region. Further optimization may be possible by reflecting the "next-worst" point rather than the "worst" point, Simplexes 3 and 4 in Figure 67.

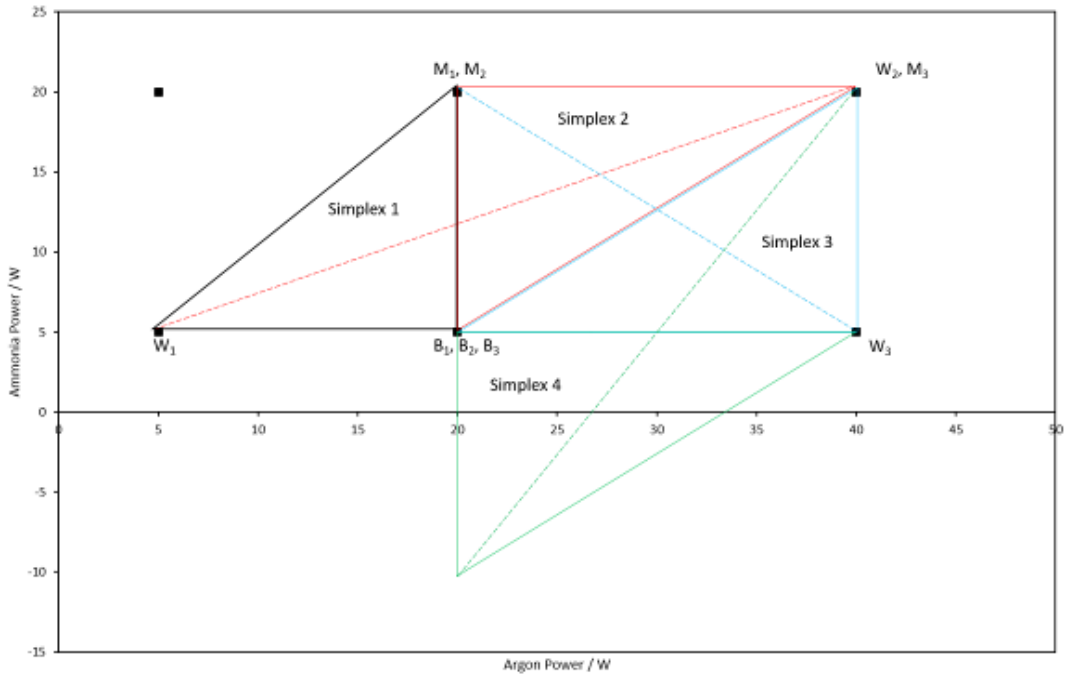

Figure 67: Simplex plasma power optimization map for fixed treatment time (120 s Ar plasma, then 120 s NH_3 plasma, 0.2 mbar), continued until no further reflections are possible. The 'worst' point in simplex triangle 1 is reflected to give simplex 2. Note that 40 W is used rather than 35 W, as the SWR meter will not accurately measure 35 W. A reflection of the 'worst' point of simplex 2 will yield an argon power of 0 W, so this is rejected. To continue with the optimization, the 'second worst' point of simplex 2 is reflected to yield simplex 3. Reflection of the 'worst' point of simplex 3 will yield simplex 2 again, and reflection of the 'second worst' point will yield the impossible simplex 4. Therefore no further optimization can be carried out using this triangle size.

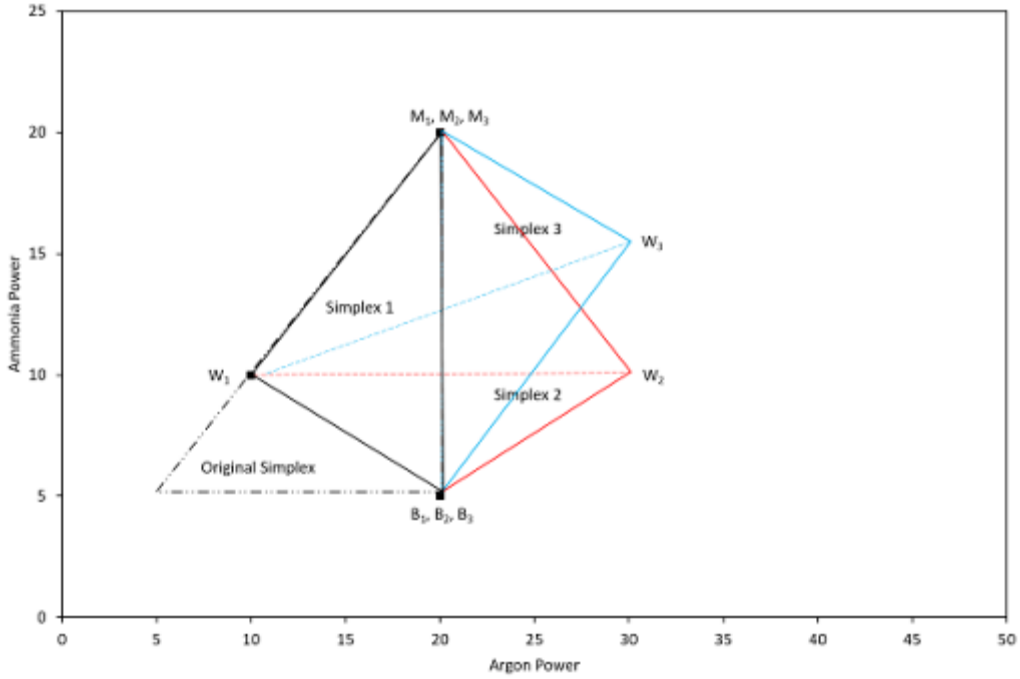

Figure 68: Simplex plasma power optimization map for fixed treatment time (120 s Ar plasma, then 120 s NH_3 plasma, 0.2 mbar) using a different simplex triangle size to improve the optimization further. The original simplex is shown by the dashed black triangle, this

includes the two best points taken from the previous simplex optimization, B1 and M1 from Figure 67. The black triangle shows the smaller simplex triangle used to improve the optimization (Simplex 1). The reflection of the worst point (W1) yields the red triangle (Simplex 2). As the triangle is not equilateral, the blue triangle is also drawn to yield a further vertex (Simplex 3).

The normal simplex methodology may be repeated but using a smaller original simplex triangle to further the optimization, Figure 68. Eventually no further optimizations using simplex triangles will be possible, and at this point the optimum combination of argon and ammonia powers has been found. A smaller simplex triangle was constructed using 10 W argon plasma and 10 W ammonia plasma treatment (Simplex 1 in Figure 68). The same simplex methodology is conducted to yield Simplex 2 and Simplex 3 which also oscillate about the optimum region.

7.3 SEM Supplementary Images

Table 66: SEM carried out using FEI Helios Nanolab Mk2 microscope using secondary electron mode, and running at 5 kV. Samples were coated with 20 nm of gold palladium prior to analysis. SEM carried out by Leon Bowen, Experimental Officer, Department of Physics, Durham University.

Plasma Treatment	SEM images	Comments
Untreated	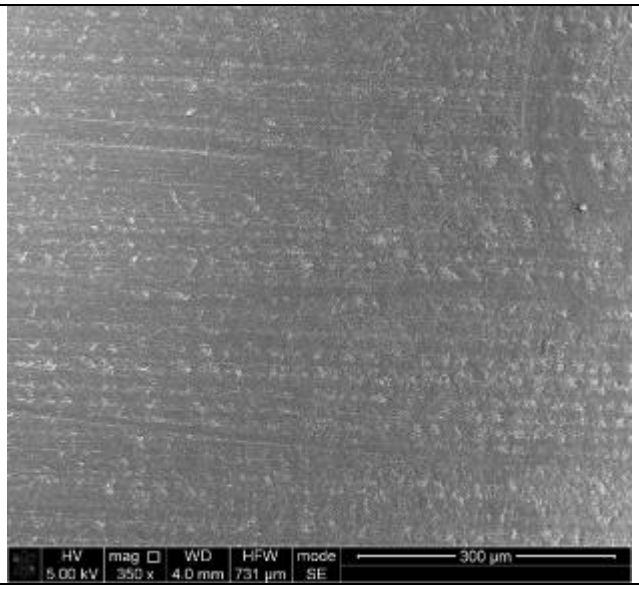	500 µm scale. Linear striations visible from the manufacturing process. Overall appears smooth and featureless.

	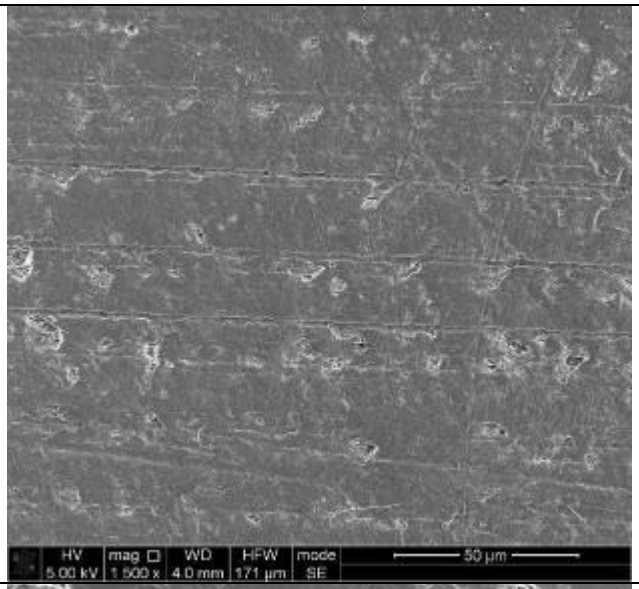	50 µm scale. Areas of the surface are distorted with indentations and imperfections. Surface is smooth.
	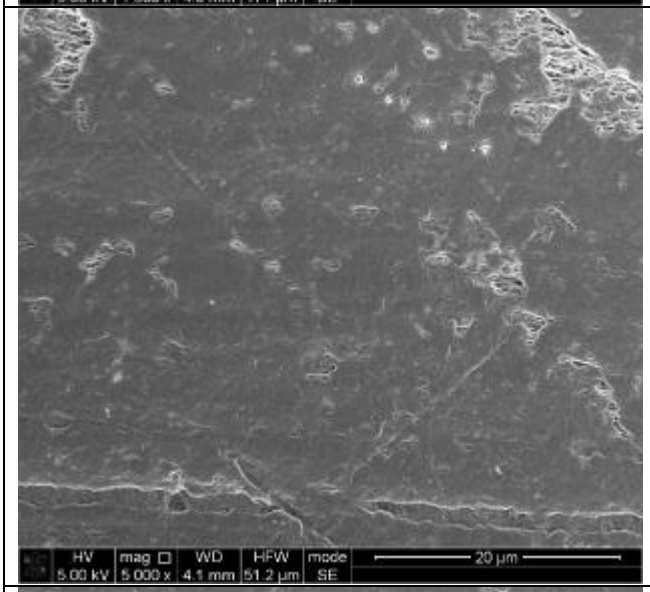	20 µm scale. Areas with imperfections visible in top left and top right corners. Overall surface appears to be smooth and featureless.
	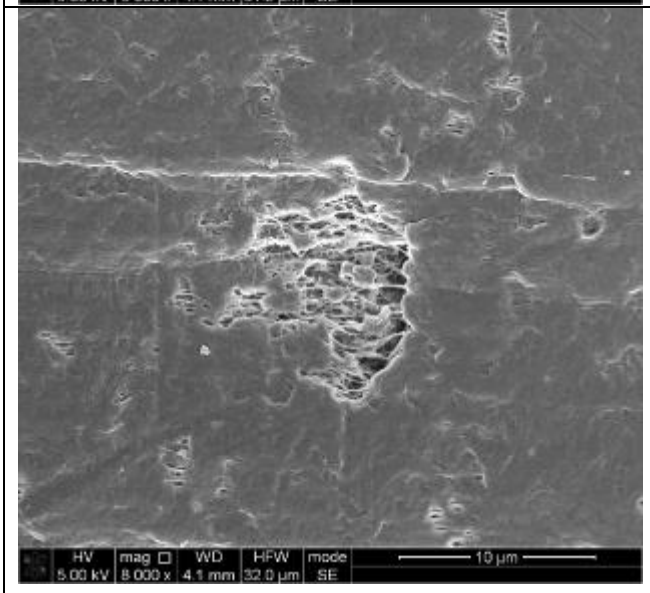	10 µm scale. Close up view of an imperfection on the surface, feature is approx. 5 µm square. Visible on SEM in Figure 18 as well. Area surrounding the “hole” is smooth and relatively featureless. Some features in the couple of micron range visible. However can see the

		polymer chains underneath for large portion of this image.
	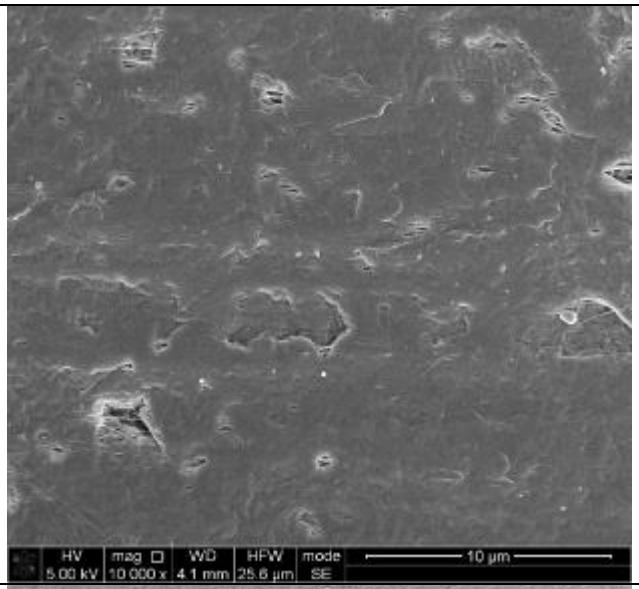	10 µm scale. Surface appears to have some indentations and features in the few micron range. No large features.
Oxygen, 50 W, 600 s	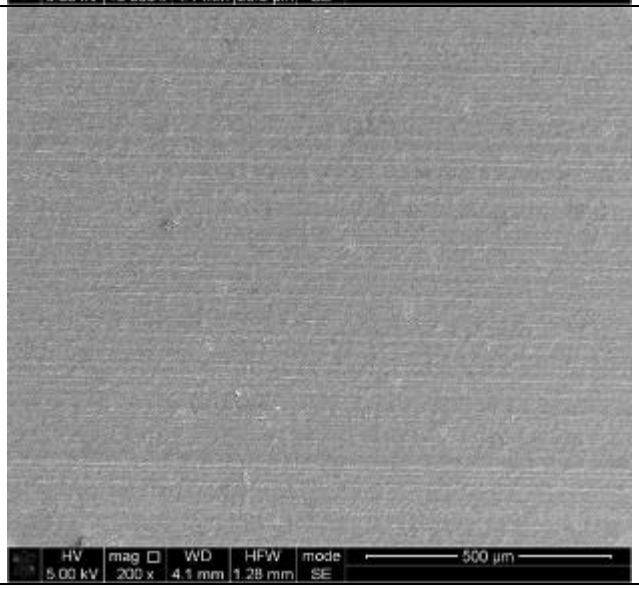	500 µm scale. Overall featureless. Linear striations visible from manufacturing process still. Appears to be some pits or dirt on the surface.

	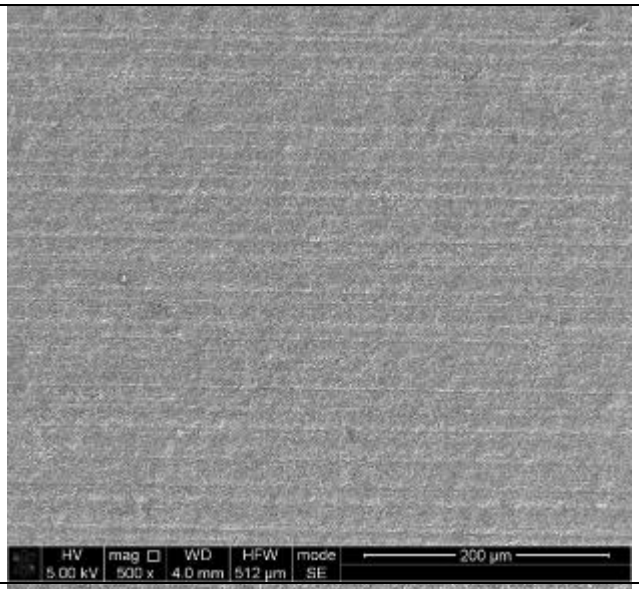	200 µm scale.
	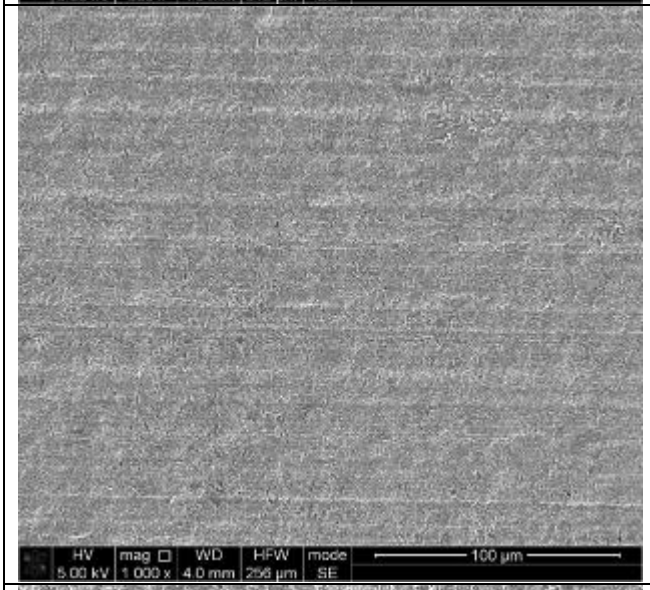	100 µm scale.
	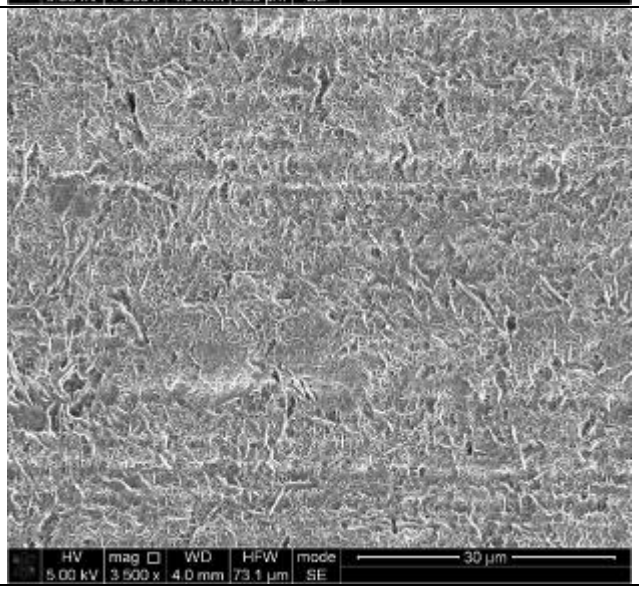	30 µm scale.

	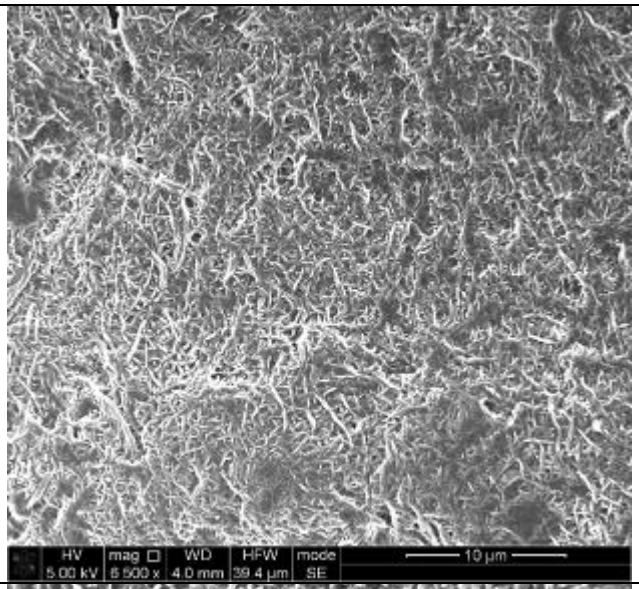	10 µm scale.
	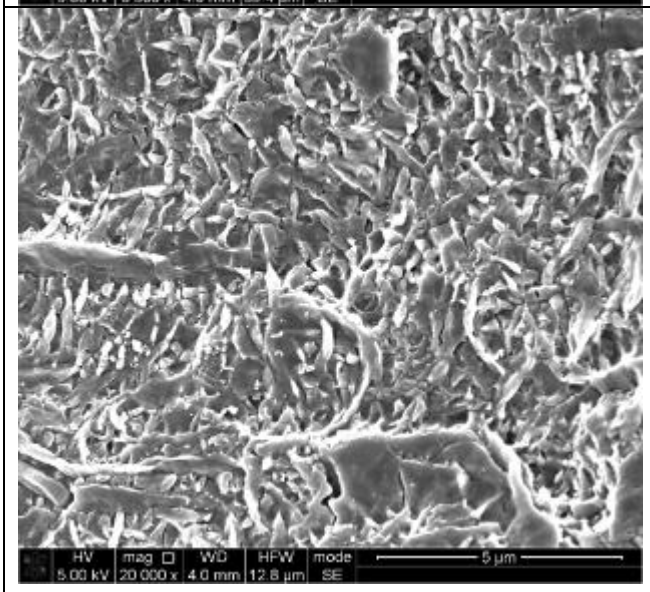	5 µm scale. Significant deformation of the surface observed. Etching of the surface is significant such that the polymer chains are exposed rather than the smooth surface. Small fragments of the original surface still visible, indicating the surface modification is not completely uniform – reflected in the error associated with the measured WCA. Droplets are 1 µL, which will occupy a much smaller area than that shown in the image. Therefore these regions where the unmodified surface is present will have an effect on the

		observed WCA.
Ammonia, 5 W, 300 s	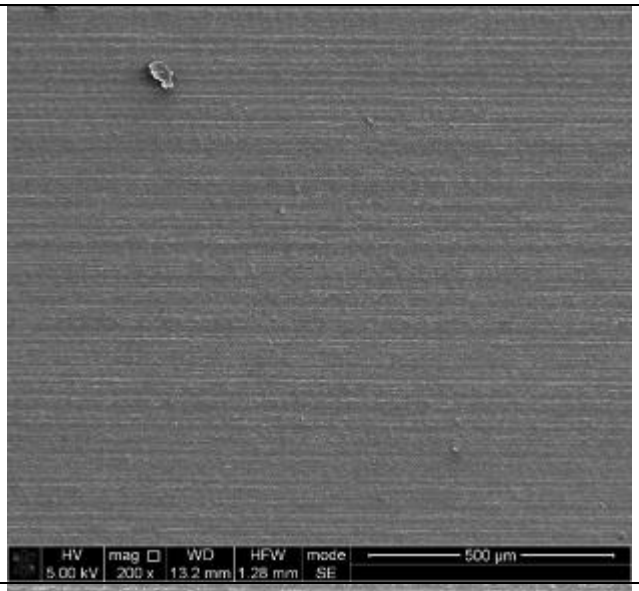	500 µm scale. Linear striations visible. Piece of dirt/debris on the surface in top right hand corner.
	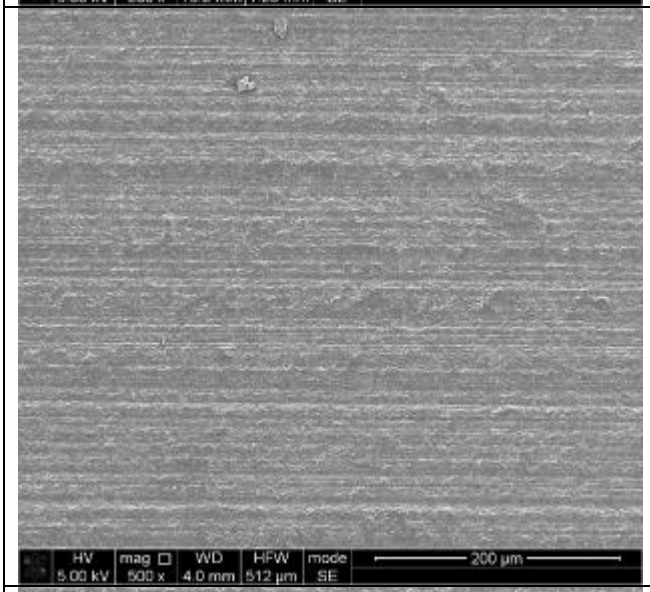	200 µm scale. Striations from the manufacturing process still visible on the surface. Some contamination present at the top of the image.
	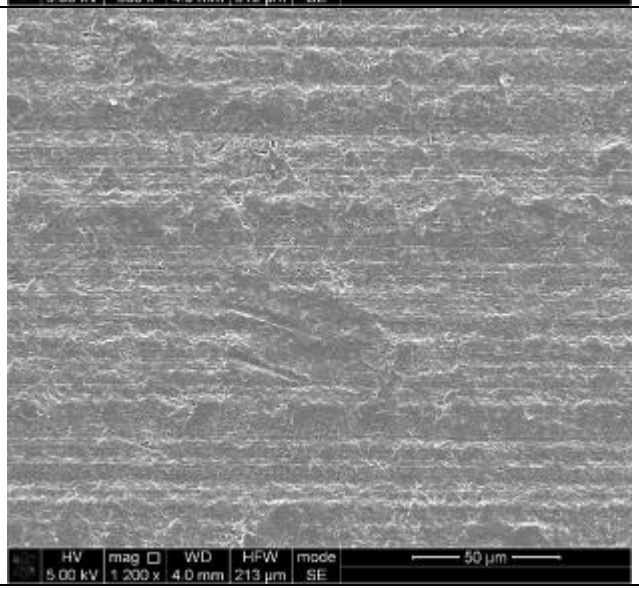	100 µm scale.

	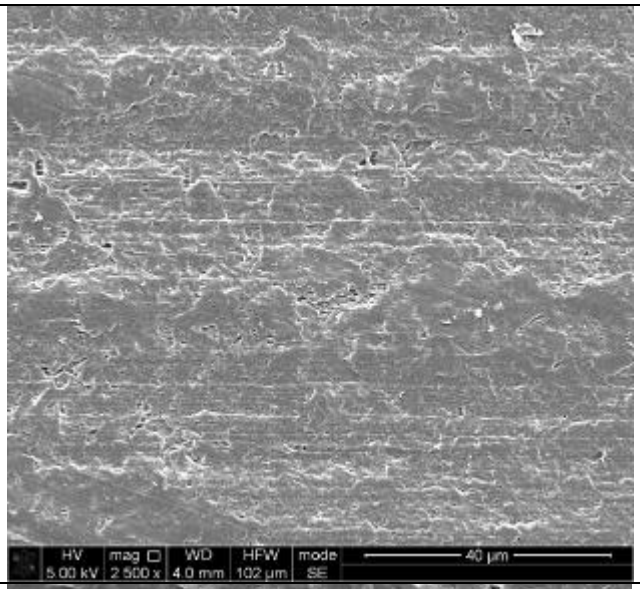	40 µm scale. Overall some damage to the surface by the plasma treatment is visible, but there are few obvious distinct features.
	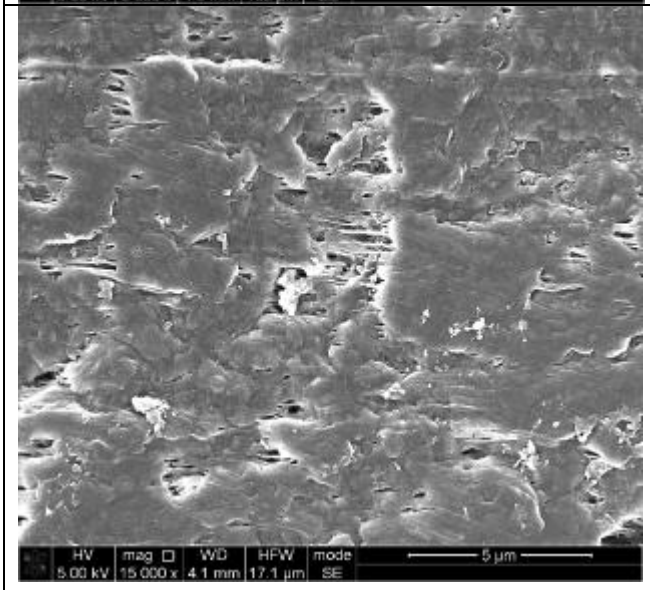	5 µm scale. Much less destruction of the surface observed after the ammonia plasma treatment than after the oxygen treatment. However still an increase in the amount of polymer chains visible through ‘holes’ in the surface compared to the untreated substrate.
Two-step: oxygen 50 W, 600 s, followed by ammonia 5 W, 300 s (unwashed)	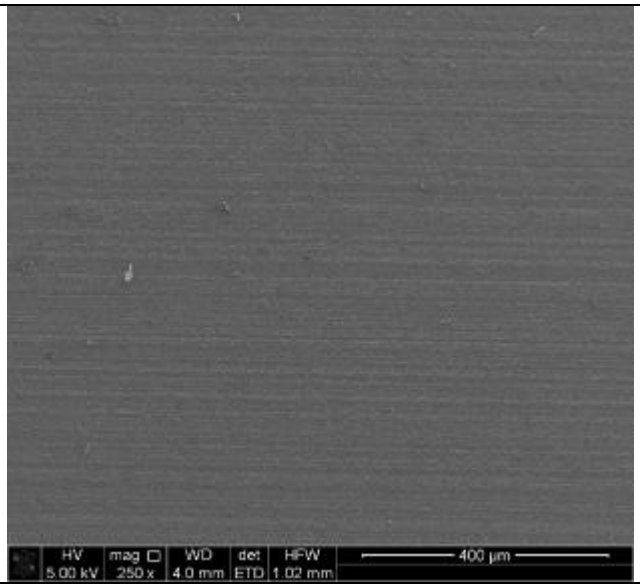	

	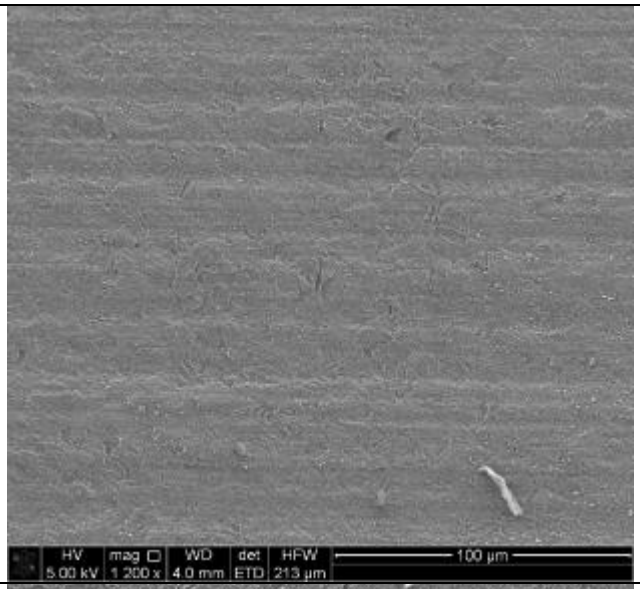 HV 5.00 kV mag 1 200 x WD 4.0 mm det ETD HFW 213 µm 100 µm	
	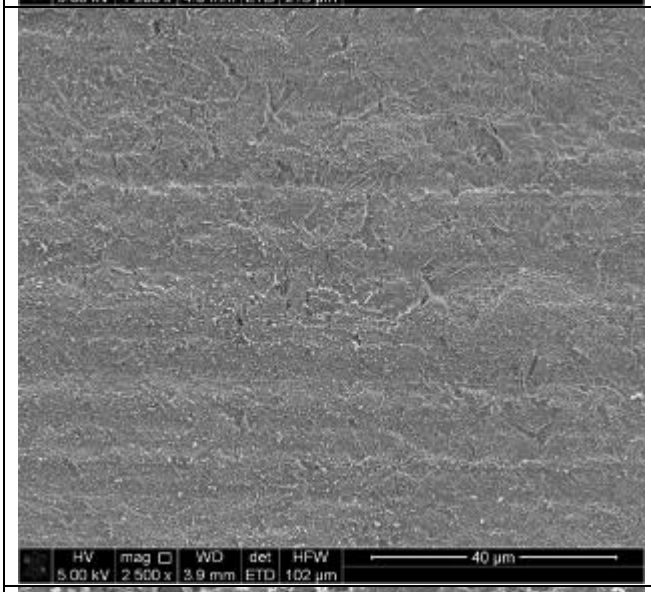 HV 5.00 kV mag 2 500 x WD 3.9 mm det ETD HFW 102 µm 40 µm	
	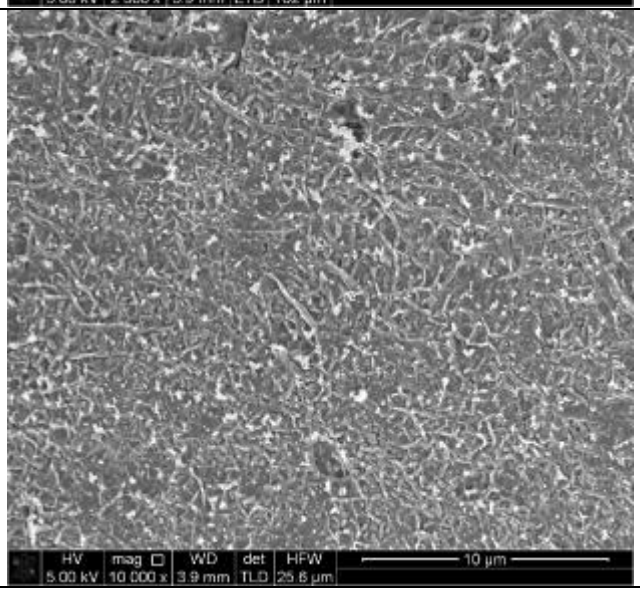 HV 5.00 kV mag 10 000 x WD 3.9 mm det TLD HFW 25.6 µm 10 µm	

Two-step: oxygen 50 W, 600 s, followed by ammonia 5 W, 300 s (solvent washed)	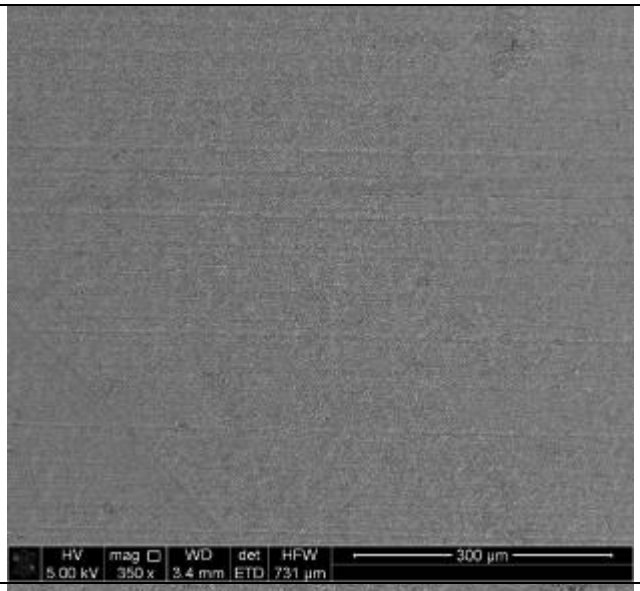	
	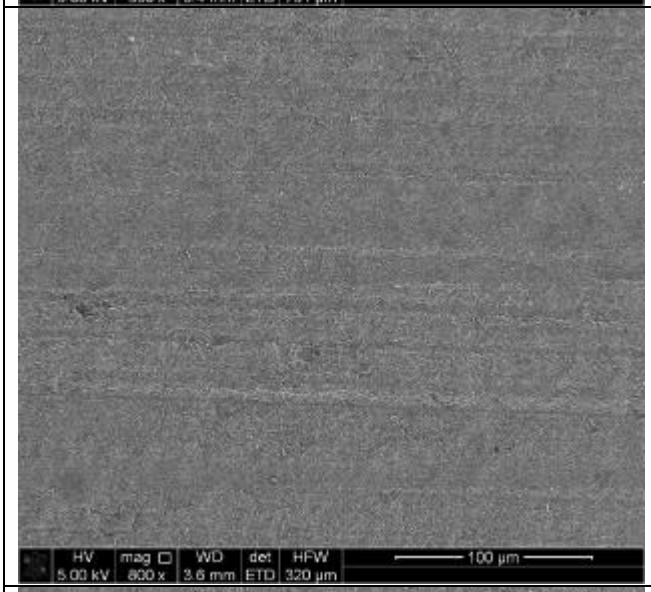	
	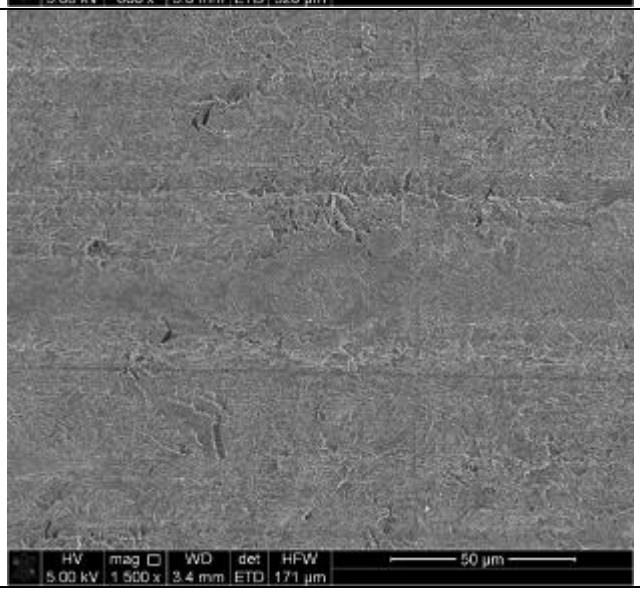	

	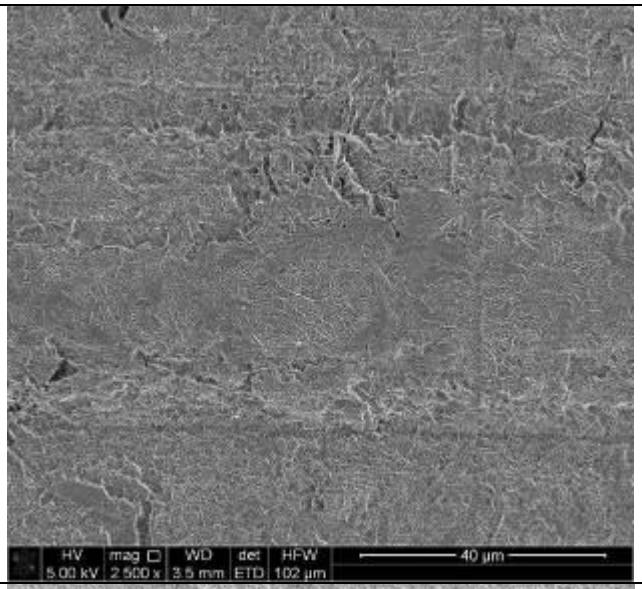 HV 5.00 kV mag 2 500 x WD 3.5 mm det ETD HFW 102 µm 40 µm	
	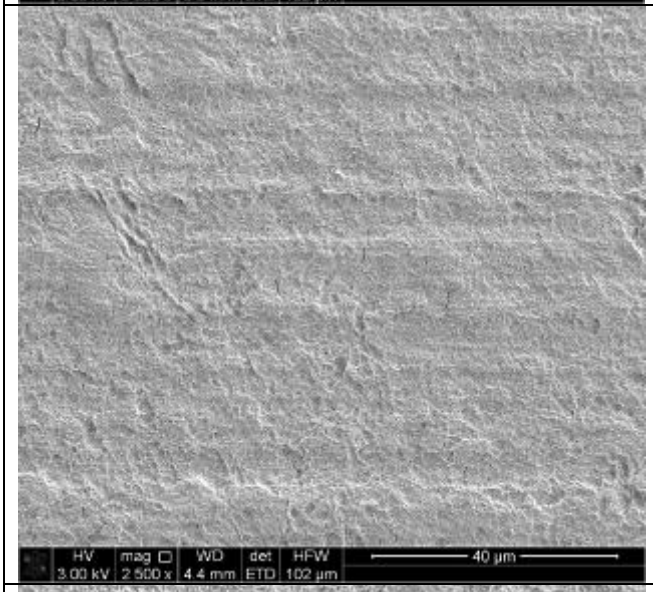 HV 3.00 kV mag 2 500 x WD 4.4 mm det ETD HFW 102 µm 40 µm	
	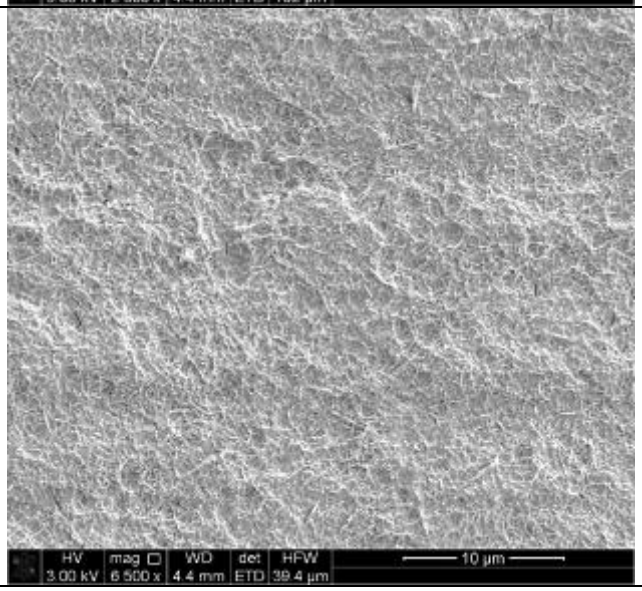 HV 3.00 kV mag 6 500 x WD 4.4 mm det ETD HFW 39.4 µm 10 µm	

	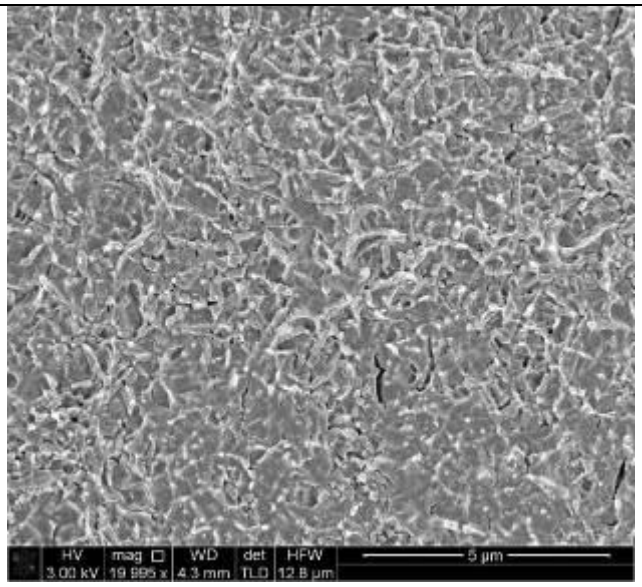 HV 3.00 kV mag 19 895 x WD 4.3 mm det TLD HFW 12.8 µm 5 µm	
	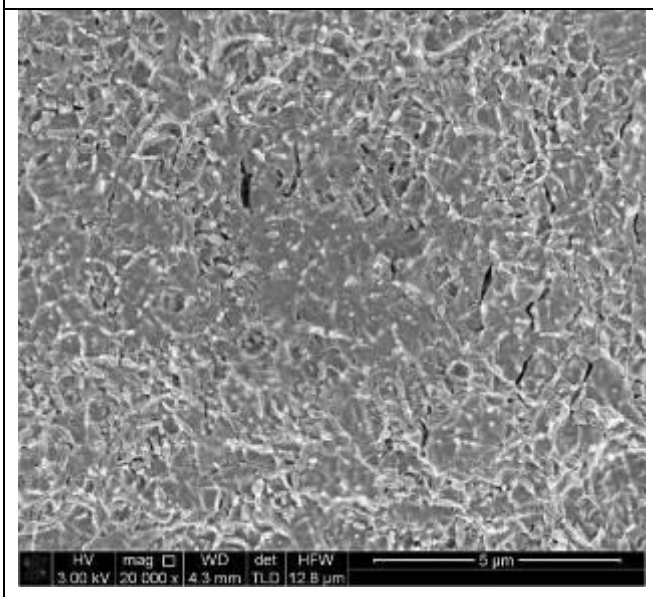 HV 3.00 kV mag 20 000 x WD 4.3 mm det TLD HFW 12.8 µm 5 µm	

7.4 XPS Fittings

Table 67: XPS of untreated washed Goodfellow PTFE, and single-step (ammonia 5 W, 300 s, 0.2 mbar; and oxygen 50 W, 600 s, 0.2mbar) and two-step (ammonia 5 W, 300 s; followed by oxygen 50 W, 600 s, all conducted at 0.2mbar) plasma-treated PTFE. (a) Survey spectra; (b) C 1s high resolution scan; (c) F 1s high resolution scan; (d) N 1s high resolution scan; and (e) O 1s high resolution scan.

	Untreated	**Conditions**	**Ammonia** plasma-treated **(5 W, 300 s)**	**Oxygen** plasma-treated **(50 W, 600 s)**	**Two-step** plasma-treated
(a)	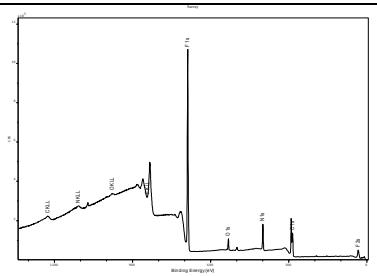	Glow Unwashed		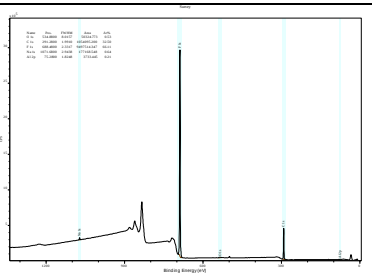	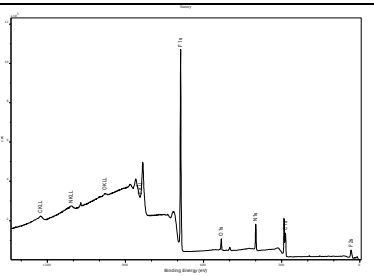
		Remote Unwashed		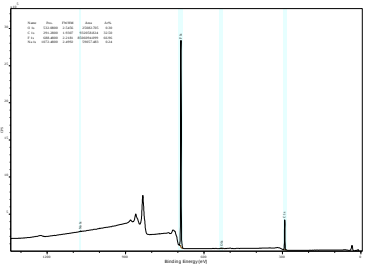	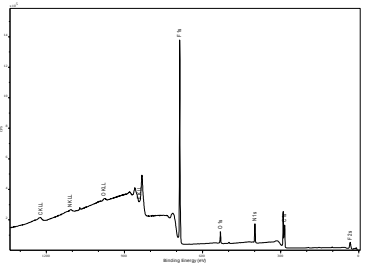

		Glow Washed		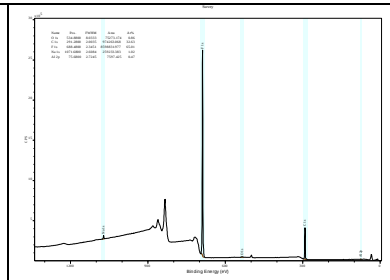	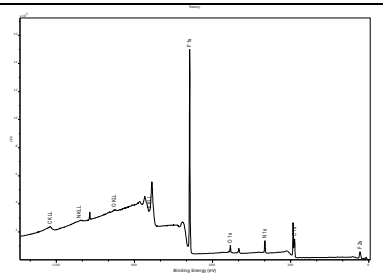
		Remote Washed		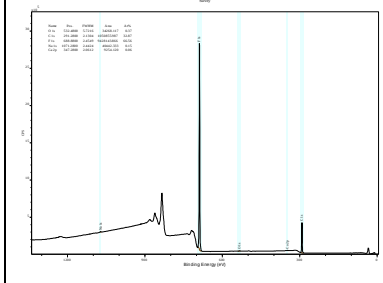	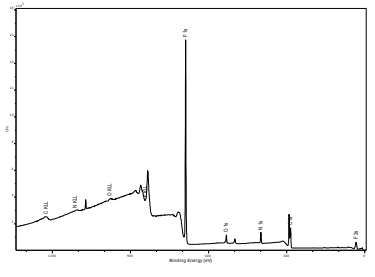
(b)		Glow Unwashed	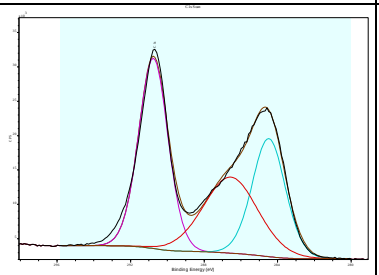	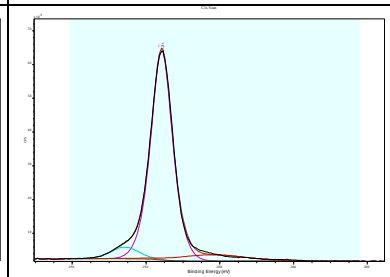	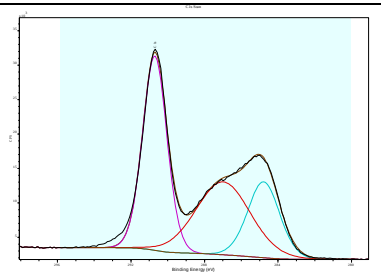

		Remote Unwashed	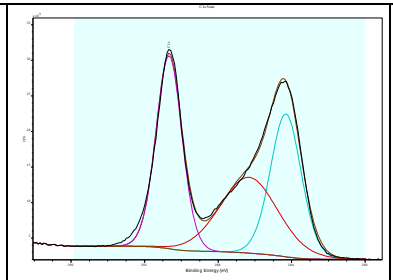	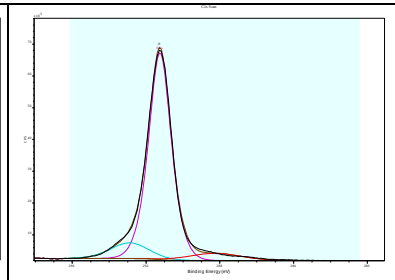	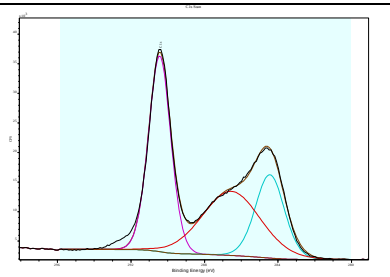
		Glow Washed	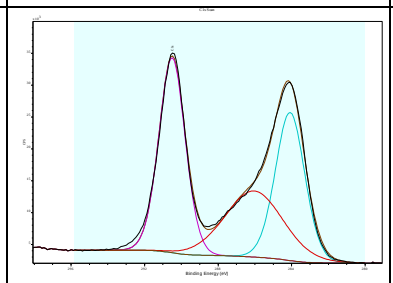	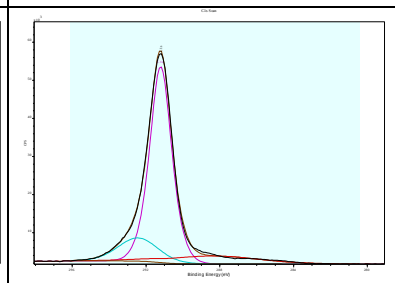	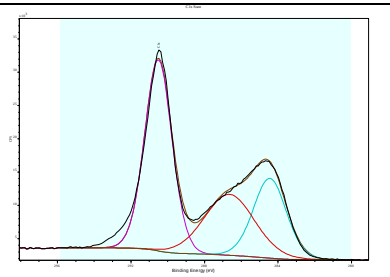
		Remote Washed	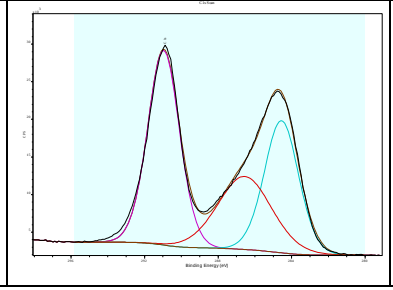	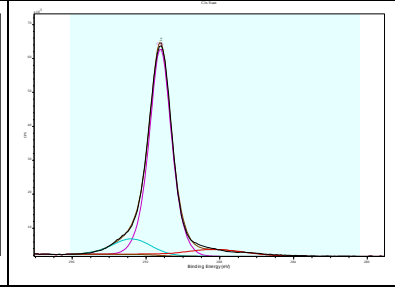	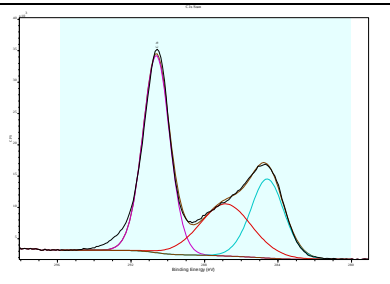

(c)		Glow Unwashed	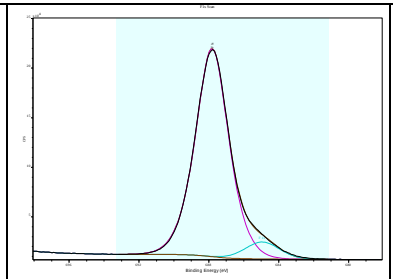	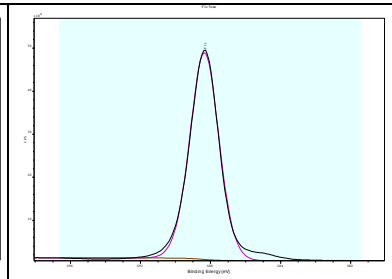	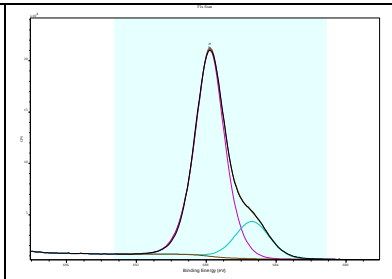
		Remote Unwashed	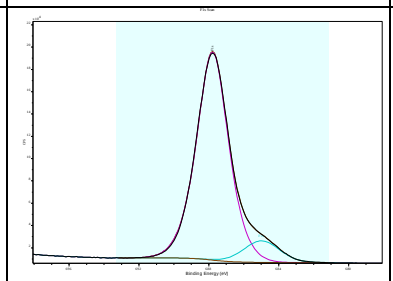	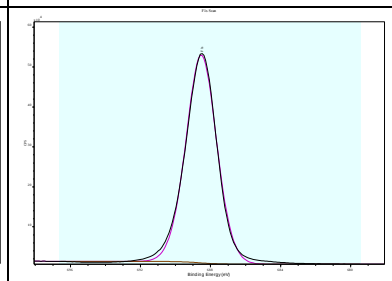	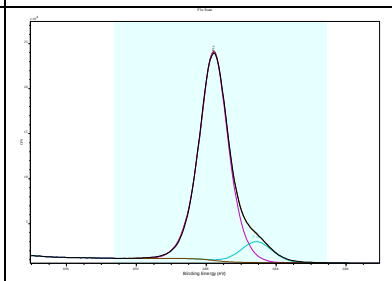
		Glow Washed	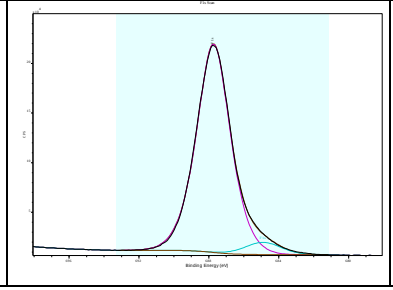	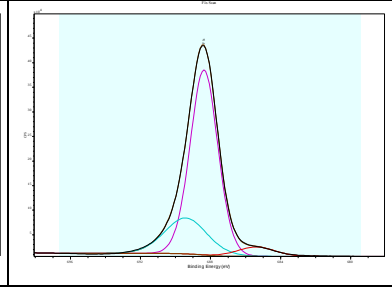	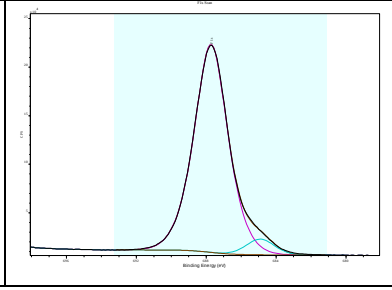

		Remote Washed	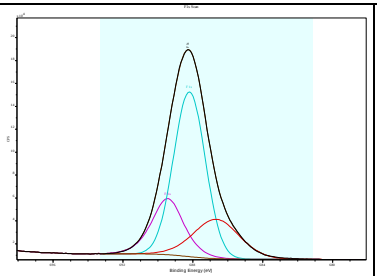	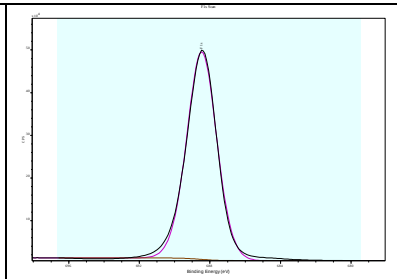	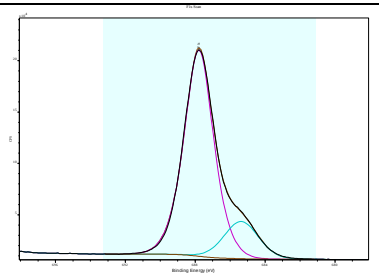
(d)		Glow Unwashed	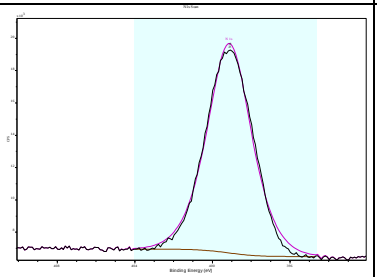	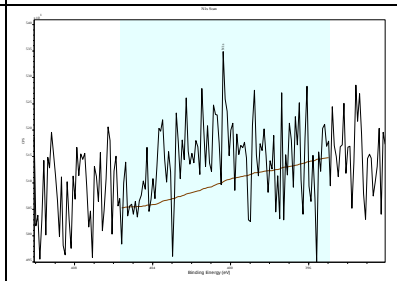	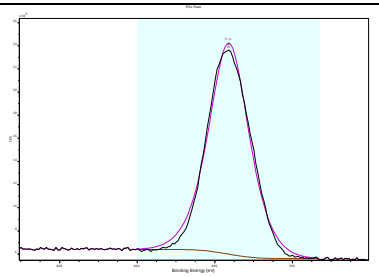
		Remote Unwashed	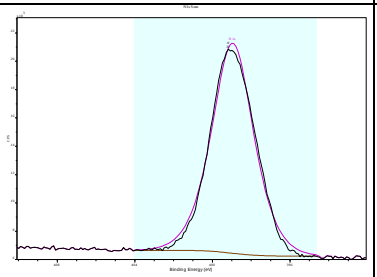	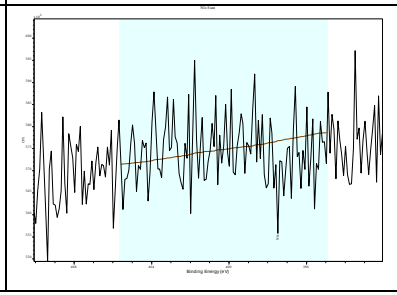	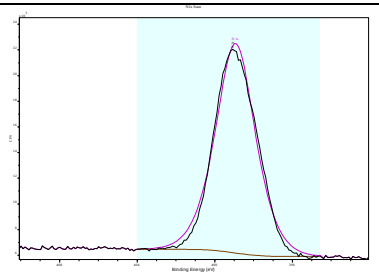

		Glow Washed	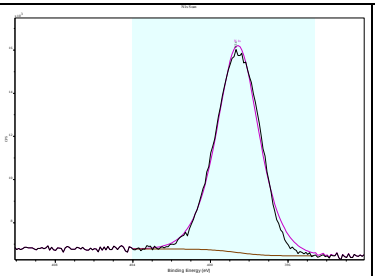	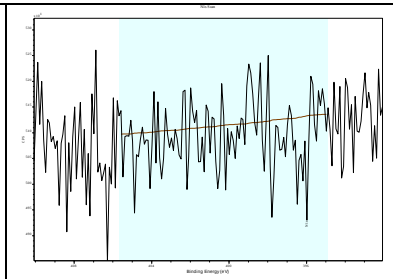	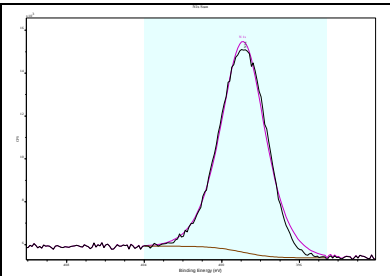
		Remote Washed	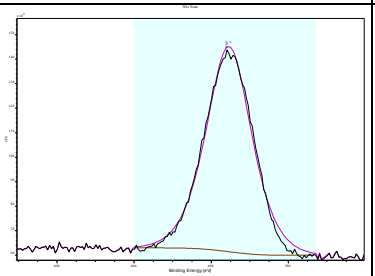	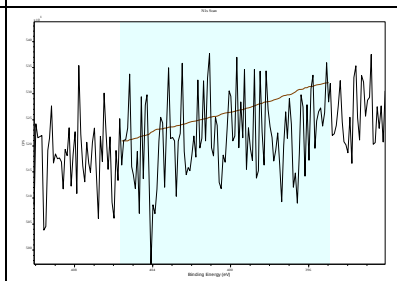	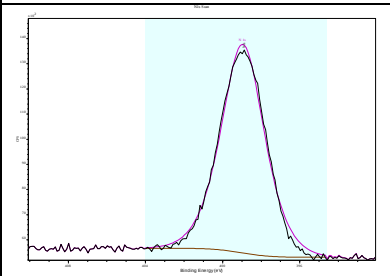
(e)		Glow Unwashed	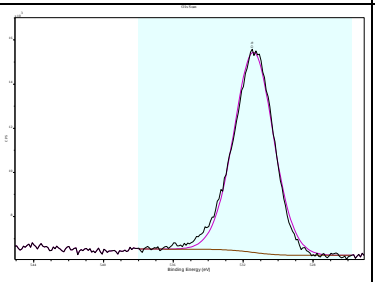	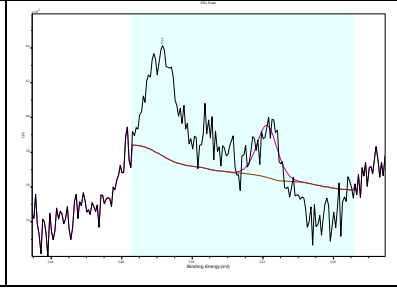	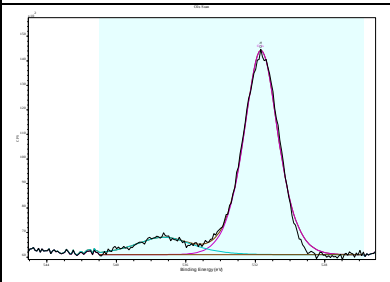

		Remote Unwashed	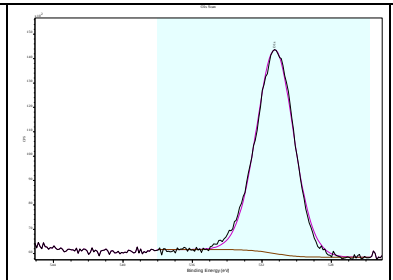	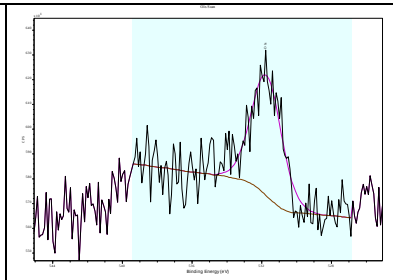	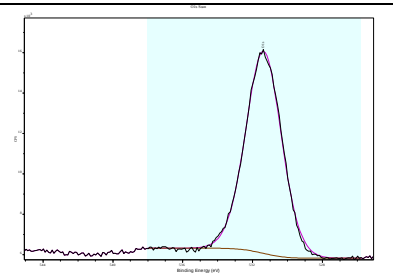
		Glow Washed	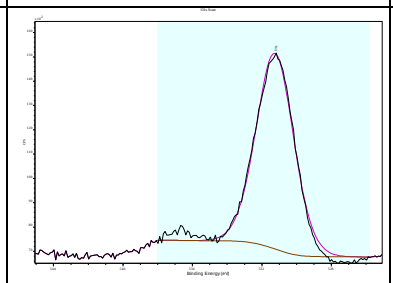	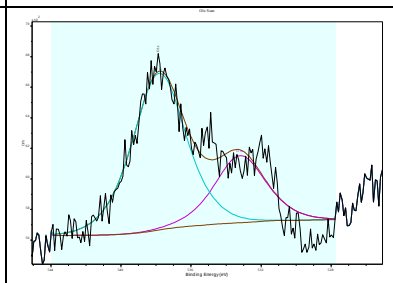	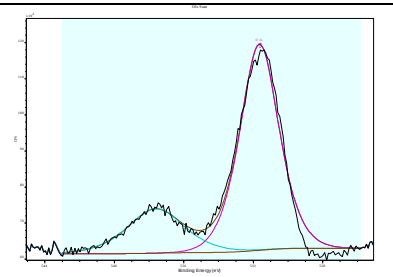
		Remote Washed	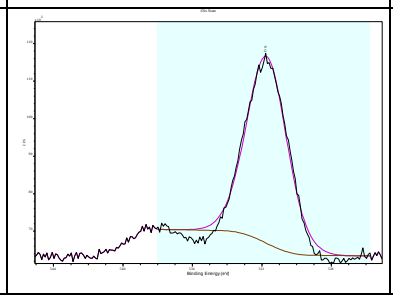	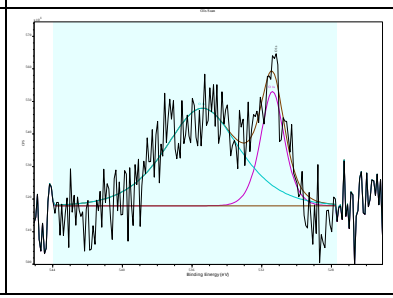	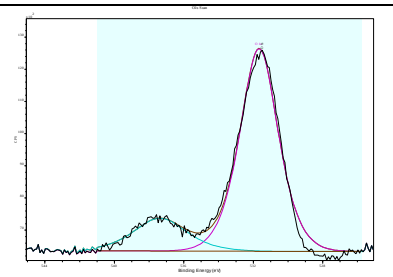

7.5 GC-MS

7.5.1 Solvent Background

Initially samples of the solvent were run as a background; propan-2-ol alone (Figure 69), cyclohexane alone (Figure 71), and the solvent wash solution (1:1 v/v solution of propan-2ol and cyclohexane),Figure 73.

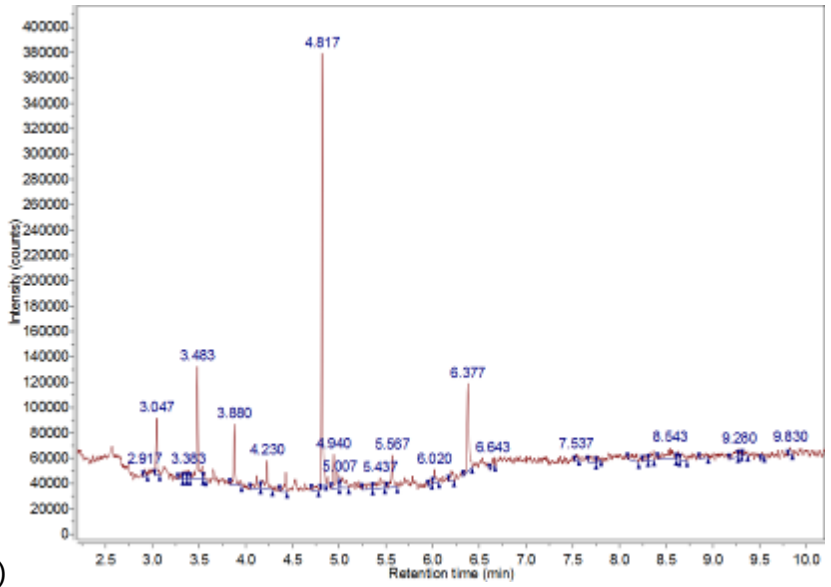

(a)

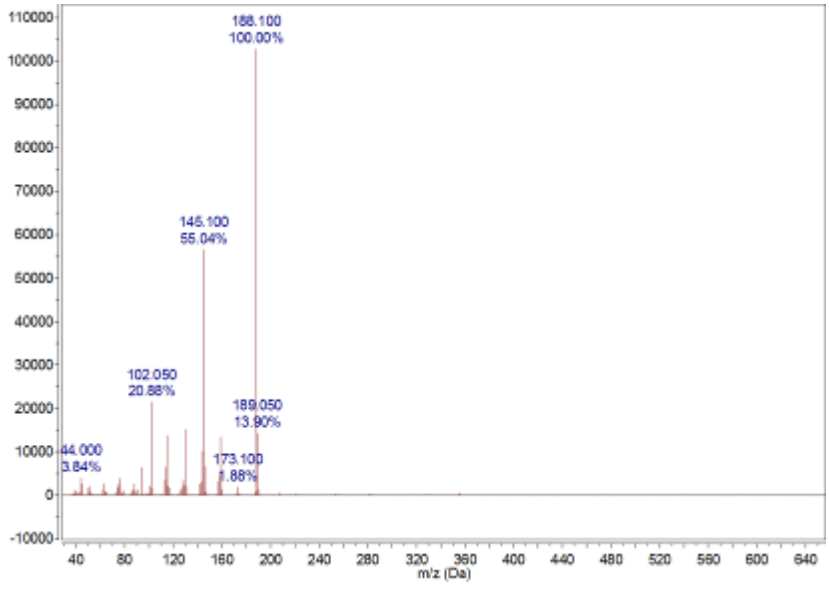

(b)

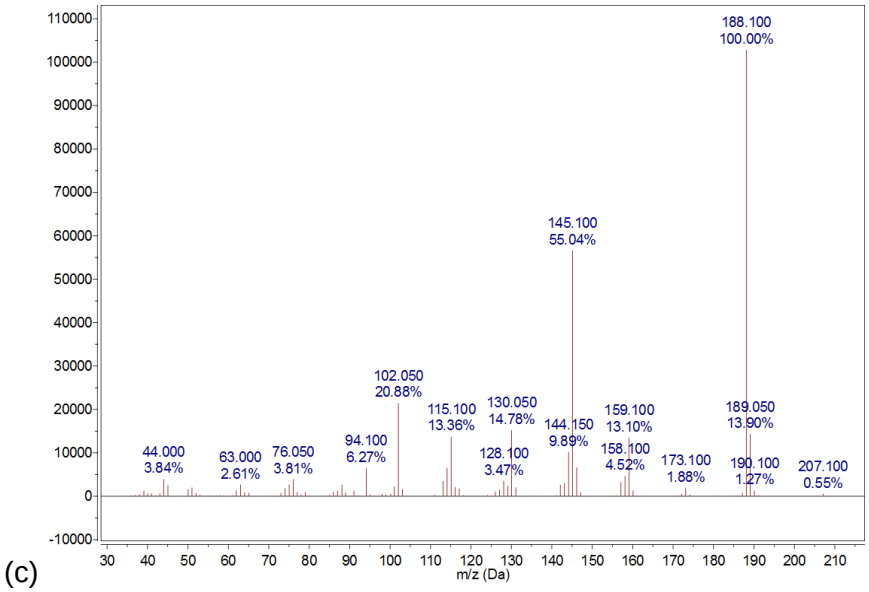

(c)

Figure 69: GC-MS results for solvent background (propan-2-ol alone). Shown is (a) the graph showing the retention time of the solvent in the column, and both (b) the whole m/z spectrum (35–650 Da), and (c) the zoomed in image (30–215 Da).

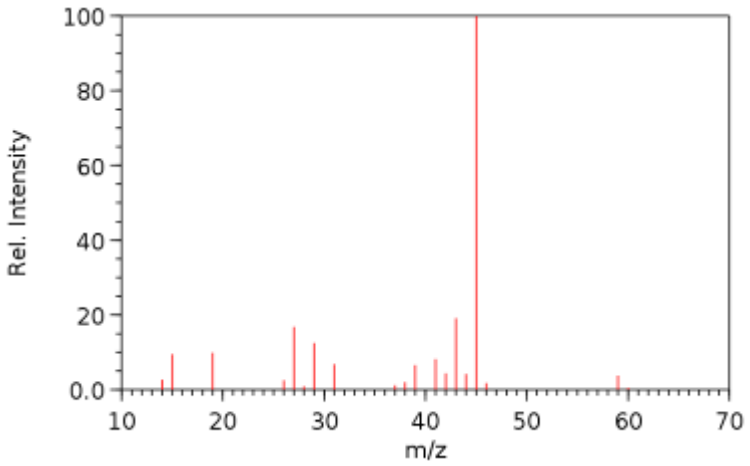

Figure 70: Literature mass spectrum of propan-2-ol taken from NIST database. Intensity of peaks is given relative to the base peak at m/z 45 Da.[430]

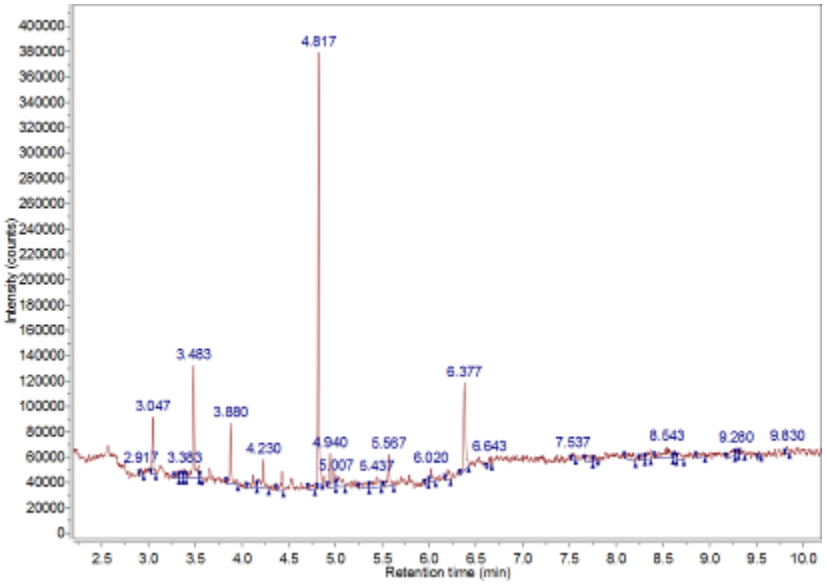
Intensity (counts)
Retention time (min)
4.817
3.483
6.377
3.047
3.880
4.230
4.940
5.567
6.020
6.643
7.537
8.543
9.280
9.830
2.917
3.383
5.007
5.437

(a)

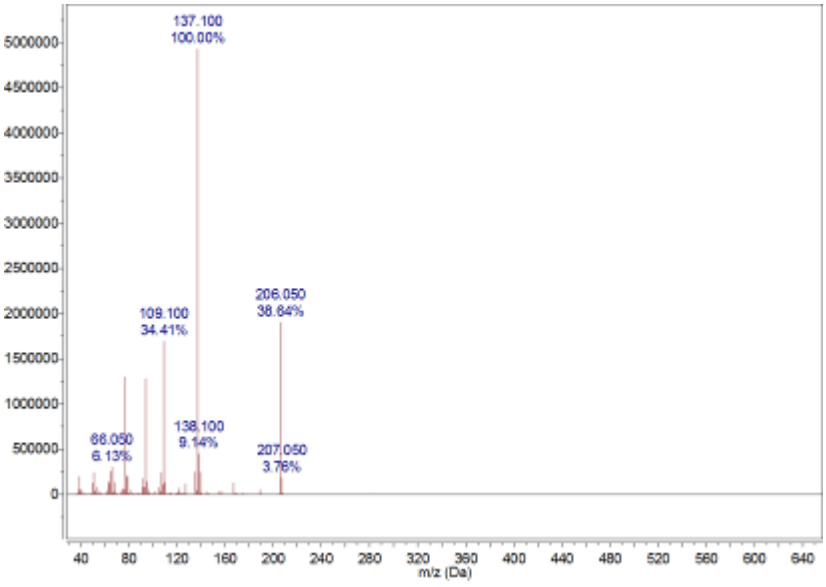
m/z (Da)
137.100
100.00%
206.050
38.64%
109.100
34.41%
138.100
9.14%
66.050
6.13%
207.050
3.76%

(b)

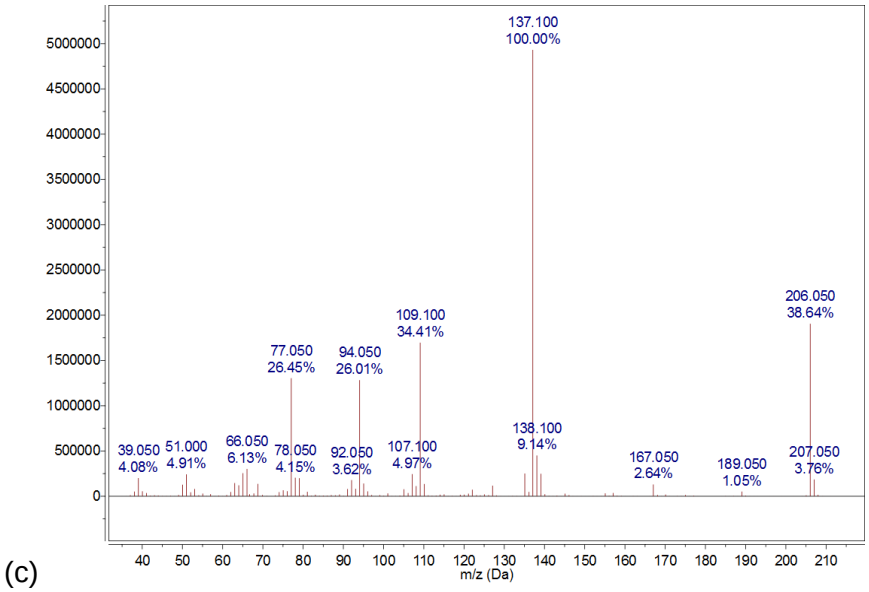

(c)

Figure 71: GC-MS results for solvent background (cyclohexane alone). Shown is (a) the graph showing the retention time of the solvent in the column, and both (b) the whole m/z spectrum (35–650 Da), and (c) the zoomed in image (35–215 Da).

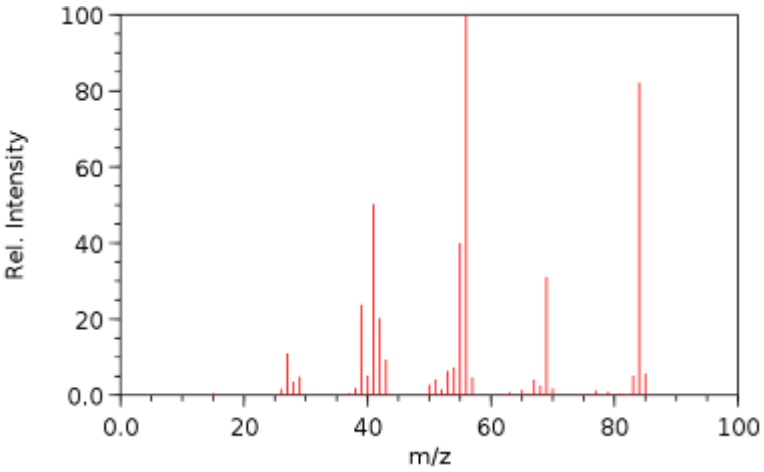

Figure 72: Literature mass spectrum of cyclohexane taken from NIST database. Intensity of peaks is given relative to the base peak at m/z 56 Da.[430]

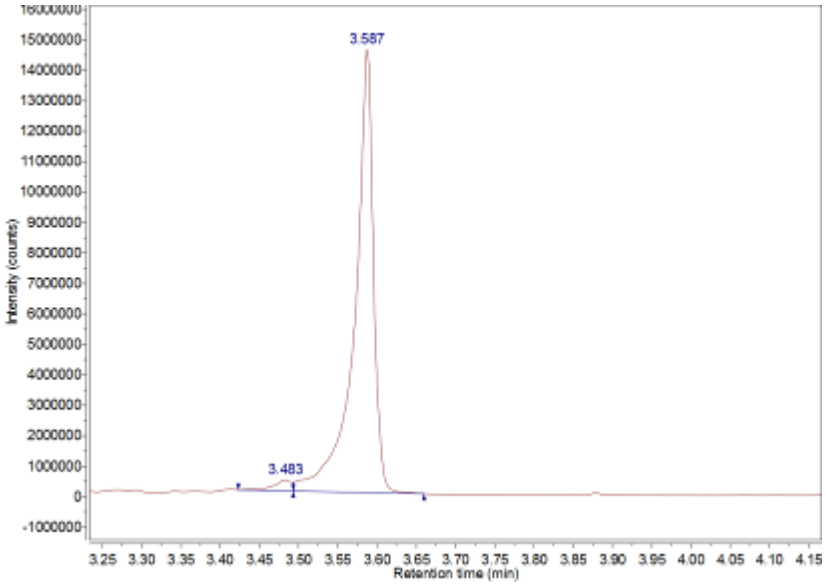
3.587
3.483
Intensity (counts)
Retention time (min)

(a)

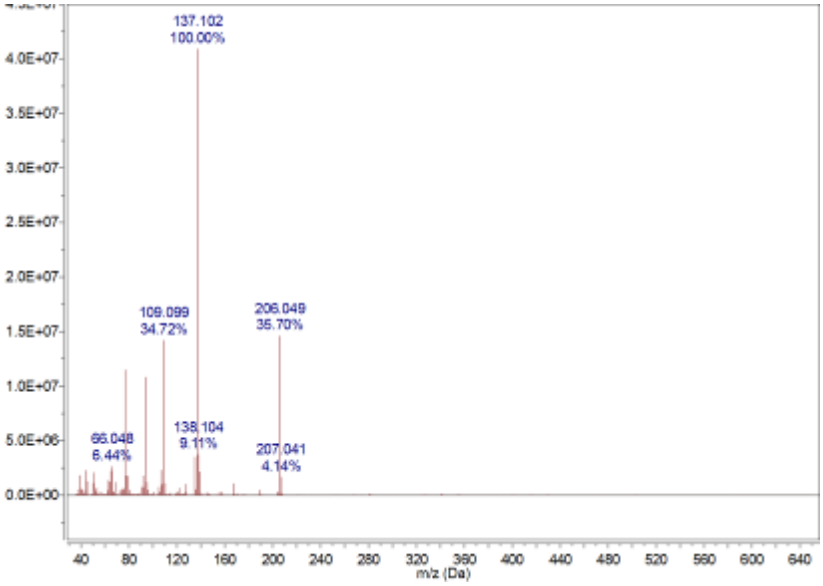
137.102
100.00%
109.099
34.72%
206.049
35.70%
66.048
6.44%
138.104
9.11%
207.041
4.14%
m/z (Da)

(b)

(c)

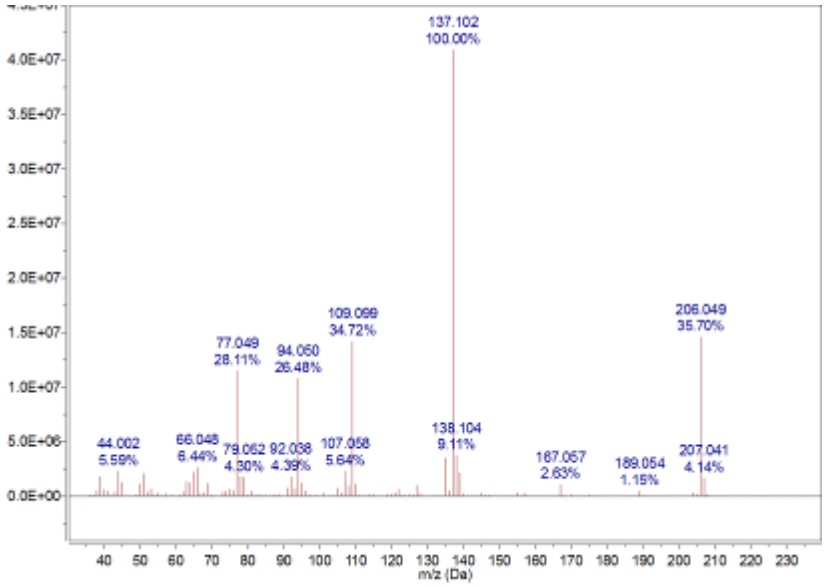

Figure 73: GC-MS results for solvent background (propan-2-ol and cyclohexane 1:1 v/v solution). Shown is (a) the graph showing the retention time of the solvent in the column, and both (b) the whole m/z spectrum (35–650 Da), and (c) the zoomed in image (35–235 Da).

Table 68: Table of reported m/z values with intensities relative to base peak (137.1 Da) for solvent background (1:1 v/v propan-2-ol and cyclohexane solution). Tabulated are the 12 most abundant m/z peaks, arranged in order of decreasing relative intensity.

Mass/Charge (m/z) / Da	Relative Intensity to Base Peak / %
137.1	100.0
206.0	35.7
109.1	34.7
77.1	28.1
94.1	26.5
138.1	9.1
66.0	6.4
107.1	5.6
44.0	5.6
92.0	4.4
78.1	4.4
207.0	4.1

8 REFERENCES

1 Chemcours, *History of Teflon™*, (https://www.chemours.com/Teflon/en_US/products/history.html), accessed 29-01-18

2 PPSTechnology.com, *The History of PTFE*, (http://ppstechnology.ca/Assets/PDF/PTFEHistory.pdf), accessed 29-01-18

3 The Essential Chemical Industry, University of York, (http://www.essentialchemicalindustry.org/polymers/polytetrafluoroethene.html), accessed 29-01-18

4 Encyclopaedia Britannica, (https://www.britannica.com/science/fluoroelastomer), accessed 12-03-18)

5 ChemGuide, (https://www.chemguide.co.uk/qandc/ptfe.html), accessed 02-02-18

6 C. Wang, G. Duscher, and S.J. Paddison, *Microscopy*, 2014, **63**, 73

7 L.W. McKeen, *Film Properties of Plastics and Elastomers*, William Andrew (Elsevier), Oxford, 4th ed., 2017, 255

8 Goodfellow, (http://www.goodfellow.com/A/Polytetrafluoroethylene-Film.html), accessed 29-01-18

9 Fluon, Molding of PTFE granular powders: Technical Service Note F1 (https://www.agccgem.com/component/jdownloads/finish/13-fluon-ptfe-resins/41-processing-note-f1-moldinng-of-ptfe-granular-powders?Itemid=0), accessed 11-07-17

10 O.D. Greenwood, J. Hopkins, and J.P.S. Badyal, *Macromolcules*, 1997, **3**, 1091

11 J. Tsibouklis, and T.G. Nevell, *Adv. Mater.*, 2003, **7**, 647

12 Processing of Dyneon PTFE Fine Powder, (http://multimedia.3m.com/mws/media/907326O/processing-of-3m-dyneon-ptfe-fine-powder-brochure.pdf?fn=Dyneon_PTFE_FinePowder_EN.pdf), accessed 02-01-18

13 R.J. Good, *J. Adhesion Sci. Technol.*, 1992, **6**, 1269

14 H.J. Butt, I.V. Roisman, M. Brinkmann, P. Papadopoulos, D. Vollmer, and C. Semprebon, *Curr. Opin. Colloid In.*, 2014, **19**, 343

15 R.N. Wenzel, *Ind. Eng. Chem. Res.*, 1936, **28**, 988

16 A.B.D. Cassie, and S. Baxter, *Trans. Faraday Soc.*, 1944, **40**, 546

17 Y. Yuan and T.R. Lee, *Surface Science Techniques*, ed. G. Bracco and B. Holst, Springer-Verlag Berlin Heidelberg, Berlin, 2013, 5–6

18 W.A. Zisman, *Contact Angle, Wettability and Adhesion Advances in Chemistry*, Fowkes, Washington DC, 1964, 1

19 A.B.D. Cassie, and S. Baxter, *Trans. Faraday Soc.*, 1944, **40**, 546

20 D. Myers, *Surfaces, Interfaces, and Colloids: Principles and Applications*, John Wiley & Sons, Inc., New York, 2nd ed., 1999, 415

21 Contact Angle Measurment, (https://www.kruss-scientific.com/services/education-theory/glossary/contact-angle), accessed 04-02-18

22 Drop Shape Analysis, (https://www.kruss-scientific.com/services/education-theory/glossary/drop-shape-analysis), accessed 04-02-18

23 A.F. Taggart, T.C. Taylor, and C.R. Ince, *Trans. Am. Inst. Min. Metall. Pet. Eng.*, 1930, **87**, 285

24 A.W. Neumann, and R.J. Good, *J. Colloid Interface Sci.*, 1996, **179**, 37

25 F.J. Montes Ruiz-Cabello, M.A. Rodriguez-Valverde, and M.A. Cabrerizo-Vilchez, *Langmuir*, 2011, **27**, 8748

26 F.J. Montes Ruiz-Cabello, M.A. Rodriguez-Valverde, A. Marmur, and M.A. Cabrerizo-Vilchez, *Langmuir*, 2011, **27**, 9638

27 J. Drelichm J.D. Miller, and R.J. Good, *J. Colloid Interface Sci.*,

28 A.F. Taggart, T.C Taylor, and C.R. Ince, *T. Am. I. Min. Met. Eng.*, 1930, **87**, 285

29 Wilhelmy Plate Method, (https://www.kruss-scientific.com/services/education-theory/glossary/wilhelmy-plate-method/), accessed 05-02-18

30 Y. Yuan and T.R. Lee, *Surface Science Techniques*, ed. G. Bracco and B. Holst, Springer-Verlag Berlin Heidelberg, Berlin, 2013, 3–34

31 Methods of surface tension measurements, (http://zzm.umcs.lublin.pl/Wyklad/FGF-Ang/2A.F.G.F.%20Surface%20tension.pdf), accessed 05-02-18

32 V. Émyde, *Wilhelmy Plate* (https://commons.wikimedia.org/w/index.php?curid=36905472), accessed 05-02-18

33 R. Shuttleworth, and G.L.J. Bailey, *Discuss. Faraday Soc.*, 1948, **3**, 16

34 E.W. Washburn, *Phys. Rev.*, 1921, **17**, 374

35 J.A. Bittencourt, *Fundamentals of Plasma Physics*, Springer Science + Business Media, New York, 3rd ed., 2004, 1

36 G.H. Yang, E.T. Kang, and K.G. Neoh, *J. Polym. Sci. Pol. Chem.*, 2000, **38**, 3498

37 W.H. Yu, E.T. Kang, and K.G. Neoh, *Langmuir*, 2005, **21**, 450

38 E.T. Kang, K.G. Neoh, W. Chen, K.L. Tan, D.J. Liaw, and C.C. Huang, *J. Adhesion Sci. Technol.*, 1996, **10**, 725

39 A. Reznickova, Z. Kolska, V. Hnatowicz, P. Stopka, and V. Svorcik, *Nucl. Instrum. Meth. B.*, 2011, **269**, 83

40 W.H. Harris, *Clin. Orthop. Relat. Res.*, 2009, **467**, 28

41 J-M. Lee, *Hip Pelvis*, 2016, **28**, 191

42 J. Charnley, *The Lancet*, 1961, **277**, 1129

43 P.C. Raynor, B.G. Kim, G, Ramachandran, M.R. Dtrommen, J.H. Horns, and A.J. Steifel, *Indoor Air*, 2008, **18**, 51

44 T. Murakami, S-I. Kuroda, and Z. Osawa, *J. Colloid Interface Sci.*, 1998, **202**, 37

45 R.K. Wells, J.P.S. Badyal, I.W. Drummond, K.S. Robinson, and F.J. Street, *J. Adhesion Sci.* Technol*., 2004,* **18**, 1279

46 T.R. Gengenbach, X. Xie, R.C. Chatelier and H.J. Greisser, *J. Adhesion Sci. Technol.*, 1994, **8**, 305

47 J. Kim, M.K. Chaudhury, M.J. Owen, and T. Orbeck, *J. Colloid Interface Sci.*, 2001, **244**, 200

48 M. Mortazavi, and M. Nosonovsky, *Appl. Surf. Sci.*, 2012, **258**, 6876

49 N. Zachariaha, J.S. Mohammed, and D.T. Eddington, *Journal of Undergraduate Research*, 2007, **1**, 67

50 D.J. Wilson, R.L. Williams, and R.C. Pond, *Surf. Interface. Anal.*, 2001, **31**, 397

51 G. Attard, and C. Barnes, *Surfaces*, Oxford University Press, Oxford, 1998, 1, 23.

52 O.D. Greenwood, J. Hopkins, and J.P.S. Badyal, *Macromolecules*, 1997, **30**, 1091

53 D.J. Guckenberger, E. Berthier, E.W.K. Young, and D.J. Beebe, *Lab. Chip.*, 2012, **12**, 2317

54 N. Vandencasteele, B. Nisol. P. Vivelle, R. Lazzaroni, D.G. Castner, and F. Reniers, *Polymer*, 2008, **5**, 661

55 L. Tong, D.T.K. Kwok, H. Wang, L. Wu, and P.K. Chu, *Adv. Eng. Mater.*, 2010, **12**, 163

56 M. Morra, E. Occhiello, and F. Garbassi, Langmuir, 1989, **5**, 872

57 S. Zanini, R. Barni, R. Della Pergola, and C. Riccardi, *J. Phys. D. Appl. Phys.*, 2014, **47**, 325202

58 A. Dekker, K. Reitsma, T. Beugeling, A. Bantjes, J. Feijen, and W.G van Aken, *Biomaterials*, 1991 **12**, 130

59 W. Hai, T. Hi, K. Shimizu, and T. Yakima, *J. Photolym. Sci. Tech.*, 2015, **28**, 479

60 N. Inagaki, S. Tasaka, and T. Umehara, *J. Adhesion Sci. Technol.*, 1989, **3**, 637

61 J.P. Badey, E. Espuche, D. Sage, B. Chabert, Y. Junget, C. Batier, and T.M. Duc, *Polymer*, 1996, **5**, 661

62 P. Favia, A. Milella, L. Iacobelli, R. d'Agostino, *Plasma Processes and Polymers*, ed. R. d'Agostino, P. Favia, C. Oehr, M.R. Wertheimer, Wiley-VCH Verlag GMBH & Co. KGaA, Weinheim, 2005, ch. 20, 271

63 S Shin, S.H. Han, and Y.S. Kim, *Han'guk Pyomyon Konghak Hoechi*, 2005, **38**, 118

64 C.Y. Tu, Y-L. Liu, K-R. Lee, and J-Y. Lai, *Polymer*, 2005, **46**, 6976

65 S. Ishikawa, K. Yukirmura, K. Matsunaga, and T. Maruyama, *Surf. Coat. Tech.*, 2000, **130**, 52

66 Z. Fang, Y. Qui, and Y. Luo, *J. Phys. D: Appl. Phys.*, 2003, **36**, 2980

67 *U.S. Pat.*, US2016/0039979, 2016

68 S. Ishikawa, K. Yukimura, K. Matsunaga, and T. Maruyama, *Jpn. J. Appl. Phys.*, 2000, **39**, 5223

69 Z. Fang, and L. Cai, *High Voltage Engineering*, 2011, **37**, 1459

70 Z. Fang, L. Hao, H. Yang, X. Xie, Y. Qui, and K. Edmund, *Appl. Surf. Sci.*, 2009, **255**, 7279

71 Z. Niu, C. Zhang, T. Shao, Z. Fang, Y. Yu, and P. Yan, *Surf. Coat. Tech.*, 2013, **228**, S578

72 F. Zhi, L. Yi, Q. Yuchung, Y. Yun, and X. Dawei, *Vacuum Science and Technology (China)*, 203, **23**, 408

73 C. Liu, N. Cui, N.M.D. Brown, and B.J. Meenan, *Surf. Coat. Tech.*, 2004, **185**, 311

74 G. Borcia, C.A. Anderson, and N.M.D. Brown, *Appl. Surf. Sci.*, 2004, **221**, 203

75 G. Borcia, C.A. Anderson, and N.M.D. Brown, *Plasma Sources Sci.*, 2003, **12**, 335

76 C. Sarra-Bournet, S. Turgeon, D. Mantovani, and G. Laroche, *J. Phys. D: Appl. Phys.*, 2006, **39**, 3461

77 C. Sarra-Bournet, S. Turgeon, D. Mantovani, and G. Laroche, *Plasma Process. Polym.*, 2006, **3**, 506

78 Encyclopaedia Britannica, (https://www.britannica.com/science/electret), accessed 12-03-18

79 Z-Y. Xi, Y-Y. Xu, L-P. Zu, F. Liu, amd B-K. Zhu, *Appl. Surf. Sci.*, 2014, **296**, 79

80 M. Gabriel, K. Niederer, C.M. Raynaud, C-F. Vahl, and H. Frey, *Bioconjugate Chem.*, 2016, **27**, 1216

81 G. Tae, R.G.H. Lammertink, J.A. Kornfield, and J.A. Hubbell, *Adv. Mater.*, 2003, **15**, 66

82 K. Szymczyk, and B. Jańczuk, *Langmuir*, 2007, **23**, 8740

83 C. Zilio, L. Sola, F. Damin, L. Faggioni, and M. Chiari, *Biomed. Microdevices*, 2014, **16**, 107

84 S. George, *Chem. Rev.*, 2010, **110**, 111.

85 S. George, A. Ott, and J. Klaus, *J. Phys. Chem.*, 1996, **100**, 13121.

86 A.K. Roy, J. Dendooven, D. Deduytsche, K. Devloo-Casier, K. Ragaert, L. Cardon, and C. Detavernier, *Chem. Comm.*, 2015, **51**, 3556

87 A. Grill, *Cold Plasma in Materials Fabrication*, IEEE Press, New York, 1994, Chapter 1

88 I. Langmuir, *Phys. Rev.*, 1929, **33**, 354

89 S. Morsch, PhD Thesis, Durham University, 2012

90 A. Solouk, B.G. Cousins, H. Mirzadeh, and A.M. Sifalian, *Biotechnol. Appl, Biochem.*, 2001, **58**, 311

91 N. Inagaki, K. Narushim, N. Tachida, and K. Miyazaki, *J. Polym. Sci. Pol. Phys.*, 2004, **42**, 3727

92 C.M. Chan, T.M. Ko, and H. Hiroaka, *Surf. Sci. Rep.*, 1996, **24**, 1

93 P. Horowitz, and W. Hill, *The Art of Electronics*, Cambridge University Press, Cambridge, 2nd ed., 1989

94 *Handbook of Advanced Plasma Processing Techniques*, ed. R.J. Shul, and S.J. Pearton, Springer-Verlay Berin Heidelberg, New York, 2000

95 P.S. Brown, PhD Thesis, Durham University, 2013

96 R.J. Good, *J. Colloid Interf. Sci.*, 1979, **71**, 283

97 J. Drelich, J.D. Miller, and R.J. Good, *J. Colloid Interface Sci.*, 1996, **179**, 37

98 D. Briggs and J.T. Grant, *Surface Analysis by Auger and X-Ray Photoelectron Spectroscopy*, ed. D. Briggs and J.T. Grant, IM Publications and Surface Spectra Limited, Chichester, 2003

99 H.G.J. Moseley, *Phil. Mag. Vi*, 1914, **27**, 195

100 E. Rutherford, *Philos. Mag. A.*, 1914, **28**, 305

101 D. Briggs, and J.C. Riviere, *Practical Surface Analysis Volume 1 - Auger and X-Ray Photoelectron Spectroscopy*, ed. D. Briggs and M.P. Seah, John Wiley & Sons Ltd, Chichester, 2nd ed., 1990

102 G. Attard, C. Barnes, *Surfaces*, Oxford University Press, Oxford, 1998

103 J.C. Riviere, *Practical Surface Analysis Volume 1 - Auger and X-Ray Photoelectron Spectroscopy*, ed. D. Briggs and M.P. Seah, John Wiley & Sons Ltd, Chichester, 2nd ed., 1990

104 G. Beamson and G. Briggs, *High Resolution XPS of Organic Polymers – The Scienta ESCA300 Database*, John Wiley & Sons, Chichester, 1992

105 J.F. Moulder, W.F. Stickle, P.E. Sobol, and K.D. Bomben, *Handbook of X-ray Photoelectron Spectroscopy*, Perkin Elmer Corporation Physical Electronics Division, Eden Prairie, 1992

106 T.J. Wood, P.S. Brown, J.P.S. Badyal, *Plasma Chem. Plasma P.*, 2014, **34**, 1019

107 The Russell Saunders Coupling Scheme, (http://wwwchem.uwimona.edu.jm/courses/RScoupling.html), accessed 23-03-18

108 P. Atkins, and J. de Paula, *Atkins' Physical Chemistry*, Oxford University Press, 7th ed., 2002, Oxford, 400–404

109 P.M.A. Sherwood, *Practical Surface Analysis Volume 1 - Auger and X-Ray Photoelectron Spectroscopy*, ed. D. Briggs and M.P. Seah, John Wiley & Sons Ltd, Chichester, 2nd ed., 1990

110 I.W. Drummond, *Surface Analysis by Auger and X-Ray Photoelectron Spectroscopy*, ed. D. Briggs and J.T. Grant, IM Publications and Surface Spectra Limited, Chichester, 2003

111 S. Tougaard, *Surface Analysis by Auger and X-Ray Photoelectron Spectroscopy*, ed. D. Briggs and J.T. Grant, IM Publications and Surface Spectra Limited, Chichester, 2003, 1

112 U. Fantz, *Plasma Sources Sci. T.*, 2006, **15**, S137

113 V. Donnelly, *J. Phys. D. Appl. Phys.*, 2004, **37**, R217

114 X.M. Zhu, and Y.K Pu, *J. Phys. D:Appl. Phys.*, 2010, **43**, 403001

115 X. Hou, and B.T. Jones, *Encyclopedia of Analytical Chemistry*, ed. R.A. Meyers, John Wiley & Sons Ltd., Chichester, 2000, 9468

116 C.B. Boss, and K.J. Fredeen, *Concepts, Instrumentation, and Techniques in Inductively Coupled Plasma Optical Emission Spectroscopy*, The Perkin Elmer Corporation, U.S.A, 2nd ed., 1997

117 I.P. Herman, *Optical Diagnostics for Thin Film Processing*, Academic Press, San Diego, 1996

118 C.A.J. Putman, K.O. Van der Werf, B.G.D. Grooth, N.F. Van Hulst, and J. Greve, *Appl. Phys. Lett.*, 1994, **64**, 2454

119 P.J. James, M. Antogonozzi, J. Tamayo, T.J. McMaster, J.M. Newton, and M.J. Miles, *Langmuir*, 2001, **17**, 349

120 D.J. Stokes, *Principles and Practice of Variable Pressure/Environmental Scanning Electron Microscopy*, John Wiley & Sons Ltd., 2008, Chichester, Chapter 1

121 T.E. Everhart, *J. Vac. Sci. Technol. B*, 1996, **14**, 3620

122 *Advances in Imaging and Electron Physics: Sir Charles Oatley and the Scanning Electron Microscope*, ed. B.C. Breton, D. McMullan, and K.C.A. Smith, Elsevier Academic Press, San Diego, 2004, 7–37

123 Understanding Cement; SEM Introduction, (https://www.understanding-cement.com/sem-introduction.html), accessed 24-1-18

124 ThermoFisher Scientific, FTIR Sample Techniques: Attenuated Total Reflection (ATR), (https://www.thermofisher.com/uk/en/home/industrial/spectroscopy-elemental-isotope-analysis/spectroscopy-elemental-isotope-analysis-learning-center/molecular-spectroscopy-information/ftir-information/ftir-sample-handling-techniques/ftir-sample-handling-techniques-attenuated-total-reflection-atr.html#), accessed 22-01-18

125 PerkinElmer, *Technical Note: FTIR Spectroscopy, ATR Accessories*, PerkinElmer Life and Analytical Sciences, 2004, New York, 1–4

126 P. Atkins, and J. de Paula, *Atkins' Physical Chemistry*, Oxford University Press, 7th ed., 2002, Oxford, 150–154

127 A.W. Adamson, *Physical Chemistry of Surfaces*, John Wiley & Sons, 1982, New York, 4

128 The Gibbs Free Energy and Helmholtz Free Enery, (http://pruffle.mit.edu/3.00/Lecture_02_web/node16.html), accessed 13-02-18

129 Helmholtz Free Energy, (http://hyperphysics.phy-astr.gsu.edu/hbase/thermo/helmholtz.html), accessed 13-02-18

130 D. Myers, *Surface, Interfaces and Colloids: Principles and Applications*, John Wiley & Sons Inc., 2nd ed., 1999, New York, 140–149

131 Gibb's Adsorption Isotherm, (http://image.sciencenet.cn/olddata/kexue.com.cn/bbs/upload/1367103_lect_Gibbs_Adsorption_-_Fall_2006_SC.pdf), accessed 27-03-18

132 Monroe Electronics Ltd., *Electrostatic Voltmeter Manual (Isoprobe Model 244)*, New York, 1979

133 R.A.W. Johnstone, and C.G. Herbert, *Mass Spectrometry Basics*¸ CRC Press LLC, 2003, Boca Raton, Chapter 36

134 V. Barwick, J. Langley, T. Mallet, B. Stein, and K. Webb, *Best Practice Guide for Generating Mass Spectra*, LGC Ltd., 2006, Teddington, 2

135 A. Reznickova, Z. Kolska, V. Hnatowicz, P. Stopka, and V. Svorcik, *Nucl. Instrum. Meth. B.*, 2011, **269**, 83

136 S.R. Kim, *J. Appl. Polym. Sci.*, 2000, **77**, 1913

137 Z. Kolska, A. Reznickova, V. Hnatowicz, and V. Svorcik, *Vacuum*, 2012, **86**, 643

138 T.K. Markkula, J.A. Hunt, F.R. Pu, and R.L. Williams, *Surf. Interface Anal.*, 2002, **34**, 583

139 N. Inagaki, S. Tasaka, and H. Kawai, *J. Adhesion Sci. Technol.*, 1989, **3**, 637

140 N. Vandencasteele, B. Nisol, P. Vivelle, R. Lazzaroni, D.G. Castner, and F. Reniers, *Plasma Process. Polym.*, 2008, **5**, 661

141 J.P.Badey, E. Espuche, D. Sage, B. Chabert, Y. Jugnet, C. Batier, and T.M. Duc, *Polymer*, 1996, **37**, 1377

142 N. Inagaki, S. Tasaka, and T. Umehara, *J. Appl. Polym. Sci.*, 1999, **71**, 2191

143 J. Nakamatsu, L.F. Delgado-Aparicio, R. Da Silva, and F. Soberon, *J. Adhesion Sci. Technol.*, 1999, **13**, 753

144 H. Xu, Z. Hu, S. Wu, and Y. Chen, *Mater. Chem. Phys.*, 2003, **80**, 278

145 A. Sarani, N. De Geyter, A.Y. Nikiforov, R. Morent, C. Leys, J. Hubert, and F. Reniers, *Surf. Coat. Technol.*, 2012, **206**, 2226

146 C. Huang, W.C. Ma, C.Y. Tsai, W.T. Hou, and R.S. Juang, *Surf. Coat. Tech.*, 2013, **231**, 42

147 W. Hai, T. Hi, K. Shimizu, and T. Yajima, *J. Photopolym. Sci. Tech.*, 2015, **28**, 479

148 T.R. Gengenbach, X. Xie, R.C. Chatelier and H.J. Greisser, *J. Adhesion Sci. Technol.*, 1994, **8**, 305

149 J. Kim, M.K. Chaudhury, M.J. Owen, and T. Orbeck, *J. Colloid Interface Sci.*, 2001, **244**, 200

150 M. Mortazavi, and M. Nosonovsky, *Appl. Surf. Sci.*, 2012, **258**, 6876

151 N. Zachariaha, J.S. Mohammed, and D.T. Eddington, *Journal of Undergraduate Research*, 2007, **1**, 67

152 O.D. Greenwood, J. Hopkins, and J.P.S. Badyal, *Macromolecules*, 1997, **30**, 1091

153 D.J. Guckenberger, E. Berthier, E.W.K. Young, D.J. Beebe, *Lab Chip.*, 2012, **12**, 2317

154 G. Attard, C. Barnes, *Surfaces*, Oxford University Press, Oxford, 1998, 1, 23.

155 V. Švorčík, V. Kotál, J. Siegel, P. Sajdl, A. Macková, and V. Hnatowicz, *Polym. Degr. Stab.*, 2007, **92**, 1645

156 J. Hyun, *Polymer*, 2001, **42**, 6473

157 H.Z. Syed, M.A.Sc. Thesis, University of Windsor, 2002

158 D.J. Wilson, R.L. Williams, and R.C. Pond, *Surf. Interface. Anal.*, 2001, **31**, 397

159 X. Xie, T.R. Gengenbach, and H.J. Greisser, *J. Adhesion Sci. Technol.*, 1992, **6**, 1411

160 T. Murakami, S-I. Kuroda, and Z. Osawa, *J. Colloid Interface Sci.*, 1998, **202**, 37

161 S. Wolf, M. Edmonds, X. Jiang, R. Droopad, N. Yoshida, L. Dong, R. Galatage, S. Siddiqui, B. Sahu, and A. Kummel, *ECS Trans*, 2016, **72**, 291

162 R. Morent, N. De Geyter, C. Leys, L. Gengembre, and E. Payen, *Surf. Coat. Tech.*, 2007, **201**, 7847

163 R.A. Lawton, C.R. Price, A.F. Runge, W.J. Doherty III, S.S. Saavedra, *Colloids Surf. A*, 2005, **253**, 213

164 K.S. Kim, C.M. Ryu, C.S. Park, G.S. Sur, and C.E. Park, *Polymer*, 2003, **44**, 6287

165 M. Tsuchida, and Z. Osawa, *Colloid Polym. Sci.*, 1994, **272**, 770

166 J. Larrieu, B. Held, H. Martinez, and Y. Tison, *Surf. Coat. Technol.*, 2005, **200**, 2310

167 H. Lim, Y. Lee, S. Han, J. Cho, and K-J Kim, *J. Vac. Sci. Technol. A*, 2001, **19**, 1490

168 Y.I. Yun, K.S. Kim, S-J. Uhm, B.B. Khatua, K. Cho, J.K. Kim, and C.E. Park, *J. Adhesion Sci. Technol.*, 2004, **18**, 1279

169 J. Nakamatsu, L.F. Delgado-Aparicio, R. Da Silva, and F. Soberon, *J. Adhesion Sci. Technol.*, 1999, **13**, 753

170 R.K. Wells, J.P.S. Badyal, I.W. Drummond, K.S. Robinson, and F.J. Street, *J. Adhesion Sci. Technol.*, 1993, **7**, 1129

171 P. Favia, A. Milella, L. Iacobelli, R. d'Agostino, *Plasma Processes and Polymers*, ed. R. d'Agostino, P. Favia, C. Oehr, M.R. Wertheimer, Wiley-VCH Verlag GMBH & Co. KGaA, Weinheim, 2005, ch. 20, 271

172 S. Shin, S.H. Han, Y.S. Kim, *Han'guk Pyomyon Konghak Hoechi*, 2005, **38**, 118

173 C.Y. Tu, Y-L. Liu, K-R. Lee, and J-Y. Lai, *Polymer*, 2005, **46**, 6976

174 L. Tong, D.T.K. Kwok, H. Wang, L. Wu, and P.K. Chu, *Adv. Eng. Mater.*, 2010, **12**, 163

175 M. Morra, E. Ochchiello, and F. Garbassi, *Langmuir*, 1989, **5**, 872

176 S. Zanini, R. Barni, R. Della Pergola, and C. Riccardi, *J. Phys. D. Appl. Phys.*, 2014, **47**, 325202

177 A. Dekker, K. Reitsma, T. Beugeling, A. Bantjes, J. Feijen, and W.G. van Aken, *Biomaterials*, 1991, **12**, 130

178 N. Vandencasteele, B. Nisol, P. Viville, R. Lazzaroni, D.G. Castner, and F. Reniers, *Plasma Process Polym.*, 2008, **5**, 661

179 N. Vandencasteele, H. Fairbrother, and F. Reniers, *Plasma Process. Polym.*, 2005, **2**, 493

180 M.E. Ryan, and J.P.S. Badyal, *Macromolecules*, 1995, **28**, 1377

181 S. Zanini, R. Barni, R. Della Pergola, and C. Riccardi, *J. Phys. D. Appl. Phys.*, 2014, **47**, 325202

182 E.C. Stancu, A.M. Stanciuc, M.D. Ionita, M. Teodorescu, L. Moldovan, and G. Dinescu, *Rom. Journ. Phys.*, 2011, **56**, 149

183 A. Reznickova, Z. Kolska, V. Hnatowicz, P. Stopka, and V. Svorcik, *Nucl. Instrum. Meth. B.*, 2011, **269**, 83

184 D.J. Wilson, R.L. Williams, and R.C. Pond, *Surf. Interface Anal*., 2001, **31**, 385

185 J. Hubert, T. Dufour, N. Vandencasteele, S. Desbief, R. Lazzaroni, and F. Reniers, *Langmiur*, 2012, **28**, 9466

186 P. Slepicka, N. Slepickova Kasalkova, E. Stranska, L. Bacakova, V. Scorcik, *Express Polym. Lett.*, 2013, **7**, 535

187 J.P.Badey, E. Espuche, D. Sage, B. Chabert, Y. Jugnet, C. Batier, and T.M. Duc, *Polymer*, 1996, **37**, 1377

188 A. Sarani, N. De Geyter, A.Y. Nikiforov, R. Morent, C. Leys, J. Hubert, and F. Reniers, *Surf. Coat. Technol.*, 2012, **206**, 2226

189 C.Y. Tu, Y.L. Liu, K.R. Lee, and J.Y. Lai, *Polymer*, 2005, **46**, 6976

190 U. Konig, M. Nitschke, M. Pilz, F. Simon, C. Arnhold, and C. Werner, *Colloid Surface B*, 2002, **25**, 313

191 B. Hergelova, T. Homola, A. Zahoranova, T. Pecenik, D. Kovacik, and J. Matousek, *WDS 2012 - Proceedings of Contributed Papers Part II*, ed. J. Safrankova, J Pavlu, Matfyzpress, Prague, 2012, 128

192 G.H. Yang, E.T. Kang, and K.G.Neoh, *J. Polym. Sci. Pol. Chem.*, 2000, **38**, 3498

193 X.P. Zou, E.T. Kang, K.G.Neoh, C.Q. Cui, and T.B. Lim, Polymer, 2001, **42**, 6409

194 H.C. Barshilia, and N. Gupta, *Vacuum*, 2014, **99**, 42

195 N. Vandencasteele, B. Nisol, P. Viville, R. Lazzaroni, D.G. Castner, and F. Reniers, *Plasma Process Polym.*, 2008, **5**, 661

196 S.M. Pelagade, N.L. Singh, R.S. Rane, S. Mukherjee, U.P. Deshpande, V. Ganesan, and T. Shrpropan-2-olthi, *JSEMAT*, 2012, **2**, 132

197 C. Huang, W.C. Ma, C.Y. Tsai, W.T. Hou, and R.S. Juang, *Surf. Coat. Tech.*, 2013, **231**, 42

198 F.J. Montes Ruiz-Cabello, M.A. Rodriguez-Valverde, and M.A. Cabrerizo-Vilchez, *Langmuir*, 2011, **27**, 8748

199 R.P. Woodward, *FTA200 Measurement Capabilities*, First Ten Angstroms, Portsmouth VA

200 R.P. Woodward, *Surface Tension Measurements Using the Drop Shape Method*, First Ten Angstroms, Portsmouth VA

201 P. Chevallier, M. Castonguay, S. Turgeon, N, Dubrelle, D. Mantovani, P.H. McBreen, J-C. Wittmann, and G. Laroche, *J. Phys. Chem. B*, 2001 **105**, 12490

202 S.J. Kang, and V.M. Donnelly, *Plasma Sources Sci. Technol.*, 2007, **16**, 265

203 J.E. Nicholas, A.I. Spiers, and N.A. Martin, *Plasma Chem. Plasma Process.*, 1986, **6**, 39

204 D.C. Carbaugh, F.J. Munno, and J.M. Marchello, *J. Chem. Phys.*, 1967, **47**, 5211

205 M.J. Kushner, *J. Appl. Phys.*, 1992, **71**, 4173

206 W.C.E.Schofield, and J.P.S. Badyal, *Polymer*, 2011, **52**, 5732

207 T. Lundstedt, E. Seifert, L. Abramo, B. Thelin, Å. Nystrom, J. Pettersen, and R. Bergman, *Chemometr. Intell. Lab.*, 1998, **42**, 3

208 Fluon, Moulding of PTFE granular powders: Technical Service Note F1 (https://www.agcchem.com/component/jdownloads/finish/13-fluon-ptfe-resins/41-processing-note-f1-molding-of-ptfe-granular-powders?Itemid=0) accessed 11-07-17

209 M. Morra, E. Ochchiello, and F. Garbassi, Langmuir, 1989, 5, 872

210 D. Lin-Vien, N.B. Colthup, W.G. Fateley, and J.G. Graselli, *The Handbook of Infrared and Raman Characteristic Frequencies of Organic Molecules*, Academic Press Inc., London, 1991, 475

211 D.D. Fazullin, G.V. Mavrin, M.P. Sokolov, and I.G. Shaikhiev, *Mod. Appl. Sci.*, 2015, **9**, 242

212 M.J. Cozad, D.A. Grant, S.L. Bachman, D.N. Grant, B.J. Ramshaw, and S.A. Grant, *J. Biomed. Mater. Res., Part B*, 2010, **94B**, 455

213 G. Wolansky, and A. Marmur, *Colloids Surf. A*, 1999, **156**, 381

214 A.B.D. Cassie, and S. Baxter, *Trans. Faraday Soc.*, 1944, **40**, 546

215 L.I. Rolo, A.I. Caço, A.J. Queimada, I.M. Marrucho, and J.A.P. Coutinho, *J. Chem. Eng. Data*, 2002, **47**, 1442

216 G. Vázquez, E. Alvarez, and J.M. Navaza, *J. Chem. Eng. Data*, 1995, **40**, 611

217 D.L. Camin, A.F. Forziati, and F.D. Rossini, *Physical Properties of Some Hydrocarbons*, 1954, **58**, 440

218 J. Rheims, J. Köser, and T. Wriedt, *Meas. Sci. Technol.*, 1997, **8**, 601

219 http://www.surface-tension.de/solid-surface-energy.htm (accessed 21-08-17)

220 J.F. Moulder W.F. Stickle, P.E. Sobol, and K.D. Bomben, *Handbook of X-ray Photoelectron Spectroscopy*, Perkin Elmer Corporation Physical Electronics Division, Eden Prairie, 1992

221 H. Liu, and Y. Liu, *Plasmas Sci. Technol.*, 2012, **14**, 728

222 A. Vesel, M. Mozetic, and A. Zalar, *Surf. Interface Anal.*, 2008, **40**, 661

223 D.J. Wilson, R.L. Williams, and R.C. Pond, *Surf. Interface Anal.*, 2001, **31**, 385

224 V. Barwick, J. Langley, T. Mallet, B. Stein, and K. Webb, *Best Practice Guide for Generating Mass Spectra*, LGC Ltd., Teddington, 2006, 24.

225 C.L. Enloe, T.E. McLaughlin, R.D. VanDyken, and K.D. Kachner, *AIAA Journal*, 2004, **42**, 589

226 G. Konesky, *Proceedings of SPIE - The International Society for Optical Engineering*, Orlando FL, 2009, 7304ON, doi: 10.1117/12.818323

227 M. Laroussi, *IEEE Trans. Plasma Sci.*, 1996, **24**, 1188

228 L.J. Ward, PhD Thesis, Durham University, 2000

229 U. Kogelschatz, B. Eliasson, and W. Egli, *J. Phys. Colloq.*, 1997, **07**, C4-47

230 H.F. Beer, PhD Thesis, Durham University, 1980

231 P. Rajasekaran, P. Mertmann, N. Bibinov, D. Wandke, W. Viöl, and P. Awakowicz, *Plasma Processes Polym.*, 2010, **7**, 665

232 C. Sarra-Bournet, G. Ayotte, S. Turgeon, F. Massines, and G. Laroche, *Langmuir*, 2009, **25**, 9432

233 C. Sarra-Bournet, S. Turgeon, D. Mantovani, and G. Laroche, *J. Phys. D. Appl. Phys.*, 2006, **39**, 3461

234 P. Rajasekaran, P. Mertmann, N. Bibinov, D. Wandke, W. Viöl, and P. Awakowicz, *Plasma Processes Polym.*, 2010, **7**, 665

235 C. Sarra-Bournet, G. Ayotte, S. Turgeon, F. Massines, and G. Laroche, *Langmuir*, 2009, **25**, 9432

236 Z. Fang, L. Hao, H. Yang, X. Xie, Y. Qiu, and K. Edmund, Appl. Surf. Sci., 2009, 255, 7279

237 D. Pavlinak, O. Galmiz, M. Zemeanek, A. Brablec, J. Cech, and M. Cernak, *Appl. Phys. Lett.*, 2014, **105**, 154102

238 S. Ishikawa, K. Yukimura, K. Matsunaga, and T. Maruyama, *Jpn. J. Appl. Phys.*, 2000, **39**, 5223

239 C. Sarra-Bournet, S. Turgeon, D. Mantovani, and G. Laroche, *J. Phys. D. Appl. Phys.*, 2006, **39**, 3461

240 C. Sarra-Bournet, S. Turgeon, D. Mantovani, and G. Laroche, *Plasma Process. Polym.*, 2006, **3**, 506

241 X-J. Shao, G-J. Zhang, J-Y. Zhan, and G-M. Xu, *IEEE T. Plasma Sci.*, 2011, **39**, 3095

242 C. Sarra-Bournet, G. Ayotte, S. Turgeon, F. Massines, and G. Laroche, *Langmuir*, 2009, **25**, 9432

243 Z. Fang, and L. Cai, *High Voltage Engineering,* 2011, **37**, 1459

244 Z. Fang, L. Hao, H. Yang, X. Xie, Y. Qiu, and K. Edmund, Appl. Surf. Sci., 2009, 255, 7279

245 C.Z. Liu, J.Q. Wu, L.Q. Ren, J. Tong, J.Q. Li, N. Cui, N.M.D. Brown, and B.J. Meenan, *Mater. Chem. Phys.*, 2004, **85**, 340

246 N. Zettsu, H. Itoh, and K. Yamamura, *Surf. Coat. Tech.*, 2008, **202**, 5284

247 D. Pavlinak, O. Galmiz, M. Zemeanek, A. Brablec, J. Cech, and M. Cernak, *Appl. Phys. Lett.*, 2014, **105**, 154102

248 Z. Niu, C. Zhang, T. Shao, Z. Fang, Y. Yu, and P. Yan, *Surf. Coat. Tech.*, 2013, **228**, S578

249 F. Zhi, L. Yi, Q. Yuchung, Y. Yun, and X. Dawei, *Vacuum Science and Technology (China),* 2003, **23**, 408

250 C. Liu, N. Cui, N.M.D. Brown, B.J. Meenan, *Surf. Coat. Tech.,* 2004, **185**, 311

251 Y. Iriyama, *J. Photopolym. Sci. Technol.*, 2010, **23**, 599

252 D.D. Pappas, A.A. Bujanda, J.A. Orlicki, and R.E. Jensen, *Surf. Coat. Tech.,* 2008, **203**, 830

253 G. Borcia, C.A. Anderson, and N.M.D. Brown, *Appl. Surf. Sci.*, 2004, **221**, 203

254 G. Borcia, C.A. Anderson, and N.M.D. Brown, *Plasma Sources Sci. T.*, 2003, **12**, 335

255 B. Hergelova, T. Homola, A. Zahoranova, T. Pecenik, D. Kovacik, and J. Matousek, *WDS 2012 - Proceedings of Contributed Papers Part II*, ed. J. Safrankova, J Pavlu, Matfyzpress, Prague, 2012, 128

256 S. Ishikawa, K. Yukimura, K. Matsunaga, and T. Maruyama, *Surf. Coat. Tech.,* 2000, **130**, 52

257 S. Trigwell, D. Boucher, and C.I. Calle, *J. Electrost.,* 2007, **65**, 401

258 K. Furuse, Y. Sawada, K. Takahashi, M. Kogoma, and K. Tanaka, *J. Photopolym. Sci. Tec.,* 2015, **28**, 465

259 Z. Lan, G.H. Lu, W. Chen, H. Pang, G.L. Zhang, and S.Z. Yang, *Chin. Phys. B,* 2011, **20**, 065206

260 Z. Fang, Y. Qiu, and Y. Luo*, J. Phys. D: Appl. Phys.,* 2003, **36**, 2980

261 *U.S. Pat.*, US2016/0039979, 2016

262 *PCT Int. Appl.*, WO9702310, 1997

263 *WIPO Pat.*, WO99/18149, 1999

264 F. Chen, S. Liu, J. Liu, S. Huang, G. Xia, J. Song, W. Xu, J. Sun, and X. Liu, *Appl. Surf. Sci.*, 2016, **360**, 207

265 K. Tanaka, M. Kogoma, *Int. J. Adhes. Adhes.,* 2003, **23**, 515

266 R. Winter, D. Korzec, N. Sprang, D. Theirich, and J. Engemann, *Surf. Coat. Tech.,* 1995, **74**, 618

267 B.E. Stein, V. Rodriguez-Santiago, A.A. Bujanda, K.E. Strawhecker, and D.D. Pappas, 2010, *NSTI-Nanotech,* **1**, 677

268 E.C. Stancu, A.M. Stanciuc, M.D. Ionita, M. Teodorescu, L. Moldovan, and G. Dinescu, *Rom. Journ. Phys.,* 2011, **56**, 149

269 A. Sarani, N. De Geyter, A.Y. Nikiforov, R. Morent, C. Leys, J. Hubert, and F. Reniers, *Surf. Coat. Technol.,* 2012, **206**, 2226

270 V. Rodriguez-Santiago, A. Bujanda, B. Stein, and D. Pappas, *Plasma Process Polym.,* 2011, **8**, 631

271 E.A.D. Carbone, N. Boucher, M. Sferrazza, and F. Reniers, *Surf. Interface Anal.,* 2010, **42**, 1014

272 J. Hubert, T. Dufour, N. Vandencasteele, S. Desbief, R. Lazzaroni, and F. Reniers, *Langmiur,* 2012, **28**, 9466

273 T. Dufour, J. Hubert, P. Viville, C.Y. Duluard, S. Desbief, R. Lazzaroni, and F. Reniers, *Plasma Process. Polym.,* 2012, **9**, 820

274 A. Mellinger, Dr. rer. nat. habil. Thesis, Potsdam University, 2004

275 P.P. Tsai, H. Schreuder-Gibson, and P. Gibson, *J. Electrost.*, 2002, **54**, 333

276 W. Pong, D. Brandt, and Z.X. HeW. Imaino, *J. Appl. Phys.*, 1985, **58**, 896

277 C-Y. Liu, and S-A. Chen, *Macromol. Rapid Commun.*, 2007, **28**, 1743

278 A. Many, and G. Rakavy, *Phys. Rev.*, 1962, **126**, 1980

279 P.W. Chudleigh, *J. Appl. Phys.*, 1977, **48**, 4591

280 D.W. Vance, *J. Appl. Phys.*, 1971, **42**, 5430

281 K. Seki, H. Tanaki, T. Ohta, Y. Aoki, A. Imamura, H. Fujimoto, H. Yamamoto, and H. Inokuchi, *Physica Scripta*, 1990, **41**, 167

282 A. Atta, and A. Abdel-Galil, *Indian Journal of Pure & Applied Physics*, 2016, **54**, 551

283 G-J. Zhang, K. Yang, W-B. Zhao, Z. Yan, *Appl. Surf. Sci.*, 2006, **253**, 1995

284 G. Attard, C. Barnes, *Surfaces*, Oxford University Press, Oxford, 1998

285 ChemGuide; Electron Affinity, (https://www.chemguide.co.uk/atoms/properties/eas.html), accessed 21-03-18

286 D.K. Davies, *Brit. J. Appl. Phys. (J. Phys. D)*, 1969, **2**, 1533

287 A.J. Dekker, *Solid State Physics*, Pan MacMillan, 1969, London, 350

288 M. Eguchi, *Philos. Mag.*, 1925, **49**, 178

289 *US Pat.*, US4291245 A, 1981

290 B.A. MacDonald, PhD Thesis, McGill University, 1990

291 J. Van Turnhout, *J. Electrost.*, 1975, **1**, 147

292 F. Gutmann, *Reviews of Modern Physics*, 1948, **20**, 457

293 Y-H. Chou, H-C. Chang, C-L. Liu, and W-C. Chen, *Polym. Chem.*, 2015, **6**, 341

294 S. Boisseau, G. Despesse, T. Ricart, E. Defay, and A. Sylvestre, *Smart Mater. Struct.*, 2011, **20**, 105013

295 J. Niu, D. Liu, and Y. Wu, *Surf. Coat. Tech.*, 2011, **205**, 3434

296 T.A. Yovcheva, I.A. Avramova, G.A. Mekishev, and T.S. Marinova, *J. Electrost.*, 2007, **65**, 667

297 A. Yagishita, H. Yamanoiuchi, and K. Ikezaki, *Jpn. J. Appl. Phys.*, 1999, **38**, 2053

298 J.A. Giacometti, S. Fedosov, and M.M. Costa, *Brazilian Journal of Physics*, 1999, **29**, 269

299 D.K. Davies, and P.J. Lock, *J. Electrochem Soc.*, 1973, **120**, 266

300 R. A. Creswell, M. M. Perlman, and M. A. Kabayama, *Dielectric Properties of Polymers*, ed. F. E. Karasz, Plenum Publishing Corp., New York, 1972, 295

301 Z. Xia, A. Buechtemann, Z. An, J. Jiang, R. Danz, and A. wedel, *J. Electrost.*, 2005, **63**, 387

302 C. Lei, X. Wang, Q. Fang, Y. Gao, D. Tu, and Q. Du, *Eur. Polym. J.*, 2007, **43**, 4523

303 D.K. Das-Gupta, *J. Electrost.*, 2001, **51-52**, 159

304 R. Kressman, G.M. Sessler, and P. Günther, *IEEE Trans. Dielectr. Electr. Insul.*, 1996, **3**, 607

305 Y Arita, S. Sha Shiratori, and K. Ikezaki, *J. Electrost.*, 2003, **57**, 263

306 S. Morsch, P.S. Brown, and J.P.S. Badyal, *J. Mater. Chem.*, 2012, **22**, 3922

307 A.A. Rychkov, V.G. Boltzov, and V.V. Shvetzm, *9th International Symposium on Electrets*, IEEE, Shanghai, 1996, 89

308 D. Rychkov, A. Kuznetsov, and A. Rychkov, *IEEE Trans. Dielectr. Electr. Insul.*, 2011, **18**, 8

309 M.M. Perlman, and S. Unger, *J. Phys. D: Appl. Phys.*, 1972, **5**, 2115

310 P. Atkins, and J. de Paula, *Atkins' Physical Chemistry*, Oxford University Press, Oxford, 7th ed., 2002, 255

311 A.M. Kamalov, and M.E. Borisova, *St. Petersburg Polytechnical University Journal: Physics and Mathematics*, 2016, **2**, 188

312 D.W. Vance, *J. Appl. Phys.*, 1971, **42**, 5430

313 R.K. Wells, PhD Thesis, Durham University, 1994

314 F. Massines, A. Rabehi, P. Decomps, R.B. Gadri, P. Segur, and C. Mayoux, *J. Appl. Phys.*, 1998, **83**, 2950

315 C.L. Enloe, T.E. McLaughlin, R.D. VanDyken, and K.D. Kachner, *AIAA Journal*, 2004, **42**, 589

316 A. Fridman, A. Chirokov, and A. Gutsol, *J. Phys. D: Appl. Phys.*, 2005, **38**, R1

317 Z. Xia, A. Buechtemann, Z. An, J. Jiang, R. Danz, and A. Wedel, *J. Electrost.*, 2005, **63**, 387

318 K. Samanta, M. Jassel, and A.K. Agrawal, *Indian J. Fibre Text. Res.*, 2006, **31**, 83

319 Z. Xia, R. Gerhard-Multhaupt, W. Künstler, A. Wedel, and R. Danz, *J. Phys. D: Appl. Phys.*, 1999, **32**, L83

320 D. Rychkov, M. Yablokov, and A. Rychkov, *Appl. Phys. A*, 2012, **107**, 589

321 D. Rychkov, A. Kuznetsov, and A. Rychkov, *IEEE Trans. Dielectr. Electr. Insul.*, 2011, **18**, 8

322 M. Nifuku, Y. Zhou, A. Kisiel, T. Kobayashi, and H. Katoh, *J. Electrost.*, 2001, **51**, 200

323 S. Haridoss, and M. Perlman, *J. Appl. Phys.*, 1984, **55**, 1332

324 M. Li, C. Li, H. Zhan, J. Xu, and X. Wang, *Appl. Phys. Lett.*, 2008, **92**, 031503

325 G. A. Mekishev, T.A. Yovcheva, and A.P. Viraneva, *J. Non-Cryst. Solids*, 2007, **353**, 4453

326 G.S. Neugschwandtner, R. Schwödiauer, S. Bauer-Gogonea, and S. Bauer, *Appl. Phys. A.*, 2000, **70**, 1

327 R. Kacprzyk, and J. Ziaja, *J. Electrost.*, 1997, **40&41**, 319

328 M.A. Noras, Trek Application Note #3002, (http://www.trekinc.com/pdf/3002-field-voltmeter.pdf), accessed 21-03-18

329 P.S. Brown, PhD Thesis, Durham University, 2013

330 F. Wang, Q. Zhang, Y. Qiu, and E. Kuffel, *Conference Record of the 2002 IEEE International Symposium on Electrical Insulation*, IEEE, Boston MA, 2002, 426

331 R. Toomer, and T.J. Lewis, *J. Phys. D: Appl. Phys.*, 1980, **13**, 1343

332 A. Cristofolini, A.A. Borghi, and G. Neretti, *J. Appl. Phys.*, 2013, **113**, 143307

333 D. Orejon, K. Sefiane, and M.E.R. Shanahan, *Appl. Phys. Lett.*, 2013, **102**, 201601

334 S.R. Kim, *J. Appl. Polym. Sci.*, 2000, **77**, 1913

335 A. Řezníčková, Z. Kolská, V. Hnatowicz, P. Stopka, and V. Švorčík, *Nucl. Instrum. Meth. B.*, 2011, **269**, 83

336 S. Morsch, PhD Thesis, Durham University, 2012

337 U. Zaghloul, B. Bushan, P. Pons, G.J. Papaioannou, F. Coccetti, and R. Plana, *Nanotechnology*, 2010, **22**, 035705

338 S. Collette, T. Dufour, and F. Reniers, *Plasma Sources Sci. Technol.*, 2016, **25**, 025014

339 W. Hai, T. Hi, K. Shimizu, and T. Yajima, *J. Photopolym. Sci. Tech.*, 2015, **28**, 479

340 L. Mecozzi, O. Gennari, R. Rega, L. Battista, P. Ferraro, and S. Grilli, *Macromol. Biosci.*, 2017, **17**, 1600307

341 L. Lin, X. Guo, and T.S. Mayer, *Conference on Alternative Lithographic Technologies VII*, ed. D.J. Resnick, and C. Bencher, SPIE, San Jose CA, 2015, 94231U

342 X. Guo, L. Lin, and T.S. Mayer, *Conference on Alternative Lithographic Technologies VIII*, ed. C. Bencher, and J.Y. Cheng, SPIE, San Jose CA, 2016, 977719

343 S.N. Jayasinghe, and A.C. Sullivan, *Sol-Gel Sci. Technol.*, 2006, **38**, 293

344 M.D. Dickey, E. Collister, A. Raines, P. Tsiartas, T. Holcombe, S.V. Sreenivasan, R.T. Bonnecaze, and C.G. Willson, *Chem. Mater.*, 2006, **18**, 2043

345 *U.S. Pat.*, US2016/0039979, 2016

346 Ch. Baquey, F. Palumbo, M.C. Porte-Durrieu, G. Legeay, A. Tressaud, and R. d'Agostino, *Nucl. Instr. and Meth. in Phys. Res. B*, 1999, **151**, 255

347 S. Turmanova, M. Minchev, K. Vassilev, and G. Danev, *J. Polym. Res.*, 2008, **15**, 309

348 C-Y. Tu, Y-L. Liu, K-R. Lee, and J-Y. Lai, *Polymer*, 2005, **46**, 6976

349 Y.K. Cho, D. Park, H. Kim, H. Lee, H. Park, H.J. Kim, and D. Jung, *Appl. Surf. Sci.*, 2014, **296**, 79

350 *U.S. Pat.*, US2016/0039979, 2016

351 Z-Y. Xi, Y-Y. Xu, L-P. Zhu, F. Liu, and B-K. Zhu, *Appl. Surf. Sci.*, 2008, **254**, 7469

352 N. Zettsu, H. Itoh, and K. Yamamura, *Surf. Coat. Tech.*, 2008, **202**, 5284

353 N. Zettsu, H. Itoh, and K. Yamamura, *Thin Solid Films*, 2008, **516**, 6683

354 A. Lin, S. Shao, H. Li, D. Yang, and Y. Kong, *J. Membr. Sci.*, 2011, **371**, 286

355 G.H. Yang, Y. Zhang, K.S. Lee, E.T. Kang, and K.G. Neoh, *J. Fluorine Chem.*, 2003, **119**, 151

356 W.H. Yu, E.T. Tang, and K.G. Neoh, *Langmuir*, 2005, **21**, 450

357 S. Lévesque, J. Thibault, M. Castonguay, R. C.-Gaudreault, and G. Laroche, Colloids Surf., B., 2002, **25**, 205

358 Z. Kolskà, S. Lupìnková, K. Výborný, N. Kasálková Slepičková, A. Řezníčková, M.Nagyová, and V. Švorčík, *Polym. Degrad. Stabil.*, 2014, **101**, P-36

359 H.S. Sundaram, X. Han, A.K. Nowinski, J.-R. Ella-Menye, C. Wimbish, P. Marek, K. Senecal, and S. Jiang, *ACS Appl. Mater. Interfaces*, 2014, **6**, 6664

360 J. Kuang, and P.B. Messersmith, *Langmuir*, 2012, **28**, 7258

361 H.-C. Yang, J. Luo, Y. Lv, P. Shen, and Z.-K. Xu, *J. Membr. Sci.*, 2015, **483**, 42

362 J. Jiang, L. Zhu, L. Zhu, H. Zhang, B. Zhu, and Y. Xu, *ACS Appl. Mater. Interfaces*, 2013, **5**, 12895

363 A. Venault, Y. Chang, H-H. Hsu, J-F. Jhong, H-S. Yang, T-C. Wei, K-L. Tung, A. Higuchi, and J. Huang, *J. Membrane Sci.*, 2013, **439**, 48

364 J.-F. Jhong, A. Venault, C.-C. Hou, S.-H. Chen, T.-C. Wei, J. Zheng, J. Huang, and Y. Chang, *ACS Appl. Mater. Interfaces*, 2013, **5**, 6732

365 Sigma-Aldrich Catalogue, (https://www.sigmaaldrich.com/catalog/product/aldrich/473170?lang=en&region=GB), accessed 22-03-18

366 M.A. Noras, Trek Application Note #3002, (http://www.trekinc.com/pdf/3002-field-voltmeter.pdf), accessed 21-03-18

367 K. Samanta, M. Jassel, and A.K. Agrawal, *Indian J. Fibre Text. Res.*, 2006, **31**, 83

368 N. Zettsu, H. Itoh, and K. Yamamura, *Surf. Coat. Tech.*, 2008, **202**, 5284

369 Table of IR Absorptions, (https://webspectra.chem.ucla.edu/irtable.html), accessed 12-02-18

370 Y. Yuan, X. Zang, F. Ai, J. Zhou, J. Shen, and S. Lin, *Polym. Int.*, 2004, **53**, 121

371 J.P.Badey, E. Espuche, D. Sage, B. Chabert, Y. Jugnet, C. Batier, and T.M. Duc, *Polymer*, 1996, **37**, 1377

372 Y. Yuan, X. Zang, F. Ai, J. Zhou, J. Shen, and S. Lin, *Polym. Int.*, 2004, **53**, 121.

373 K.M. Sim, H-S. Park, G-N. Bae, and J.H, Jung, *Sci Total Environ.*, 2015, **533**, 266.

374 P.C. Raynor, B.G. Kim, G. Ramachandran, M.R. Strommen, J.H. Horns, and A.J. Streifel, *Indoor Air*, 2008, **18**, 51.

375 P.C. Raynor, and S.J. Chae, *J. Occup. Environ. Hyg.*, 2004, **1**, 463.

376 S. George, *Chem. Rev.*, 2010, **110**, 111.

377 S. George, A. Ott, and J. Klaus, *J. Phys. Chem.*, 1996, **100**, 13121.

378 A. Brozena, C. Oldham, G. Parsons, *J. Vac. Sci. Technol. A*, 2016, **34**, 010801-1.

379 G.B. Lee, K. Son, S. Park, J. Shim, and B-H. Choi, *ECS Transactions*, 2012, **50**, 89

380 Q. Xu, J. Yang, J. Dai, Y. Yang, X.Chen, and Y. Wang, *J. Membrane Sci.*, 2013, **448**, 215

381 Q. Xu, J. Yang, X. Wang, Z. Wang, W. Jin, J. Huang, and Y. Wang, *J. Membrane Sci.*, 2012, **415**, 435

382 A.K. Roy, J. Dendooven, D. Deduytsche, K. Devloo-Casier, K. Ragaert, L. Cardon, and C. Detavernier, *Chem. Comm.*, 2015, **51**, 3556

383 R. Edy, X. Huang, Y. Guo, J. Zhang, and J. Shi, *Nanoscale Res. Lett.*, 2013, **8**, 79

384 G.C. Correa, B. Bao, and N.C. Strandwitz, *ACS Appl. Mater. Interfaces*, 2015, **7**, 14816

385 T. Shi, M. Shao, H. Zhang, Q. Yang, and X. Shen, *Appl. Surf. Sci.*, 2011, **258**, 1474

386 Z. Kolska, A. Reznickova, V. Hnatowicz, and V. Svorcik, *Vacuum*, 2012, **86**, 643

387 J.P. Badey, E. Espuche, D. Sage, and B. Chabert, *Polymer*, 1996, **37**, 1377

388 V. Gauvreau, P. Chevallier, K. Vallieres, E. Petitclerc, R.C. Gaudreault, and G. Laroche, *Bioconjug. Chem.*, 2004, **15**, 1146

389 N. Vandencasteele, H. Fairbrother, and F. Reniers, *Plasma Process. Polym.*, 2005 **2**, 493

390 E.T. Kang, K.L. Tan, K. Kato, Y. Uyama, and Y. Ikada, *Macromolecules*, 1997, **30**, 1091

391 S. Wu, E.T. Kang, K.G. Neoh, and K.L. Tan, *Polymer*, 1999, **40**, 6955

392 T. Wang, E.T. Kang, K.G. Neoh, K.L. Tan, C.Q. Cui, and T.B. Lim, *J. Adhesion Sci. Technol.*, 1997, **11**, 679

393 M. Morra, E. Ochchiello, and F. Garbassi, *Surf. Interface Anal.*, 1990, **16**, 412

394 E.A.D. Carbone, N. Boucher, M. Sferrazza, and F. Reniers, *Surf. Interface Anal.*, 2010, **42**, 1014

395 X.P. Zou, E.T. Kang, K.G. Neoh, C.Q. Cui, and T.B. Lim, *Plasma Polym.*, 2000, **5**, 219

396 H. Liu, and Y. Liu, *Plasmas Sci. Technol.*, 2012, **14**, 728

397 A. Reznickova, Z. Kolska, V. Hnatowicz, and V. Svorick, *J. Nanopart. Res.*, 2011, **13**, 2929

398 S.R. Kim, *J. Appl. Polym. Sci.*, 2000, **77**, 1913

399 E.C. Stancu, A.M. Stanciuc, M.D. Ionita, M. Teodorescu, L. Moldovan, and G. Dinescu, *Rom. Journ. Phys.*, 2011, **56**, 149

400 J.P. Badey, E. Espuche, Y. Jugnet, B. Chabert, and T.M. Duct, *Int. J. Adhes. Adhes.*, 1996, **16**, 173

401 C. Wang, J.R. Chen, and R. Li, *Appl. Surf. Sci.*, 2008, **254**, 2882

402 L. Zhou, G.H. Lu, W. Chen, H. Pang, G.L. Zhang, and S.Z. Yang, *Chin. Phys. B*, 2011, **20**, 065206

403 A. Vesel, M. Mozetic, and A. Zalar, *Surf. Interface Anal.*, 2008, **40**, 661

404 D.J. Wilson, R.L. Williams, and R.C. Pond, *Surf. Interface Anal*., 2001, **31**, 385

405 J.P. Badey, E. Espuche, Y. Jugnet, B. Chabert, and T. M. Duct, *Int. J. Adhes. Adhes.*, 1996, **16**, 173

406 H.J. Zhang, Z.Z. Zhang, and F. Guo, *J. Appl. Polym. Sci.*, 2009, **114**, 3980

407 L. Tong, D.T.K. Kwok, H. Wang, L. Wu, and P.K.Chu, *Adv. Eng. Mater. 2010, **12**, 163*

408 Y. Yamada, T. Yamasa, S. Tasaka, N. Inagaki, M*acromolecules*, 1996, **29**, 4331

409 N. Inagaki, *Macromol. Symp.*, 2000, **159**, 151

410 N. Inagaki, S. Tasaka, K. Narushima, and K. Teranishi, *J. Appl. Polym. Sci.*, 2001, **83**, 340

411 C.L. Li, C.Y. Tu, K.R. Lee, and J.Y. Lai, *J. Appl. Polym. Sci.*, 2006, **102**, 909

412 H. Hunke, N. Soin, T.H. Shah, E. Kramer, A. Pascual, M.S.L. Karuna, and E. Siores, *Materials*, 2015, **8**, 2258

413 J.C. Carao, U. Lappan, and K. Lunkwitz, *Surf. Coat. Tech.*, 1999, **116**, 762

414 N. Inagaki, S. Tasaka, and T. Umehara, *J. Appl. Polym. Sci.*, 1999, **71**, 2191

415 H.J. Zhang, Z.Z. Zhang, and F. Guo, *J. Appl. Polym. Sci.*, 2009, **114**, 3980

416 N. Encinas, M. Pantoja, M. Torres-Remiro, and M. Martinez, *J. Adhesion*, 2011, **87**, 709

417 S.W. Lee, *Macromolecular Research*, 2015,**23**, 325

418 J. Nakamatsu, L.F. Delgado-Aparicio, R. Da Silva, and F. Soberon, *J. Adhesion Sci. Technol.*, 1999, **13**, 753

419 Z. Fang, and L. Cai, *High Voltage Engineering*, 2011, **37**, 1459

420 D. Rychov, M. Yablokov, and A. Rychov, *Appl. Phys. A-Mater.*, 2012, **107**, 589

421 F. Zhi, L. Yi, Q. Yuchung, Y. Yun, and X. Dawei, *J. Vac. Sci. Technol. A*, 2003, **23**, 408

422 M. Yuguang, Y. Meilin, L. Dehou, and S. Jiacong, *Chem. J. Chinese U.*, 1990, **11**, 1307

423 H.J. Greisser, *Polym. Mater. Sci. Eng.*, 1990, **62**, 872

424 S. Hai-Xing, Z. Lin, C. Hong, and C. Huan-Lin, *Desalination*, 2006, **192**, 271

425 H. Xu, Z. Hu, S. Wu, and Y. Chen, *Mater. Chem. Phys.*, 2003, **80**, 278

426 J. Hubert, T. Dufour, N. Vandencasteele, S. Desbief, R. Lazzaroni, and F. Reniers, *Langmiur*, 2012, **28**, 9466

427 C.L. Lai, R.M. Liou, S.H. Chen, G.W. Huang, and K.R. Lee, *Desalination*, 2011, **267**, 184

428 D.J. Hook, T.G. Vargo, J.A. Gardella Jr., K.S. Litwiler, and F.V. Bright, *Langmuir*, 1991, **7**, 142

429 J.N. Miller, and J.C. Miller, *Statistics and Chemometrics for Analytical Chemistry*, Pearson Education Ltd, Harlow, 5th ed, 2005

430 NIST Chemistry WebBook, http://webbook.nist.gov/chemistry (accessed 28-11-17)